Science with e-ASTROGAM

A space mission for MeV-GeV gamma-ray astrophysics

Draft 1
November 2nd 2017

Editors

Alessandro De Angelis, Vincent Tatischeff, Isabelle A. Grenier,
Julie McEnery, Manuela Mallamaci

A. De Angelis*,[1,2,3,4] V. Tatischeff*,[5] I. A. Grenier*,[6] J. McEnery*,[7] M. Mallamaci*,[1] M. Tavani,[8,9,10] U. Oberlack,[11] L. Hanlon,[12] R. Walter,[13] A. Argan,[14] P. Von Ballmoos,[15] A. Bulgarelli,[16] A. Bykov,[17] M. Hernanz,[18] G. Kanbach,[19] I. Kuvvetli,[20] M. Pearce,[21] A. Zdziarski,[22] J. Conrad,[23] G. Ghisellini,[24] A. Harding,[25] J. Isern,[26] M. Leising,[27] F. Longo,[28,29] G. Madejski,[30] M. Martinez,[31] M. N. Mazziotta,[32] J. M. Paredes,[33] M. Pohl,[34] R. Rando,[1,35] M. Razzano,[36,37] A. Aboudan,[35,2] M. Ackermann,[38] A. Addazi,[39] C. Albertus,[40] M. Ajello,[27] J. M. Álvarez,[41] G. Ambrosi,[42] S. Antón-Castillo,[43] L. A. Antonelli,[44] A. Babic,[45] B. Baibussinov,[1] M. Balbo,[46] L. Baldini,[36,47] S. Balman,[48] C. Bambi,[49,50] U. Barres de Almeida,[51] J. A. Barrio,[52] R. Bartels,[53] D. Bastieri,[35,1,54] W. Bednarek,[55] D. Bernard,[11] E. Bernardini,[56,38] T. Bernasconi,[13] A. Biland,[57] E. Bissaldi,[58,32] V. Bonvicini,[29] V. Bosch-Ramon,[33] E. Bottacini,[35,1] V. Bozhilov,[59] T. Bretz,[60] M. Branchesi,[61,62] V. Brdar,[63] T. Bringmann,[64] A. Brogna,[11] C. Budtz-Jørgensen,[20] G. Busetto,[35] S. Buson,[7] M. Busso,[42,65] S. Camera,[66,67,68,69] R. Campana,[16] P. Caraveo,[70] M. Cardillo,[8] P. Carlson,[71] S. Celestin,[72] M. Cermeño,[40] C. C Cheung,[73] E. Churazov,[74,75] S. Ciprini,[44,42] A. Coc,[5] A. Coleiro,[76,77] W. Collmar,[78] P. Coppi,[79] R. Curado da Silva,[80] S. Cutini,[44,42] B. De Lotto,[81] D. de Martino,[82] A. De Rosa,[8] L. Delgado,[18] R. Diehl,[78] S. Dietrich,[83] A D. Dolgov,[84,85] A. Domínguez,[52] D. Dominis Prester,[86] I. Donnarumma,[8] D. Dorner,[87] M. Doro,[1,35] M. Fabrizio,[44,88] V. Fioretti,[16] L. Foffano,[35,1] N. Fornengo,[66,67] L. Foschini,[24] A. Franceschini,[35] A. Franckowiak,[89] S. Funk,[90] F. Fuschino,[16] G. Gaggero,[53] G. Galanti,[91] F. Gargano,[32,92] D. Gasparrini,[44,42] R. Gehrz,[93] P. Giammaria,[88] N. Giglietto,[58,32] P. Giommi,[94] F. Giordano,[32] G. Ghirlanda,[24,95] N. Godinovic,[45] C. Gouiffés,[96] J. E. Grove,[97] C. Hamadache,[5] D. H. Hartmann,[27] M. Hayashida,[98] A. Hryczuk,[64] P. Jean,[99] T. Johnson,[100] J. José,[101] S. Kaufmann,[102] J. Kiener,[5] J. Knödlseder,[103] M. Kole,[13] J. Kopp,[104] V. Kozhuharov,[59] C. Labanti,[16] S. Lalkovski,[59] P. Laurent,[105] O. Limousin,[106] L. Nava,[24,107] E. Lindfors,[108] J. Liu,[109] S. Lombardi,[44,88] F. Loparco,[32,92] M. López Moya,[52] B. Lott,[110] P. Lubrano,[42] D. Malyshev,[111] N. Mankuzhiyil,[112] K. Mannheim,[87] A. Marcianò,[39] B. Marcote,[113] M. Mariotti,[1] M. Marisaldi,[114] S. McBreen,[12] S. Mereghetti,[115] A. Merle,[116] R. Mignani,[117,118] G. Minervini,[8] A. Moiseev,[119] A. Morselli,[10] K. Nakazawa,[120] D. Nieto,[52] M. Orio,[121,2] E. Orlando,[30] P. Orleanski,[122] S. Paiano,[2] R. Paoletti,[36] A. Papitto,[88] B. Patricelli,[123,36] M. Á. Pérez-García,[40] M. Persic,[107] G. Piano,[8] A. Pichel,[124] M. Pimenta,[4] C. Pittori,[44,88] T. Porter,[30] J. Poutanen,[108] E. Prandini,[35,1] N. Prantzos,[125] N. Produit,[13] S. Rainó,[58,32] A. Raklev,[64] M. Regis,[66,67] I. Reichardt,[126] J. Rico,[127] G. Rodriguez Fernandez,[10] M. Roncadelli,[128] L. Roso,[129] A. Rovero,[124] R. Ruffini,[130] G. Sala,[101] M. A. Sánchez-Conde,[131] A. Santangelo,[132] P. Saz Parkinson,[133,134] T. Sbarrato,[95] A. Shearer,[135] R. Shellard,[51] K. Short,[53] T. Siegert,[78] P. Spinelli,[32] A. Stamerra,[123] S. Starrfield,[136] A. Strong,[78] I. Strümke,[137] F. Tavecchio,[24] R. Taverna,[35] T. Terzić,[86] D. J. Thompson,[138] O. Tibolla,[102] R. Turolla,[35] A. Ulyanov,[12] A. Ursi,[139] A. Vacchi,[81] J. Van den Abeele,[64] G. Vankova-Kirilovai,[59] F. Verrecchia,[44,88] P. Vincent,[140] X. Wang,[141] C. Weniger,[53] X. Wu,[142] G. Zaharijaš,[143] L. Zampieri,[2] S. Zane,[144] S. Zimmer,[145] A. Zoglauer,[146] and the e-ASTROGAM collaboration

[1] *Istituto Nazionale di Fisica Nucleare, Sezione di Padova, I-35131 Padova, Italy*
[2] *INAF - Osservatorio Astronomico di Padova, I-35122, Padova, Italy*
[3] *Dipartimento di Matematica, Informatica e Fisica, Università di Udine, I-33100 Udine, Italy*
[4] *Laboratorio de Instrumentaçao e Particulas and Instituto Superior Tecnico, Lisboa, Portugal*
[5] *CSNSM, CNRS and University of Paris Sud, F-91405, Orsay, France*
[6] *Laboratoire AIM, CEA-IRFU/CNRS/Université Paris Diderot, C.E.A. Saclay, France*
[7] *NASA Goddard Space Flight Center, Greenbelt, MD 20771, USA*
[8] *INAF/IAPS, via del Fosso del Cavaliere 100, I-00133, Roma, Italy*
[9] *University of Roma "Tor Vergata", I-00133, Roma, Italy*
[10] *Istituto Nazionale di Fisica Nucleare, Sezione di Roma "Tor Vergata", I-00133 Roma, Italy*
[11] *Institute of Physics and PRISMA Excellence Cluster, Johannes Gutenberg University Mainz, 55099 Mainz, Germany*
[12] *School of Physics, University College Dublin, Ireland*
[13] *University of Geneva, Switzerland*
[14] *INAF Headquarters, Viale del Parco Mellini, 84, I-00136, Roma, Italy*
[15] *IRAP Toulouse, 9 av. du Colonel-Roche - BP 44 346, F-31028 Toulouse Cedex 4, France*
[16] *INAF/IASF Bologna, Via Gobetti 101, I-40129 Bologna, Italy*
[17] *Ioffe Institute, St.Petersburg 194021, Russia*
[18] *Institute of Space Sciences (CSIC-IEEC), Campus UAB, C/ Can Magrans s/n, 08193 Cerdanyola del Vallés (Barcelona), Spain*
[19] *Max-Planck-Institut fur Extraterrestrische Physik, Postfach 1312, 85741 Garching, Germany*
[20] *DTU Space, National Space Institute, Technical University of Denmark, Kgs. Lyngby, Denmark*
[21] *KTH Royal Institute of Technology, Dept. of Physics, 10691 Stockholm, Sweden*
[22] *Nicolaus Copernicus Astronomical Center, Polish Academy of Sciences, Bartycka 18, PL-00-716 Warszawa, Poland*

[23] *Oskar Klein Centre for Cosmoparticle Physics Fysikum, Stockholm University AlbaNova University Centre, SE-10961, Stockholm, Sweden*
[24] *INAF - Osservatorio Astronomico di Brera, I-23807 Merate, Italy*
[25] *NASA/Goddard Space Flight Center, Greenbelt, MD 20771, USA*
[26] *ICE (CSIC-IEEC), Campus UAB, Carrer Can Magrans s/n, E-08193 Cerdanyola del Valles, Barcelona, Spain*
[27] *Department of Physics and Astronomy, Clemson University, Clemson, SC 29634, USA*
[28] *Dipartimento di Fisica, Università di Trieste, I-34127 Trieste, Italy*
[29] *Istituto Nazionale di Fisica Nucleare, Sezione di Trieste, I-34127 Trieste, Italy*
[30] *W.W. Hansen Experimental Physics Laboratory, Kavli Institute for Particle Astrophysics and Cosmology, Stanford University, Stanford, CA, 94305, USA*
[31] *IFAE-BIST, Edifici Cn. Universitat Autonoma de Barcelona, E-08193 Bellaterra, Spain*
[32] *Istituto Nazionale di Fisica Nucleare, Sezione di Bari, I-70126 Bari, Italy*
[33] *Departament de Física Quàntica i Astrofísica, Institut de Ciències del Cosmos (ICCUB), Universitat de Barcelona, IEEC-UB, Martí i Franquès 1, E08028 Barcelona, Spain*
[34] *Institute of Physics and Astronomy, University of Potsdam, 14476 Potsdam, Germany*
[35] *Dipartimento di Fisica e Astronomia* "G. Galilei"*, Università di Padova, I-35131 Padova, Italy*
[36] *Istituto Nazionale di Fisica Nucleare, Pisa, Italy*
[37] *Dipartimento di Fisica, Università di Pisa, Italy*
[38] *Deutsches Elektronen Synchrotron (DESY), Platanenallee 6, D-15738 Zeuthen, Germany*
[39] *Center for Field Theory and Particle Physics & Department of Physics, Fudan University, 200433 Shanghai, China*
[40] *Department of Fundamental Physics and IUFFyM University of Salamanca, Plaza de la Merced s/n 37008 Spain*
[41] *Spanish Center for Pulsed Lasers (CLPU), M5 Bldg. Science Park, Villamayor, Salamanca (Spain)*
[42] *Istituto Nazionale di Fisica Nucleare, Sezione di Perugia, I-06123, Perugia, Italy*
[43] *University of Aveiro, Portugal*
[44] *Space Science Data Center, Agenzia Spaziale Italiana, I-00133, Roma, Italy*
[45] *University of Split, Croatia*
[46] *Department of Astronomy, University of Geneva, Switzerland*
[47] *Pisa University, Italy*
[48] *Department of Physics, Middle East Technical University, Ankara, Turkey*
[49] *Fudan University, 200433 Shanghai, China*
[50] *Eberhard-Karls Universität Tübingen, 72076 Tübingen, Germany*
[51] *Brazilian Center for Research in Physics, Rio de Janeiro, Brazil*
[52] *Unidad de Partículas y Cosmología (UPARCOS), Universidad Complutense, E-28040 Madrid, Spain*
[53] *GRAPPA and Institute of Physics, University of Amsterdam, Science Park 904, 1098XH Amsterdam, The Netherlands*
[54] *Center for Astrophysics, Guangzhou University, Guangzhou 510006, China*
[55] *Department of Astrophysics, University of Lodz, ul. Pomorska 149/153, 90-236 Lodz, Poland*
[56] *Institut für Physik, Humboldt-Universität zu Berlin, D-12489 Berlin, Germany*
[57] *ETH, Zürich, Switzerland*
[58] *Dipartimento di Fisica "M. Merlin" dell'Università e del Politecnico di Bari, I-70126 Bari, Italy*
[59] *Faculty of Physics, University of Sofia* "St. Kl. Ohridski"*, Sofia 1164, Bulgaria*
[60] *RWTH Aachen University, D-72074 Aachen, Germany*
[61] *GSSI, L'Aquila, Italy*
[62] *Istituto Nazionale di Fisica Nucleare, Laboratori Nazionali del Gran Sasso, L'Aquila, Italy*
[63] *Max Planck Institut für Kernphysik, 69117 Heidelberg, Germany*
[64] *Department of Physics, University of Oslo, Box 1048, NO-0371 Oslo, Norway*
[65] *Università di Perugia, I-06123 Perugia, Italy*
[66] *Dipartimento di Fisica, Università degli Studi di Torino, Via P. Giuria 1, 10125 Torino, Italy*
[67] *Istituto Nazionale di Fisica Nucleare, Sezione di Torino, Via P. Giuria 1, 10125 Torino, Italy*
[68] *Istituto Nazionale di Astrofisica, Osservatorio Astrofisico di Torino, Strada Osservatorio 20, 10025 Pino Torinese, Italy*
[69] *Department of Physics & Astronomy, University of the Western Cape, Cape Town 7535, South Africa*
[70] *INAF, Milano, Italy*
[71] *Physics Department, Royal Institute of Technology (KTH), 10691 Stockholm, Sweden*
[72] *LPC2E, University of Orléans, CNRS, France*
[73] *Space Science Division, Naval Research Laboratory, Washington, DC 20375-5352, USA*
[74] *MPI für Astrophysik, Garching D-85741, Germany*
[75] *Space Research Institute, Moscow 117997, Russia*
[76] *Instituto de Física Corpuscular (CSIC - Universitat de València) c/ Catedrático José Beltrán, 2 E-46980 Paterna, Valencia, Spain*
[77] *APC, Université Paris Diderot, CNRS/IN2P3, CEA/Irfu, Observatoire de Paris, Sorbonne Paris Cité, France*

[78] *Max Planck Institut für extraterrestrische Physik, D-85748 Garching, Germany*
[79] *Department of Astronomy, Yale University, P.O. Box 208101, New Haven, CT 06520-8101, USA*
[80] *LIP, Departamento de Física Universidade de Coimbra, P-3004-516 Coimbra, Portugal*
[81] *University of Udine and INFN GC di Udine, via delle Scienze, I-33100 Udine, Italy*
[82] *INAF - Osservatorio Astronomico di Capodimonte, Salita Moiariello 16, I-80131 Napoli, Italy*
[83] *ISAC-CNR, Roma, Italy*
[84] *Novosibirsk State University, 630090 Novosibirsk, Russia*
[85] *ITEP, 117259 Moscow, Russia*
[86] *University of Rijeka - Department of Physics, Radmile Matejčić 2, 51000 Rijeka, Croatia*
[87] *University Würzburg, D-97074 Würzburg, Germany*
[88] *INAF - Osservatorio Astronomico di Roma, I-00078, Monte Porzio Catone, Italy*
[89] *Deutsches Elektronen Synchrotron (DESY), Platanenallee 6, D-15738, Zeuthen, Germany*
[90] *Erlangen Centre for Astroparticle Physics, D-91058 Erlangen, Germany*
[91] *Dipartimento di Fisica, Università dell'Insubria,Via Valleggio 11, I-22100 Como, Italy*
[92] *Dipartimento di Fisica "M. Merlin" dell'Università e del Politecnico di Bari, I-70126 Bari, Italy*
[93] *University of Minnesota, Minneapolis, MN 55455, USA*
[94] *Agenzia Spaziale Italiana, Roma, Italy*
[95] *Dipartimento di Fisica G. Occhialini, Università di Milano Bicocca, Piazza della Scienza 3, I-20126 Milano, Italy*
[96] *Laboratoire AIM, UMR 7158, CEA/DRF, CNRS,*
Université Paris Diderot, IRFU/SAp, F-91191 Gif-sur-Yvette, France
[97] *U.S. Naval Research Laboratory, 4555 Overlook Ave SW, Washington, DC 20375, USA*
[98] *Institute for Cosmic Ray Research, the University of Tokyo, Kashiwa, Chiba, 277-8582, Japan*
[99] *IRAP, 9 av. colonel Roche, BP 44 346, 31028 Toulouse Cedex 4, France*
[100] *College of Science, George Mason University, Fairfax, VA 22030, USA,*
resident at Naval Research Laboratory, Washington, DC 20375, USA
[101] *Departament de Física, EEBE, UPC, 08019 Barcelona, Spain*
[102] *Mesoamerican Center for Theoretical Physics (MCTP),*
Universidad Autonoma de Chiapas (UNACH), 29050 Tuxtla Gutierrez, Chiapas, Mexico
[103] *IRAP Toulouse, 9 av. du Colonel-Roche - BP 44 346, 31028 Toulouse Cedex 4, France*
[104] *Johannes Gutenberg-Universität Mainz, 55099 Mainz, Germany*
[105] *Laboratoire APC, UMR 7164, CEA/DRF CNRS, Université Paris Diderot, Paris, France*
[106] *CEA/Saclay IRFU/Department of Astrophysics, Bat. 709, F-91191, Gif-Sur-Yvette, France*
[107] *INAF - Osservatorio Astronomico di Trieste, via G. B. Tiepolo 11, I-34143 Trieste, Italy*
[108] *Tuorla observatory, University of Turku, FIN-21500 Piikkiö, Finland*
[109] *Enrico Fermi Institute, University of Chicago, Chicago, IL 60637, USA*
[110] *IN2P3/CNRS, Université Bordeaux 1, BP120, Gradignan Cedex, France*
[111] *Erlangen Centre for Astroparticle Physics, Erwin-Rommel-Str. 1, Erlangen, Germany*
[112] *Astrophysical Sciences Division, BARC, Mumbai - 400085, India*
[113] *Joint Institute for VLBI ERIC, Postbus 2, 7990 AA Dwingeloo, The Netherlands*
[114] *University of Bergen, Norway*
[115] *INAF/IASF, Via Bassini 15, I-20133 Milano, Italy*
[116] *Max-Planck-Institut für Physik, 80805 Munich, Germany*
[117] *INAF-Istituto di Astrofisica Spaziale, Milano, Italy*
[118] *University of Zielona Gora, Poland*
[119] *CRESST/NASA/GSFC and University of Maryland, College Park, USA*
[120] *Department of Physics, the University of Tokyo, 7-3-1 Hongo, Bunkyo-ku, Tokyo 113-0033*
[121] *Department of Astronomy, University of Wisconsin, Madison WI 53704, USA*
[122] *Space Research Center of Polish Academy of Sciences, Bartycka 18a, PL-00-716 Warszawa, Poland*
[123] *Scuola Normale Superiore, Pisa, Italy*
[124] *Instituto de Astronomía y Física del Espacio (IAFE, CONICET-UBA), Buenos Aires, Argentina*
[125] *Institut d'Astrophysique de Paris, F-75014, Paris, France*
[126] *Universitat Rovira i Virgili, Carrer de l'Escorxador, E-43003 Tarragona, Spain*
[127] *Institut de Física d'Altes Energies (IFAE), The Barcelona Institute of*
Science and Technology (BIST), E-08193 Bellaterra (Barcelona), Spain
[128] *Istituto Nazionale di Fisica Nucleare, Sezione di Pavia,*
Via A. Bassi 6, I-27100 Pavia, Italy, and INAF
[129] *University of Salamanca (USAL), Plaza de la Merced s/n, 37008, Salamanca (Spain)*
[130] *ICRANET Roma, Italy*
[131] *Instituto de Física Teórica (IFT UAM-CSIC) and Departamento de Física Teórica,*
Universidad Autónoma de Madrid, ES-28049 Madrid
[132] *Institute of Astronomy and Astrophysics, University of Tübingen, Germany*
[133] *Santa Cruz Institute for Particle Physics, University of California, Santa Cruz, CA, USA*
[134] *Dept. of Physics & Laboratory for Space Research, University of Hong Kong, Hong Kong*
[135] *Centre for Astronomy, NUI Galway, Ireland*

[136] *Arizona State University, Tempe, AZ 85287-1504, USA*
[137] *University of Bergen, Institute for Physics and Technology, Postboks 7803, N-5020 Bergen, Norway*
[138] *NASA Goddard Space Flight Center, Greenbelt, MD, USA*
[139] *INAF-IAPS, Roma, Italy*
[140] *LPNHE, CNRS/IN2P3 and Université Pierre et Marie Curie, F-75252 Paris, France*
[141] *High Energy Physics Division, Argonne National Laboratory, Argonne, IL 60439, USA*
[142] *University of Geneva, Department of Nuclear and Particle Physics, 24 quai Ernest-Ansermet, CH-1211 Geneva 4, Switzerland*
[143] *Center for Astrophysics and Cosmology, University of Nova Gorica, Nova Gorica, Slovenia*
[144] *Mullard Space Science Laboratory, University College London, Holmbury St. Mary, Dorking, Surrey, RH5 6NT, UK*
[145] *Department for Nuclear and Particle Physics, University of Geneva, Switzerland*
[146] *University of California at Berkeley, Space Sciences Laboratory, 7 Gauss Way, Berkeley, CA 94720, USA*

* Editors of this White Book

CONTENTS

The e-ASTROGAM mission:

exploring the extreme Universe with gamma rays in the MeV–GeV range

Abstract

e-ASTROGAM ('enhanced ASTROGAM') is a breakthrough Observatory space mission, with a detector composed by a Silicon tracker, a calorimeter, and an anticoincidence system, dedicated to the study of the non-thermal Universe in the photon energy range from 0.3 MeV to 3 GeV – the lower energy limit can be pushed to energies as low as 150 keV, albeit with rapidly degrading angular resolution, for the tracker, and to 30 keV for calorimetric detection. The mission is based on an advanced space-proven detector technology, with unprecedented sensitivity, angular and energy resolution, combined with polarimetric capability. Thanks to its performance in the MeV-GeV domain, substantially improving its predecessors, e-ASTROGAM will open a new window on the non-thermal Universe, making pioneering observations of the most powerful Galactic and extragalactic sources, elucidating the nature of their relativistic outflows and their effects on the surroundings. With a line sensitivity in the MeV energy range one to two orders of magnitude better than previous generation instruments, e-ASTROGAM will determine the origin of key isotopes fundamental for the understanding of supernova explosion and the chemical evolution of our Galaxy. The mission will provide unique data of significant interest to a broad astronomical community, complementary to powerful observatories such as LIGO-Virgo-GEO600-KAGRA, SKA, ALMA, E-ELT, TMT, LSST, JWST, Athena, CTA, IceCube, KM3NeT, and LISA.

1 Introduction

e-ASTROGAM [12, 11] is a gamma-ray mission concept proposed as a response to the European Space Agency (ESA) Call for the fifth Medium-size mission (M5) of the *Cosmic Vision* Science Programme. The planned launch date is 2029.

The main constituents of the e-ASTROGAM payload will be:

- A **Tracker** in which the cosmic γ-rays can undergo a Compton scattering or a pair conversion, based on 56 planes of double-sided Si strip detectors, each plane with total area of $\sim$1 m^2;
- A **Calorimeter** to measure the energy of the secondary particles, made of an array of CsI (Tl) bars of 5×5×80 mm^3 each, with relative energy resolution of 4.5% at 662 keV;
- An **Anticoincidence system** (AC), composed of a standard plastic scintillator AC shielding and a Time of Flight, to veto the charged particle background.

If selected, e-ASTROGAM will operate in a maturing gravitational wave and multimessenger epoch, opening up entirely new and exciting synergies. The mission will provide unique and complementary data of significant interest to a broad astronomical community, in a decade of powerful observatories such as LIGO-Virgo-GEO600-KAGRA, SKA, ALMA, E-ELT, LSST, JWST, Athena, CTA and the promise of LISA.

The core mission science of e-ASTROGAM addresses three major topics of modern astrophysics.

- ***Processes at the heart of the extreme Universe: prospects for the Astronomy of the 2030s***

  Observations of relativistic jet and outflow sources (both in our Galaxy and in active galactic nuclei, AGNs) in the X-ray and GeV–TeV energy ranges have shown that the MeV–GeV band holds the key to understanding the transition from the low energy continuum to a spectral range shaped by very poorly understood particle acceleration processes. e-ASTROGAM will: (1) determine the composition (hadronic or leptonic) of the outflows and jets, which strongly influences the environment – breakthrough polarimetric capability and spectroscopy providing the keys to unlocking this long-standing question; (2) identify the physical acceleration processes in these outflows and jets (e.g. diffusive shocks, magnetic field reconnection, plasma effects), that may lead to dramatically different particle energy distributions; (3) clarify the role of the magnetic field in powering ultrarelativistic jets in gamma-ray bursts (GRBs), through time-resolved polarimetry and spectroscopy. In addition, measurements in the e-ASTROGAM energy band will have a big impact on multimessenger astronomy in the 2030s. Joint detection of gravitational waves and gamma-ray transients would be groundbreaking.

- ***The origin and impact of high-energy particles on galaxy evolution, from cosmic rays to antimatter***

  e-ASTROGAM will resolve the outstanding issue of the origin and propagation of low-energy cosmic rays affecting star formation. It will measure cosmic-ray diffusion in interstellar clouds and their impact on gas dynamics and state; it will provide crucial diagnostics about the wind outflows and their feedback on the Galactic environment (e.g., Fermi bubbles, Cygnus cocoon). e-ASTROGAM will have optimal sensitivity and energy resolution to detect line emissions from 511 keV up to 10 MeV, and a variety of issues will be resolved, in particular: (1) origin of the gamma-ray and positron excesses toward the Galactic inner regions; (2) determination of the astrophysical sources of the local positron population from a very sensitive observation of pulsars and supernova remnants (SNRs). As a consequence e-ASTROGAM will be able to discriminate the backgrounds to dark matter (DM) signals.

- ***Nucleosynthesis and the chemical enrichment of our Galaxy***

  The e-ASTROGAM line sensitivity is more than an order of magnitude better than previous instruments. The deep exposure of the Galactic plane region will determine how different isotopes are created in stars and distributed in the interstellar medium; it will also unveil the recent history of supernova explosions in the Milky Way. Furthermore, e-ASTROGAM will detect a significant number of Galactic novae and supernovae in nearby galaxies, thus addressing fundamental issues in the explosion mechanisms of both core-collapse and thermonuclear supernovae. The γ-ray data will provide a much better understanding of Type Ia supernovae and their evolution with look-back time and metallicity, which is a pre-requisite for their use as standard candles for precision cosmology.

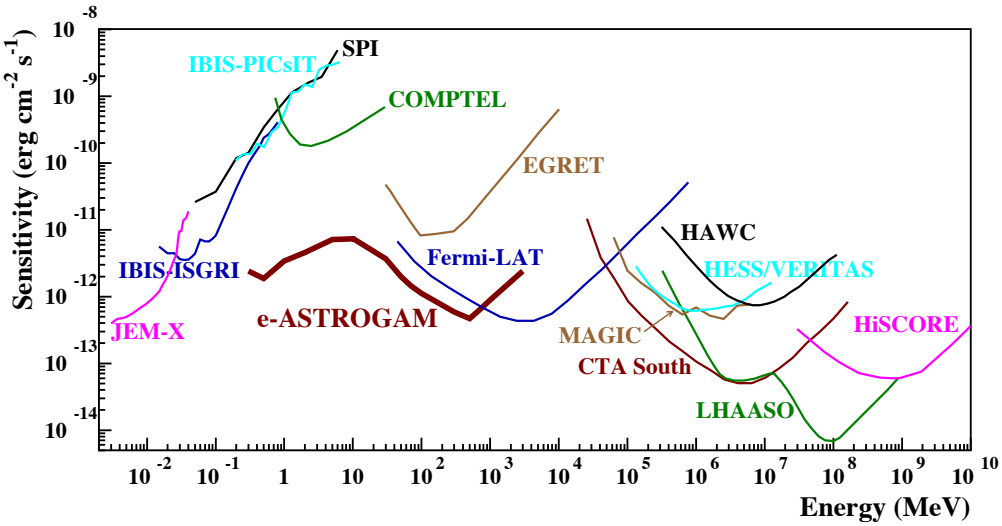

Figure 1: Point source continuum differential sensitivity of different X- and γ-ray instruments. The curves for *INTEGRAL*/JEM-X, IBIS (ISGRI and PICsIT), and SPI are for an effective observation time $T_{\rm obs}$ = 1 Ms. The COMPTEL and EGRET sensitivities are given for the typical observation time accumulated during the ∼9 years of the *CGRO* mission (see Fig. 1 in [19]). The *Fermi*/LAT sensitivity is for a high Galactic latitude source in 10 years of observation in survey mode. For MAGIC, VERITAS (sensitivity of H.E.S.S. is similar), and CTA, the sensitivities are given for $T_{\rm obs}$ = 50 hours. For HAWC $T_{\rm obs}$ = 5 yr, for LHAASO $T_{\rm obs}$ = 1 yr, and for HiSCORE $T_{\rm obs}$ = 1000 h. The e-ASTROGAM sensitivity is calculated at 3σ for an effective exposure of 1 year and for a source at high Galactic latitude.

In addition to addressing its core scientific goals, e-ASTROGAM will achieve many serendipitous discoveries (the unknown unknowns) through its combination of wide field of view (FoV) and improved sensitivity, measuring in 3 years the spectral energy distributions of thousands of Galactic and extragalactic sources, and providing new information on solar flares and terrestrial gamma-ray flashes (TGF). e-ASTROGAM will become a key contributor to multiwavelength time-domain astronomy. The mission has outstanding discovery potential as an Observatory facility that is open to a wide astronomical community.

e-ASTROGAM is designed to achieve:

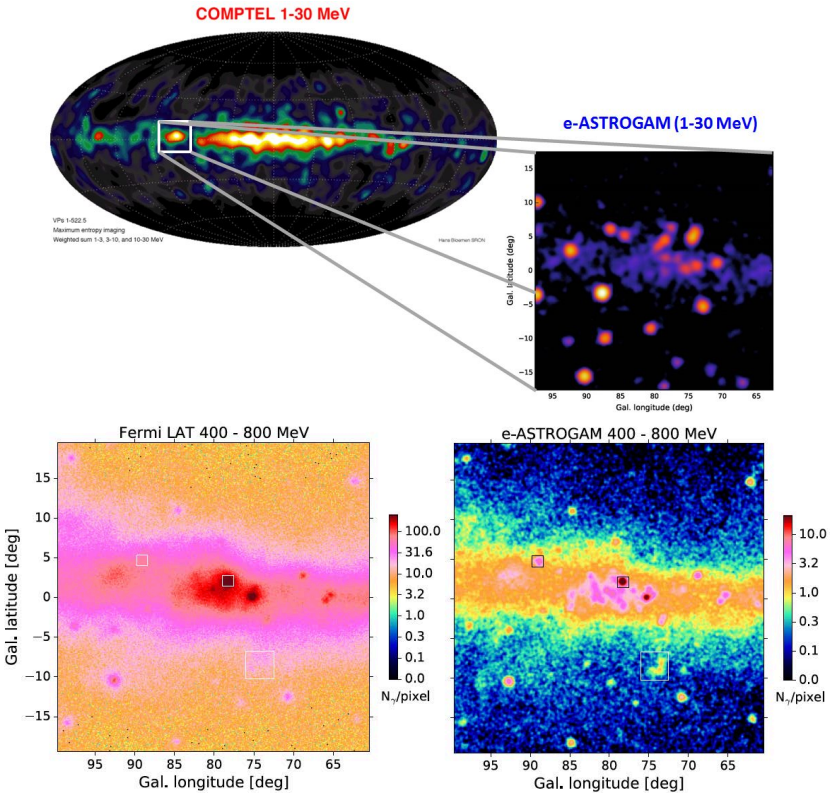

Figure 2: An example of the capability of e-ASTROGAM to transform our knowledge of the MeV-GeV sky. Upper panel: The upper left figure shows the 1-30 MeV sky as observed by COMPTEL in the 1990s; the lower right figure shows the simulated Cygnus region in the 1-30 MeV energy region from e-ASTROGAM . Lower panel: comparison between the view of the Cygnus region by Fermi in 8 years (left) and that by e-ASTROGAM in one year of effective exposure (right) between 400 MeV and 800 MeV.

- Broad energy coverage (0.3 MeV to 3 GeV), with one-two orders of magnitude improvement in continuum sensitivity in the range 0.3 MeV – 100 MeV compared to previous instruments (the lower energy limit can be pushed to energies as low as 150 keV, albeit with rapidly degrading angular resolution, for the tracker, and to 30 keV for calorimetric detection);
- Unprecedented performance for γ-ray lines, with, for example, a sensitivity for the 847 keV line from Type Ia SNe 70 times better than that of INTEGRAL/SPI;
- Large FoV (>2.5 sr), ideal to detect transient sources and hundreds of GRBs;
- Pioneering polarimetric capability for both steady and transient sources;
- Optimized source identification capability afforded by the best angular resolution achievable by state-of-the-art detectors in this energy range (about 0.15 degrees at 1 GeV);
- Sub-millisecond trigger and alert capability for GRBs and other cosmic and terrestrial transients;
- Combination of Compton and pair-production detection techniques allowing model-independent control on the detector systematic uncertainties.

e-ASTROGAM will open the MeV region for exploration, with an improvement of one-two orders of magnitude in sensitivity (Fig. 1) compared to the current state of the art, much of which was derived from the COMPTEL instrument more than two decades ago. It will also achieve a spectacular improvement in terms of source localization accuracy (Fig. 2) and energy resolution, and will allow to measure the contribution to the radiation of the Universe in an unknown range (Fig. 3). The sensitivity of e-ASTROGAM will reveal the transition from nuclear processes to those involving electro- and hydro-dynamical, magnetic and gravitational interactions.

An important characteristic of e-ASTROGAM is its ability to measure polarization in the MeV range, which is afforded by Compton interactions in the detector. Polarization encodes information about the geometry of magnetic fields and adds a new observational pillar, in addition to the temporal and spectral, through which fundamental processes governing the MeV emission can be determined. The addition of

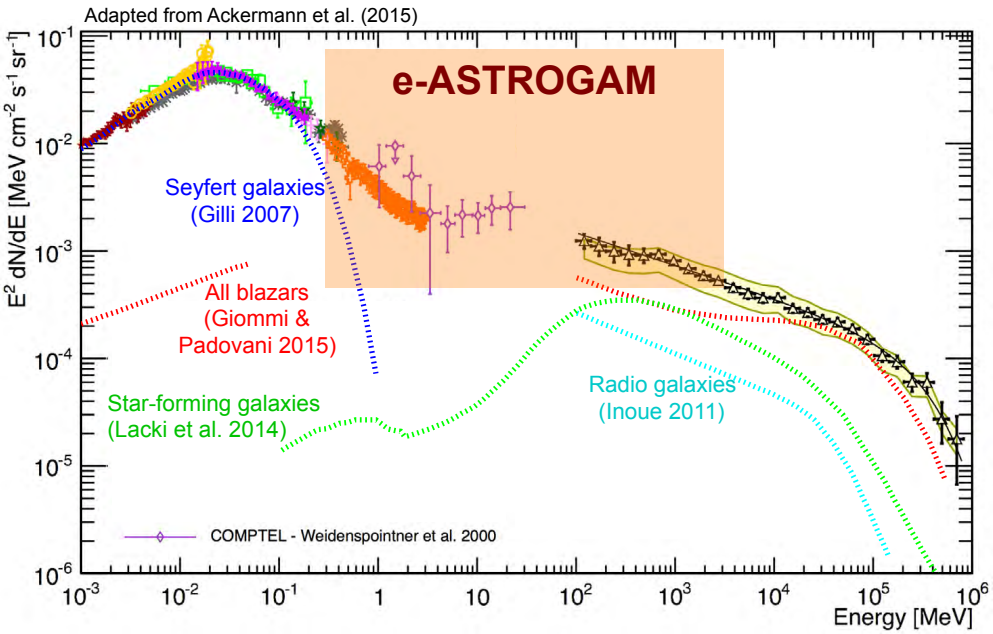

Figure 3: Compilation of the measurements of the total extragalactic gamma-ray intensity between 1 keV and 820 GeV [2], with different components from current models; the contribution from MeV blazars is largely unknown. The semi-transparent band indicates the energy region in which e-ASTROGAM will dramatically improve on present knowledge.

polarimetric information will be crucial for a variety of investigations, including accreting black-hole (BH) systems, magnetic field structures in jets, and the emission mechanisms of GRBs. Polarization will provide definitive insight into the presence of hadrons in extragalactic jets and the origin of ultra-high-energy cosmic rays (CR).

2 Scientific Requirements

e-ASTROGAM's requirements to achieve its core science objectives, such as the angular and energy resolution, the field of view, the continuum and line sensitivity, the polarization sensitivity, and the timing accuracy, are summarized in Table 1.

- The very large spectral band covered by the telescope in the standard gamma-ray acquisition mode will give a complete view of the main nonthermal processes at work in a given astrophysical object, for the first time with a single instrument. The e-ASTROGAM energy band includes the 511 keV line from e^+e^- annihilation, the nuclear de-excitation lines, the characteristic spectral bump from pion decay, the typical domains of nonthermal electron bremsstrahlung and IC emission, as well as the high-energy range of synchrotron radiation in sources with high magnetic field ($B \gtrsim 1$ G). The designed wide energy band is particularly important for the study of blazars, GRBs, Galactic compact binaries, pulsars, as well as the physics of CRs in SNRs and in the ISM.
- The large energy band covered by the Calorimeter in the burst search mode of data acquisition is primarily designed for the triggering and study of GRBs. It is also well adapted to the broadband emissions of TGFs and solar flares.
- The wide field of view of the telescope is especially important to enable the measurement of source flux variability over a wide range of timescales both for a-priori chosen sources and in serendipitous observations. Coupled with the scanning mode of operation, this capability enables continuous monitoring of source fluxes that will greatly increase the chances of detecting correlated flux variability with other wavelengths. The designed wide field of view is particularly important for the study of blazars, GRBs, Galactic compact objects, supernovae, novae, and extended emissions in the Milky Way (CRs, radioactivity). It will also enable, for example, searches of periodicity and orbital modulation in binary systems.
- One of the main requirements of e-ASTROGAM is to improve dramatically the detection sensitivity in a region of the electromagnetic spectrum, the so-called MeV domain, which is still largely unknown.

Table 1: e-ASTROGAM scientific requirements.

Parameter	Value
Energy bands:	0.3 MeV – 3 GeV (Gamma-ray imager: Tracker + Calorimeter) 30 keV – 200 MeV (Calorimeter burst search)
Gamma-ray imager FOV (at 100 MeV)	≥ 2.5 sr
Gamma-ray imager Continuum flux sensitivity at 3σ confidence level	$< 2\times10^{-5}$ MeV cm^{-2} s^{-1} at 1 MeV ($T_{obs} = 10^6$ s effective observation time) $< 5\times10^{-5}$ MeV cm^{-2} s^{-1} at 10 MeV ($T_{obs} = 10^6$ s, high-latitude source) $< 3\times10^{-6}$ MeV cm^{-2} s^{-1} at 500 MeV ($T_{obs} = 10^6$ s, high-latitude source)
Gamma-ray imager Line flux sensitivity at 3σ confidence level	$< 5\times10^{-6}$ ph cm^{-2} s^{-1} for the 511 keV line ($T_{obs} = 10^6$ s effective obs. time) $< 5\times10^{-6}$ ph cm^{-2} s^{-1} for the 847 keV SN Ia line ($T_{obs} = 10^6$ s) $< 3\times10^{-6}$ ph cm^{-2} s^{-1} for the 4.44 MeV line from LECRs ($T_{obs} = 10^6$ s)
Gamma-ray imager angular resolution	≤ 1.5° at 1 MeV (FWHM of the angular resolution measure) ≤ 1.5° at 100 MeV (68% containment radius) ≤ 0.2° at 1 GeV (68% containment radius)
AC particle background rejection efficiency	> 99.99 %
Polarization sensitivity	MDP < 20% (99% c.l.) for a 10 mCrab source (0.3-2 MeV, T_{obs} = 1 yr) Detection of a polarization fract. ≥ 20% in more than 20 GRBs per year
ΔE/E (Gamma-ray imager)	3.0% at 1 MeV 30% at 100 MeV
ΔE/E (Calorimeter burst)	< 25% FWHM at 0.3 MeV < 10% FWHM at 1 MeV < 5% FWHM at 10 MeV
Time tagging accuracy	1 microsecond (at 3 sigma)
Impulsive event acquisition logic (Calorimeter burst)	sub-millisecond trigger and photon-by-photon acquisition capability
Orbit	Low Earth Orbit, equatorial with inclination i < 2.5°, eccentricity e < 0.01, altitude: 550-600 km
Average scientific telemetry	> 1.4 Mbit/s (after data compression)
Satellite attitude reconstruction	1' (at 3 sigma)
Satellite pointing modes	1. pointing mode (1 or 2 pointings per orbit); 2. survey zenith pointing mode.
Target of Opportunity observations	within 6 – 12 hours from alert (goal of 3 – 6 hours)
Mission duration	3 years + provision for a 2+ year extension

The sensitivity requirement is relevant to all science drivers discussed above. Thus, the goal of detecting a significant number ($N > 5$) of SN Ia in gamma rays after 3 years requires a sensitivity in the 847 keV line $< 5 \times 10^{-6}$ ph cm^{-2} s^{-1} in 1 Ms of integration time (Table 1).

- Another major requirement for a future gamma-ray observatory is to improve significantly the angular resolution over past and current missions, which have been severely affected by a spatial confusion issue. Thus, the e-ASTROGAM angular resolution will be excellent in the MeV range and above a few hundreds of MeV, improving *CGRO*/COMPTEL and *Fermi*-LAT by almost a factor of 4 at 1 MeV and 1 GeV, respectively. The targeted angular resolution given in Table 1 is close to the physical limits: for Compton scattering, the limit is given by the Doppler broadening induced by the velocity of the atomic electrons, while for low-energy pair production, the limit is provided by the nuclear recoil. e-ASTROGAM angular resolution will allow a number of currently unidentified gamma-ray sources (e.g. 992 sources in the 3FGL catalog [14]) to be associated with objects identified at other wavelengths. The GC region is the most challenging case, for which the e-ASTROGAM capability will be fully employed.

- The polarization sensitivity of e-ASTROGAM is designed to enable measurements of the gamma-ray polarization fraction in more than 20 GRBs per year (GRBs being promising candidates for highly gamma-ray polarized sources, see, e.g., [16]). Such measurements will provide important information on the magnetization and content (leptons, hadrons, Poynting flux) of the relativistic outflows, and, in the case of GRBs at cosmological distance, will address fundamental questions of physics related to vacuum birefringence and Lorentz invariance violation (e.g., [13]). With the designed polarization sensitivity, e-ASTROGAM will also be able to study the polarimetric properties of more than 50 pulsars, magnetars, and black hole systems in the Galaxy.

- The spectral resolution of e-ASTROGAM is well adapted to the main science drivers of the mission. Thus, the main gamma-ray lines produced in SN explosions or by LECR interactions in the ISM are significantly broadened by the Doppler effect, and a FWHM resolution of 3% at 1 MeV is adequate. In the pair production domain, an energy resolution of 30% will be more than enough to measure accurately putative spectral breaks and cutoffs in various sources and distinguish the characteristic pion-decay bump from leptonic emissions.

- The timing performance of e-ASTROGAM is mainly driven by the physics of magnetars and rotation-powered pulsars, as well as by the properties of TGFs. The targeted microsecond timing accuracy is already achieved in, e.g., the AGILE mission [20].

The e-ASTROGAM requirements reflect the dual capacity of the instrument to detect both Compton scattering events in the 0.3 (and below) – 10 MeV range and pair-producing events in the 10 MeV – 3 GeV energy range; a small overlap around 10 MeV allows (although in a limited energy band) cross-calibration, thus reducing systematic uncertainties. The main instrument features of e-ASTROGAM necessary to meet the scientific requirements in Table 1, are described in Sect. 4.

The sensitivity performance is consistent with the requirement of an equatorial low-Earth orbit (LEO) of altitude in the range 550 – 600 km. Such an orbit is preferred for a variety of reasons. It has been demonstrated to be only marginally affected by the South Atlantic Anomaly and is therefore a low-particle background orbit, ideal for high-energy observations. The orbit is practically unaffected by precipitating particles originating from solar flares, a virtue for background rejection. Finally, both ESA and ASI have satellite communication bases near the equator (Kourou and Malindi) that can be efficiently used as mission ground stations.

Table 1 also includes the most important system requirements such as the satellite attitude reconstruction, telemetry budget, and pointing capability. e-ASTROGAM is a multi-purpose astrophysics mission with the capability of a very flexible observation strategy. Two main scientific observation modes are to be managed by the Mission Operation Center (MOC):

- pointing mode;
- survey mode.

The pointing mode can be implemented either in a fixed inertial pointing or in the more efficient double-pointing per orbit mode. In the latter case, the e-ASTROGAM satellite is required to be able to perform two sky pointings per orbit, lasting approximately 40 minutes each. The survey mode consists in a continuous pointing to the zenith to perform a scan of the sky at each orbit. This mode can be activated at any time in principle, and depending on the scientific prioritization and on the mission schedule foreseen by the Science Management Plan, can lead to an optimized all-sky survey.

Requirements for the Ground Segment are standard for an observatory-class mission. Target of Opportunity observations (ToOs) are required to follow particularly important transient events that need a satellite

Type	3 yr	New sources
Total	3000 – 4000	∼1800 (including GRBs)
Galactic	∼ 1000	∼400
MeV blazars	∼ 350	∼ 350
GeV blazars	1000 – 1500	∼ 350
Other AGN (<10 MeV)	70 – 100	35 – 50
Supernovae	10 – 15	10 – 15
Novae	4 – 6	4 – 6
GRBs	∼600	∼600

Table 2: Estimated number of sources of various classes detectable by e-ASTROGAM in 3 years. The last column gives the number of sources not known before in any wavelength.

repointing. The e-ASTROGAM mission requirement for ToO execution is within 6–12 hours, with the goal of reaching 3–6 hours. The speed of repointing depends on the torque of the reaction wheels. We expect a repointing velocity similar to Fermi (∼ 30 degrees/min, which grants to have a visible object in FoV within less than 5').

e-ASTROGAM does not use any consumable and could in principle be operated for a duration up to 10-20 years (well within the foreseen operation duration of 3 years with a possible extension of two), limited mainly by orbital instabilities and by the risk of accidents. Radiation damage in LEO, with almost equatorial inclination, is negligible. As an example, the degradation of Fermi, whose inclination implies significant crossing of the South Atlantic Anomaly, is negligible for what concerns electronics, negligible for what concerns Tracker aging, and around 1%/year in terms of loss in light yield of the Calorimeter crystals.

Table 2 summarizes our conservative estimates of the number of sources detectable by e-ASTROGAM in 3 years, based on current knowledge and $\log N - \log S$ determinations of Galactic and extragalactic sources, including GRBs. It takes information from the the *Swift*-BAT 70-Month Hard X-ray survey catalog [5], the 4th *INTEGRAL*-IBIS catalog [8], and the 3rd *Fermi*-LAT catalog [14]. Noteworthy, the latter catalog contains more than 1000 unidentified sources in the 100 MeV – 300 GeV range with no counterparts at other wavelength, and most of them will be detected by e-ASTROGAM, in addition to a relevant number of new unidentified sources. The discovery space of e-ASTROGAM for new sources and source classes is very large.

The e-ASTROGAM mission concept aims to fill the gap in our knowledge of astronomy in the medium-energy (0.3–100 MeV) gamma-ray domain by increasing the number of known sources in this field by more than an order of magnitude and providing polarization information for many of them. Between 3000 and 4000 sources are expected to be detected during the first three years of mission operation. The e-ASTROGAM gamma-ray instrument inherits from its predecessors such as *AGILE*[20] and *Fermi*[3], as well as from the MEGA prototype[14], but takes full advantage of recent progress in silicon detectors and readout microelectronics to achieve excellent spectral and spatial resolution by measuring the energy and 3D position of each interaction within the detectors. The e-ASTROGAM mission concept is presented at length in Ref. [12]. Here, we first give an overview of the proposed observatory (Sect. 3) and then outline the breakthrough capability of the e-ASTROGAM telescope for gamma-ray polarimetric observations of some of the main targets of the mission: active galactic nuclei (AGN), gamma-ray bursts (GRBs), the Crab pulsar/nebula system, and microquasars.

3 The e-ASTROGAM observatory

The payload of the e-ASTROGAM satellite (Figure 4) consists of a single gamma-ray telescope operating over more than four orders of magnitude in energy (from about 150 keV to 3 GeV) by the joint detection of photons in both the Compton (0.15 – 30 MeV) and pair (> 10 MeV) energy ranges. It is attached to a mechanical structure at a distance of about 90 cm from the top of the spacecraft platform, the space between the payload and the platform being used to: (i) host a time-of-flight (ToF) unit designed to discriminate between particles coming out from the telescope and those entering the instrument from below; (ii) host several units of the payload (the back-end electronics modules, the data handling unit, and the power supply unit) and (iii) accommodate two fixed radiators of the thermal control system, each of 5.8 m^2 area (Figure 4). This design has the advantage of significantly reducing the instrument background due to prompt and delayed gamma-ray emissions from fast particle reactions with the platform materials.

The e-ASTROGAM telescope is made up of three detection systems (Figure 5): a silicon Tracker in which

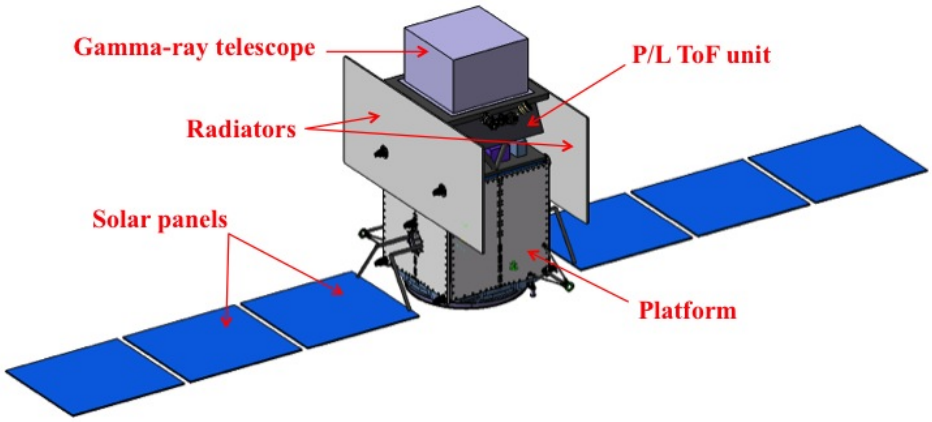

Figure 4: e-ASTROGAM spacecraft with solar panels deployed.

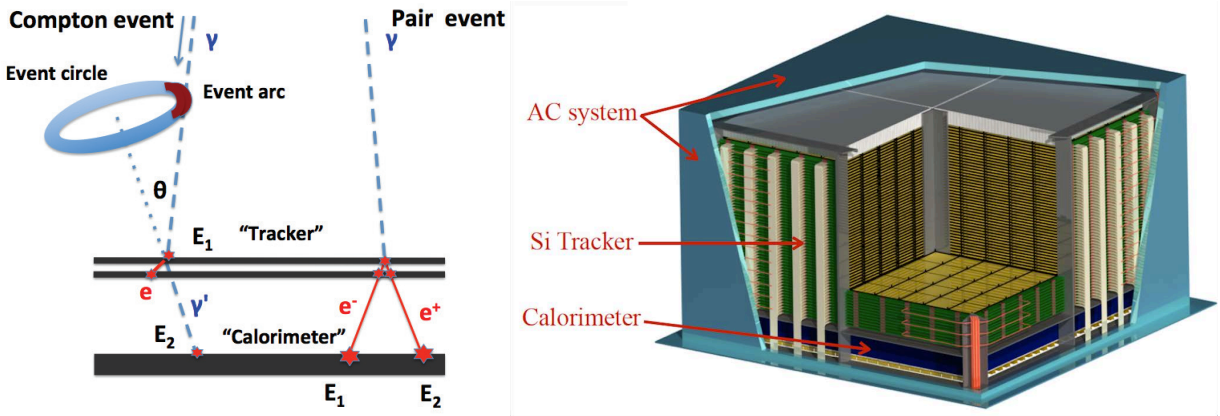

(a) (b)

Figure 5: (a) Representative topologies for a Compton event and for a pair event. Photon tracks are shown in pale blue, dashed, and electron and/or positron tracks are in red, solid. (b) Overview of the e-ASTROGAM payload.

the cosmic gamma-rays undergo a Compton scattering or a pair conversion (see Figure 5a); a Calorimeter to absorb and measure the energy of the secondary particles and an anticoincidence (AC) system to veto the prompt-reaction background induced by charged particles. The telescope has a size of $120\times120\times78$ cm^3 and a mass of 1.2 tons (including maturity margins plus an additional margin of 20% at system level).

The Si Tracker comprises 5600 double-sided strip detectors (DSSDs) arranged in 56 layers. It is divided in four units of 5×5 DSSDs, the detectors being wire bonded strip to strip to form 2-D ladders. Each DSSD has a geometric area of 9.5×9.5 cm^2, a thickness of 500 μm, and a strip pitch of 240 μm. The total detection area amounts to 9025 cm^2. Such a stacking of relatively thin detectors enables efficient tracking of the electrons and positrons produced by pair conversion, and of the recoil electrons produced by Compton scattering. The DSSD signals are read out by 860,160 independent, ultra low-noise and low-power electronics channels with self-triggering capability.

The Calorimeter is a pixelated detector made of a high-Z scintillation material – Thallium activated Cesium Iodide – for efficient absorption of Compton scattered gamma-rays and electron-positron pairs. It consists of an array of 33,856 parallelepiped bars of CsI(Tl) of 8 cm length and 5×5 mm^2 cross section, read out by silicon drift detectors (SDDs) at both ends, arranged in an array of 529 ($= 23 \times 23$) elementary modules each containing 64 crystals. The depth of interaction in each crystal is measured from the difference of recorded scintillation signals at both ends. Accurately measuring the 3D position and deposited energy of each interaction is essential for a proper reconstruction of the Compton events. The Calorimeter thickness – 8 cm of CsI(Tl) – makes it a 4.3 radiation-length detector having an absorption probability of a 1-MeV photon on-axis of 88%.

The third main detector of the e-ASTROGAM payload consists of an Anticoincidence system composed

of two main parts: (1) a standard Anticoincidence, named Upper-AC, made of segmented panels of plastic scintillators covering the top and four lateral sides of the instrument, requiring a total active area of about 5.2 m^2, and (2) a Time of Flight (ToF) system, aimed at rejecting the particle background produced by the platform. The Upper-AC detector is segmented in 33 plastic tiles (6 tiles per lateral side and 9 tiles for the top) coupled to silicon photomultipliers (SiPM) by optical fibers. The bottom side of the instrument is protected by the ToF unit, which is composed of two plastic scintillator layers separated by 50 cm, read out by SiPMs connected to Time Digital Converters. The required timing resolution is 300 ps.

For best environmental conditions, the e-ASTROGAM satellite should be launched into a quasi-equatorial (inclination $i < 2.5°$) low-Earth orbit (LEO) at a typical altitude of 550 – 600 km. The background environment in such an orbit is now well-known thanks to the Beppo-SAX[10] and *AGILE*[20] missions. In addition, such a LEO is practically unaffected by precipitating particles originating from solar flares, a virtue for background rejection.

Extensive simulations of the instrument performance using state-of-art numerical tools[21, 9] and a detailed numerical mass model of the satellite together with a thorough model for the background environment have shown that e-ASTROGAM will achieve:

- Broad energy coverage (∼0.15 MeV to 3 GeV), with nearly two orders of magnitude improvement of the continuum sensitivity in the range 0.3 – 100 MeV compared to previous missions;
- Excellent sensitivity for the detection of key gamma-ray lines e.g. sensitivity for the 847 keV line from thermonuclear supernovae 70 times better than that of the *INTEGRAL* spectrometer (SPI);
- Unprecedented angular resolution both in the MeV domain and above a few hundreds of MeV i.e. improving the angular resolution of the COMPTEL telescope on board the *Compton Gamma Ray Observatory* (*CGRO*) and that of the *Fermi*/LAT instrument by a factor of ∼4 at 5 MeV and 1 GeV, respectively (e.g. the e-ASTROGAM Point Spread Function (68% containment radius) at 1 GeV is 9').
- Large field of view (> 2.5 sr), ideal to detect transient Galactic and extragalactic sources, such as X-ray binaries and gamma-ray bursts;
- Timing accuracy of 1 μs (at 3σ), ideal to study the physics of magnetars and rotation-powered pulsars, as well as the properties of terrestrial gamma-ray flashes;
- Pioneering polarimetric capability for both steady and transient sources, as illustrated in the next Section.

e-ASTROGAM will be sensitive to the linear polarization of incident gamma-rays over its entire bandwidth. In the Compton range, the polarization signature is reflected in the probability distribution of the azimuthal scatter angle. In the pair production domain, the polarization information is given by the distribution of azimuthal orientation of the electron-positron plane. e-ASTROGAM will have a breakthrough capacity for gamma-ray polarimetry thanks to the fine 3D position resolution of both the Si Tracker and the Calorimeter, as well as the light mechanical structure of the Tracker, which is devoid of any heavy absorber in the detection volume.

The measurement of polarization in the pair creation range, using the azimuthal orientation of the electron-positron plane, is complex and a precise evaluation of the unfolding procedures and performance requires accurate simulation and testing [6]. In the following, we focus on the e-ASTROGAM performance for polarimetry in the Compton domain. We discuss in particular the polarimetric capability of e-ASTROGAM for the study of active galactic nuclei (AGN), gamma-ray bursts (GRBs), the Crab pulsar and nebula, as well as microquasars. e-ASTROGAM will explore for the first time the polarimetric properties of celestial sources above 1 MeV. Thus, as the mission will open a new window, it is difficult to assess what will be discovered. Anyway, we could expect to make detailed studies of jet non-thermal components observed from AGN, stellar black holes and GRBs. We might also expect a better description of particle acceleration processes in, for example, pulsars and supernova remnants.

4 Instrument Response

The scientific performance of the e-ASTROGAM instrument was evaluated by extensive numerical simulations with the software tools MEGAlib [21] and BoGEMMS (Bologna Geant4 Multi-Mission Simulator, [9]), together with detailed background model including the effects on the instrument response of the cosmic diffuse gamma-ray radiation (both Galactic and extragalactic), the Galactic cosmic-ray protons and electrons modulated by the geomagnetic field, the secondary semi-trapped protons, electrons and positrons, as well as the atmospheric gamma-rays and the secondary albedo neutrons. The environmental conditions in

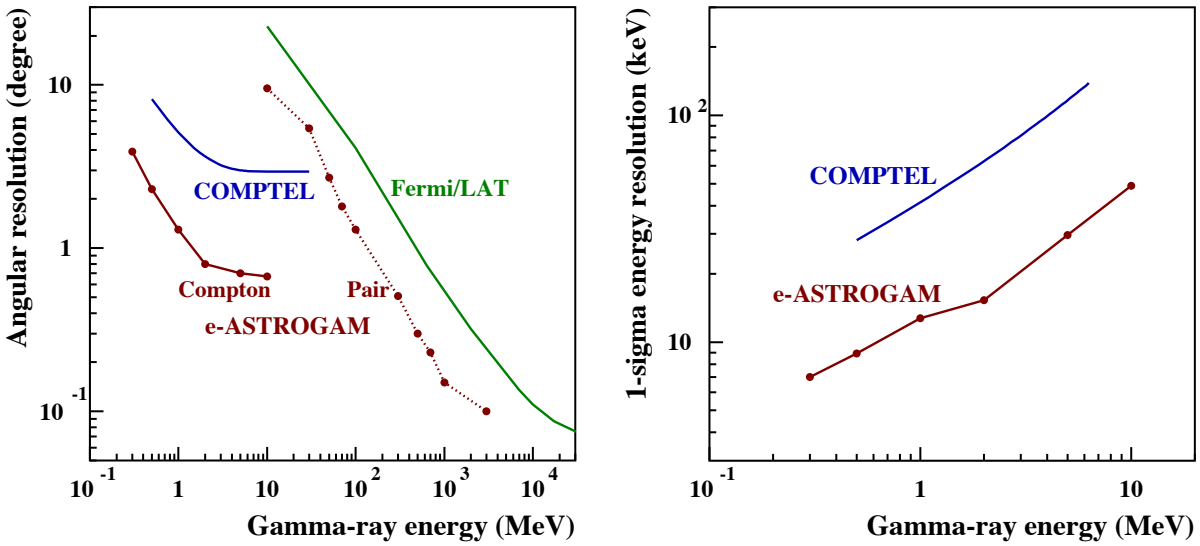

Figure 6: *Left panel* – e-ASTROGAM on-axis angular resolution compared to that of COMPTEL and *Fermi*/LAT. In the Compton domain, the presented performance of e-ASTROGAM and COMPTEL is the FWHM of the angular resolution measure (ARM). In the pair domain, the point spread function (PSF) is the 68% containment radius for a 30° point source. The Fermi/LAT PSF is from the Pass 8 analysis (release 2 version 6) and corresponds to the FRONT and PSF event type. *Right panel* – 1σ energy resolution of COMPTEL and e-ASTROGAM in the Compton domain after event reconstruction and selection on the ARM.

the quasi-equatorial (inclination $i < 2.5°$) low Earth orbit (typical altitude of 550 km) of e-ASTROGAM is now well-known, thanks to the Beppo-SAX mission, which measured the radiation environment on a low-inclination ($i \sim 4°$), 500 – 600 km altitude orbit almost uninterruptedly during 1996 – 2002 [10] and the on-going *AGILE* mission, which has been scanning the gamma-ray sky since 2007 from a quasi-equatorial orbit at an average altitude of 535 km [20].

The numerical mass model of e-ASTROGAM used to simulate the performance of the instrument includes passive material in the detector and its surroundings, true energy thresholds and energy and position measurement accuracy, as well as a roughly accurate spacecraft bus mass and position.

4.1 Angular and spectral resolution

e-ASTROGAM will image the Universe with substantially improved angular resolution both in the MeV domain and above a few hundreds of MeV, i.e. improving the angular resolution of the *CGRO*/COMPTEL telescope and that of the *Fermi*/LAT instrument by a factor of ∼4 at 1 MeV and 1 GeV, respectively.

In the pair production domain, the PSF improvement over *Fermi*/LAT is due to (i) the absence of heavy converters in the Tracker, (ii) the light mechanical structure of this detector minimizing the amount of passive material within the detection volume and thus enabling a better tracking of the secondary electrons and positrons, and (iii) the analog readout of the DSSD signals allowing a fine spatial resolution of about 40 μm (∼1/6 of the microstrip pitch). In the Compton domain, thanks to the fine spatial and spectral resolutions of both the Tracker and the Calorimeter, the e-ASTROGAM angular resolution will be close to the physical limit induced by the Doppler broadening due to the velocity of the target atomic electrons.

Figure 2 shows an example of the e-ASTROGAM imaging capability in the MeV domain compared to COMPTEL. The e-ASTROGAM synthetic map of the Cygnus region was produced from the third *Fermi* LAT (3FGL) catalog of sources detected at photon energies $E_\gamma > 100$ MeV [14], assuming a simple extrapolation of the measured power-law spectra to lower energies. It is clear from this example that e-ASTROGAM will substantially overcome (or eliminate in some cases) the confusion issue that severely affected the previous and current generations of gamma-ray telescopes. The e-ASTROGAM imaging potential will be particularly relevant to study the various high-energy phenomena occurring in the GC region.

e-ASTROGAM will also significantly improve the energy resolution with respect to COMPTEL, e.g. by a factor of ∼3.2 at 1 MeV, where it will reach a 1σ resolution of $\Delta E/E = 1.3\%$ (Figure 6). In the pair production domain above 30 MeV, the simulated spectral resolution is within 20–30%.

Table 3: e-ASTROGAM performance in the Compton domain simulated with MEGAlib v2.26.01. The 3σ continuum sensitivity is for the detection of a point source on axis after an observation time $T_{\rm obs} = 10^6$ s.

E (MeV)	ΔE spectrum[(a)] (MeV)	Angular selection[(b)]	Effective area after selection[(c)] (cm^2)	Background rate after selection[(d)] (count s^{-1})	Sensitivity (photon cm^{-2} s^{-1})	Notes
0.3	0.15 – 0.45	4.3°	560	28	2.8×10^{-5}	Without e-tracking
0.5	0.25 – 0.75	2.5°	446	3.5	1.3×10^{-5}	Without e-tracking
1	0.5 – 1.5	1.5°	297	1.4	1.2×10^{-5}	Without e-tracking
2	1.0 – 3.0	1.1°	117	0.097	8.0×10^{-6}	With e-tracking
5	2.5 – 7.5	0.8°	105	0.031	5.0×10^{-6}	With e-tracking
10	5 – 15	0.8°	50	0.007	5.0×10^{-6}	With e-tracking

(a) Source spectrum is an E^{-2} power-law in the range ΔE.
(b) ARM radius. Note that the best sensitivity results are obtained for a selection on the ARM radius slightly larger than the optimal ARM.
(c) Effective area after event selection optimized for sensitivity.
(d) Total background including the atmospheric γ-ray background, the cosmic γ-ray background, the activation induced by primary and semi-trapped particles (mainly protons), and the prompt reactions from primary (i.e. cosmic-ray) protons, as well as from secondary protons and leptons (electrons and positrons).

4.2 Field of View

The e-ASTROGAM field of view was evaluated from detailed simulations of the angular dependence of the sensitivity. Specifically, the width of the field of view was calculated as the half width at half maximum (HWHM) of the inverse of the sensitivity distribution as a function of the polar, off-axis angle, for a constant azimuthal angle $\phi = 22.5°$. In the Compton domain, the sensitivity remains high within 40° to 50° off-axis angle and then degrades for larger incident angles. For example, the field of view at 1 MeV amounts to 46° HWHM, with a fraction-of-sky coverage in zenith pointing mode of 23%, corresponding to $\Omega = 2.9$ sr.

In the pair-production domain, the field-of-view assessment is also based on in-flight data from the *AGILE* and *Fermi*-LAT gamma-ray imager detectors. With the e-ASTROGAM characteristics (size, Si plane spacing, overall geometry), the field of view is found to be > 2.5 sr above 10 MeV.

4.3 Effective area and continuum sensitivity

Improving the sensitivity in the medium-energy gamma-ray domain (1–100 MeV) by one to two orders of magnitude compared to previous missions is the main requirement for the proposed e-ASTROGAM mission. Such a performance will open an entirely new window for discoveries in the high-energy Universe. Tables 3 and 4 present the simulated effective area and continuum sensitivity in the Compton and pair-production domains. The sensitivity below 10 MeV is largely independent of the source location (inner galaxy vs. high latitude), because the diffuse gamma-ray background is not a major background component in the Compton domain.

Figure 1 shows the e-ASTROGAM continuum sensitivity for a 1-year effective exposure of a high Galactic latitude source. Such an effective exposure will be reached for broad regions of the sky after 3 years of operation, given the very large field of view of the instrument. We see that e-ASTROGAM would provide an important leap in sensitivity over a wide energy band, from about 200 keV to 100 MeV. At higher energies, e-ASTROGAM would also provide a new vision of the gamma-ray sky thanks to its angular resolution, which would reduce the source confusion that plagues the current *Fermi*-LAT and *AGILE* images near the Galactic plane (see, e.g., the 3FGL catalog [14]).

Table 4: e-ASTROGAM performance in the pair-production domain simulated with BoGEMMS v2.0.1, together with Kalman v1.5.0 and Trigger v1.0.0. All results are for a 30° off-axis source and for $T_{\rm obs} = 10^6$ s. The King function used to fit the PSF, derived from the model of XMM data, is defined, e.g., in [15].

E (MeV)	**ΔE spectrum[(a)] (MeV)**	**PSF[(b)]**	**Effective area[(c)] (cm^2)**	**Inner Galaxy Backgr. rate (count s^{-1})**	**Inner Galaxy Sensitivity (ph cm^{-2} s^{-1})**	**Galactic Center[(d)] Sensitivity (ph cm^{-2} s^{-1})**	**Extragal. Backgr. rate (count s^{-1})**	**Extragal. Sensitivity 3σ (ph cm^{-2} s^{-1})**
10	7.5 - 15	9.5°	215	3.4×10^{-2}	7.7×10^{-6}	1.3×10^{-5}	3.8×10^{-3}	2.6×10^{-6}
30	15 - 40	5.4°	846	1.6×10^{-2}	1.4×10^{-6}	2.4×10^{-6}	1.6×10^{-3}	4.3×10^{-7}
50	40 - 60	2.7°	1220	4.0×10^{-3}	4.6×10^{-7}	8.0×10^{-7}	3.4×10^{-4}	1.4×10^{-7}
70	60 - 80	1.8°	1245	1.3×10^{-3}	2.6×10^{-7}	4.5×10^{-7}	1.0×10^{-4}	7.2×10^{-8}
100	80 - 150	1.3°	1310	5.1×10^{-4}	1.6×10^{-7}	2.7×10^{-7}	3.2×10^{-5}	3.9×10^{-8}
300	150 – 400	0.51°	1379	4.8×10^{-5}	4.5×10^{-8}	7.8×10^{-8}	1.1×10^{-6}	6.9×10^{-9}
500	400 – 600	0.30°	1493	1.4×10^{-5}	2.2×10^{-8}	3.8×10^{-8}	1.8×10^{-7}	3.3×10^{-9}
700	600 – 800	0.23°	1552	6.3×10^{-6}	1.5×10^{-8}	2.5×10^{-8}	7.6×10^{-8}	3.2×10^{-9}
1000	800 – 2000	0.15°	1590	2.1×10^{-6}	8.3×10^{-9}	1.4×10^{-8}	2.1×10^{-8}	3.1×10^{-9}
3000	2000 - 4000	0.10°	1810	3.3×10^{-7}	2.9×10^{-9}	5.0×10^{-9}	2.9×10^{-9}	2.8×10^{-9}

(a) Source spectrum is an E^{-2} power-law in the range ΔE.
(b) Point Spread Function (68% containment radius) derived from a single King function fit of the angular distribution.
(c) Effective area after event selection.
(d) The background for the Galactic Center is assumed to be 3 times larger than that of the Inner Galaxy.

Table 5: e-ASTROGAM line sensitivity (3σ in 10^6 s) compared to that of *INTEGRAL*/SPI[18].

E (keV)	**FWHM (keV)**	**Origin**	**SPI sensitivity (ph cm^{-2} s^{-1})**	**e-ASTROGAM sensitivity (ph cm^{-2} s^{-1})**	**Improvement factor**
511	1.3	Narrow line component of the e+/e- annihilation radiation from the Galactic center region	5.2×10^{-5}	4.1×10^{-6}	13
847	35	^{56}Co line from thermonuclear SN	2.3×10^{-4}	3.5×10^{-6}	66
1157	15	^{44}Ti line from core-collapse SN remnants	9.6×10^{-5}	3.6×10^{-6}	27
1275	20	^{22}Na line from classical novae of the ONe type	1.1×10^{-4}	3.8×10^{-6}	29
2223	20	Neutron capture line from accreting neutron stars	1.1×10^{-4}	2.1×10^{-6}	52
4438	100	^{12}C line produced by low-energy Galactic cosmic-ray in the interstellar medium	1.1×10^{-4}	1.7×10^{-6}	65

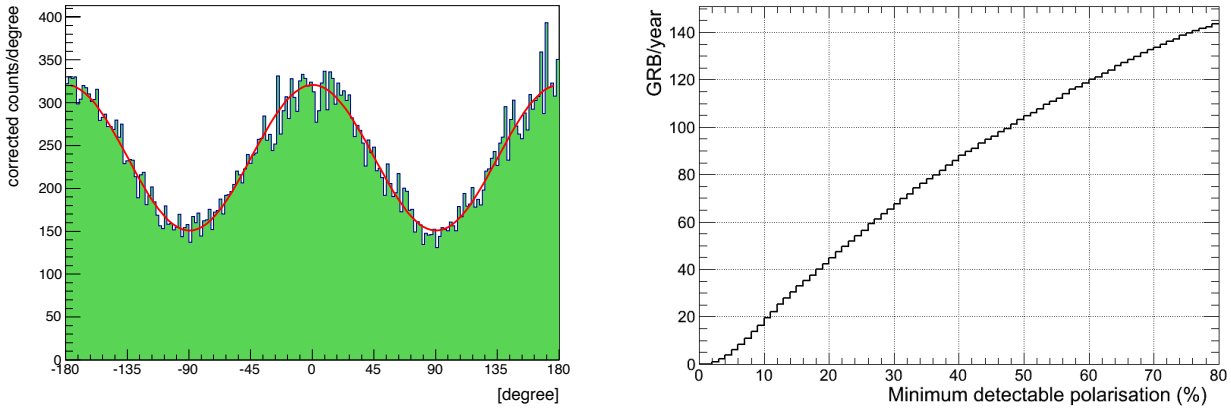

Figure 7: *Left panel* – e-ASTROGAM polarization response (polarigramme) in the 0.2 – 2 MeV range for a 100% polarized, 10 mCrab-like source observed on axis for 10^6 s. The corresponding modulation is $\mu_{100} = 0.36$. *Right panel* – Cumulative number of GRBs to be detected by e-ASTROGAM as a function of the minimum detectable polarization at the 99% confidence level.

4.4 Line sensitivity

Table 5 shows the e-ASTROGAM 3σ sensitivity for the detection of key gamma-ray lines from pointing observations, together with the sensitivity of the *INTEGRAL* Spectrometer (SPI). The latter was obtained from the *INTEGRAL* Observation Time Estimator (OTE) assuming 5×5 dithering observations. The reported line widths are from SPI observations of the 511 and 847 keV lines (SN 2014J), and from theoretical predictions for the other lines. Noteworthy, the neutron capture line from accreting neutron stars can be significantly redshifted and broadened (FWHM between 10 and 100 keV) depending on the geometry of the mass accretion [7].

We see that e-ASTROGAM will achieve a major gain in sensitivity compared to SPI for all gamma-ray lines, the most significant improvement being for the 847 keV line from Type Ia SNe.

4.5 Polarization response

Both Compton scattering and pair creation partially preserve the linear polarization information of incident photons. In a Compton telescope, the polarization signature is reflected in the probability distribution of the azimuthal scattering angle. In the pair domain, the polarization information is given by the distribution of azimuthal orientation of the electron-positron plane. e-ASTROGAM will be able to perform for the first time at these energies polarization measurements thanks to the fine 3D position resolution of both the Si Tracker and the Calorimeter, as well as the light mechanical structure of the Tracker, which is devoid of any heavy absorber in the detection volume.

The left panel of Figure 7 shows an example of a polarigramme in the 0.2 – 2 MeV range (i.e. in the Compton domain), simulated with MEGAlib. The calculations assume a 100% polarized emission from a 10 mCrab-like source observed on axis. The systematic effects of instrumental origin were corrected by simulating the azimuthal response of the instrument to an unpolarized source with the same spectral distribution and position in the field of view as the polarized source. From the obtained modulation ($\mu_{100} = 0.36$), we find that at low energies (0.2 – 2 MeV), e-ASTROGAM will be able to achieve a Minimum Detectable Polarization (MDP) at the 99% confidence level as low as 0.7% for a Crab-like source in 1 Ms (statistical uncertainties only). After one year of effective exposure of the GC region, the achievable MDP_{99} for a 10 mCrab source will be 10%. With such a performance, e-ASTROGAM will be able to study the polarimetric properties of many pulsars, magnetars, and black hole systems in the Galaxy.

The right panel of Figure 7 shows the number of GRBs detectable by e-ASTROGAM as a function of MDP_{99} in the 150–300 keV band. The total number of GRBs detected by e-ASTROGAM will be ∼600 in 3 years of nominal mission lifetime. Here, the GRB emission spectrum has been approximated by a typical Band function [19] with $\alpha = -1.1$, $\beta = -2.3$, and $E_{\mathrm{peak}} = 0.3$ MeV, and the response of e-ASTROGAM to linearly polarized GRBs has been simulated at several off-axis angles in the range $[0°; 90°]$. The number of GRBs with polarization measurable with e-ASTROGAM has then been estimated using the Fourth BATSE GRB Catalog [20]. We see in Figure 7 that e-ASTROGAM should be able to detect a polarization fraction of 20% in about 42 GRBs per year, and a polarization fraction of 10% in ∼16 GRBs per year. This polarization information, combined with spectroscopy over a wide energy band, will provide unambiguous

answers to fundamental questions on the sources of the GRB highly relativistic jets and the mechanisms of energy dissipation and high-energy photon emission in these extreme astrophysical phenomena.

The measurement of polarization using the azimuthal orientation of the electron-positron plane is complex and a precise evaluation of the unfolding procedures and performance requires accurate simulation and testing [6]. Thus, using a simplified model for pair production and multiple scattering of electrons and positrons, a MDP of ∼45% at 3σ has been estimated for the Crab Nebula in 10^6 s in the range from 10 to 100 MeV.

5 Summary

e-ASTROGAM is a concept for a gamma-ray space observatory that can revolutionize the astronomy of medium/high-energy gamma rays by increasing the number of known sources in this field by more than an order of magnitude and providing polarization information for many of these sources – thousands of sources are expected to be detected during the first 3 years of operations. Furthermore, the proposed wide-field gamma-ray observatory will play a major role in the development of time-domain astronomy, and provide valuable information for the localization and identification of gravitational wave sources.

The instrument is based on an innovative design, which minimizes any passive material in the detector volume. The instrument performance has been assessed through detailed simulations using state-of-the-art tools and the results fully meet the scientific requirements of the proposed mission.

e-ASTROGAM will operate as an observatory open to the international community. The gamma-ray observatory will be complementary to ground and space instruments, and multifrequency observation programs will be very important for the success of the mission. In particular, e-ASTROGAM will be essential for investigations jointly done with radio (VLA, VLBI, ALMA, SKA), optical (JWST, E-ELT and other ground telescopes), X-ray and TeV ground instrument (CTA, HAWC, LHAASO and other ground-based detectors). Special emphasis will be given to fast reaction to transients and rapid communication of alerts. New astronomy windows of opportunity (sources of gravitational waves, neutrinos, ultra high-energy cosmic rays) will be fully and uniquely explored.

Acknowledgements. The contribution by P. Couzin (TAS-F), G. Cluzet (TAS-F), X. Roser (TAS-F), A. Laurens (CNES), D. Delrieu (CNES), M.-F. DelCastillo (CNES), C. Contini (CGS), P. Lattanzi (CGS), B. Morelli (CGS), A. Spalla (CGS), is acknowledged.

References

[1] Acero, F., *et al.*, 2015, ApJS, 218, 23
[2] Ackermann, M., *et al.*, 2015, ApJ, 799, 1
[3] Atwood, W. B., Abdo, A. A., Ackermann, M., et al. 2009, ApJ, 697, 1071
[4] Band, D., *et al.*, 1993, ApJ, 413, 281
[5] Baumgartner, W.H., *et al.*, 2013 ApJS, 207, 19
[6] Bernard, D., 2013, Nuclear Instr. and Methods in Phys. Res. A, 729, 765
[7] Bildsten, L., Salpeter, E. E., & Wasserman, I., 1993, ApJ, 408, 615
[8] Bird, A.J., *et al.*, 2010, ApJS, 186, 1
[9] Bulgarelli, A., *et al.*, 2012, Proceedings of the SPIE 8453, 845335
[10] Campana, R., *et al.*, 2014, Experimental Astronomy, 37, 599
[11] De Angelis A., Tatischeff, V. & Giusti, M. (*eds.*), 2017, "e-ASTROGAM scientific workshop", eBook (Lulu), http://www.lulu.com/shop/alessandro-de-angelis/e-astrogam-scientific-workshop/ebook/product-23158421.html
[12] De Angelis, A., Tatischeff, V., *et al.*, 2017, Exp. Astronomy 44, 25, arXiv:1611.02232
[13] Götz, D., Laurent, P., Antier, S., et al. 2014, MNRAS, 444, 2776
[14] Kanbach, G., *et al.*, 2005, Nucl. Instr. Methods A, 541, 310
[15] Kirsch, M.G.F., *et al.*, 2004, "XMM-Newton (cross)-calibration", arXiv:astro-ph/0407257
[16] McConnell, M. L. 2016, accepted for publication in New Astronomy Review, arXiv:1611.06579
[17] Paciesas, W. S., *et al.*, 1999, ApJS, 122, 465
[18] Roques, J.P., *et al.*, 2003, A&A, 411, L91
[19] Takahashi, T., Uchiyama, Y., & Stawarz, L. 2013, Astroparticle Physics, 43, 142
[20] Tavani, M., *et al.*, 2009, A&A, 502, 995
[21] Zoglauer, A., Andritschke, R. & Schopper, F., 2006, New Astronomy Review, 50, 629

Processes at the heart of the extreme universe

Conveners: Gabriele Ghisellini
Lorraine Hanlon
Greg Madejski
Martin Pohl
Massimiliano Razzano

Electromagnetic counterparts to gravitational wave transients in the MeV range

Barbara Patricelli,[1,2] *Antonio Stamerra,*[1] *Massimiliano Razzano,*[2,3] *Marica Branchesi* [4,5]

[1] *Scuola Normale Superiore, Pisa, Italy*
[2] *Istituto Nazionale di Fisica Nucleare (INFN), Pisa, Italy*
[3] *Dipartimento di Fisica, Università di Pisa, Italy*
[4] *GSSI, L'Aquila, Italy*
[5] *INFN, Laboratori Nazionali del Gran Sasso, L'Aquila, Italy*

Science questions – The long-standing quest for the observation of gravitational waves (GWs) met with success on September 14, 2015 when the two Advanced LIGO interferometers detected the signal from the final inspiraling, merging and ring-down of a coalescing binary system formed by two stellar black holes (BBH; the event was named GW150914 [1]). After this first event, the LIGO scientific collaboration and the Virgo collaboration reported the GW detection of other three BBH mergers: GW151226 [2], detected during the first observing run (O1, September 2015 - January 2016) and GW170104 [3] and GW170814, detected during the second observing run (O2, November 2016 - August 2017). In particular, GW170814 was the first detection made by the LIGO-Virgo network, since Advanced Virgo joined O2 on August 1, 2017. During O2, LIGO and Virgo also detected GW170817, the first signal from the coalescence of two neutron stars 1.7 s before the gamma-ray signal detected by the *Fermi*-GBM instrument. Thanks to a dedicated follow-up campaign, electromagnetic counterparts to GW170817 were found in the visible, X-ray and radio bands [6], marking the first multimessenger observation done with electromagnetic and gravitational waves.

In fact, besides BBHs the most promising transient sources that emit GWs at the frequencies at which Advanced LIGO and Advanced Virgo are sensitive (20 Hz - 20 kHz) are the coalescences of binary systems composed by two neutron stars (NS-NS) or a neutron star and a stellar mass black hole (NS-BH). These sources are expected to have also an associated electromagnetic (EM) emission. Specifically, these systems are expected to be the progenitors of short Gamma-ray Bursts (GRBs): intense flashes of gamma-rays lasting less then 2 s, sometimes followed by a long lasting multi-wavelength afterglow emission (see [4] for a review). Furthermore, NS-NS mergers are theoretically predict to entail significant mass ejection which interacts with the surrounding medium on timescales of years, producing a remnant in which accelerated electrons can produce gamma-ray emission [8]. The association between GW170817 and the GRB 170817A by *Fermi*-GBM [7] supports the connection between NS-NS mergers and short GRBs.

Joint GW and EM observations are key to obtain a more complete knowledge of the sources and their environments, since they provide complementary informations. From one side, GW signals provide information about the physics of the source such as, e.g., the mass and the distance; on the other hand, the identification of the possible EM counterpart pinpoints the location of the burst, possibly identifying the host galaxy and properly defining the astrophysical context. Finally, the detection of the gamma-ray counterpart with e-ASTROGAM will help understand if also NS-BH systems are progenitors of short GRBs and to characterize the astrophysical properties of the source. These results will also improve our knowledge of the stellar population of our Galaxy, with a particular focus on the progenitor of merging binary systems.

Importance of gamma-ray observations – The search for the EM counterpart to GW transient events is challenging for several reasons. First of all, the sky localization provided by the current ground-based interferometers is in order of tens to hundreds of square degrees (see, e.g., [9]), therefore large field-of-view (FOV) instruments are essential to properly cover the large GW error boxes. Furthermore, within such large GW error boxes, a huge number of EM transients is expected, making it difficult a clear and univocal identification of an EM counterpart to the GW event (e.g., the number of optical transients spatially and temporally coincident with GW events is expected to be of the order of hundreds, see e.g. [10]); this is somewhat mitigated at gamma-ray energies, where the number of transient events is much smaller than at lower energies (for instance, the *Fermi*-GBM transient catalog comprises only a few events in an area of 100 square degrees, see [11]).

In the gamma-ray domain, the favourite EM counterparts to NS-NS mergers are short GRBs, possibly accompanied by a thermal signal associated to the "kilonova" emission (see [12, 13]). The EM emission from short GRBs is believed to be beamed and the observed sources are typically the on-axis ones, i.e. the ones for which the angle between the line-of-sight and the jet axis is less than the jet opening angle.

However, the majority NS-NS merger events will correlate to off-axis short GRBs, as suggested by simple geometrical arguments based on the presumable small opening angle $\theta \sim 10^\circ$ of the jet [14]. Taking into consideration that the observed flux from on-axis GRBs is enhanced by beaming, off-axis GRBs flux is dramatically weaker and very sensitive gamma-ray instruments are needed to reveal nearby off-axis GRBs associated to GW events.
From the observational point of view, the follow-up of GW170817 conducted in optical, IR and UV revealed the presence of an electromagnetic counterpart with emission consistent with a kilonova, while X-ray and radio data are interpreted as due to an off-axis afterglow emission [6].
Polarization is expected if the jet launching is driven by magnetic energy and depending on the magnetic field configuration. Off-axis observations can introduce an anisotropy that enhances the degree of polarization [13, 16]. In case a high-energy MeV-GeV component is observed, polarization can help to discriminate between different emission processes such as inverse Compton acceleration of leptons (no polarization) and synchrotron polarized emission from hadrons. Measurement of the gamma-ray polarization in GW triggered events could provide a new tool in the interpretation of the GW/EM emission.

Expected results with e-ASTROGAM – e-ASTROGAM fills the gap in the energy region from X-rays up to GeV and TeV gamma-rays, providing a MeV gamma-ray detector operating at the same time as facilities such as SKA and CTA. e-ASTROGAM may coincide with the third generation of ground-based interferometer projects, such as the Einstein Telescope and Cosmic Explorer, with an order of magnitude increase in sensitivity (see e.g. [17, 18]). Furthermore, the space detector eLISA will open GW observations to massive, $10^4 - 10^6 M_\odot$ BHs, which could have magnetized circumbinary disks powering EM emission. Within the GW-sGRB paradigm, on-axis GRBs associated to GW events shall be favourably detected with e-ASTROGAM. The presence of a GW signal naturally selects nearby GRBs, thus favouring the detection of the prompt emission and possibly of the delayed afterglow. When Advanced LIGO and Advanced Virgo will operate at design sensitivity, the expected range for the detection is 200 Mpc for NS-NS mergers and $\approx$ 1 Gpc for BH-NS systems [9]. Considering a maximum GRB jet opening angle of 30° (see, e.g., [19]) and taking into account the updated NS-NS merger rate estimates [20], the expected detection rate of GRB prompt emission by e-ASTROGAM in coincidence with a GW detection is between ~ 0.6 yr^{-1} and ~ 9 yr^{-1} ; these numbers will double after the incorporation of KAGRA and LIGO-India into the GW network, which should happen several years before 2029. e-ASTROGAM will also play a key role in the multiwavelength study of GW events: in fact, its large FoV will maximize the detection probability and provide accurate sky localization ($<$ 1 sq. deg at 1 MeV), thus allowing the follow-up of the GW events by other telescopes. This capability will be crucial for the identification and the multiwavelength characterization of the GW progenitor and of its host galaxy.
The joint GW and EM detection rate is expected to increase if off-axis GRBs are taken into accout. To verify the capability of e-ASTROGAM to detect also these sources, we estimate the minimum luminosity $L_{\rm min}$ for a short GRB to be detected at a distance equal to the horizon of Advanced LIGO at design sensitivity. We simulate a short GRB spectrum assuming the Band function, with the parameters estimated for short GRBs observed by *Fermi*-GBM [21] and different values for the luminositiy of the source; we then compare the predicted flux with the sensitivity of e-ASTROGAM in the energy range 0.2-2 MeV for an observation period of 1 s [22], that is 0.05 ph cm^{-2} s^{-1}: we obtain $L_{\rm min} \sim 10^{48}$ erg/s. This value is much lower than the typical luminosity of short GRB (see, e.g., [23]): this suggest that e-ASTROGAM will be able to detect also off-axis sources, with the consequent sizeable increase in the detection rates. e-ASTROGAM will also be able to detect events like GRB170817. This GRB is characterized by an isotropic peak luminosity L=1.6 10^{47} erg/s, a luminosity distance 40 Mpc and its spectrum is well described by an exponentially cut-off power law (see [24, 25]; the expected flux in the 0.2-2 MeV energy range for such an event is ~ 0.8 ph cm^{-2} s^{-1}, that is above the e-ASTROGAM sensitivity [22].

e-ASTROGAM will be capable also to detect the MeV gamma-ray emission associated to kilonovae, provided that the sources are located at a distance less than 10 Mpc, where the expected flux for ~ 1 MeV photons is of the order of $10^{-11} - 10^{-12}$ erg/cm2/s [13].

e-ASTROGAM will also allow to measure the polarization of the brightest events with the highest fluence, typically of the order of $10^{-4} - 10^{-5}$ erg/cm^2 down to the level of 10-20% [22]. The possible detection of polarization from GRB associated to GW events with e-ASTROGAM shall have a tremendous impact on the interpretation of the formation of the jet and radiation mechanisms.

Finally, the detection of the gamma-ray counterpart with e-ASTROGAM will help understand if and which binary systems are progenitors of short GRBs and to characterize the astrophysical properties of the source. Simultaneous GW/EM emission will transform our understanding of the formation, evolution, properties and environment of different mass compact objects through cosmic history.

References

[1] Abbott B. P. et al. (LVC) 2016a, Physical Review Letters, 116, 061102
[2] Abbott B. P. et al. (LVC) 2016b, Physical Review Letters, 116, 241103
[3] Abbott B. P. et al. (LVC) 2017, Physical Review Letters, 118, 221101
[4] Berger E. 2014, Annual Review of Astronomy and Astrophysics, 43, 52
[5] Abbott, B. P., Abbott, R., Abbott, T. D., et al. 2017, Physical Review Letters, 119, 161101
[6] Abbott, B. P., Abbott, R., Abbott, T. D., et al. 2017, ApJL, 848, L12
[7] Goldstein, A., Veres, P., Burns, E., et al. 2017, ApJL, 848, L14
[8] Takami H., 2014, Physical Review D, 89, 063006
[9] Abbott B. P. et al. (LVC), 2016c, Living Reviews in Relativity, 19, 1
[10] Nissanke S. et al., 2013, ApJ, 767, 124
[11] Jenke P.A. et al. 2016, ApJ, 826, 228
[12] Barnes J. et al. 2016, ApJ, 829, 110
[13] Hotokezaka K. et al. 2016, MNRAS, 459, 35
[14] Fong W et al. 2014, ApJ, 780, 118
[15] Ghisellini G. & Lazzati D., 1999, MNRAS, 309, 7
[16] Granot J. 2002, ApJ, 570, 61
[17] Hild S. et al. 2011, Class. Quantum Grav. 28, 094013
[18] Dwyer S. E. et al. 2015, Phys. Rev. D 91, 082001
[19] Patricelli B. et al. 2016, JCAP, 11, 056
[20] Abbott B.P. et al. (LVC) 2017, PRL, 119, 161101
[21] Nava L. et al. 2011, MNRAS, 415, 3153
[22] Tatischeff, V., et al. 2017, arXiv: 1706.07031
[23] D'Avanzo P. et al. 2014, MNRAS, 442, 2342
[24] Abbott B.P. et al. 2017, ApJL, 848, 13
[25] Goldstein A. et al. 2017, ApJ, 846, 5

Synergies between neutrino telescopes and e-ASTROGAM

Elisa Bernardini[1,2], *Sara Buson*[3], *Alexis Coleiro*[4,5], *Alessandro De Angelis*[6]

[1] *Institut für Physik, Humboldt-Universität zu Berlin, D-12489 Berlin, Germany*
[2] *Deutsches Elektronen Synchrotron (DESY), Platanenallee 6, D-15738 Zeuthen, Germany*
[3] *NASA Postdoctoral Program Fellow, NASA GSFC, 8800 Greenbelt Rd, Greenbelt, MD 20771* [4] *Instituto de Física Corpuscular (CSIC - Universitat de València) c/ Catedrático José Beltrán, 2 E-46980 Paterna, Valencia, Spain*
[5] *APC, Univ Paris Diderot, CNRS/IN2P3, CEA/Irfu, Obs de Paris, Sorbonne Paris Cite, France*
[6] *INFN & INAF, Padova; Udine and Padova Universities*

Science questions – Neutrinos are unique probes to study high-energy cosmic sources. Contrary to cosmic rays (CRs), they are not deflected by the magnetic fields and unlike high-energy photons, they are not absorbed by pair production via $\gamma\gamma$ interactions. Astrophysical high-energy neutrinos at TeV–PeV energies are generated by the decay of charged pions produced in inelastic photo-hadronic ($p\gamma$) or hadronuclear (pp) processes, involving protons ~ 20 times more energetic than the resulting neutrinos. Photoproduction of νs (and photons) via pion decay has a kinematical threshold, and it happens mainly via the Δ^+ resonance slightly above this threshold: $p\gamma \to \Delta^+ \to N\pi$. The energy of the proton has to be $E_p \gtrsim 350\ \mathrm{PeV}/\epsilon$, where ϵ is the target photon energy in eV. For UV photons, as expected in AGN jets, this translates into $E_p \gtrsim 10$ PeV, i.e., above the knee: photoproduction of neutrinos on optical/UV photons is a likely indicator of UHECR acceleration. A simultaneous emission of hadronic gamma-rays is also expected from both processes. An approximate relation holds *at emission* between the spectral production rates of neutrinos and γ-rays in hadronic production:

$$E_\nu^2 \frac{dN_\nu(E_\nu)}{dE_\nu} \sim \frac{3K}{4} E_\gamma^2 \frac{dN_\gamma(E_\gamma)}{dE_\gamma}$$

with $K = 1(2)$ for $\gamma p\,(pp)$. Depending on the source optical depth, such photons may escape or further cascade, complicating time and energy correlation between neutrinos and electromagnetic counterparts.

A diffuse flux of cosmic neutrinos has been detected by IceCube [1], the sources of which are still unknown. Identifying those sources and their association with electromagnetic counterparts, would provide unique insights into the long-standing problem of the origin of cosmic rays. Many astrophysical source classes have been suggested as responsible for the IceCube signal, like star-forming and/or start-burst galaxies, GRBs, or AGNs. Galactic sources like microquasars are also expected to be emitters of astrophysical neutrinos. For a review on neutrino source candidates and multi-messenger connections see e.g. [2]. In conventional GRBs, the neutrino emission is expected to be in temporal coincidence with the prompt gamma-ray emission. Recent results from IceCube [3] disfavour them as the sources of the highest energy cosmic rays and neutrinos. Such conclusions however would not apply if the central engine is surrounded by dense material envelope, like the chocked jets proposed in [4]. For AGNs, predicted fluxes strongly vary with the assumed emission mechanisms. A recent IceCube analysis [5] suggests that blazars contribute at most 27% of the observed IceCube intensity. However neutrinos could be emitted during flaring events, making simultaneous observation of neutrino and gamma-ray signals mandatory to probe this scenario. Recently, the TANAMI collaboration reported that the detection of the third PeV neutrino by IceCube occurred during a major and long-lasting gamma-ray ($0.1 - 300$ GeV) outburst of the blazar PKS B1424-418 with a small *a posteriori* chance coincidence probability of $\sim 5\%$ [6]. While a genuine association of the PeV neutrino and the gamma-ray flare seems unlikely [8], this result illustrates well the great importance of gamma-ray monitoring of high-energy sources to the search of astrophysical neutrino counterparts. Another potentially compelling evidence happened on September 2017, when the *Fermi*-LAT observed enhanced gamma-ray emission from a blazar positionally consistent with the neutrino IC170922A [9, 10]. More recently, a candidate γ-ray precursor to one IceCube ν event has been observed by the AGILE satellite, with a 3.9σ post-trial significance [7].

Importance of γ-ray observations – One of the main challenges in neutrino astronomy is the detection of excesses of events due to astrophysical sources amongst background. To this end, directional, energy and time information are used to differentiate the signal emission from the background. Focusing on high-energy events with neutrinos vertices inside the detector volume allows to select candidates with a high probability of astrophysical origin [1], however at the price of much lower effective area compared

to through-going events. Several attempts to look for very-high-energy (VHE) gamma-rays counterparts of high-energy neutrino events have been inconclusive so far ([11] but see also [12]). The lack of VHE gamma-ray counterparts of IceCube events can indicate that the gamma-rays emitted in association with neutrinos are absorbed, either in the sources themselves or during propagation over large redshifts. In the first case, the overall isotropic extragalactic γ-ray background (IGBR) measured by *Fermi*-LAT provides strong constraints on source populations (see e.g. [13]). If on the other hand ν sources are optically thin to gamma-rays, missing VHE counterparts may indicate that the source are either too distant or too faint, making the quest for their origin more challenging.

The ANTARES and IceCube neutrino telescopes [14, 15] operate extensive programs of real-time multi-wavelength follow-up [16, 17]. They enable to search for an electromagnetic counterpart to astrophysical neutrino candidates by generating alerts whenever an interesting neutrino event is detected (namely a significant multiplet of events, an energetic event or an event whose direction is compatible with a local galaxy [16, 18]). Broad-band data, from the radio domain to the very-high-energy gamma-ray regime, are requested as Target-of-Opportunity (ToO) observations to the partners. In particular, high-energy data from the X-ray (keV) to the gamma-ray (GeV) domains are among the most decisive if they are performed within some hours after the neutrino trigger, since they allow for the detection of transient cataclysmic events which might involve hadronic processes. While such programs have not yet provided a significant evidence for cosmic sources associated with high-energy neutrinos, a few possible associations have been already claimed [6, 7] and a set of serendipitous discoveries is emerging [19, 20].

Both IceCube and ANTARES data have also been extensively looked at for a space and time neutrino emission correlated with the high-energy electromagnetic emission of a transient or flaring source. Selecting only neutrino events coincident with the electromagnetic flare allows for a much better background rejection, and thus a better sensitivity. Such studies generally assume a correlation between X-ray/gamma-ray flares and neutrino emission, and thus require lightcurves measured by X-ray/gamma-ray instruments as an input, with largest time coverage possible. Such studies have also failed so far in finding the sources of cosmic neutrinos, but still yielded important model constraints (see e.g. [3, 21]).

Expected results with e-ASTROGAM– The next generation of neutrino telescopes is currently under deployment. In the Northern hemisphere, KM3NeT will succeed ANTARES in the coming years and will greatly improve both the sensitivity to neutrino point-sources and the angular resolution ($\sim 0.2^\circ$ for muon track events and $\sim 1.5^\circ$ for showers). In parallel, IceCube-Gen2 should increase the performances of the current detector by one order of magnitude with the deployment of 120 new detection lines by the next decade. Those upgrades will enable significant improvement on the electromagnetic follow-up activities and will benefit from the multi-wavelength facilities operating at the same time. As stated above, a joint detection of a neutrino and a X-ray/gamma-ray transient source might lead to the first significant association and consequently to the first incontrovertible identification of the electromagnetic counterpart of astrophysical neutrinos.

e-ASTROGAM can play a decisive role. In particular, the ToO capabilities of the satellite should allow for a repointing of the instrument within 6–12 hours, with the goal of reaching 3–6 hours, while its large field-of-view (FoV) will maximize the detection probability and provide an accurate sky localization. Those low-latency follow-up abilities will be important to test a potential association between high-energy neutrino candidates and various classes of transient astrophysical events, and will continue the programs currently performed with the Swift and *Fermi* satellites. Moreover, by connecting the $p\gamma$ and $\gamma\gamma$ optical depths, it as been claimed recently that the potential sources of the astrophysical neutrinos detected by IceCube may be opaque to 1–100 GeV gamma-rays if the neutrino flux originates from photo-hadronic processes [13]. This result consequently suggests a population of cosmic-ray accelerators invisible in GeV–TeV gamma-rays but bright in the X-ray and MeV domains (see e.g. [4]).

Furthermore, thanks to its wide FoV (> 2.5 sr at 10 MeV) in survey mode, e-ASTROGAM will detect and follow variable point-like sources (microquasars, AGNs, etc). It will provide with a good sampling of their MeV lightcurves that will be used to search for neutrino counterparts. More specifically, the typical double-humped spectral energy distribution of blazars peaks at MeV energy and can be explained by both hadronic and leptonic processes. In photo-hadronic models, the neutrino flux F_ν can be related to the bolometric high-energy electromagnetic flux F_γ (integrated from 1 keV to 5 GeV) with $F_\nu \approx F_\gamma$ [22], which makes the MeV photon flux a good proxy of the neutrino emission from blazars. Thanks to its high sensitivity in the MeV domain, e-ASTROGAM will be perfectly suited to select the best blazar candidates for a neutrino emission and will help to interpret the neutrino observations. In addition, its unique polarimetric capability will enable to reveal the structure of the magnetic field and test the presence of hadrons in relativistic jets. e-ASTROGAM should also observe ~ 600 GRBs during the first three years of its mission. Its sub-millisecond trigger and alert capabilities will enable to look for neutrino counterparts of GRBs in nearly real-time and will then take over from Swift, INTEGRAL and *Fermi* instruments.

Finally, one of the yet unanswered question is the nature of the process generating the observed cosmic neutrinos ($p\gamma$ or pp processes). If IceCube neutrinos are mainly produced by pp interactions, their sources should significantly contribute to the IGBR and any source-class should not violate it. Recent studies (see e.g. [23]) show that pp models are in tension with the IGBR, disfavoring the pp origin of the cosmic neutrino flux observed by IceCube. Further understanding the contribution of different source populations to the extragalactic gamma-ray background (EGB) is therefore crucial. Measurement of spectral features in the 10 – 200 MeV range with e-ASTROGAM will help to constrain the population models of the EGB and will consequently have an important impact on the interpretation of the multi-messenger connection between gamma-rays and neutrinos.

References

[1] Aartsen M.G. et al. (IceCube collaboration), 2013, Science, 779, 132
[2] Ahlers M., Halzen F., 2015, Rep. Prog. Phys., 78, 126901
[3] Aartsen M.G. et al. (IceCube collaboration), 2016, ApJ, 824, 115
[4] Senno N. et al., 2016, Phys. Rev. D, 93, 083003
[5] Aartsen M.G. et al. (IceCube collaboration), 2017, ApJ, 835, 45
[6] Kadler M. et al., 2016, Nature Physics, 12, 807-814
[7] Lucarelli F. et al., 2017, ApJ, 846, 121
[8] Gao S. et al., 2017, ApJ, 843, 2
[9] GCN IceCube EHE 50579430_130033
[10] Tanaka et al., 2017, Astronomer's Telegram, 10791
[11] Santander M. et al., 2017, PoS, (ICRC2017), 618
[12] the MAGIC Collaboration, 2017, Astronomer's Telegram, 10817
[13] Murase K. et al., 2016, Phys. Rev. Lett., 116, 071101
[14] Ageron M. et al. (ANTARES collaboration), 2011, Nucl. Instrum. Meth. A, 656, 11-38
[15] Abbasi R. et al. (IceCube collaboration), 2009, Nucl. Instrum. Meth. A, 601, 294
[16] Ageron M. et al. (ANTARES collaboration), 2012, Astropart. Phys., 35, 530-536
[17] Aartsen M.G. et al. (IceCube collaboration), 2017, Astropart. Phys., 92, 30-41
[18] The IceCube, MAGIC and VERITAS collaborations, 2016, JINST, 11, 11009
[19] Dornic D. et al. (for the ANTARES collaboration), 2017, PoS, (ICRC2017), 985
[20] Aartsen M.G. et al. (IceCube collaboration), 2015, ApJ, 811, 52
[21] Albert A. et al. (ANTARES Collaboration), 2017, JCAP, 04, 019
[22] Krauss F. et al., 2014, A&A, 566, L7
[23] Bechtol K. et al., 2017, ApJ, 836, 47

Gamma Ray observations of Clusters of Galaxies with e-ASTROGAM

Stephan Zimmer

Department for Nuclear and Particle Physics, University of Geneva, Switzerland

Science questions – Galaxy Clusters are the largest virialized structures that have formed through a hierarchical build up of structures from small galaxy groups that later merged and formed a cluster. Observations with radio frequencies reveal a number of large Mpc-scale diffuse halos of polarized synchrotron emission in a large number of merging clusters, indicating the presence of a population of relativistic electrons [see e.g., [11], for a review]. However, to date the mechanism of how these cosmic ray (CR) electrons traverse out into the virial volume pose a puzzle: due to the short cooling time, primary CR electrons (escaping from the denser core region) would lose energy too fast to account for the radio emission. Since the ambient gas emits soft X rays, one would also expect to observe hard X rays originating from the Inverse Compton (IC) scattering of these CR electrons and the soft X rays, and possibly γ rays, provided the correct magnetic field strength and configuration, the latter which remain largely unknown and precise measurements being limited to a small number of otherwise well-studied clusters.[1] In addition, the distribution of cosmic rays (both protons and electrons) is *a priori* unknown and neither X-ray nor radio observations are sufficient to disentangle the two scenarios and more importantly to study the role of CR protons in galaxy clusters, the latter which carry the imprint of the cosmic evolution of a cluster including prior mergers.

Finally, as clusters have high mass to light ratios, they are interesting candidates to indirectly search for signatures of Dark Matter decay and annihilation [see e.g., [9], for a review]. Notably, the predicted astrophysical factor of the nearest clusters are about 1-2 orders of magnitude smaller than what is found in nearby dwarf spheroidal galaxies, but clusters are significantly more numerous [13].[2] Since the Coma cluster hosts the prototype of a giant radio halo and is among the best studied systems in addition to being suggested as second cluster candidate to be studied with the upcoming Cherenkov Telescope Array in the context of its key science program [8], we limit our case study of e-ASTROGAM to this cluster.

Importance of gamma-ray observations – To address the emergence of large scale radio emission, two solutions have been proposed: the *pure hadronic* scenario and situations in which primary CRs, both electrons and protons are subject to *in-situ re-acceleration*, providing the necessary ingredients to account for the measured radio emission [see, e.g., [6], for a review]. In both cases, the release of kinetic energy associated with major mergers is thought to provide a sufficient source for the acceleration of these particle populations. In the pure hadronic scenario high energy CR protons interact with the ambient gas in inelastic *pp*-collisions producing pions, both charged and neutral ones. The radio emission then emerges from the decay of charged pions into highly energetic (secondary) CR electrons. The neutral pions on the other hand decay into two photons, yielding a significant flux of γ-rays from the intracluster medium (ICM), a signature that has long been sought for but has yet to be serendipitously attributed to the ICM and not due to foreground (or host) galaxies. In re-acceleration scenarios CRs are accelerated for instance through turbulence, which may be induced by the aforementioned merger processes, as re-acceleration is not limited to CRs alone, γ-rays also emerge from the re-accelerated CR protons undergoing *pp*-collisions such as in the hadronic scenario. γ-ray observations of clusters, especially at low energies, are essential since unlike radio emission they offer a direct probe to study CR protons. If γ rays were observed from clusters, the emergence of the pion-decay cutoff at around 130 MeV (equal to the rest mass of the π^0 meson) would provide a remarkable feature in the spectrum.

During its now close to 10 years of observation, the *Fermi* Large Area Telescope (LAT) has provided important constraints that severely limit the remaining parameter space [see, e.g., [2]-[4], [12], [14]-[16], to list but a few]. Together with observations at the highest energies with imaging air Cherenkov telescopes, the lack of γ-rays from clusters implies that CR acceleration has to be significantly less sufficient than previously thought or that the volume-averaged CR to thermal pressure ratio of protons in the ICM is less than $\sim 1\%$ [1]. In re-acceleration models, the predicted γ-ray flux is typically lower, thus existing

[1] The lack of evidence for hard X-rays from clusters allows to place lower limits on the magnetic field strength, as the radio-producing CR electrons upscatter the cosmic microwave background, whose energy density is well known.

[2] In this contribution we focus on the conventional astrophysics scenario rather than on the indirect Dark Matter prospects. For the latter the reader is referred to the Dark Matter contribution in this book.

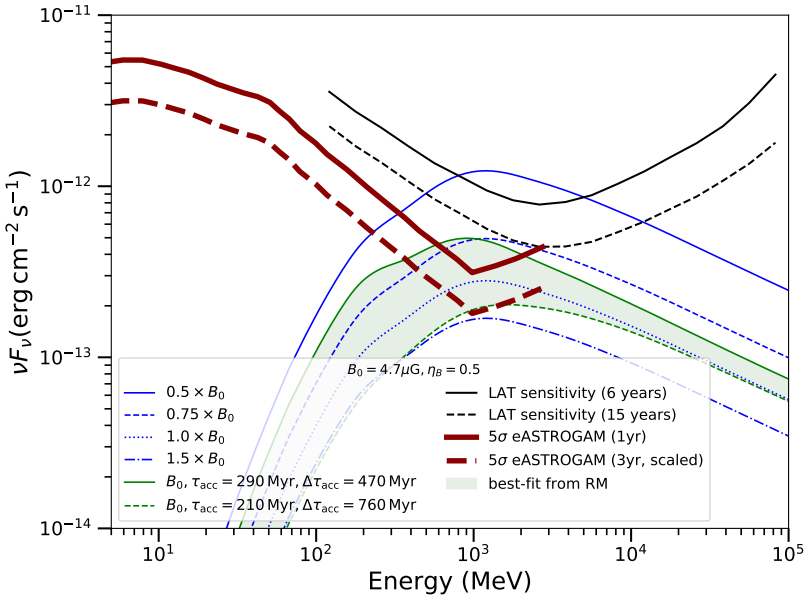

Figure 1: Figure re-produced from [7]. Predicted γ-ray spectra for the most promising scenarios of turbulent re-acceleration assuming a variety of magnetic field configurations (blue curves) and re-acceleration assumptions (green lines). The green-shaded area reflects the parameter space of models which are compatible with the best-fit values of B_0 and η_B from FR measurements. The nominal re-acceleration parameter configuration assumed an acceleration time, $\tau_{\rm acc} = 260\,$Myrs and a period $\Delta\tau_{\rm acc} = 720\,$Myrs, respectively. Black lines correspond to the sensitivity of *Fermi*-LAT (solid for 6 years, dashed for 15 years, respectively). The bold red curves are the same as in Fig. 1 in Sec. 1, showing the e-ASTROGAM point-source sensitivity at high Galactic latitude for 1 year (solid) and rescaled to 3 years (dashed).

constraints are weaker. However, while the computation of the predicted γ-ray spectrum from hadronic scenarios typically depends only on the assumption of the magnetic field in the cluster as well as the parent CR proton distribution, re-acceleration models are more complex, adding additional degrees of freedom to the problem (such as the $re-acceleration$ time $\tau_{\rm acc}$ and period $\Delta\tau_{\rm acc}$) and enlarging the allowed parameter space. Recent work indicates that current observations of the Coma cluster [3] are sufficiently deep to probe a meaningful part of the parameter space [7], and if observations with *Fermi* continued, emission at the $3-5\sigma$ level may be detectable for a small number of scenarios. Note however that γ-ray observations of clusters are more challenging than e.g. observations of point sources as the predicted emission is in many cases spatially extended. Since the processes present in clusters that produce γ-ray emission are not much unlike what governs our own Galaxy, one has to be careful in trying to disentangle the Galactic diffuse emission component from any low brightness emission that may be associated with the ICM. These aforementioned recent observations of the Coma cluster with *Fermi* were associated with uncertainties of the order of $30-50\%$ due to diffuse emission modeling alone [3].

Expected results with e-ASTROGAM – In [7] we showed that existing γ-ray constraints obtained from the observation of the Coma cluster by the LAT severely increase the existing tension of the predictions of hadronic models and the observed $B_0 = 4.7\mu G$ magnetic field and $\eta_B = 0.5$ obtained from Faraday Rotation (FR) measurements [5]. We also identified that a number of re-acceleration models can be effectively probed by continued LAT exposure. Fig. 1 shows the most promising re-acceleration models from our study along with the expected sensitivity of the LAT based on the published 6 year likelihood analysis and its extension to an observation time of 15 years. In order to account for the difference in sensitivity towards extended ICM emission (as opposed to a point-like emission source), model predictions have been rescaled by a common scaling factor that corresponds to the ratio between the observed upper limits for each model after 6 years [see [7], for further details]. Note that these sensitivity curves require a likelihood test statistic value above 25 and at least 3 photons being attributed to the cluster emission. Further note that the sensitivity curves have been computed with the predicted counts associated with the Galactic foreground emission

serving as proxy for the background estimate.[3] The bold-faced red curves correspond to the predicted 1 year sensitivity (3 years re-scaled assuming a scaling of $\propto 1/\sqrt{t}$) with e-ASTROGAM [10]. As can be seen from this figure, e-ASTROGAM, already after the first year will effectively allow us to probe a number of models with magnetic fields that are within a factor of ~ 2 from the current best-fit value for the magnetic field in Coma. The remainder of models will be probed during the lifetime of the e-ASTROGAM mission. Note however, that these numbers do not take into consideration the potential uncertainties related to the diffuse emission modeling.

References

[1] Ackermann, M., Ajello, M., Albert, A., et al. 2014, ApJ, 787, 18

[2] Ackermann, M., Ajello, M., Allafort, A., et al. 2010, ApJL, 717, L71

[3] Ackermann, M., Ajello, M., Albert, A., et al. 2016, ApJ, 819, 149

[4] Arlen, T., Aune, T., Beilicke, M., et al. 2012, ApJ, 757, 123

[5] Bonafede, A., Feretti, L., Murgia, M., et al. 2010, A&A, 513, A30

[6] Brunetti, G., & Jones, T. W. 2014, International Journal of Modern Physics D, 23, 1430007

[7] Brunetti, G., Zimmer, S., & Zandanel, F. 2017, MNRAS, 472, 1506

[8] Acharya, B. S., et al. (The Cherenkov Telescope Array Consortium) 2017, ArXiv e-prints, arXiv:1709.07997

[9] Conrad, J., Cohen-Tanugi, J., & Strigari, L. E. 2015, Soviet Journal of Experimental and Theoretical Physics, 121, 1104

[10] De Angelis, A., Tatischeff, V., Tavani, M., et al. 2017, Experimental Astronomy, 44, 25

[11] Ferrari, C., Govoni, F., Schindler, S., Bykov, A. M., & Rephaeli, Y. 2008, Space Sci. Rev., 134, 93

[12] Griffin, R. D., Dai, X., & Kochanek, C. S. 2014, ApJL, 795, L21

[13] Lisanti, M., Mishra-Sharma, S., Rodd, N. L., & Safdi, B. R. 2017, ArXiv e-prints, arXiv:1708.09385

[14] Prokhorov, D. A. 2014, MNRAS, 441, 2309

[15] Prokhorov, D. A., & Churazov, E. M. 2014, A&A, 567, A93

[16] Zandanel, F., & Ando, S. 2014, MNRAS, 440, 663

[3] The LAT sensitivity curves were computed assuming the same analysis choices (binning, energy range) as in [3].

The most massive high redshift and jetted black holes in the universe

Gabriele Ghisellini[1], *Fabrizio Tavecchio*[1], *Tullia Sbarrato*[2], *Sarah Kaufmann*[3], *Omar Tibolla*[3]

[1] *INAF–Osservatorio Astronomico di Brera, via Bianchi 46, I-23807 Merate Italy*
[2] *Università di Milano Bicocca, piazza della Scienza 3, I–20126 Milano, Italy*
[3] *Mesoamerican Center for Theoretical Physics (MCTP), Universidad Autonoma de Chiapas (UNACH), 29050 Tuxtla Gutierrez, Chiapas, Mexico*

Science questions – Flat Spectrum Radio Quasars at high redshift ($z > 2$) are the most persistent powerful hard X–ray sources in the Universe. As such, they are well suited both to study the physics of jets and of accretion along the cosmic history, and to be used as probes to shed light on the far Universe. Their 15–150 keV spectrum, as seen by the Burst Alert Telescope (BAT) onboard *Swift* is invariably very flat (photon spectral index $\Gamma_{\rm X} < 1.5$): this, together with γ–ray data from *Fermi*/LAT, suggests that their high energy SED peaks around 0.5–3 MeV, where most of their electromagnetic power comes out. All the high–z FSRQ of [3] (10 objects at $z > 2$, and 5 at $z > 3$) have a [15–55 keV] luminosity $L_{\rm X} > 2 \times 10^{47}$ erg s^{-1}, and a bolometric one exceeding 10^{48} erg s^{-1}. The same is true for the extended sample of [5]. Recent *NuSTAR* observations of some of these FSRQs confirmed and refined this view. In PMN J0641–0320 the observed X–ray spectrum was extremely flat, with $\Gamma_{\rm X} \sim 1$, allowing to get information on the region of the jet where most of the power comes out and on the details of the acceleration/cooling of the emitting electrons. In this and in other FSRQs (see Fig. 1 the example of S5 0014+813 at $z = 3.366$) the optical emission is dominated by the accretion disk component (since the synchrotron emission peaks at smaller frequencies). Often, it is possible to observed the peak of the disk emission: once it is fitted with a standard disk model, we can infer the black hole (BH) mass and the accretion rate with an uncertainty smaller than what allowed by the virial method (based on the FWHM of the broad emission lines). *All* black holes in $z > 2$ FSRQs detected in the hard X–rays turned out to have masses $M > 10^9 M_\odot$. Benefitting from the completeness of the SLOAN optical sample, [7] reconstructed the number density as a function of z of massive BH with $M > 10^9 M_\odot$ and that are *active*, e.g. with a disk luminosity exceeding 10% the Eddington one. The right panel of Fig. 1 shows the corresponding number density. For radio–quiet quasars it peaks at $z \sim 2$–2.5 and decays exponentially after the peak. The number density of radio–loud quasars is surprisingly different. It peaks at $z \sim 4$. This result suggests that there are 2 preferred epochs of formation of massive BH, and that systems with jets form earlier. Is the jet helping the mass accretion rate or is a large accretion rate required to have a jet?

Importance of gamma-ray observations – The electromagnetic output of high–z powerful FSRQs peaks just in the band of e–ASTROGAM. Therefore e–ASTROGAM can discover several of new sources of this kind. With each source we can find the BH mass, the accretion rate and the jet power. Since the emission from these sources are beamed toward us, for each detected source there must exist (several) other sources pointing in other directions. Since the produced radiation is collimated within an angle $\sim 1/\Gamma$ (where Γ is the bulk Lorentz factor) each detected source corresponds to other $2\Gamma^2$ sources pointing elsewhere, but with the same intrinsic properties of the detected one. We could start to evaluate how the number density of massive BH with jets behave as a function of BH mass. Are BH holes with – say – $M = 10^8 M_\odot$ formed at $z = 4$ or later (i.e. smaller z)?

Expected results with e–ASTROGAM – Powerful FSRQs are characterized by an hard ($\Gamma_{\rm X} < 1.5$) spectrum. Therefore e–ASTROGAM can find them either selecting hard spectrum sources below 1 MeV, and then cross correlating with the radio emission, to pinpoint the arcsec position. If no redshift is already known for the source, a spectroscopic follow–up is needed.

Alternatively, the best candidates could be selected by the upcoming X–ray surveys (i.e. by e–ROSITA) in the 2–10 keV. Again, we have to select the hardest sources, cross correlate them with the radio (> 1 mJy is enough) samples, and find the redshift if unknown. Given the expected sensitivity of e–ASTROGAM, this second option is to be preferred, since in this case the selected FSRQ would be a pointed target, with adequate exposure. If the sensitivity for one year of exposure is 10^{-11} erg cm^{-2} s^{-1} at $\sim$10 MeV, scaling with $t^{1/2}$ implies to reach a limiting flux ten times more (10^{-10}) in 3.6 days of effective exposure. At $z = 1$, this corresponds to a luminosity $L_{\rm X} \sim 5 \times 10^{47}$ erg s^{-1}.

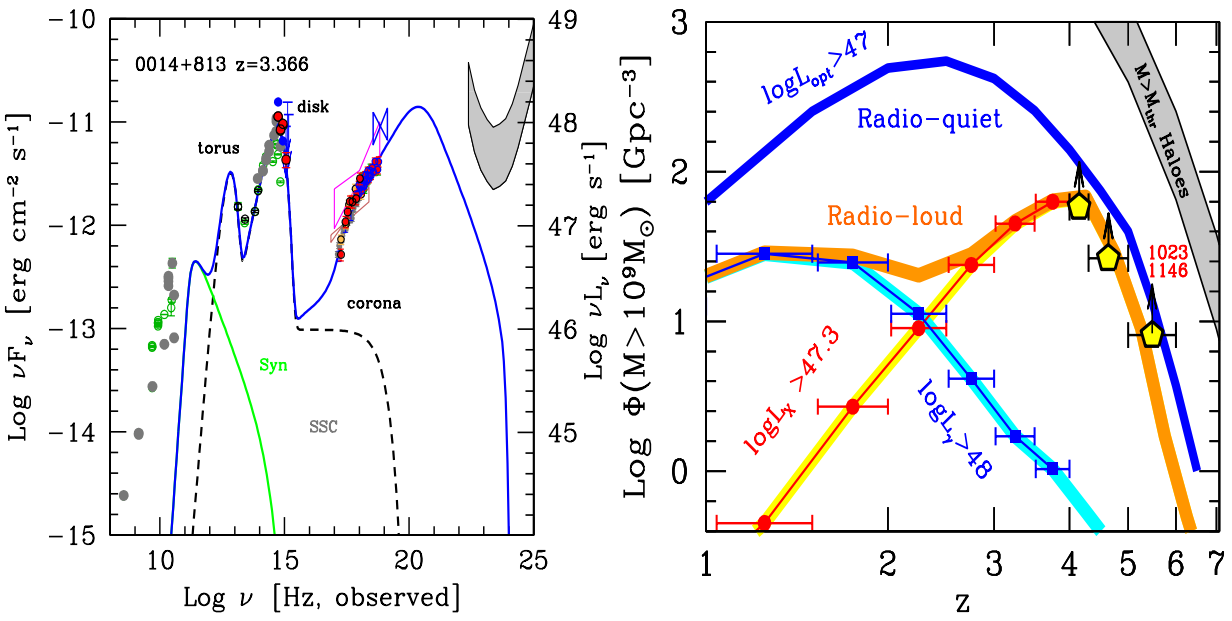

Figure 1: Left: Broad band SED of S5 0014+81 with X–ray data from Swift and *NuSTAR*. Note the large Compton dominance, the optical peak unveiling the contribution of the accretion disk and the fact that his FSRQs **has not** been detected by Fermi. Th BH mass for this source is of the order of $M \sim 10^{10} M_\odot$ (from [7]). Right: The number density of black holes with $M > 10^9 M_\odot$ as a function of redshift. While massive black holes in active radio quiet quasars (i.e. accreting at >10% the Eddington rate) appear to form at $z \sim 2$, the ones in jetted sources appear to form earlier, at $z > 4$. Adapted from [6].

With these new detected FSRQs we can start to refine the current ideas of the relation about the jet and the accretion rate. Currently, the results (using with *Fermi* blazars whose maximum redshift is ∼3 and mostly located at $z \sim 1$, see [5]) indicate that the jet power is greater than the luminosity of the accretion disk. Selecting new sources where the jet emission peaks (i.e. at ∼1 MeV) could imply to find even more dominant jets. In turn, this impacts on our understanding of the generation process of jets itself: is it really the Blandford–Znajek mechanism? Or can we explain these results assuming that part of the gravitational energy of the accreting matter goes into amplifying the magnetic field, instead of heating the disk? In this case we can have sub–Eddington disc luminosities with super–Eddington accretion rates. This possibility could also explain why jetted sources have black holes that grows at earlier epochs than in radio–quiet quasars.

References

[1] Ajello M., Costamante L., Sambruna R.M. et al., 2009, ApJ, 699, 603

[2] Ajello M., Ghisellini G., Paliya V.S., 2016, ApJ, 826, 76

[3] Blandford R.D. & Znajek R.L., 1977, MNRAS, 179, 433

[4] Baumgartner W.H., Tueller J., Markwardt C.B., Skinner G.K., Barthelmy S., Mushotzky R.F., Evans P.A., Gehrels N., 2013, ApJS, 207, 19

[5] Ghisellini G., Tavecchio F., Maraschi L., Celotti A., Sbarrato T., 2014, Nature 515, 376

[6] Sbarrato T., Ghisellini G., Tagliaferri G., Foschini L., Nardini M., Tavecchio F., Gehrels N., 2015, MNRAS, 446, 2483

[7] Sbarrato T., Ghisellini G., Tagliaferri G. et al., 2016, MNRAS, 462, 1542

On The Origin of the Extragalactic MeV Background

Marco Ajello [1], *Dieter Hartmann* [1], *Markus Ackermann* [2]

[1] *Department of Physics and Astronomy, Clemson University, Kinard Lab of Physics, Clemson, SC 29634-0978, USA*
[2] *Deutsches Elektronen Synchrotron DESY, D-15738 Zeuthen, Germany*

Science questions – The origin of the MeV background, in the ∼0.2-100 MeV gap region, remains a long-standing issue in astrophysics. The first measurements by the APOLLO 15/16 missions [13] displayed an intriguing 'MeV bump' that was not later confirmed by HEAO-4 , SMM and COMPTEL [6, 14, 15]. These latter missions characterized the MeV background spectrum as a power-law extension of the cosmic X-ray background (up to ∼3 MeV) [2]. Up to this day there is no clear understanding of which source population, or emission mechanism, may account for the intensity of the MeV background.

Importance of gamma-ray observations – Dark matter annihilation [4], non-thermal emission from Seyfert galaxies [7], nuclear decays from Type Ia supernovae [5, 11], and emission from blazars [3] and radio-galaxies [8] are among the candidates that were put forth to explain part or the totality of the MeV background. Blazars, radio-galaxies, and type Ia supernovae have been detected at MeV energies and as such their contribution to the MeV background is guaranteed. On the other hand the contribution from the putative dark matter interaction or the non-thermal emission of Seyfert galaxies is less secure. The latter is however worth of attention because by invoking the presence of non-thermal electrons in AGN coronae, it makes radio-quiet AGN a population able to account for both the X-ray and MeV backgrounds, justifying at the same time the power-law shape of the low-energy part of the MeV background. On the other hand, the < 3 MeV part of the MeV background spectrum can be accounted for by the emission of extremely powerful blazars, which are easily detected in the hard X-ray range and display very hard power-law spectra [3]. The most interesting aspect is that in order to connect the X-ray and the γ-ray (i.e. GeV) background, the spectrum of the MeV background must harden at around 40-60 MeV (see Fig. 1). This implies that either at least two source classes are major contributors to the MeV background or that another source class that exhibits a spectral bump needs to be considered. Star-forming galaxies, whose MeV to GeV emission is powered by cosmic rays, may be this additional population [10].

Expected results with e-ASTROGAM – e-ASTROGAM will provide a new, accurate, measurement of the MeV background at > 300 keV and up to a *few* GeV providing good overlap with the X-ray and the γ-ray backgrounds. At the same time e-ASTROGAM will detect hundreds of sources providing direct insight into which populations can explain the MeV background. The measurements of luminosity functions (for e.g. populations like blazars, star-forming and radio galaxies) will provide direct prediction of the contributions of those source classes to the background.

The measurement of the MeV background will require careful modeling of the Galactic diffuse emission and of the instrumental background. The former can be achieved using predictions of Galactic cosmic ray propagation models [12] tuned to fit the e-ASTROGAM data, while the latter will require detailed Monte Carlo simulations and an event selection that minimizes non celestial signal.

Thanks to its excellent point-source detection sensitivity, e-ASTROGAM will detect hundreds of sources. Spectroscopic campaigns will be needed to determine their redshift and ultimately their luminosity function. For the unresolved component of the MeV background, both a stacking analysis and the analysis of the angular fluctuations [9] of the background will be able to provide further insight into its origin.

References

[1] Ackermann, M., et al. 2015, ApJ, 799, 86
[2] Ajello, M., Greiner, J., Sato, G., et al. 2008, ApJ, 689, 666
[3] Ajello M., Costamante L., Sambruna R.M. et al., 2009, ApJ, 699, 603
[4] Ahn, K., & Komatsu, E. 2005, Phys. Rev. D, 72, 061301
[5] Clayton, D. D., & Ward, R. A. 1975, ApJ, 198, 241
[6] Kinzer, R. L., Jung, G. V., Gruber, D. E., Matteson, J.-L., & Peterson, L. E. 1997, ApJ, 475, 361
[7] Inoue, Y., Totani, T., & Ueda, Y. 2008, ApJ, 672, 5

[8] Inoue, Y., 2011, ApJ, 733, 66
[9] Inoue, Y., 2013, ApJ, 776, 33
[10] Lacki, B., et al., 2014, ApJ, 786, 1
[11] Ruiz-Lapuente, P., et al., 2016, ApJ, 820
[12] Strong, A. & Moskalenko I., 1998 ApJ, 509, 212S
[13] Trombka, J. I., Dyer, C. S., Evans, L. G., et al. 1977, ApJ, 212, 925
[14] Watanabe, K., Leising, M., Share, G., & Kinzer, R. 1999b, BAAS, 31, 702
[15] Weidenspointner, G., Varendorff, M., Kappadath, S. C., et al. 2000, in AIP Conf. Proc. 510, The Fifth Compton Symposium, ed. M. L. McConnell, & J. M. Ryan (Melville, NY: AIP), 581

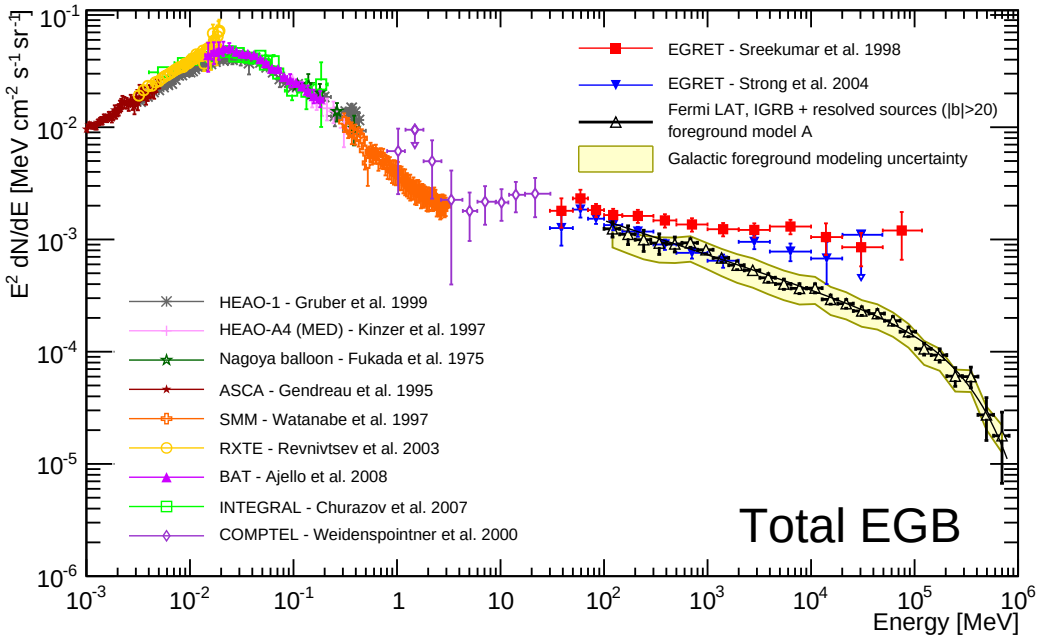

Figure 1: Spectrum of the high-energy background from X-ray to GeV γ-rays. Adapted from [1].

MeV blazars: understanding emission processes and blazar evolution at high-redshift

Sarah Kaufmann [1], *Omar Tibolla* [1], *Stefano Ciprini* [2,3], *Gabriele Ghisellini* [4], *Fabrizio Tavecchio*[4], *Carlotta Pittori* [2,5], *Francesco Verrecchia* [2,5]

[1] *Mesoamerican Center for Theoretical Physics (MCTP), Universidad Autonoma de Chiapas (UNACH), 29050 Tuxtla Gutierrez, Chiapas, Mexico*
[2] *Space Science Data Center, Agenzia Spaziale Italiana, I-00133, Roma, Italy*
[3] *Istituto Nazionale di Fisica Nucleare, Sezione di Perugia, I-06123, Perugia, Italy*
[4] *INAF - Osservatorio Astronomico di Brera, Via Bianchi 46, I-2380 Merate, Italy*
[5] *INAF - Osservatorio Astronomico di Roma, I-00078, Monte Porzio Catone, Italy*

Science questions – Blazars with a high luminosity at MeV energies (so-called **MeV-blazars**) are the most luminous objects of their class. Blazars describe the class of AGN which are detected at a very small angle between the rotational axis of the accretion disc and the line of sight of the observer, hence in the direction of the jet. This class contains the flat spectrum radio quasars (FSRQ) and the BL Lac objects.

In the first COMPTEL source catalog and in the subsequent re-analysis of the COMPTEL database (0.75-30 MeV), evidence for MeV emission of several blazars both in the lower (< 3 MeV) and upper (> 3 MeV) COMPTEL energy bands were reported [1], [2].

Only few MeV-blazars have been detected so far ([3],[2],[4],[5],[6],[7],[8]). These very luminous objects are mostly found at high redshifts (z>2) [6], they are thought to be fueled by super-massive black holes ($M \geq 10^9 M_\odot$) [9], and they have luminous accretion disk photon fields [10]. At high luminosities and redshift, the accretion disc is expected to become visible in FSRQs, which could testify a sequence in physical parameters and in the dominance of the inverse Compton emission.

External photon field: BLR or Torus:
The spectral energy distribution (SED) represents the clear Compton dominance of the MeV blazars (see Fig. 1), in which the ratio of the inverse Compton to synchrotron luminosity is of the order of ~ 100. The optical and UV radiation is dominated by the thermal emission from the accretion disk [4], which is strengthen by the fact of lack of variability in these bands. As described by e.g. [6], an external photon field, in addition to the photons produced by the synchrotron, is needed to account for the high inverse Compton flux, since the synchrotron Self-Compton model would produce a much less luminous Compton peak. There are two favorable locations for this external photon field which could yield to this large Compton dominance (see [11], [12]): the broad line region (BLR) and the torus region. In both locations, the ratio between radiation and magnetic energy density are large enough to explain the Compton dominance ([6]). The size of the emitting region is a good indicator to distinguish between the two options for the location of the photon field responsible for the Compton dominance. The size can be identified by the variability time scale of the X-ray and gamma-ray emission, e.g. day time scale for the BLR and five times longer for the torus option ([6]).
Understanding cause of violent outbursts:
As [4] stated, one need to understand the cause of the violent outbursts at hard X-rays, which are expected to be detected as well in the MeV range and what is their duty cycle. The time scale of the variability gives an estimation of the size of the emission region and hence clues about the most reasonable external photon fields.
High-redshifts studies of blazars:
The very luminous objects are mostly found at high redshifts (z>2-3)([6]). Therefore they are the best cases to study the redshift evolution of blazars. As mentioned in [6], the Burst Alert Telescope (BAT) on-board Swift detected 26 FSRQ of which $\sim 40\%$ are located at $z > 2$ and Fermi-LAT instead detected > 400 FSRQ of which only $\sim 12\%$ are with $z > 2$. Although currently the number of detected MeV blazars is very small, they enlarge the redshift range, e.g. one MeV blazar is detected at redshift of 5.3 ([7]).
MeV background:
Ajello et al[5] pointed out, that MeV blazars can contribute to the MeV background. Moreover the mass density of heavy black holes might be constrained by the measurements on MeV blazars [9].

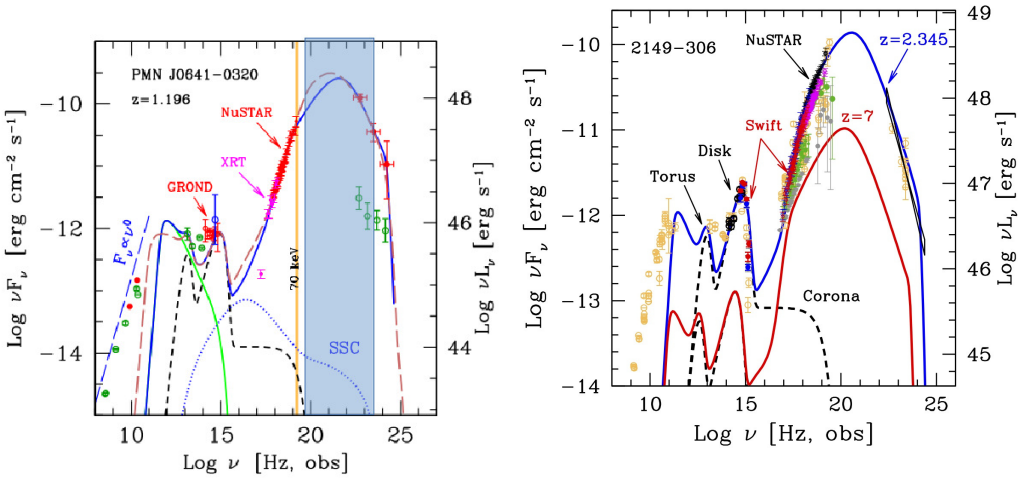

Figure 1: Left: Spectral energy distribution and model of the MeV blazar PMN J0641-0320 taken from [6]. Observations with quasi-simultaneous observations by GROND, Swift, NUSTAR and Fermi-LAT (in red). The black dashed curve represents to contribution of the torus, accretion disk and X-ray corona. The solid green line shows the synchrotron emission. The solid blue line represents a model with external photon field in the BLR, while the dashed brown model takes into account a photon field of the region between the BLR and the Torus. In blue the energy range of e-ASTROGAM is marked to illustrate the coverage of the MeV energy where we have a gap of observations due to the lack of an instrument like e-ASTROGAM. Right: Spectral energy distribution and model of the MeV blazar PKS 2149-306 (redshift of z=2.345), which was observed by NuSTAR together with multi-wavelength instruments and discussed in [8]. Additionally, a model, illustrating how such source might appear at a redshift of z=7, was added. Hence, e-ASTROGAM will have the sensitivity (given enough exposure time) to detect this kind of source even at a redshift of z=7.

Importance of gamma-ray observations – The physical parameters of MeV blazar jets need to be studied in detail and only higher statistics of MeV bright blazars can give a good parameter space to describe this class of very luminous blazars. Moreover, very few high-redshift blazars could yet be studied at MeV and GeV energies.

The detailed modeling of the Compton dominated SED is crucial to identify the underlying physical properties of the MeV blazars. Moreover, the measurement of the time scale of flux variability in the gamma-rays together with X-ray observations (e.g. e-ROSITA heritage, ATHENA and further future X-ray monitoring satellites) , gives the indication about the location of the external photon fields necessary to explain the Compton emission. In addition cross-correlation studies with mm/infrared data (for example from ALMA, JWST, WFIRST) will also be very important.

The redshift distribution of the MeV blazars can reach much higher redshift than the GeV detected blazars due to the absorption by the extragalactic background light (EBL) at gamma-ray energies. This is also a crucial issue that the study of high-redshift blazars at MeV energies gives a very detailed information about the source intrinsic spectra. This intrinsic spectra are important to verify the current EBL model predictions for TeV blazars.

Expected results with e-ASTROGAM – The hard continuum spectrum at hard X-rays and the peak (in νF_ν presentation) of the Compton component at MeV energies makes them a wonderful target for e-ASTROGAM observations, especially due to the current lack of data in the 100keV-100 MeV energy band. A numerous detection of MeV blazars are expected with the covered broad energy range from 0.3 MeV to 3 GeV and its planned high sensitivity of e-ASTROGAM, which, e.g. in the range 0.3-100 MeV will be one to two orders of magnitude better than that of previous instruments [14]. This will give rise to a more detailed study of the underlying emission processes and to identify the characteristic parameters for the general class of blazars. Based on the number of FSRQ mentioned in the Fermi LAT catalog 3FGL([14]) for which the gamma-ray spectrum can be described with a photon index of $\Gamma > 2$ and which hence could be good candidates for high luminosity at MeV energies, we expect that at least more than 450 blazars (a conservative estimation) will be detected with a high flux in the MeV range.

Gamma-ray observations in the MeV energy range are important to increase the number statistics of the MeV blazars to verify, if Compton dominance is a general characteristics of them and hence that external photon fields are necessary to explain their high luminosity at MeV energies. A combination and interplay

of external-jet infrared photon field Comptonization and in-jet synchrotron self-Compton, both producing gamma-rays, can be unveiled and well studied only with sensitive observations in the MeV gamma-ray regime. The 0.1-100MeV region is a new discovery window for the possible emergence of multi-component and multi-process gamma-ray signatures observable in this poorly known portion of the blazars SED.

The increase number of detections, based on e-ASTROGAM, will enlarge the redshift distribution of blazars up to highest redshifts, which is very important for the study of the evolution models. Blazar with highest redshift, even up to z=7, are expected to be detected with e-ASTROGAM, as illustrated in Fig. 1. Therefore e-ASTROGAM will be crucial to study the evolution of blazars.

MeV-blazars have their peak emission in the high sensitivity range of e-ASTROGAM, which will detect hundreds of these sources up to high redshifts, revolutionizing our understanding of blazar emission processes and evolution.

References

[1] Schoenfelder, V., Bennett, K., Blom, J. J., et al., 2000, A&AS, 143, 145
[2] Collmar, W., 2006, ASP Conference Series, Vol. 350, 120
[3] Bloom, S. D. and Marscher, A. P., 1996, ApJ, 461, 657
[4] Sambruna, R. M., Markwardt, C. B., Mushotzky, R. F., et al., 2006, ApJ, 646, 23
[5] Ajello, M., Costamante, L., Sambruna, R. M., et al. 2009, ApJ, 699, 603
[6] Ajello, M., Ghisellini, G., Paliya, V. S., et al., 2016, Astrophysical Journal, 826, 76
[7] Sbarrato, T., Tagliaferri, G., Ghisellini, G., et al., 2013, ApJ, 777, 147
[8] Tagliaferri, G., Ghisellini, G., Perri, M., et al., 2015, ApJ, 807, 167
[9] Ghisellini, G., Della Ceca, R., Volonteri, M., et al., 2010, MNRAS, 405, 387
[10] Ghisellini, G.; Righi, C.; Costamante, L., et al. 2017, MNRAS, 469, 255
[11] Ghisellini, G. and Tavecchio, F., 2009, MNRAS, 397, 985
[12] Sikora, M., Stawarz, L., Moderski, R., et al., 2009, ApJ, 704, 38
[13] De Angelis, A., Tatischeff, V., Tavani, M., et al. 2016, arXiv:1611.02232D
[14] Acero, F. et al. (Fermi-LAT collaboration), 2015, ApJS, 218, 23

Unraveling Active Galactic Nuclei using Time-resolved Spectral Energy Distributions

Daniela Dorner[1], *Thomas Bretz*[2]

[1] *University Würzburg, D-97074 Würzburg, Germany*
[2] *RWTH Aachen University, D-72074 Aachen, Germany*

Science questions – The importance of studying the spectral energy distribution (SED) of Active Galactic Nuclei with e-ASTROGAM and the relevance of its all-sky survey have already been highlighted in other chapters.

For Active Galactic Nuclei, one of the most fundamental and still open questions is the origin of the high energy emission, i.e. the identification of the processes in the central engine responsible for the highest energy photons. While stationary spectral energy distributions can be explained with a variety of models, some of the most intriguing variability features are still not understood. Leptonic models predict simultaneous flux increases in the low energy and high energy peak, while lepto-hadronic models can accommodate more complex variability patterns depending on the dominant process responsible for the gamma-ray emission.

Bright blazars, such as Markarian 421 and Markarian 501, are well studied in different energy bands (e.g. [1, 2, 3, 4, 5, 6]). Their quiescent-state spectral energy distributions are well described by leptonic or hadronic models. Also the broadband spectral energy distributions of individual high-states can be explained tuning the parameters of the models. While usually the different flux states are studied in detail but individually, the temporal evolution is rarely considered. Figure 1 shows an example of spectral energy distributions of the flat spectrum radio quasar 3C 279 in different flux states. While snapshot spectral energy distributions can be explained by a variety of models, their temporal evolution challenges stationary models. Only few first approaches as the one shown feature time-dependent modeling. To overcome the sparse sampling at very high energies, the gamma-ray telescope FACT [7] is monitoring bright TeV blazars providing an excellent temporal coverage allowing for time-resolved spectral energy distributions [8].

In the framework of Synchrotron Self-Compton models, a quadratic dependence between the synchrotron- and the inverse-Compton flux is predicted. Apart from effects due to the shift of the peak-frequency, the observation of this simple correlation is expected. The continuous gain during the assumed Fermi-I acceleration will produce a time lag between lower and higher energy photons (hard lag) in each hump. The ratio between the acceleration timescales of electrons and protons is expected to produce a very clear time lag between the two synchrotron components (e.g. [9]).

For blazars, another peculiar phenomenon challenging especially leptonic models are orphan flares, i.e. outbursts in gamma rays not accompanied by a low energy counterpart. Continuous monitoring of the spectral energy distribution is needed to allow to distinguish such events from time lags and from changes in the spectral shape.

Also periodic modulations of the gamma-ray emission have been derived from a number of models of the core regions of blazars. Their observation would put constraints on the possible intrinsic source processes. An example was found in a multi-wavelength campaign [10], which combined gamma-ray measurements from Fermi LAT with data from optical- and radio-waveband long-term monitoring. It revealed a possible quasi-periodic oscillation in PG 1553+113 on a time-scale of about two years. The paper also lists numerous proposed models for periodic emission such as binary black hole systems (e.g. [11, 12]), accretion flow instabilities (e.g. [13, 10]) or helical jet motion [14, 10].

Importance of gamma-ray observations – To draw conclusions on the mechanisms in the central engine of Active Galactic Nuclei not only the spectral but also the temporal coverage of e-ASTROGAM is important.

Depending on the position of the high energy peak of the source, the e-ASTROGAM observations will allow to probe different ranges of the high energy part of the spectral energy distribution. Although, for blazars the time resolution will be limited since measurements take place in the gap between high- and low-energy bump where fluxes are low, e-ASTROGAM's unprecedented sensitivity will allow for a time-resolution good enough to yield additional model constraints. For other Active Galactic Nuclei with lower peak position, the studies can be carried out with better timing resolution. In the context of multi-wavelength studies, unprecedented time-resolved spectral energy distributions can be studied and allow to constrain models and draw conclusions on the dominating emission process. Measurements of different classes of Active Galactic

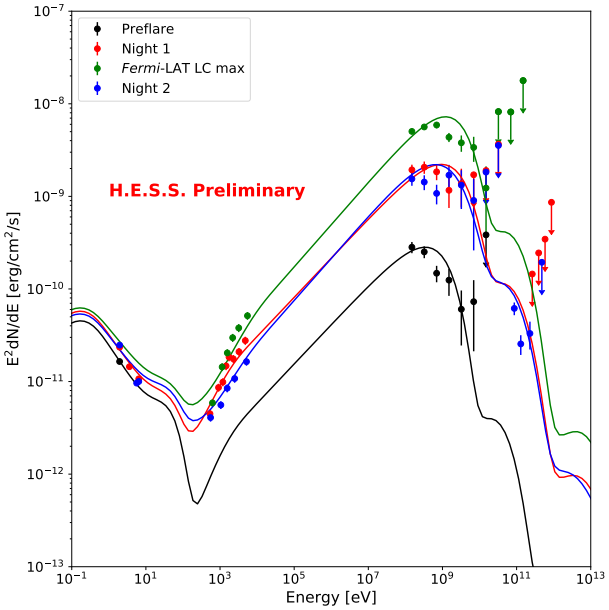

Figure 1: Multi-wavelength spectral energy distribution (Swift-XRT, Fermi LAT and H.E.S.S.) for different flux states superimposed with fits of an hadronic model. *Courtesy: arXiv:1708.00882*

Nuclei can be compared. In this way, e-ASTROGAM provides an essential contribution to the measurement and understanding of the high-energy peak.

After the Fermi LAT era, e-ASTROGAM will be the only instrument monitoring the non-thermal sky not only in space but also in time. This fits very well with future monitoring programs of the planned Cherenkov Telescope Array (CTA). Although targeted on single sources, CTA will extend the e-ASTROGAM measurements to higher energies. Only together, both measurements will allow to study time-resolved spectral energy distributions with unprecedented sensitivity and precision.

Expected results with e-ASTROGAM – The time evolution of all measured sources is a natural by-product of the proposed cataloging of the MeV sky.

New MeV sources will be detected extending and complementing the catalog of Active Galactic Nuclei. For unidentified sources, only e-ASTROGAM will be able to provide the crucial time evolution and spectral information helping to classify them. In case an association at other wavelengths is found, e-ASTROGAM will at that time be the only instrument available to provide time-resolved spectra of a large number of sources simultaneously.

With this valuable information, numerous models on periodicity or acceleration processes can be tested and excluded or further constrained. Thus, the existence of the time evolution from the only all-sky survey instrument available in the inverse-Compton regime and the only MeV instrument available will render exceptionally useful.

e-ASTROGAM will provide an essential contribution to the multi-wavelength picture of Active Galactic Nuclei. Covering a large energy range in gamma rays, it fills a gap in the spectral energy distributions which is important to constrain the models. While snapshots of spectral energy distributions can be explained with a variety of models, studying the temporal evolution will allow to further constrain models by enforcing a smooth evolution of the model parameters with time or comparing it to time-dependent models. The continuous coverage will also allow to search for orphan flares from others sources than blazars and allow to distinguish these special flares from time lags between the low and high energy peak and from changes in the spectral shape.

With increased source statistics from the all-sky survey, it is not needed anymore to generalize the result obtained from a single source, but population studies allow for a wider and more general picture.

References

[1] Abdo, A. A., Ackermann, M., Ajello, M., et al. 2011a, ApJ, 727, 129.

[2] Acciari, V. A., Arlen, T., Aune, T., et al. 2011, ApJ, 729, 2.

[3] Abdo, A. A., Ackermann, M., Ajello, M., et al. 2011b, ApJ, 736, 131.

[4] Fossati, G., Buckley, J. H., Bond, I. H., et al. 2008, ApJ, 677, 906.
[5] Pian, E., Tuerler, M., Fiocchi, M., et al. 2013, ArXiv e-prints.
[6] Lichti, G. G., Bottacini, E., Ajello, M., et al. 2008, AAP, 486, 721.
[7] Anderhub et al. 2013, JINST, 8, P06008.
[8] Dorner et al. 2017, PoS(ICRC2017) 608.
[9] Spanier, F. & Weidinger, M. 2012, Int. Journal of Modern Physics Conf. Series, 8, 293.
[10] Ackermann et al. 2015, APJ L, 813 (2), L 41.
[11] Begelmann, Blandford and Rees 1980, Reviews of modern Physics, 11, 288-291.
[12] Komossa 2003, In Centrella, J. M., editor, AIP C, 686, 161174.
[13] Honma et al 1992, Publications of the Astronomical Society of Japan, 44, 529535.
[14] Rieger 2004, APJ, 615 (1), L5-L8.

Extreme blazars with e-ASTROGAM: testing the limit of particle acceleration in the jet

Elisa Prandini,[1,2] *Eugenio Bottacini,*[1,2] *Luca Foffano,*[1,2] *Simona Paiano,*[1] *Ulisses Barres de Almeida* [3]

[1] *Dipartimento di Fisica e Astronomia* "G. Galilei"*, Università di Padova, I-35131 Padova, Italy*
[2] *Istituto Nazionale di Fisica Nucleare, Sezione di Padova, I-35131 Padova, Italy*
[3] *Brazilian Center for Research in Physics, Rio de Janeiro*

Science questions – Blazars are supermassive black holes accreting material and ejecting part of it in a jet almost aligned to the line of sight of the observer. They are the most powerful persistent accelerators of the known Universe. The blazar spectral energy distribution (SED) is dominated by the jet emission and encodes the particle acceleration. The SED is, in fact, characterized by a low frequency peak (from 10^{12} to $> 10^{18}$ Hz), due to synchrotron radiation emitted by ultra-relativistic electrons and a second peak at higher frequencies ($> 10^{21}$ Hz). The nature of this second peak is still largely discussed, in particular a dibated issue is the contribution of hadrons in addition to the inverse-Compton emission, as discussed for example in [1]. Blazars are further divided into flat spectrum radio quasars (FSRQs) and BL Lac objects (BL Lacs), depending on the characteristics of their optical spectrum.

Very remarkably, the analysis of the SEDs revealed that blazars display an anti-correlation between the bolometric luminosity and the location of the synchrotron peak (the so called blazar sequence [2, 3]). FSRQs display the synchrotron peak at low frequencies (IR - optical) while BL Lacs feature a lower luminosity and the peak shifted to higher frequencies. The subclasses of low/intermediate/and high synchrotron peaked BL Lac objects (LBL, IBL, and HBL respectively) reflect this behaviour.

In the MeV domain, the blazar SED may feature the second peak (FSRQs), the valley between the two peaks (LBL and IBL) or even part of the synchrotron peak (HBL). The analysis of a number of "extreme blazars" [4] showing the synchrotron peak at energies exceeding the hard X-ray band, and therefore not well constrained yet, raised the question about the limit of particles acceleration in the blazar jets. Moreover, in some extreme blazars, like 1ES 0229+200, the high-energy part of the SED shows clear evidence of a non-negligible hadronic component in the jet. A precise, complete sampling of the SED is therefore necessary to fully characterize it and disentangle between the leptonic and hadronic contributions. **We propose to measure with *e-ASTROGAM* the missing part of the SED for the most luminous extreme blazars known.**

With this measure we aim at answering the following questions:

- How do the synchrotron peak and the second peak connect in such extreme objects?
- What is the maximum energy reached by electrons in the jet of blazars?
- Is the SED obtained in agreement with the standard model of particle acceleration in the blazar jet?
- What is the hadronic contribution to the overall power emitted in a jet of an extreme blazar?
- Is there any additional, unexpected component in the spectrum of extreme blazars at MeV energies?

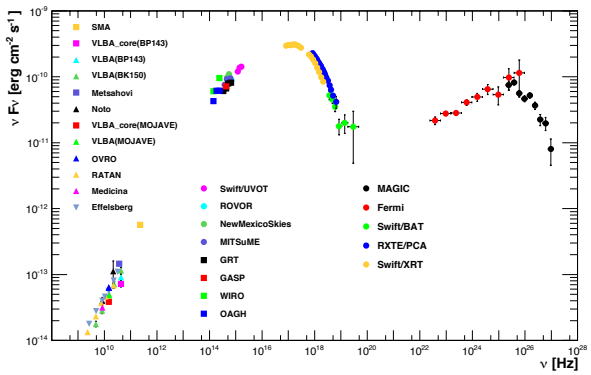

Figure 1: Overall SED of the TeV blazar Mkn 421. Multi-wavelength observations of the source emission, from radio to TeV energies, allowed for an accurate measurement of the acceleration mechanisms of the electrons in the jet [5]. In this HBL object the synchrotron emission lies in the optical/soft X-ray energy range. Therefore, the synchrotron peak of the source could be precisely determined and modelled.

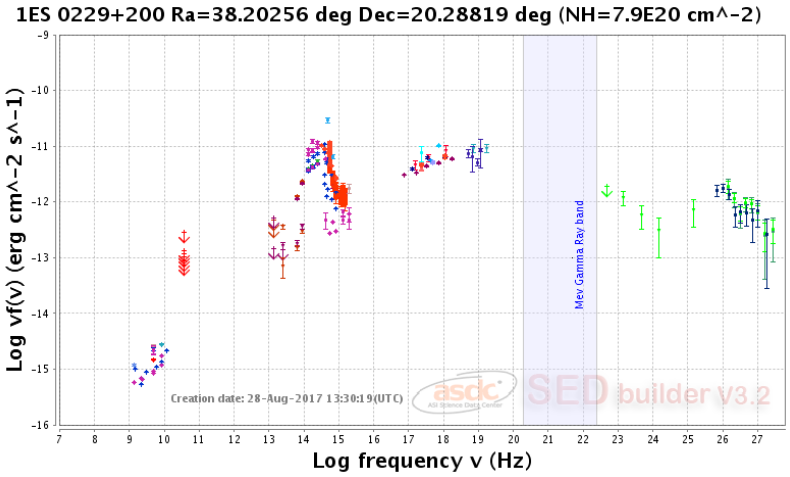

Figure 2: SED of the extreme blazar 1ES 0229+200. In this case, the peak of the synchrotron emission is not well determined due to the lack of measurements at frequencies above 10^{20} Hz. From ASDC website.

Importance of gamma-ray observations – A large number of blazars has been detected at energies above *100 MeV* by current generation of gamma-ray satellites (*Fermi*-LAT and AGILE). One of the most updated Fermi-LAT blazar catalogs is the so-called 3LAC [6] containing 1591 sources mainly belonging to three categories, which are unknown type of blazars, FSRQs, and BL Lacs. Of the latter two categories, only a minor fraction emits up to the highest energies, the so-called *very high-energy gamma rays (VHE, E > 100 GeV)*. The TeV catalog counts, in mid 2017, $\sim$ 70 sources, mainly HBLs. This drop in the number of sources is mainly due to the fact that only the most powerful and nearby objects reach such high energies with a sufficient flux to be detected by current generation of instruments. The Cherenkov telescope array (CTA) will start the operations in few years from now and is expected to detect more than 1000 sources above 100 GeV, thanks to its unprecedented sensitivity.

At energies *below 100 MeV*, the number of blazars with a significant gamma-ray emission detected by the most recent instrument (COMPTEL, in orbit from 1991 to 2000) is very low in comparison to the sources reported in the 3LAC (only $\sim$1%). The reason is twofold: the potential of source detection of COMPTEL was quite poor in comparison to that of *Fermi*-LAT, due to its low sensitivity (two orders of magnitude above). Moreover, most of the BL Lacs are expected to have a dip of the emission at these energies, due to the transition from the synchrotron emission to the inverse-Compton one. Interestingly, some objects (FSRQs and extreme HBLs) presumibly emits a large fraction of their power in this band, and is still largely undetected.

In the last decade, there is an increasing number of blazars that have been intensively studied at different bands, from radio to VHE gamma rays. The characterization of the SED over more than a decade in energy allowed very detailed studies of the physical conditions responsible for the emission at the site. *In general, a precise characterization of the first peak of the SED, the synchrotron peak,allows to determine the electron acceleration in the jet, while the study of the high-energy emission helps to constrain the eventual hadronic component in the jet or the presence of external radiation fields.* An example is Mkn 421, whose SED collected during a multi-wavelength campaign carried out in 2009 is displayed in Fig. 1. For this HBL object the synchrotron emission lies in the optical/soft X-ray energy range. Therefore, the synchrotron peak of the source could be precisely determined and modelled. The overall SED from Mkn 421 including th esecond peak is well modelled by a standard, synchrotron self-Compton model, where no additional contribution (e.g. hadronic emission or external radiation fields) is needed.

Another deeply studied blazar is the BL Lac object 1ES 0229+200, located at redshift 0.14. It is one of the few EHBLs detected at TeV energies [7]. The SED of 1ES 0229+200 is displayed in Fig 2, obtained from the ASDC website[1].

From its SED we can conclude that:

- The X-ray emission is detected up to $\sim$100 keV without any significant cut-off [8], meaning that the synchrotron peak is located at extremely high frequencies;
- The luminosity of the source is orders of magnitude below that of Mkn 421, as foreseen by the blazar sequence (extreme = faint);
- Once corrected for the effect of absorption due to the extragalactic background light (EBL), the VHE spectrum of 1ES 0229+200 is very hard at TeV energies, which is in tension with the classical, leptonic model of blazar emission.

[1] https://tools.asdc.asi.it/SED

The last point had a great relevance for the astrophysical community. The hard spectrum was used to set new constraints on the EBL itself in the IR regime [7], and to determine an upper limit on the intergalactic magnetic field [9, 10]. Several authors proposed a hadronic origin for the peculiar TeV spectrum [11, 12], suggesting that they could be responsible for a significant neutrino emission and could also be the site of ultra-high energy cosmic ray acceleration. A better knowledge of the MeV spectrum, being related to the synchrotron emittion of the electrons, could be of particular relevance to constrain the leptonic component of the emission.

Expected results with e-ASTROGAM – We propose to carry out a multi-wavelength observation campaign on a sample of extreme blazars including for the first time e-ASTROGAM observations. The target list can be extracted from [13], which collects the most promising extreme blazars known to date. In addition, we propose to include Mkn 501 during flaring states, since this source usually features an extreme behaviour in such circumstances. Goal of the campaign is to achieve the most accurate and complete characterization of the SED of a sample of extreme blazars. In particular, the goals of e-ASTROGAM observations are the measurement of the flux level at MeV energies and, possibly, the spectral slope. This will allow, for the first time, to determine the location of the synchrotron peak of these extreme, intriguing sources.

References

[1] M. Böttcher, A. Reimer, K. Sweeney, and A. Prakash. *ApJ*, 768:54, 2013.
[2] G. Fossati, L. Maraschi, A. Celotti, A. Comastri, and G. Ghisellini. *MNRAS*, 299:433–448, 1998.
[3] G. Ghisellini, C. Righi, L. Costamante, and F. Tavecchio. *MNRAS*, 469:255–266, 2017.
[4] L. Costamante, et al. *A&A*, 371:512–526, 2001.
[5] A. A. Abdo, et al. *ApJ*, 736:131, August 2011.
[6] M. Ackermann, et al. *ApJ*, 810:14, 2015.
[7] F. Aharonian, et al. *A&A*, 475:L9–L13, 2007.
[8] S. Kaufmann, S. J. Wagner, O. Tibolla, and M. Hauser. *A&A*, 534:A130, 2011.
[9] A. M. Taylor, I. Vovk, and A. Neronov. *A&A*, 529:A144, 2011.
[10] J. D. Finke, et al. *ApJ*, 814:20, 2015.
[11] M. Cerruti, A. Zech, C. Boisson, and S. Inoue. *MNRAS*, 448:910–927, 2015.
[12] F. Tavecchio and G. Bonnoli. *ArXiv e-prints*, 2015.
[13] G. Bonnoli, F. Tavecchio, G. Ghisellini, and T. Sbarrato. *MNRAS*, 451:611–621, 2015.

Gravitationally lensed MeV blazars

Stefano Ciprini[1,2], *Carlotta Pittori*[1,3], *Chi C Cheung*[4], *Sara Buson*[5], *Francesco Verrecchia*[1,3], *Dario Gasparrini*[1,2], *Sara Cutini*[1,2]

[1] *Space Science Data Center, Agenzia Spaziale Italiana, I-00133, Roma, Italy*
[2] *Istituto Nazionale di Fisica Nucleare, Sezione di Perugia, I-06123, Perugia, Italy*
[3] *INAF - Osservatorio Astronomico di Roma, I-00078, Monte Porzio Catone, Italy*
[4] *Space Science Division, Naval Research Laboratory, Washington, DC 20375-5352, USA*
[5] *NASA Goddard Space Flight Center, Greenbelt, MD 20771, USA*

Science questions − Blazars, namely BL Lac objects and flat-spectrum radio quasars (FSRQs), are a small but important fraction of the entire population of active galactic nuclei (AGN, e.g. [18]). For blazar populations which are typically distributed at larger distances, such as the FSRQs, the sub-GeV and MeV gamma-ray emission can dominate the electromagnetic radiative bolometric power. This makes them optimal probes of the distant and young Universe ([15, 13, 2, 14]), and targets for astrophysical "tomography" in the MeV regime. The sky in the 0.2-30 MeV energy region is, however, insufficiently covered with only a few tens of steady sources detected.

In parallel, strong gravitational lensing of electromagnetic radiation from distant sources (predicted in Einstein's theory of General Relativity [12]), has been discovered and studied in hundreds of radio/optical lens systems, since the first detection of multiple images of SBS 0957+561 [20]. When the distant source, the lensing galaxy/quasar, and observer lie along a straight line a circle, known as the Einstein ring, may be formed [19].

An example of (spatially unresolved) strong-lensing is the case of the powerful, MeV-peaked FSRQ, PKS 1830−211 ($z = 2.507$, routinely detected in GeV band by AGILE and *Fermi*, Fig. 1 and [11, 1]). PKS 1830−211 is the brightest strong lens in the sky at cm, hard X-ray, MeV gamma-ray energies, and detected already by COMPTEL [7] in 0.75−30 MeV band. The the two lines of sight to this object have been used in the past also as a cosmological probe [5]. S3 0218+35 (lens B0218+357, $z = 0.6847$) is another GeV lensed blazar detected by *Fermi* (and by MAGIC at $E > 100$ GeV, [3]), representing the smallest-separation lens known. For S3 0218+35 the first gamma-ray delay measurement was possible thanks to *Fermi* LAT data. This opened to the possibility of delay measurements for other distant lensed gamma-ray FSRQs. In the MeV regime (before/around/after the emission peak), the largest amplitude for flares and variability patterns occurs, enriching the statistics in strong-lensing/microlensing gamma-ray temporal features.

How we can substantially improve the spatial resolution of the central engine and identify the sizes and locations of gamma-ray emission regions from distant sources? How independent gamma-ray delay measurements and radio-delays are related in strong macro-lensing? Which is the role of micro/milli lensing (a view into astrophysical emission regions or a probe for dark-matter substructure and subhalos)? Can high-redshift, lensed MeV blazars, help us in the detection of cosmic neutrinos from the distant Universe? Are, at the end, distant gravitationally lensed MeV blazars a potential and unexplored gold-mine for multi-messenger and fundamental physics?

Importance of gamma-ray observations − A gravitational lens magnify the radiation emitted from a distant blazars and produce time delays between the diffraction mirage images, with delays depending on the position of the emitting regions in the source plane. Time delays in AGN/galaxy-scale lenses typically range from hours to weeks. The possibility to obtain independent gamma-ray delay measurements from strong macro-lensing, and to derive accurate measurements of the projected size of the gamma-ray emission regions in cnetral engine and the jet, disentangling micro-lensing temporal features, was attested for S3 0218+35 [6] and PKS 1830−211 [16, 4, 17, 4]. The evidence for micro/milli-lensing effects in strong lensed quasars is increasing in general. These can introduce a variability in the flux ratio of the two images, in addition to an intrinsic energy-dependent source structure and the different region sizes, resulting in a "chromatic" spectral variability [1, 11, 16]. The study of variability of gravitationally lensed blazars emitting in the 0.2MeV−3GeV band, can open interesting perspectives:

• MeV data are important to understand blazar particle acceleration and emission processes, the combination and interplay of different leptonic inverse-Compton mechanisms (SSC, BLR, torus,

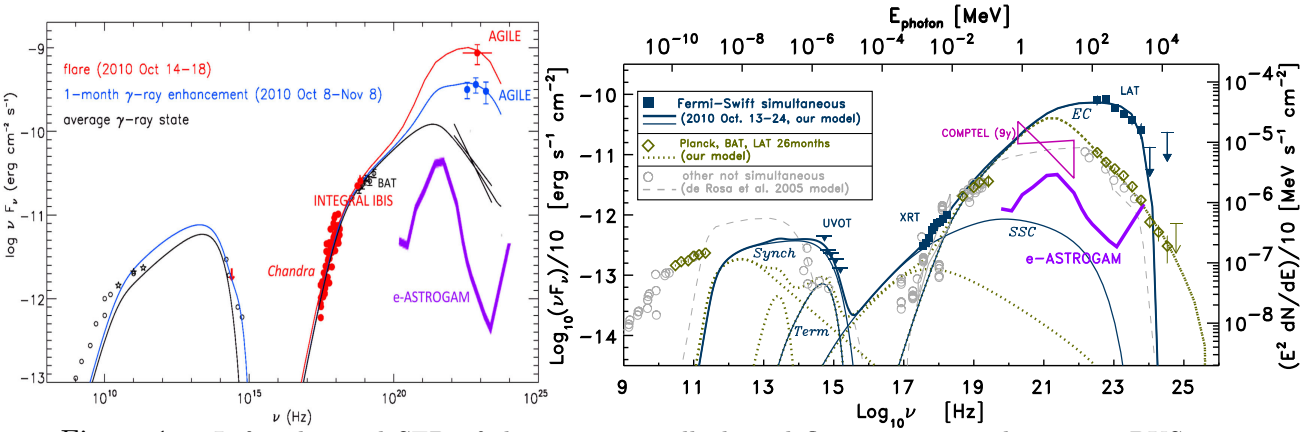

Figure 1: Left: observed SED of the gravitationally lensed flat spectrum radio quasar PKS 1830−211 ($z = 2.507$), built with archival data and Oct.-Nov. 2010 simultaneous data from the multi-wavelength campaign led by AGILE (models magnified by a factor of 10× for the lensing). Adapted from [11]. Right: observed SED of PKS 1830−211 built with simultaneous LAT and *Swift* XRT and UVOT data, averaged over the Oct. 13-24, 2010 period of the multi-frequency campaign led by *Fermi*. Past 26-month LAT, 58-month BAT, *Planck* ERCSC, Gemini-N, *Hubble*-ST, *Chandra* and INTEGRAL IBIS [10], COMPTEL and EGRET data are also reported (corrected for lensing by a factor of 10×). Adapted from [1]. This study is an example of a possible future confluence in e-ASTROGAM [14] of synergetic legacy science from teams of the NASA-DoE *Fermi*, ASI AGILE and ESA INTEGRAL missions.

diffuse dust photon fields) or hadronic emission processes (photopion, e.m. cascades, proton synchrotron, Bethe-Heitler).

• MeV temporal/spectral variability produced by unresolved lensing of distant FSRQs is able to probe the central engine and jet structures and the origin of the HE emission, this also in synergy with facilities like SKA, ALMA ([16]), LSST and Euclid.

• MeV data, placed around the emission peak with more pronounced variability and flares, enhance the detection of temporally delayed events and micro-lensing signals. *Fermi* LAT already observed common 1-day GeV flares of factors 3-10× compared to few-10% increases in mm/radio bands.

• More, small separation, lenses that cannot be resolved, can be discovered in MeV band thanks to measured delays. This is also relevant for unidentified *Fermi* LAT point sources.

• Gravitational lensing might help to enhance the sensitivity to cosmic neutrinos emitted by hadronic-dominated gamma-ray FSRQs that are typically placed at much larger distances with respect to other expected neutrino sources. The neutrino signal magnification by astrophysical lenses is of much interest for the next large-scale neutrino detectors. Lens multiple paths might induce also neutrino quantum interference and oscillations [8].

• Pseudoscalar axion-like particles (ALPs) generically couple to two photons, giving rise to possible oscillations with gamma-ray photons emitted by a FSRQ in the intergalactic/intervening-galaxy magnetic fields. Strong lensing of a background MeV FSRQ has some, speculative, possibility to enhance the flux of non-isotropic/streaming ALPs. Anomalies in the flux ratios of lensed images are foreseen by some DM theories. Time-variable lenses are also probes on the behavior of DM substructure in the intervening galaxy halo.

• Depending from particle properties, cosmological parameters, masses and separations of elements in the lensing system, differential arrival times of multi-messenger particles (gamma-ray photons, massive-neutrinos, gravitational waves, even massive axions and gravitons) are expected. Multi-messenger detections of different time delays from a lensed MeV FSRQ would be an unexplored fundamental physics phenomenon.

Expected results with e-ASTROGAM – The capability of e-ASTROGAM [14] to obtain independent gamma-ray delay measurements from unresolved strong macro-lensing, and to identify variability features related to micro-lensing, in the case of MeV blazars, will be already a very useful goal. e-ASTROGAM is expected to discover several new high-redshift FSRQs undetected by the *Fermi* LAT because of GeV cutoffs, and to see many MeV gamma-ray flares, including

those from lensed FSRQs. In addition, space-borne wide field imaging observatories, such as ESA's Euclid space telescope, would soon produce hundreds of new useful strong lenses to be searched for a MeV detection. Time-series and spectral analysis of gamma-ray variability, combined with the properties of the lens from radio observations (SKA, ALMA, etc.) or IR/optical observations (LSST, Euclid, JWST, etc.) can yield an improvement in spatial resolution at gamma-ray energies by a factor of 10^4 [4, 17]. Multi-messenger studies using FSRQ sources with candidate hadronic processes, will also be potentially opened by e-ASTROGAM, in conjunction with the, foreseen, large scale neutrino array experiments (KM3NeT and other). The lens magnification of the neutrino flux is expected to be equal to that of gamma-ray photon flux, and this could drive to the measure the intrinsic neutrino luminosity of powerful MeV-GeV FSRQs. MeV gamma-ray lensed blazar might also be of interest for, speculative, hypotheses in multi-messenger and fundamental physics.

References

[1] Abdo, A. A., Ackermann, M., Ajello, M., et al. 2015, ApJ, 799, 143
[2] Ackermann, M., Ajello, M., Baldini, L., et al. 2017, ApJ Lett, 837, L5
[3] Ahnen, M. L., Ansoldi, S., Antonelli, L. A., et al. 2016, A&A, 595, A98
[4] Barnacka, A., Geller, M. J., Dell'Antonio, I. P., & Benbow, W. 2015, ApJ, 809, 100
[5] Blandford, R. D., & Narayan, R. 1992, ARA&A, 30, 311
[6] Cheung, C. C., Larsson, S., Scargle, J. D., et al. 2014, ApJ Lett., 782, L14
[7] Collmar, W. 2006, ASP Con. Ser. 350, 120
[8] Crocker, R. M., Giunti, C., & Mortlock, D. J. 2004, Phys. Rev. D, 69, 063008
[9] De Angelis, A., Tatischeff, V., Tavani, M., et al. 2017, Experim. Astron., 44, 25
[10] de Rosa, A., Piro, L., Tramacere, A., et al. 2005, A&A, 438, 121
[11] Donnarumma, I., De Rosa, A., Vittorini, V., et al. 2011, ApJ Lett., 736, L30
[12] Einstein, A. 1936, Science, 84, 506
[13] Ghisellini, G., Tavecchio, F., Sbarrato, T., Kauffman, S., & O. Tibolla 2017, this volume.
[14] Ghisellini, G., Tavecchio, F., Maraschi, L., Celotti, A., & Sbarrato, T. 2014, Nature, 515, 376
[15] Kaufmann, S., Tibolla, O., Ciprini, S., et al. 2017, this volume.
[16] Martí-Vidal, I., Muller, S., Combes, F., et al. 2013, A&A, 558, A123
[17] Neronov, A., Vovk, I., & Malyshev, D. 2015, Nature Phys., 11, 664
[18] Padovani, P., Alexander, D. M., Assef, R. J., et al. 2017, A&ARev, 25, 2
[19] Schneider, P., Ehlers, J., & Falco, E. E. 1992, Gravitational Lenses, XIV, 560 pp., Berlin: Springer-Verlag
[20] Weymann, R. J., Chaffee, F. H., Jr., Carleton, N. P., et al. 1979, ApJ Lett., 233, L43

Narrow-Line Seyfert 1 galaxies: high accretion rates and low black hole masses

Sarah Kaufmann[1], *Omar Tibolla*[1], *Luigi Foschini*[2]

[1]*Mesoamerican Center for Theoretical Physics (MCTP), Universidad Autonoma de Chiapas (UNACH), 29050 Tuxtla Gutierrez, Chiapas, Mexico*
[2]*INAF Osservatorio Astronomico di Brera, 23807 Merate, Italy*

Science questions – Radio-loud Narrow-Line Seyfert 1 galaxies have been established as a new class of gamma-ray emitting AGN with relatively low black hole masses, but near-Eddington accretion rates. The mass of the central black hole is much smaller ($10^6 - 10^8 M_\odot$, e.g. [1]) and the accretion rate much higher than those estimated for the class of blazars (see [2] for a review).

Narrow-Line Seyfert 1 (NLSy1) galaxies are characterized by broad permitted and narrow forbidden lines in their optical spectra, classifying them as Seyfert 1 galaxies. However, the permitted lines are narrower than usual with FWHM(Hβ) < 2000kms^{-1}, the ratio of [O III] to Hβ is smaller than 3, and a bump due to Fe II exist (see, e.g. [3] for a review). A larger study by [4] based on SDSS Data Release 3 identified a sample of 2011 NLSy1 galaxies. Only a small fraction of NLSy1 galaxies are radio loud ($S_{4.85\mathrm{GHz}}/S_{440\mathrm{nm}} > 10.$), e.g. 7% in the study of [5].

The detection of high-energy gamma-rays and its variability ([6],[7]) confirmed the existence of powerful relativistic jets in radio-loud NLSy1 galaxies (see [8] for a review), which therefore can be now named as jetted NLS1, according to the classification recently proposed by Padovani [9].

MeV peaked emission - high energetic jet:
An important feature, that NLSy1 galaxies have in common with the other class of jetted AGN (e.g. FSRQ), is the MeV peaked spectral emission, which should be studied in more detail. Figure 1 illustrate two prominent examples of radio-loud NLSy1 galaxies with detected GeV emission. The keV-GeV peak (in νF_ν presentation) is generally described by the Synchrotron-Self-Compton (SSC) emission from the high energetic jet and the External Compton (EC) emission in which the relativistic electrons interact with a photon field close to the jet (generally from the broad-line region). The EC component is generally necessary to describe the detected GeV gamma-ray emission. It is still needed to understand the different contributions of the SSC and EC in the high energy band, which are currently difficult to establish precisely. Measurements of the polarization will help to distinguish between the SSC (polarized) and the EC (un-polarized) emission.

High accretion rate and low black hole mass:
As can be seen clearly in Fig. 2, the radio-loud NLSy1 galaxies have much lower black hole masses than the class of FSRQ and BL Lac objects (class of object observed in the direction of the high energetic jet). In addition, the accretion rate is very high, comparable to the ones of FSRQs. The important idea was established by [11], that the sequence of NLSy1 galaxies to FSRQ to BL Lac objects, going from small-mass black holes with high accretion rate to large-mass black holes and low accretion rate, could describe the cosmological evolution of the same type of object. Hence, the NLSy1 galaxies represent the young state with low black hole masses and their study will give the opportunity to understand better the cosmological evolution of Active Galactic Nuclei.

Comparable characteristics to X-ray binaries:
One hot topic of discussion is the simultaneous existence of the jet and a very high accretion rate. The investigation about the flux variability will give more insight in this question. As shown in [6],[12], the gamma-ray emission of NLSy1 galaxies is variable. Hence, the jet may be formed accompanying with relatively weak soft X-ray, as was commonly seen in X-ray binaries.

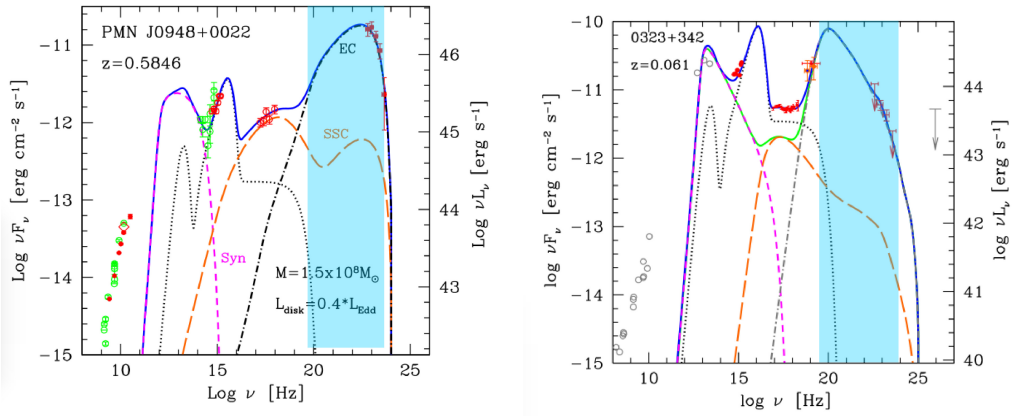

Figure 1: Left: Spectral energy distribution of PMN J0948+0022 taken from [6]. The dotted line shows the contribution from the infrared torus and accretion disk. The synchrotron Self-Compton (SSC) is shown in dashed and the Inverse Compton from external photon fields (EC) is shown with a dot-dashed line. The blue area represents the energy range of e-Astrogam. Right: 1H 0323+342 is the closest among the gamma-ray emitting NLSy1. The spectral energy distribution is taken from [7]. The black hole mass is assumed to be $M_{BH} \sim 10^7 M_\odot$ and accretion disk luminosity of $L_{\rm disk} = 0.9 \times L_{\rm Edd}$ ([7]). Based on its characteristics in optical/X-rays, 1H 0323+342 seem to represent a transitional case in which the inner disk heats up and blows up to a torus configuration, as the accretion rate goes down ([12]).

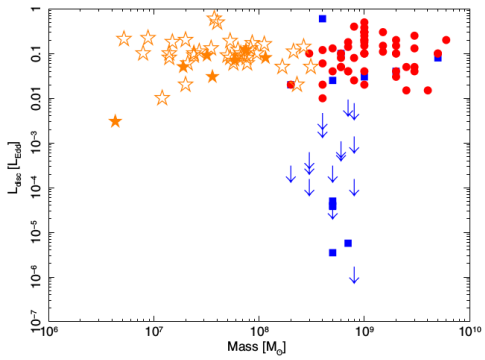

Figure 2: Accretion disk luminosity in Eddington units versus the mass of the central black hole, taken from the survey study of [10]. The orange stars represent the characteristics of the radio-loud NLSy1 galaxies. The red circles show the FSRQs and the blue squares and arrows the BL Lac objects.

Importance of gamma-ray observations – Based on survey studies by [10] with multi wavelength spectral studies of jetted NLSy1 galaxies, a peak of the gamma-ray emission in the MeV energy band is expected, as in the other jetted AGN. There is a current lack of data in the 100keV-100 MeV energy band, in which luminous emission is expected from all jetted NLSy1 galaxies. As can be seen in Figure 1, the spectral energy distribution (SED) of NLSy1 galaxies is rather complex. In the energy range from keV to MeV, the dominant emission process seems to be the Synchrotron-Self-Compton (SSC) emission from the high energetic jet and the External Compton (EC) emission in which the relativistic electrons interact with the broad line region photon field close to the jet. The EC component is necessary to describe the detected GeV gamma-ray emission. Constraints on the model can be obtained with gamma-ray observations on jetted NLSy1 galaxies which will provide a good coverage of the current gap in the MeV energy band. The currently not well determined ratio between the SSC and EC components can be defined more precise with such measurements. By using polarization measurements, it will be possible to disentangle SSC (polarized) from EC (not polarized). Especially, it is very important to fix the SSC contribution to be able to estimate the strength of the magnetic field.

Due to the variability in X-rays with changing spectral behavior, it will be important to observe

simultaneously in the gamma-ray and lower energy range (e.g. monitoring observations expected from eROSITA or triggered, pointed observations with current X-ray satellites). The measurement of the time scale of the flux variability in the X-ray and gamma-ray range will also give indications about the location of the external photon field responsible for the IC emission.

Another point is the study of gamma-ray emission from the parent population of beamed NLS1. A steeper gamma-ray spectrum is expected [13], and therefore the detection below 100 MeV could be an asset with respect to Fermi LAT.

Expected results with e-ASTROGAM – The peak (in νF_ν presentation) of the Compton component at MeV energies makes jetted NLSy1 galaxies a wonderful target for e-ASTROGAM observations, especially due to the current lack of data in the 100keV-100 MeV energy band. A large number of detections are expected with the covered broad energy range from 0.3 MeV to 3 GeV and its planned high sensitivity of e-ASTROGAM, which, e.g. in the range 0.3-100 MeV will be one to two orders of magnitude better than that of previous instruments [14]. This will give rise to a more detailed study of the underlying emission processes and to identify the characteristic parameters.

Based on the sample of radio-loud NLSy 1 galaxies by [10], in which the SED of 42 NLSy1 galaxies have been studied in detail, we expect a large number of MeV peaked NLSy1 galaxies (based on the spectral characteristics in the X-ray regime) to be easily studied with e-Astrogam.

Berton et al. [15] performed simulations indicating that SKA will detect thousands of jetted NLS1 for which a multi-wavelength coverage will be required (and Fermi will likely be no more available, and CTA has a too high low-energy threshold).

References

[1] Boroson, T. A. 2002, ApJ, 565, 78

[2] Foschini, L. 2013, Proceedings of the Conference *Nuclei of Seyfert galaxies and QSOs - Central engine & conditions of star formation*, arXiv: 1301.5785

[3] Pogge, R. W. 2000, New Astron. Rev., 44, 381

[4] Zhou, H.-Y., Wang, T., Yuan, W., et al. 2006, ApJS, 166, 128

[5] Komossa, S., Voges, W., Xu, D., et al. 2006, AJ, 132, 531

[6] Abdo, A. A., et al. (Fermi-LAT collaboration) 2009a, ApJ, 699, 976

[7] Abdo A.A., et al. (Fermi-LAT collaboration) 2009b, ApJ, 707, L142

[8] Foschini, L. 2014, in High-Energy Phenomena in Relativistic Outflows (HEPRO IV), eds. F. A. Aharonian, F.

[9] Padovani, P., 2017, Nature Astronomy, 1, 194

[10] Foschini, L., Berton, M., Caccianiga, A., et all., 2015, A&A, 575, A13

[11] Foschini, L. 2017, Proceedings of the Conference "Quasars at All Cosmic Epochs". Frontiers in Astronomy and Space Science., arXiv:1705.10166

[12] Tibolla, O., Kaufmann, S., Foschini, L., et al., 2013, ICRC 2013 proceedings paper, arXiv: 1306.4017

[13] Liao, N.-H., Liang, Y.-F., Weng, S.-S., et al. 2015, arXiv:1510.05584

[14] De Angelis, A., Tatischeff, V., Tavani, M., et al. 2016, arXiv:1611.02232D

[15] Berton, M., Foschini, L., Caccianiga, A., et al., 2015, Proceedings of "The many facets of extragalactic radio surveys: towards new scientific challenges", arXiv:1601.05791

Estimation of magnetic-to-particle energy density ratio of BL Lac objects

Nijil Mankuzhiyil

Astrophysical Sciences Division, BARC, Mumbai - 400085, India

Science questions – Blazars are class of Active Galactic Nuclei (AGN) whose relativistic plasma jet points towards the line of sight of observer. BL Lacs, one of the sub class of blazars are characterized by the weakness, or even the absence of emission lines in their optical spectra. The overall radio to γ-rays Spectral Energy Distribution (SED) of these objects display two broad non-thermal continuum peaks. The low energy peak is thought to arise from the synchrotron process, while the leptonic models, which are popular models used in literature, suggest that the second peak forms out of inverse Compton (IC) emission. If the low energy photons which undergo the IC process are the synchrotron photons, the process is known as the Synchrotron Self Compton (SSC) emission [6]. In the current scenario, SSC models can satisfactorily reproduce the observed flux of blazars in optical-to-γ-rays broad band window.

The electron energy distribution responsible for the non-thermal emission can be represented by a double power-law

$$N(\gamma) = \begin{matrix} \mathrm{K}\gamma^{-\mathrm{n}_1} & ;\gamma_{\mathrm{min}} < \gamma < \gamma_{\mathrm{br}} \\ \mathrm{K}\gamma_{\mathrm{br}}^{\mathrm{n}_2-\mathrm{n}_1}\gamma^{-\mathrm{n}_2} & ;\gamma_{\mathrm{br}} < \gamma < \gamma_{\mathrm{max}} \end{matrix}$$

where γ_{min}, γ_{br}, and γ_{max} are the lowest, break, and highest Lorentz factors of the electron energy distribution, K is the normalization constant, and n_1 and n_2 are, respectively, the slopes below and above the break. The kinetic energy density of relativistic electrons can be estimated as

$$\mathrm{U_e} = \mathrm{m_e c^2} \int_{\gamma_{\mathrm{min}}}^{\gamma_{\mathrm{max}}} \gamma\, \mathrm{N}(\gamma)(\gamma - 1)\mathrm{d}\gamma \simeq \mathrm{m_e c^2 N} < \gamma >$$

where, N is the integrated electron density. In general case, where $\mathrm{n}_1 \approx 2$, the average Lorentz factor of the particle can be written as

$$< \gamma > \simeq \gamma_{\mathrm{min}} \ln(\gamma_{\mathrm{br}}/\gamma_{\mathrm{min}})$$

Therefore, γ_{min} plays the major role in estimating $U_\mathrm{e}/U_\mathrm{b}$ ratio of the jet, where U_b is the magnetic energy density. The present estimates of U_e/U_b hint that, the situation is far from particles-field equilibrium (except for a few sources), with electrons dominating over the field by orders of magnitude [4, 7, 3].

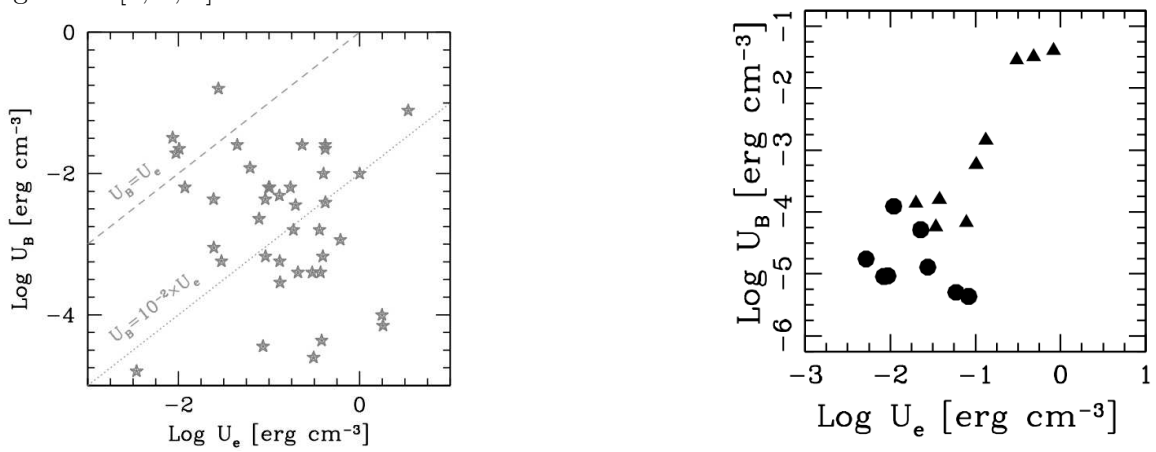

Figure 1: Left: Magnetic energy density and relativistic electron density estimated from SEDs of 45 BL Lac objects [7]. Right: Same, for Mrk 421 (triangles) and Mrk 501 (circles) in different activity states [4].

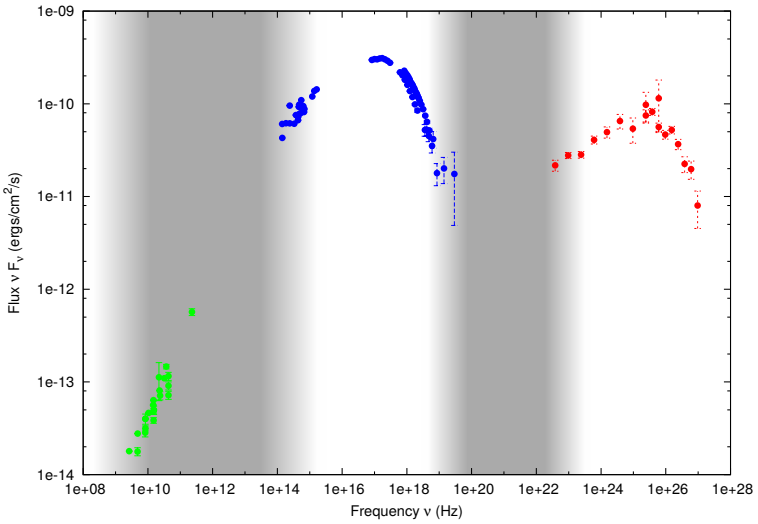

Figure 2: SED of Mrk 421 measured in muti-wavelength campaigns including *Fermi* and MAGIC telescopes [2]. The green circles corresponds to the radio emission from an extended region of the jet. The blue and red circles denote synchrotron and SSC emission respectively. The shaded area corresponds to the most appropriate frequency band, in order to constrain $\gamma_{\rm min}$.

Importance of gamma-ray observations – The detection of BL Lac objects in γ-rays have been significantly increased after the launch of *Fermi*-LAT. The third catalog of AGN of *Fermi*-LAT [1] lists $\sim$ 600 BL Lac objects. Due to the relatively lower sensitivities of the current generation Cherenkov Telescopes, and the γ-γ attenuation from the Extragalactic Background Light (which is significant for high redshift sources; z $\gtrsim$ 0.5), the number of BL Lacs detected in the Very High Energy γ-ray (VHE) range is significantly lower ($\sim$ 50). However, the recent advancement in the simultaneous multi-wavelength campaigns on BL Lacs have significantly improved our understanding on the jet energetics.

The non-thermal emission parameters of blazars are inferred from the observational quantities, like the peak frequencies (together with their peak luminosities) of the synchrotron and inverse Compton peaks, spectral slopes, flux variability of the source etc. However, the spectral information at the rising part of the synchrotron or SSC peak is essential to constrain $\gamma_{\rm min}$. As a demonstration to the current observational scenario, we show an SED of Mrk 421 [2], averaged over the observations taken during the multi-frequency campaign from 2009 January 19 to 2009 June 1 . The shaded area corresponds to the frequency band to constrain $\gamma_{\rm min}$. Even though the rising part of the synchrotron peak falls at the radio band (in which, a wide coverage of observation is accessible), the emission at this frequency band is self absorbed, and significantly dominated by the emission from the extended region of the jet. That would in turn make the rising part of the SSC peak as the unique band to probe $\gamma_{\rm min}$.

Expected results with e-ASTROGAM – We compare the fitted SSC models for Mrk 421 [5] and Mrk 501 [4] with the sensitivity of e-ASTROGAM in Fig. 3 (right). The predicted flux of these sources in the e-ASTROGAM range show the feasibility of detection of such sources. In Fig. 3 (left) we show the behavior of SSC model curve as a function of $\gamma_{\rm min}$. It is very evident that the variation in $\gamma_{\rm min}$ clearly reflects in the frequency band of e-ASTROGAM. Hence, e-ASTROGAM observations, together with simultaneous multi-wavelength observation of optical to VHE instruments can provide a robust limit to the non-thermal emission parameters, especially $\gamma_{\rm min}$. This would in turn increase the precision of the current U_e/U_b estimations, in which the value of $\gamma_{\rm min}$ arbitrarily chosesn from $\sim$1 to 10^4 [5, 4, 8]. Hence, the observation of BL Lac objects using e-ASTROGAM will address the energetics of jets, which is one of the most fundamental questions on blazars.

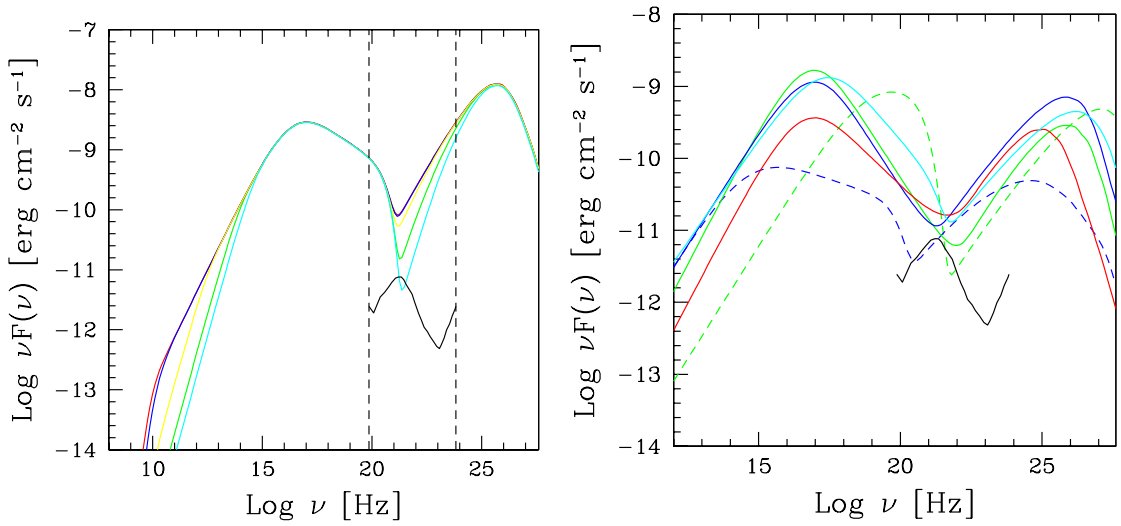

Figure 3: Left: SSC emission models produced by varying $\gamma_{\rm min}$, while keeping other emission parameters as constant. Red ($\gamma_{\rm min}$=1), blue ($\gamma_{\rm min}$=100), yellow ($\gamma_{\rm min}$=1000), green ($\gamma_{\rm min}$=5000), and cyan ($\gamma_{\rm min}$=10000) model curves show a significant difference at the e-ASTROGAM range (dashed vertical lines), and the radio region (where the emission from the extended region dominate). The black line corresponds to the sensitivity of e-ASTROGAM. Right: SSC model curves considering the SEDs of Mrk 501 (continuous line [4]) and Mrk 421 (dotted line [5]), which can be detected by e-ASTROGAM. The different colors indicate different activity levels.

References

[1] Ackerman M., et al., 2015, ApJ, 810, 14
[2] Ackerman M., et al., 2011, ApJ, 743, 171
[3] Kino, M., Takahara, F. & Kusunose, M., 2002, ApJ, 564, 97
[4] Mankuzhiyil N., et al., 2012, ApJ, 753, 2
[5] Mankuzhiyil N., et al., 2011, ApJ, 733, 1
[6] Maraschi L., Ghisellini G.& Celotti A., 1992, ApJ, 397, 5
[7] Tavecchio F. & Ghisellini G., 2016, MNRAS, 456, 3
[8] Tavecchio F., et al., 2010, MNRAS, 401, 1570

The physics of Gamma Ray Bursts through the polarized eyes of e-ASTROGAM

Tancredi Bernasconi,[1] *Merlin Kole,*[1] *Nicolas Produit,*[1] *Roland Walter,*[1] *Alexei Ulyanov,*[2] *Sheila McBreen,*[2] *Lorraine Hanlon,*[2] *Rui Curado da Silva*[3]

[1] *University of Geneva, Switzerland*
[2] *School of Physics, University College Dublin, Ireland*
[3] *LIP, Departamento de Física Universidade de Coimbra, P-3004-516 Coimbra, Portugal*

Science questions – Gamma Ray Bursts (GRBs) have been discovered in 1967 by the Vela satellites. BATSE detected several bursts per month and discovered that GRBs have different and highly structured light curves [1] and feature an isotropic distribution, indicating their extragalactic origin [2]. GRBs are the most luminous events in the Universe and the probable signature of the birth of black holes. They are classified in two categories, short (<2 seconds) and long. Long bursts are generally believed to be produced by the collapse of a massive star, while the short ones are linked to the merging of two compact objects like neutron stars. The latter are particularly interesting because of the link with the recent gravitational wave detections. GRBs have two distinct phases: the prompt and the afterglow. The prompt is an initial burst of high energy and is widely accepted to be generated by a jet forming during the gravitational collapse. The afterglow is a long-lasting multi-wavelength emission that occurs when the jet interacts with the ambient medium [3, 4]. The physical origin of the high-energy gamma rays during the prompt emission of GRBs is not yet understood.

Importance of gamma ray observations – e-ASTROGAM will be a very effective instrument to not only detect and localize GRBs, but also to measure their MeV-GeV characteristics and polarization in the prompt and after-glow phases. e-ASTROGAM will be able to study the evolution of the GRB spectral energy distribution, identify the various spectral components and their correlations, where GRBs have the peak of their luminosity. If the prompt emission originates from synchrotron emission of particles carried away from the central engine, variable moderate to high linear polarization is expected [5, 6] and several predictions have been made:

- The ordered-field model (SO) assumes that an helical magnetic field is advected from the central engine and producing a highly polarized emission. The emitted photons would not be uniformly polarized, as there would be patches of different polarization over the emitting shell. Such patches would produce a polarization angle variable over time when they emit in the line of sight [7, 8, 9].

- The random-field model (SR) suggests that collisionless shocks formed in the jet can produce sizable magnetic fields with random directions on plasma skin depth scales which in turn produce synchrotron emission and axisymmetric polarization angles along the line of sight. In this case, the polarization vectors will roughly cancel each-other out and the measured polarization will be small. On the other hand, if the viewing angle is off-axis, the polarization vectors do not fully cancel out and its amplitude will be between 30 and 50% depending on the Lorentz bulk factor [8, 10, 9].

- The synchrotron model with random fields on hydrodynamic scales (SH) is very similar to the previous model except that the depth of the shock exceeds the skin depth scale. In this case, the overall polarization will remain small [11, 12].

Alternatively the gamma-rays could be emitted radiatively from a photosphere (photospheric model) where they are beamed towards the expansion direction. As the polarization is produced by the last inverse Compton scattering the linear polarization degree is correlated with the luminosity and the level of photon anisotropy. The maximal polarization degree predicted by this model is 40% [13, 12]. Other models [14] predict that the high-energy photons are emitted by inverse Compton scattering of the prompt MeV radiation in a thermal plasma behind the forward shock with time delays, strength and spectral shape depending on the surrounding wind density.

All these models can produce very similar signatures of individual GRBs and a single observation is not enough to rule out any model. However from the correlation of the polarization degree and angle with other parameters, such as the peak energy, the physics at play can be deduced.

Finally, quantum gravity allows Lorentz invariance violation, which could be searched for using time-delays and polarization changes in the MeV range [12, 15].

Expected results with e-ASTROGAM – e-ASTROGAM will detect a large fraction of the GRBs and study them over the full energy range covering the prompt emission with excellent timing and energy resolutions. For very bright GRBs, it will be possible to study the variability of the polarization during the prompt phase for the first time. Valuable information on the delay between GRBs and gravitational waves will be obtained as well as new limits for the Lorentz invariance violation over a very wide energy range.

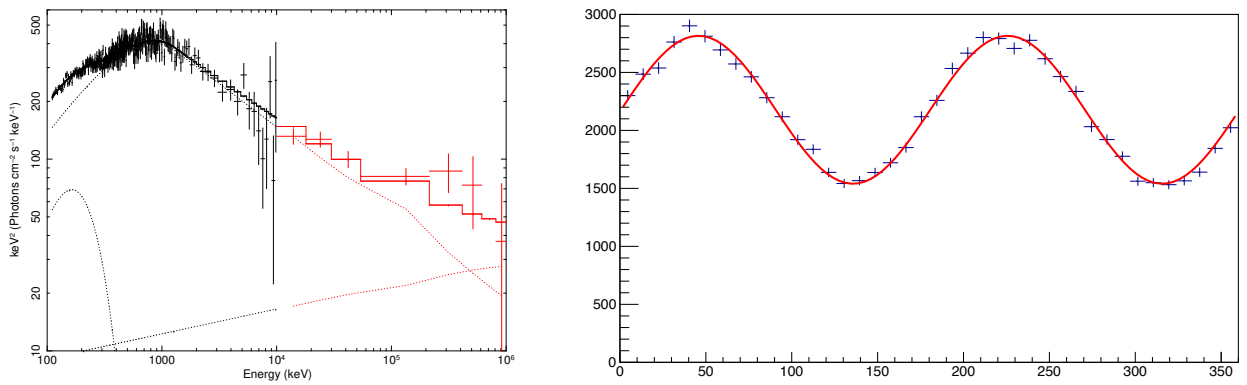

Figure 1: e-Astrogam spectra (left) and 0.1-1 MeV photon modulation with polarization angle in degrees (right) expected for a 100% polarized GRB 080916C.

To fully demonstrate the capabilities of e-ASTROGAM, we modeled the expected spectrum of the bright GRB 080916C [16] as a black-body, Band function and cutoff power-law, see Figure 1. The minimum polarization which could be detected with a 99% confidence level [17] is

$$\mathrm{MDP} = \frac{4.29}{\mu_{100} R_{src}} \sqrt{\frac{R_{src} + R_{bg}}{T}} \tag{1}$$

where T is the burst duration, R_{src} and R_{bg} are the source and background count rates, and $\mu_{100} = 30\%$ is the modulation of the signal for a fully polarized GRB. For GRB 080916C, the MDP ranges from 4.67% (0.1-1 MeV) to 38.5% (1-10 MeV). Below 1 MeV, a measurement with MDP=10% can be obtained every 18 seconds, allowing to probe its variability during the prompt emission (70 sec in the case of 080916C). e-ASTROGAM is expected to detect approximately 10 GRBs per year with a fluence similar to that of 080916C while approximately 1 per year will be detected with a fluence more than 10 times higher.

To further characterize the expected performance of e-ASTROGAM in polarization measurements, we simulated GRBs at several different angles with respect to the telescope axis. For each off-axis angle, the azimuth scatter distribution observed for a polarized GRB was corrected for the asymmetry of the detector acceptance, using the azimuth scatter distribution obtained for an unpolarized source. As shown in Figure 2, polarization of bright bursts can be detected at very

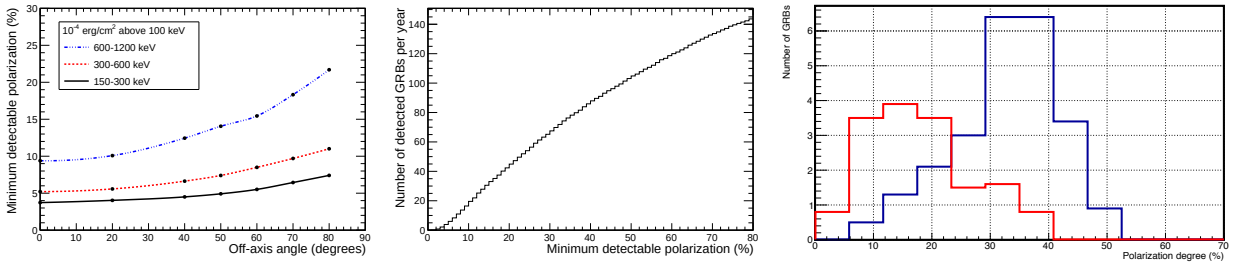

Figure 2: Left: Minimum polarization fraction detectable by e-ASTROGAM in three energy bands as a function of the off-axis angle. Centre: Cumulative number of GRBs to be detected by e-ASTROGAM as a function of the MDP. Right: Expected measured distribution of polarization degrees achieved using 1 year of data for the photospheric emission model (red) and the synchrotron with highly ordered magnetic field model (blue).

large off-axis angles. Here, the GRB emission spectrum was approximated by a Band function [19] with average GRB parameters of $\alpha = -1.1$, $\beta = -2.3$, and $E_{\rm peak} = 0.3\,{\rm MeV}$. The GRB duration was assumed to be 50 s.

The number of GRBs with polarization measurable with e-ASTROGAM was then estimated using the GRB fluences and durations from the Fourth BATSE GRB Catalog [20]. The central plot of Figure 2 indicates that e-ASTROGAM will be able to detect a polarization fraction as low as 20% in about 40 GRBs per year, and a polarization fraction of 10% will be detectable in ∼16 GRBs per year. The polarization distribution was finally established for two different models (right panel) to illustrate the model discrimination power of e-ASTROGAM.

References

[1] Marani G. F., Nemiroff R. J., Norris J. and al., 1997 Bull. American Astron. Society, 29, 839
[2] Metzger M. R., Djorgovski S. G., Kulkarni S. R. and al., 1997, Nature, 387, 878
[3] Gehrels N., 2004, American Institute of Physics Conference Series, 727, 637
[4] Mészáros P., 2006, Reports on Progress in Physics, 69, 2259
[5] Fan Y. Z., Wei D. M., Zhang B., 2004, MNRAS, 354, 1031
[6] Zhang B., Yan H., 2011, ApJ, 726, 90
[7] Lyutikov M., Pariev V. I. and Blandford R. D., 2003, ApJ, 597, 998
[8] Granot J., 2003, ApJ, 596, L17
[9] Toma K. and al., 2009, ApJ, 98, 1042
[10] Nakar E., Piran T. and Waxman E., 2003, J. Cosmology Astropart. Phys., 10, 005
[11] Inoue T., Shimoda J., Ohira Y. and Yamazaki R., 2013, ApJ, 772, L20
[12] Toma K., 2013, ArXiV
[13] Beloborodov A. M., 2011, ApJ, 737, 68
[14] Beloborodov A. M., Hascoët R. and Vurm I., 2014, ApJ, 788, 36
[15] Rybicki G. B., Lightman A.P., 1979, Radiative processes in astrophysics
[16] Guiriec s. et al., 2015, ApJ, 737, 68
[17] Weisskopf M. C., Elsner R. F. and O'Dell S. L., 2010, Proc. SPIE, 7732, 77320E
[18] Weisskopf M. C., Elsner R. F. and O'Dell S. L., 2010, Proc. SPIE, 7732, 77320E
[19] Band, D. et al., 1993, ApJ, 413, 281.
[20] Paciesas, W. S. et al., 1999, ApJS, 122, 465.

e-ASTROGAM contribution to the understanding of Gamma Ray Burst prompt emission

Giancarlo Ghirlanda[1,2], *Lara Nava*[1,3]

[1]*INAF - Osservatorio di Brera, via E. Bianchi 46, I-23807 Merate, Italy*
[2]*Dipartimento di Fisica G. Occhialini, Università di Milano Bicocca, Piazza della Scienza 3, I-20126 Milano, Italy*
[3]*INAF - Osservatorio Astronomico di Trieste, via G. B. Tiepolo 11, I-34143 Trieste, Italy*

Science questions – Since their discovery, Gamma-Ray Bursts (GRBs) have raised several questions about their origin and the nature of the physical mechanisms involved [20]. Both in long GRBs, produced by the core collapse of massive stars, and short GRBs, originating from the merger of two compact objects (NS–NS or NS–BH,), the central engine is most likely a compact object (BH or highly magnetized NS - magnetar) which is able to release (through neutrino and/or magnetic processes) a (isotropic equivalent) energy of 10^{52-54} erg within the short duration of 0.1-100 seconds in the form of high energy keV-MeV photons. This *prompt* emission phase is accompanied by a long lasting (days/months) fading emission (the *afterglow*).

Among the most compelling questions about GRBs is the nature of the prompt emission mechanism. Energised electrons (accelerated either by internal shocks or magnetic reconnection events) are expected to radiate via synchrotron emission [25, e.g.]. The apparent discrepancy between the observed keV–MeV spectral shape and the expected synchrotron spectrum [30, 11, 10, 33, 26, 18, 31] seems to find a possible solution in recently published results [28], supporting synchrotron radiation in a regime of moderately fast cooling. These recent findings are the results of an improved characterization of the low energy part of the prompt spectrum, namely below the νF_ν peak energy ~ 300 keV. *What remains highly unexplored is the shape of the high energy part of GRB prompt emission, i.e. in the 1 MeV – 100 MeV energy range.* Above the peak energy, the spectrum is expected to display a powerlaw shape $N(E) \propto E^\beta$, with photon index β directly related to the power-law index describing the energy spectrum of the emitting electrons.

The present knowledge of the prompt MeV energy range is mainly based on Fermi/GBM and Fermi/LAT observations. The Fermi/GBM with the BGO detectors extends nominally to 40 MeV, but the reduced effective area at such energies prevented a detailed study of the prompt emission high energy spectral tail. Fig.1 shows the spectral index β of the high energy powerlaw (obtained from the Fermi/GBM spectral catalog - Gruber et al. 2014[1]) versus its uncertainty. $\sim$25% of the population has a poorly constrainted β (rightward of the green line). Clear cutoff have been detected in a few cases by the LAT, sensitive down to $\sim$30 MeV. [32] reported the existence of two remarkable cases (GRB 100724B and GRB 160509A) where the combined GBM-LAT data show that the prompt keV–MeV spectrum has an evident softening (located at 20–60 MeV and 80–150 MeV, respectively), well modelled by an exponential cutoff. These detections led to estimated Lorentz factors in the range $\Gamma = 100 - 300$ for both GRBs. In other cases, the presence of a cutoff has been inferred after comparing the powerlaw extrapolation of the GBM spectrum with the lack of detection by the LAT. Using this method, [5] were able to infer the presence of a cutoff only in six cases out of a sample of 288 GRBs, deriving Lorentz factors in the range ~ 200 to ~ 600.

Beside the prompt emission, there is another spectral component contributing to the emission at energies above 10-50 MeV. The presence of this additional component was first identified by EGRET (e.g. Gonzales et al. 2004) and later confirmed by the Agile/GRID [16, 9, 24, 17] and by the Fermi/LAT (20 MeV–300 GeV) [4, 6, 3, 2, 1]. The LAT is detecting GRBs at an approximate rate of 14 yr^{-1} [2]. In most cases, however, the high-energy emission lasts much longer ($\gtrsim$ a factor

[1]https://heasarc.gsfc.nasa.gov/W3Browse/fermi/fermigbrst.html
[2]http://fermi.gsfc.nasa.gov/ssc/observations/types/grbs/lat_grbs/table.php

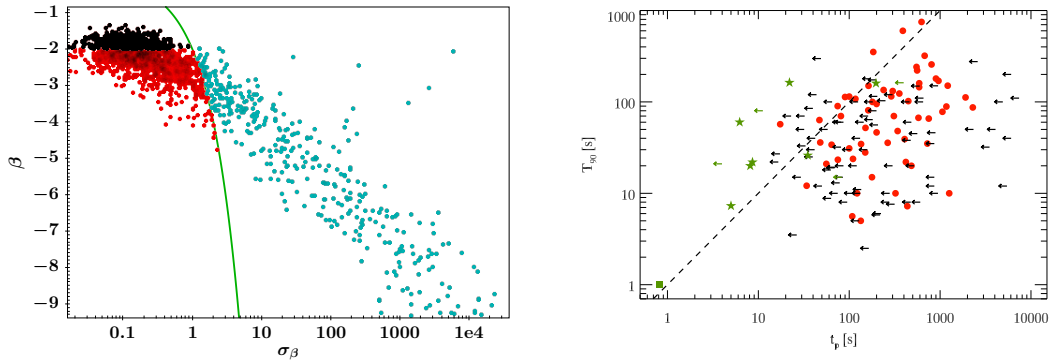

Figure 1: Left: high energy powerlaw spectral index β ($N(E) \propto E^{\beta}$) versus its relative uncertainty for the population of Fermi GRBst. The green line separates (leftward) GRBs with well constrained β (75% of the Fermi population) from (rightward) the GRBs with unconstrained β (25&). Right: GRB duration versus time of the fireball deceleration ($t_{\rm p}$) both measured in the observer frame (Figure from Ghirlanda et al. 2017). Green symbols show the GRBs detected by LAT.

10) than the prompt, its onset is delayed by few seconds, and its spectrum is generally harder than the extrapolation of the keV–MeV component [14, 29]. This component is successfully interpreted as synchrotron emission from external shocks [14, 19] or Inverse Compton [7].

The MeV–GeV luminosity after the deceleration time (i.e., after the peak) has been proven to be a robust proxy for the total energy content of the fireball, and has been used to constrain the efficiency of external shocks in accelerating electrons, the strength and configuration of the magnetic field, and the efficiency of the prompt dissipation mechanism [21, 27, 8].

Importance of gamma ray observations – An improved study of the spectrum at MeV-GeV energies would reveal fundamental properties of mildly relativistic shocks, and/or acceleration in magnetic reconnection. The physics of both these acceleration processes is poorly known. The high energy powerlaw behaviour is expected to break at energies where $\gamma - \gamma$ absorption within the source becomes relevant, producing a cutoff in the high energy part of the spectrum. The exact location of the cutoff depends on the value of the bulk Lorentz factor. The detection (or the lack) of this feature can then be used to estimate (or place constraints on) the bulk Lorentz factor.

The afterglow component produces a peak in the light curve when the outflow, engulfed by the interstellar material, is substantially decelerated. This peak, observed also in MeV–GeV lightcurves, allows a direct estimate of the bulk velocity before the deceleration (i.e. the maximum velocity attained during the fireball expansion). This is a fundamental and poorly constrained parameter for the modeling of GRB emission (i.e. relativistic beaming plays a major role in GRBs). The largest Γ_0 have been measured, so far, through the peak of the GeV light curve of Fermi/LAT GRBs [12, 13, 23, 22].

Disentangling between the two emission components (prompt and afterglow) that partially overlap in time is fundamental in order to understand the shape of the high energy part of the prompt spectrum and the properties of the high energy synchrotron afterglow spectrum. Observations in the 10 MeV–1 GeV range are fundamental to achieve this goal.

Expected results with e-ASTROGAM – e-ASTROGAM is going to cover a poorly explored energy range of the emission spectrum of GRBs, that receives contribution both from the prompt and from the afterglow emission. Presently, the 0.3 MeV – 100 MeV prompt emission phase of GRBs is characterized mostly through the GBM on board Fermi but only for the brightest events. Key questions that e-ASTROGAM will answer through systematic studies of larger samples of GRBs will be (a) whether the high energy prompt emission spectrum is a powerlaw or has a cutoff; (b) how it evolves in time (softening or hardening). These data will provide unique opportunities to study the properties of the electron distribution (shedding light on the acceleration mechanism) and

the effect of $\gamma - \gamma$ internal absorption (shedding light on the dynamics of the outflow). Moreover, e-ASTROGAM will allow to (c) disentangle the high energy tail of the prompt emission from the afterglow component, (d) measure the delay time with respect to the prompt keV–MeV component, (e) estimate the luminosity of the afterglow components. This will allow us to estimate the highest bulk Lorentz factors in long and (for the first time systematically) in short GRBs, the properties of ultra-relativistic shocks (particle acceleration efficiency, magnetic field amplification and decay), the fireball energy content during the afterglow phase and (from the comparison with the prompt radiated energy) and the efficiency of the prompt mechanism.

References

[1] Abdo, A. A., Ackermann, M., Ajello, M., et al., 2009, ApJL, 706, L138
[2] Abdo, A. A., Ackermann, M., Arimoto, M., et al. 2009, Science, 323, 1688
[3] Ackermann, M. & Ajello, e. a. 2010, ApJL, 717, L127
[4] Ackermann, M., Ajello, M., Asano, K., et al. 2014, Science, 343, 42
[5] Ackermann, M., Ajello, M., Baldini, L., et al. 2012, ApJ, 754, 121
[6] Ackermann, M., Asano, K., Atwood, W. B., et al. 2010, ApJ, 716, 1178
[7] Beloborodov, A. M., Hascoët, R., & Vurm, I. 2014, ApJ, 788, 36
[8] Beniamini, P., Nava, L., Duran, R. B., & Piran, T. 2015, MNRAS, 454, 1073
[9] Del Monte, E., Barbiellini, G., Donnarumma, I., et al. 2011, A&A, 535, A120
[10] Frontera, F., Guidorzi, C., Montanari, E., et al. 2009, ApJS, 180, 192
[11] Ghirlanda, G., Celotti, A., & Ghisellini, G. 2003, A&A, 406, 879
[12] Ghirlanda, G., Ghisellini, G., & Nava, L. 2010, A&A, 510, L7
[13] Ghirlanda, G., Nava, L., Ghisellini, G., et al. 2012, MNRAS, 420, 483
[14] Ghisellini, G., Ghirlanda, G., Nava, L., & Celotti, A. 2010, MNRAS, 403, 926
[15] Ghirlanda, G., Nappo, F., Ghisellini, G., et al., 2017, A&A, in press.
[16] Giuliani, A., Fuschino, F., Vianello, G., et al. 2010, ApJL, 708, L84
[17] Giuliani, A., Mereghetti, S., Marisaldi, M., et al. 2014, ArXiv:1407.0238
[18] Goldstein, A., Burgess, J. M., Preece, R. D., et al. 2012, ApJS, 199, 19
[19] Kumar, P. & Barniol Duran, R. 2010, MNRAS, 409, 226
[20] Kumar, P. & Zhang, B. 2015, Physics Reports, 561, 1
[21] Lemoine, M., Li, Z., & Wang, X.-Y. 2013, MNRAS, 435, 3009
[22] Liang, E.-W., Li, L., Gao, H., et al. 2013, ApJ, 774, 13
[23] Liang, E.-W., Yi, S.-X., Zhang, J., et al. 2010, ApJ, 725, 2209
[24] Longo, F., Barbiellini, G., Del Monte, E., et al. 2011, ArXiv:1111.2040
[25] Meszaros, P. & Rees, M. J. 1993, ApJL, 418, L59
[26] Nava, L., Ghirlanda, G., Ghisellini, G., & Celotti, A. 2011, A&A, 530, A21
[27] Nava, L., Vianello, G., Omodei, N., et al. 2014, MNRAS, 443, 3578
[28] Oganesyan, G., Nava, L., Ghirlanda, G., & Celotti, A. 2017, ApJ, 846, 137
[29] Panaitescu, A. 2017, ApJ, 837, 13
[30] Preece, R. D., Briggs, M. S., Mallozzi, R. S., et al. 2000, ApJS, 126, 19
[31] Sakamoto, T., Barthelmy, S. D., Baumgartner, W. H., et al. 2011, ApJS, 195, 2
[32] Vianello, G., Gill, R., Granot, J., et al. 2017, ArXiv:1706.01481
[33] Vianello, G., Götz, D., & Mereghetti, S. 2009, A&A, 495, 1005

Cosmic rays interactions

Conveners: Andrei Bykov
Isabelle A. Grenier

Cosmic Rays and Supernova Remnants at MeV energies

Martina Cardillo [1], *Martin Pohl* [2], *Sarah Kaufmann* [3], *Omar Tibolla* [3]

[1] *INAF-IAPS, via Del Fosso del Cavaliere 100, Roma, Italy*
[2] *Institute of Physics and Astronomy, University of Potsdam, 14476 Potsdam, Germany*
[3] *Mesoamerican Center for Theoretical Physics (MCTP), Universidad Autonoma de Chiapas (UNACH), 29050 Tuxtla Gutierrez, Chiapas, Mexico*

Science questions Cosmic Rays are very high energy particles (mainly protons and nuclei) with an energy spectrum extended up to $E \sim 10^{20}$ eV and a Galactic component likely accelerated at the shocks of Supernova Remnants (SNRs) [9], persistent sources of nonthermal radiation that can be resolved in nearly all wavebands [17]. There is evidence of hadronic cosmic rays in middle-aged SNRs, based on their gamma-ray emission spectra, but it is unclear what fraction of these particles is freshly accelerated and not re-accelerated. Studying directly accelerated particles is fundamental for finding the sources of cosmic rays, and SNRs are ideal systems to observe on account of their persistence and resolvability. The insights on the micro-physics of particle acceleration can be extrapolated to other outflow systems, where the process operates as well, but observations as detailed as those of SNRs are not possible.

Consequently, here we highlight some aspects of inquiry with e-ASTROGAM:

1. Search for the direct proof of the presence of freshly accelerated (and not re-accelerated) cosmic rays in a SNR shocks through the detection of the "pion bump" in young sources;
2. Search for non-thermal bremsstrahlung from energetic electrons for correlating with radio synchrotron emission and determining environmental parameters such as the level of magnetic-field amplification driven by cosmic rays.
3. Search for nuclear de-excitation lines to infer the elemental composition of cosmic rays at their acceleration site and to determine the supernova environment that is most conducive to particle acceleration.
4. Measuring the extent of re-acceleration of Galactic cosmic rays at the shock fronts of SNRs and its impact on the elemental composition of cosmic rays at Earth.

Importance of gamma-ray observations – In the last decade AGILE and Fermi-LAT satellites detected for the first time gamma-ray emission below $E \sim 200$ MeV from two very bright SNRs, W44 and IC443 [10, 1, 5]. The measurement of the specific shape of the hadronic gamma-ray spectrum, the so-called "pion bump", was claimed to be direct proof of the acceleration of cosmic-ray nuclei at the shock of SNRs. The issue is not so simple though. First of all, the cosmic-ray spectra needed to reproduce the hadronic gamma-ray spectra from these remnants are far from those than one would expect on theoretical grounds [13], and active research targets the relation between the instantaneous particle spectra and that of cosmic rays released over the entire lifetime of the remnant [11]. Then, the two SNRs with confirmed pion bump are middle-aged ($t_{age} > 10^4$ yrs) and consequently have slow shocks with $v_{sh} \sim 100$ km/s [16]. The cosmic-ray acceleration efficiency is strictly correlated with shock velocity and should be low at shocks that slow. It may be that for older SNRs re-acceleration of pre-existing Galactic cosmic rays dominates over acceleration of low-energy particles [22, 12, 6] . As the composition of Galactic cosmic rays includes elements that are not abundant in the interstellar medium, a significant re-acceleration of cosmic rays would modify the required source abundances and would have strong impact on our understanding of the propagation history of cosmic rays in the Galaxy. We need spatially resolved studies of older SNRs with slow shocks to infer the role of cosmic-ray re-acceleration in late phases of SNR evolution, which require an excellent angular resolution and high continuum sensitivity.

Simulations suggest that re-acceleration of Galactic cosmic rays is at most a secondary process in young SNRs [20, 19, 14], and primary particles would dominate. The detection below 200 MeV

of bremsstrahlung from primary electrons would offer invaluable insights. A comparison of the bremsstrahlung flux with the radio synchrotron emission of the same electrons provides a direct measure of the strength of the turbulently amplified magnetic field [7], arguably the most critical ingredient in particle acceleration theory [4]. This measurement would also remove the degeneracy in the interpretation of TeV-band gamma-ray emission. At the same time, we could measure the electron/ion ratio in cosmic rays at the source, which would significantly advance our understanding of the injection processes into diffusive shock acceleration. It is evident that an improved low-energy sensitivity would also be very useful for the study of young SNRs.

Several de-excitation lines will be visible in e-ASTROGAM energy range. Supernovae often expand into enriched material provided by the progenitor wind or nearby earlier supernovae. Heavy elements among the accelerated particles and in the ambient medium will collide and eventually radiate nuclear de-excitation lines that are characteristic of the element, thus allowing abundance tomography. From the quasi-spontaneously de-excitation, unique features arise due to C and O lines in the 4-6 MeV band, while the lines induced by the Ne-Fe group will dominate in the 1-3 MeV band. For the historic SNR Cas A we can estimate the line flux in the 4.4 MeV line from ^{12}C and use that as a proxy for all the other lines. This particular supernova expands into the wind zone of a red supergiant that is not rich in heavy elements, and so it is particle acceleration at the reverse shock running into the ejecta of the supernova explosion that provides a detectable line flux on the order 10^{-10} erg/cm^2/s, which is well above the sensitivity limit of e-ASTROGAM.

Combined with isotopic abundance measurements performed near Earth, in particular those of unstable isotopes such as ^{60}Fe [2], line observations provide direct insight into the environment in which cosmic rays are accelerated. A high energy resolution is needed for studies of nuclear de-excitation lines.

Expected results with e-ASTROGAM – It is easy to understand the importance of an instrument like e-ASTROGAM. Its sensitivity in the range $0.3-100$ MeV will be one to two orders of magnitude better than that of previous instruments [8]. As shown in Fig. 1, e-ASTROGAM should detect many SNRs within one year of operation. The angular resolution offered by e-ASTROGAM is unprecedented, reaching 0.15 degrees at 1 GeV [8], which will be decisive for resolving sources and avoiding source confusion in the galactic plane.

The expected results with e-ASTROGAM include:

1. Observation of gamma-ray emission below 200 MeV from known young SNRs, like Cas A or Tycho, and from yet undetected young SNRs, that is expected to come from freshly accelerated cosmic rays on account of the high shock speed in these sources.
2. Measurement of electron bremsstrahlung below 100 MeV from a number of SNRs. For a magnetic-field strength of 250 μG, we expect a bremsstrahlung flux from Cas A of $EF(E) \simeq 10^{-11}$ erg cm^{-2} s^{-1}, which is more than twice the one-year sensitivity level of e-ASTROGAM. This measurement would be decisive in determining the magnetic-field strength and in the separation of leptonic and hadronic contributions to the gamma-ray emission.
3. Detection of nuclear de-excitation lines from a number of SNRs. Indicates that in particular the carbon and oxygen lines from Cas A should stand out clearly and would likely constitute one of the early breakthrough results with e-ASTROGAM. Moreover, we will be able to measure element abundances by studying line ratios. In fact, with e-ASTROGAM data we may derive the spallation rate of heavy nuclei measuring their impact on the abundance of lighter elements and providing a new estimate of their primordial abundances.
4. Distinction of the gamma-ray emission from the remnant from that of nearby molecular clouds that are illuminated with freshly accelerated cosmic rays. For older SNRs such as W44 or IC443 this measurement will permit the study of re-acceleration of existing cosmic rays which, if efficient, would revolutionize our understanding of cosmic-ray physics and would also have an impact on indirect searches for dark matter using cosmic-ray annihilation products.

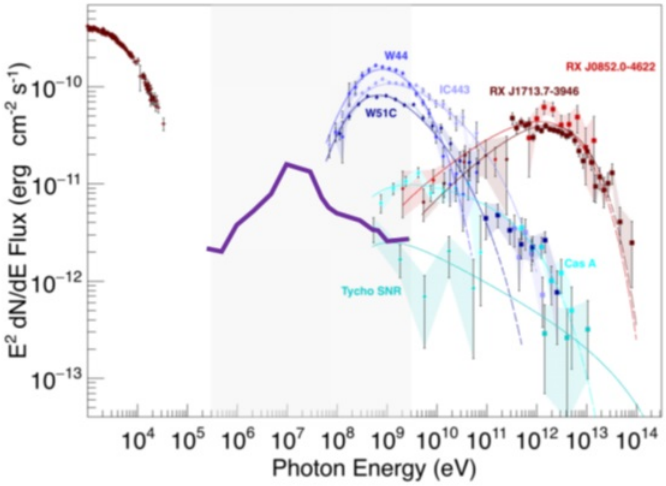

Figure 1: e-ASTROGAM sensitivity for 1-year exposure (thick purple line) compared to typical gamma-ray energy spectra for several SNRs; young SNRs (<1000 years) are shown in green [8].

References

[1] Ackermann, M., Ajello, M., Allafort, A. et al. 2013, Science, 339, 807-811 (A13)

[2] Binns, W. R., Israel, M. H., Christian, E. R., et al. 2016, Science, 352, 677

[3] Blandford, R. D. & Cowie, L. L. 1982, ApJ, 260, 625

[4] Blandford, R., & Eichler, D. 1987, Phys. Rep., 154, 1

[5] Cardillo, M., Tavani, M., Giuliani, A. et al. 2014, A&A, 565, 74

[6] Cardillo M., Amato, E. & Blasi, P. 2016, A&A, 595, 58C

[7] Cowsik, R., & Sarkar, S. 1980, MNRAS, 191, 855

[8] De Angelis, A., Tatischeff, V., Tavani, M., Oberlack, U., Grenier, Isabelle A. & et al. 2016, arXiv:1611.02232D

[9] Ginzburg, V. L. & Syrovatsky, S.I. 1961, Prog. Theor. Phys. Suppl.,20, 1.

[10] Giuliani, A., Cardillo, M., Tavani, M., et al. 2011, Astrophys. J. 742, 30-34

[11] Hanusch, A., Liseykina, T., & Malkov, M. 2017, arXiv:1707.02744

[12] Lee, S., Patnaude, D. J., Raymond, J., C. et al. 2015, ApJ, 806, 71

[13] Malkov, M. A., Diamond, P. H., & Sagdeev, R. Z. 2011, Nature Communications, 2, 194

[14] Pohl, M., Wilhelm, A., & Telezhinsky, I. 2015, A&A, 574, A43

[15] Ramaty, R., Kozlovsky, B., & Lingenfelter, R. E. 1975, SpSRv, 18, 341

[16] Reach, W.T. & Rho, J. 2000, AJ, 544, 843-858

[17] Reynolds, S. P. 2008, Ann. Rev. A&A, 46, 89

[18] Summa, A., Elsässer, D., & Mannheim, K. 2011, A&A, 533, A13

[19] Telezhinsky, I., Dwarkadas, V. V., & Pohl, M. 2013, A&A, 552, A102

[20] Telezhinsky, I., Dwarkadas, V. V., & Pohl, M. 2012, Astroparticle Physics, 35, 300

[21] Tibolla, O., Mannheim, K., Paravac, A., Greiner, J., & Kanbach, G. 2011, Nuovo Cimento C Geophysics Space Physics C, 34, 41

[22] Uchiyama, Y., Blandford, R. D., Funk, S. et al. 2010, ApJ, 723, 122

Cosmic rays acceleration in stellar winds

Ronald Walter, Matteo Balbo

Department of Astronomy, University of Geneva, Switzerland

Science questions – Diffusion of galactic cosmic-rays leads to particle energy densities dominating the pressure in the central regions of galaxies. This pressure might be sufficient to generate galactic winds and central outflows [1, 2]. These galactic cosmic-rays are likely produced through Fermi acceleration processed in supernova remnant shocks and in other exotic sources. Identifying the different contributors to cosmic ray acceleration in galaxies is fundamental to understand galactic processes, how Fermi acceleration works in various environments, and the feed-back between cosmic-rays acceleration, galactic magnetic fields and the dynamics of the interstellar medium. γ-ray observation are particularly enlightening as they are the main signature of particle acceleration, free of the pollution from thermal processes. Variable sources are the most interesting as the correlated observations in various energy bands provide key signatures of the physical processes at play and allow to understand how particle acceleration takes place and the luminosity of the source in the different particle species.

Importance of gamma-ray observations – η Carinae is the most luminous massive binary system of our galaxy and the first one to have been detected at very high energies, without hosting a compact object. The relative separation of the two stars varies by a factor ~ 20, reaching its minimum at periastron, when the two objects pass within a few AU of each other (the radius of the primary star is estimated as 0.5 AU). In these extreme conditions their supersonic winds interact forming a colliding wind region of hot shocked gas where charged particles can be accelerated via diffusive shock acceleration up to high energies. [3] have analysed the Fermi LAT data of η Carinae. (Fig. 1). The 10-300 GeV flux peaked during the 2005 periastron, decreased slightly towards apastron and did not increase again during the 2014 periastron. Instead the 0.3-10 GeV flux varied similarly for the two periastrons and, when combined, a higher resolution lightcurve could be obtained. To estimate the expected non thermal emission They also calculated the maximum energies that could be reached by electrons and hadrons in every cells of the hydrodynamic simulations presented by [4], assuming a dipolar magnetic field at the surface of the primary star. As expected, most of the shock power is released on both sides of the wind collision zone and in the cells downstream of the wind-collision region [5]. The photon-photon opacity could also be estimated as $< 10^{-2}$, excluding a significant effect on the observed GeV spectrum.

Electron cooling, through inverse-Compton scattering, is very efficient and the corresponding γ-rays are expected to peak just before periastron. A secondary inverse-Compton peak could be expected above phase 1.05 although its spectral shape could be very different as the UV seed thermal photons will have lower density when compared to the location of the primary shock close to the center of the system. The situation is different for hadrons. Unless the magnetic field would be very strong ($>$ kG) hadronic interactions mostly take place close to the center and a single peak of neutral pion decay is expected before periastron.

Figure 1 shows the X and γ-ray lightcurves predicted by the simulations for a magnetic field of 500 G and assuming that 1.5% and 2.4% of the mechanical energy is used to respectively accelerate electrons and protons. To ease the comparison between observations and simulations, the results of the latter were binned in the same way as the observed data. Both the predicted inverse-Compton emission and the observed (0.3-10 GeV) LAT lightcurve show a broad peak extending on both sides of periastron, as expected from the evolving shock geometry. The combined lightcurve is very similar to the prediction of the simulation for the inverse-Compton luminosity. The only notable exception is that the observed second broad peak is slightly shifted towards earlier phases and has a lower luminosity when compared to the simulation. The phase difference could be related to the

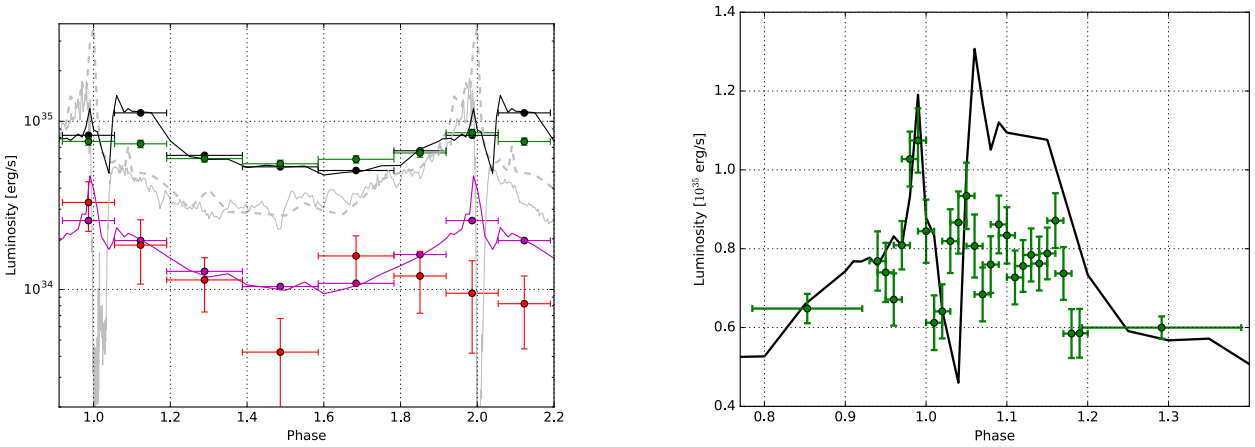

Figure 1: Left: Simulated and observed X-ray and γ-ray lightcurves of η Carinae. The black and purple lines and bins show the predicted inverse-Compton and neutral pion decay lightcurves. The green and red points show the observed Fermi-LAT lightcurves at low (0.3-10 GeV) and high (10-300 GeV) energies. The dim grey lightcurves show the observed (continuous) and predicted (dash, without obscuration) thermal X-ray lightcurves. Right: A merged Fermi LAT analysis (0.3-10 GeV) of the two periastrons for narrower time bins.

eccentricity ($\epsilon = 0.9$) assumed in the simulation, which is not well constrained observationally [6, 7] and that has an important effect on the inner shock geometry.

The distribution of γ_e, weighted by the emissivity, is relatively smooth and the expected photon distribution is very smooth. The difference of the electron spectral shape on both sides of the wind collision zone cannot explain the two components of the γ-ray emission as suggested by [8]. The simulated pion induced γ-ray lightcurve show a single peak of emission centred at periastron, in good agreement with the observations of the first periastron. The results of the observations of the second periastron are different. It has been suggested that the change of the X-ray emission after that periastron was the signature of a change of the wind geometry, possibly because of cooling instabilities. A stronger disruption or clumpier wind after the second periastron could perhaps induce a decrease of the average wind density and explain that less hadronic interactions and less thermal emission took place, without affecting much inverse-Compton emission. Hadrons could be accelerated up to 10^{15} eV around periastron and reach 10^{14} eV on average. η Carinae can therefore probably accelerate particles close to the knee of the cosmic-ray spectrum.

γ-ray observations can probe the magnetic field and shock acceleration in details, however the quality of the current data below 100 MeV and above 1 GeV does not yet provide enough information to test hydrodynamical models including detailed radiation transfer (inverse-Compton, pion emission, photo-absorption). More sensitive γ-ray observations will provide a wealth of information and allow to test the conditions and the physics of the shocks at a high level of details, making of η Carinae a perfect laboratory to study particle acceleration in wind collisions. η Carinae could yield to 10^{48-49} erg of cosmic-ray acceleration, a number close to the expectation for an average supernova remnant [9].

Expected results with e-ASTROGAM – The spectral energy distribution of η Carinae features an excess of emission at hard X-rays, beyond the extrapolation of the thermal emission [10] that should connect to the Fermi spectrum in a yet unknown manner. In the above section we have presented a model where electrons and protons are accelerated (as initially proposed by [11]). The fraction of the shock mechanical luminosity accelerating electrons appears to be slightly smaller than the one that accelerates protons. These results contrast with the efficiencies derived from the latest particle-in-cell simulations [12], involving low magnetic fields, radiation and particle densities and favouring hadronic acceleration in the context of SNR. Purely hadronic acceleration has been proposed [13] to explain the GeV spectrum of η Carinae. In that case the two spectral components are related to the different hadron interaction times observed on the two sides of the wind sepa-

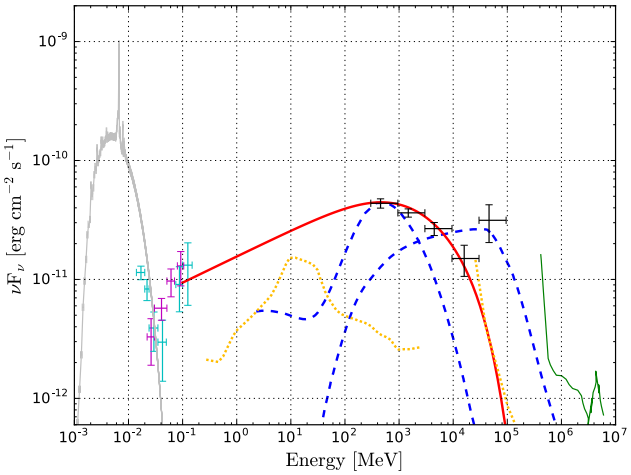

Figure 2: Spectral energy distribution of η Carinae from 1 keV to 10 GeV. The data are from NuStar (grey), Swift/BAT (cyan), INTEGRAL (purple), Fermi/LAT (black) and the upper limits from HESS (green). The predictions are from mostly hadronic (dashed blue line) and lepto-hadronic (red line for the leptonic part) models. The sensitivity curves of e-Astrogam (in the galactic plane) and CTA are also indicated (dotted yellow lines).

ration surface, largely because of the contrast in density and magnetic field. In our simulations this effect is smoothed by the many zones of the model, each characterized by different conditions. Even if the shock on the companion side does contribute more at high energies, the resulting pion decay spectrum does not feature two distinct components. e-Astrogam [14] will easily discriminate between the lepto-hadronic and the hadronic models for the gamma-ray emission as the inverse Compton leptonic emission of the former would be much stronger than predicted by the latter (Fig. 2). e-Astrogam can therefore decide which is the model likely to explain the high energy emission of Eta Carinae and strongly constrain the acceleration physics (through the hadronic over leptonic luminosity ratio) in more extreme conditions than found in SNR.

References

[1] Pakmor, R., Pfrommer, C., Simpson, C. M., and Springel, V., ApJ**824** (2016) L30.
[2] Simpson, C. M. et al., ApJ**827** (2016) L29.
[3] Balbo, M. and Walter, R., ArXiv e-prints (2017).
[4] Parkin, E. R., Pittard, J. M., Corcoran, M. F., and Hamaguchi, K., ApJ**726** (2011) 105.
[5] Reimer, A., Pohl, M., and Reimer, O., ApJ**644** (2006) 1118.
[6] Damineli, A. et al., ApJ**528** (2000) L101.
[7] Corcoran, M. F., Ishibashi, K., Swank, J. H., and Petre, R., ApJ**547** (2001) 1034.
[8] Bednarek, W. and Pabich, J., A&A**530** (2011) A49.
[9] Becker Tjus, J., Eichmann, B., Kroll, M., and Nierstenhöfer, N., Astroparticle Physics **81** (2016) 1.
[10] Panagiotou, C. and Walter, R., A&A (2017) in preparation.
[11] Eichler, D. and Usov, V., ApJ**402** (1993) 271.
[12] Park, J., Caprioli, D., and Spitkovsky, A., Physical Review Letters **114** (2015) 085003.
[13] Ohm, S., Zabalza, V., Hinton, J. A., and Parkin, E. R., MNRAS**449** (2015) L132.
[14] De Angelis, A. et al., Experimental Astronomy (2017).

Cosmic-ray production in star-forming regions

Isabelle A. Grenier [1], *Andrei Bykov* [2], *Elena Orlando* [3], *Andrew Strong* [4]

[1] *Laboratoire AIM, CEA-IRFU/CNRS/Université Paris Diderot, C.E.A. Saclay, France*
[2] *Ioffe Institute, St.Petersburg, Russia, 194021*
[3] *W.W. Hansen Experimental Physics Laboratory, Kavli Institute for Particle Astrophysics and Cosmology, Stanford University, Stanford, CA, 94305, USA*
[4] *Max Planck Institut für extraterrestrische Physik, D-85748 Garching, Germany*

Science questions – Understanding the complex interplay between stars, gas, and cosmic rays (CRs) in star-forming regions is of fundamental importance for astrophysics. Multi-wavelength studies of the highly obscured molecular clouds that actively form stars in the Galaxy together with studies of extreme examples of massive stellar clusters in the Large Magellanic cloud and in starburst galaxies have revealed a wealth of information on the physics of star formation and on the radiation impact of massive stars on their parent cloud. Yet, little is known about the activity of such sites in terms of CR production, nor on their ability to confine and modify Galactic CRs as they diffuse through those turbulent sites. Recent data have provided a wealth of details on local CRs, from direct spectral measurements in and near the heliosphere, to remote γ-ray observations in interstellar clouds within a few hundred parsecs [1]. Yet, we lack a global and resolved description of the CR distribution in the Milky Way and we don't know how much of an imprint star-forming regions leave on this distribution. This imprint must be significant, in spectrum and in composition. On the one hand, *Fermi LAT* observations have detected a cocoon of anomalously hard CRs in the Cygnus X superbubble that has been blown by multiple OB associations [2]. On the other hand, ACE abundance measurements of heavy CR nuclei indicate that 20% of the local CRs come from massive-star outflows and ejecta, the rest having been probably swept up from the interstellar medium (ISM) by the supernova shock waves that have accelerated them [3]. Massive stars are clustered in space and time, so are their massive supersonic winds and the ensuing core-collapse supernovae. Thus what happens to CRs freshly escaping from their accelerators? Are they confined for some time and potentially reaccelerated in the highly turbulent medium of star-forming regions? What impact do they have on the surrounding ISM? Our views on the diffusion properties of Galactic CRs have largely been inferred locally. Could they be significantly biased by our viewpoint inside the Local Bubble and the Gould Belt which is characterized by its numerous OB associations [4]? The recent detection of radioactive ^{60}Fe in the local CRs does imply that the time required for acceleration and transport to the Solar System does not greatly exceed 2.6 Myr and that the supernova source of ^{60}Fe lied within 1 kpc [5].

Importance of gamma-ray observations – Multiple powerful winds of early-type stars and supernova remnants were suggested as the favorable sites of CR acceleration in rich stellar clusters (see [6, 7] for review). The extended superbubbles are created by those winds and supernovae over a time scale of $\sim 10^7$ years. They are filled with hot X-ray emitting gas where numerous weak and strong shocks can amplify the turbulent magnetic fields. The efficiency of the ensemble of MHD shocks to transfer kinetic power to (re-)accelerate CRs may exceed 10%. This may result in a substantial temporal evolution of the CR spectra over 10 Myr. Non-linear modelling predicted the time-asymptotic spectra of CRs to be a power law with an index close to 2 in the MeV-TeV regime [8, 9]. This is consistent with the γ-ray spectrum observed in the Cygnus cocoon (shown in Fig. 1), assuming that the main radiation mechanism is due to the inelastic collisions of CR nuclei in the ambient gas and to the production of pions and γrays. The concomitant production of high-energy neutrinos was estimated to be large enough to be detected with the *IceCube Observatory* [10].

Gamma-ray observations provide key probes of the particle content of superbubbles, in relativistic nuclei and in high-energy electrons as they up-scatter the ambient radiation fields from the

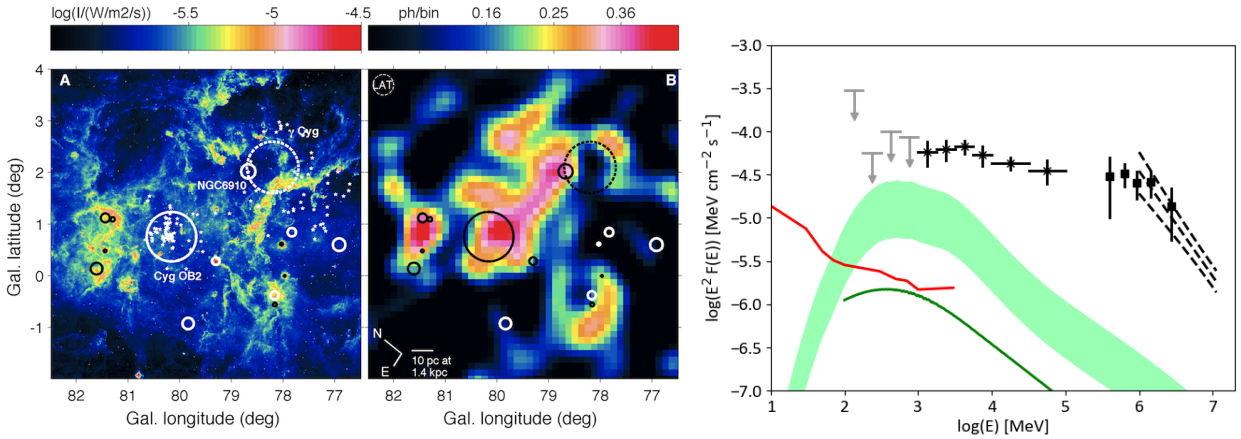

Figure 1: Left: 8 μm intensity map of the Cygnus X region from *MSX* showing the heated contours of the superbubble. OB stars (white stars), OB associations (white circles), and the supernova remnant γCygni (dashed circle) are overlaid [2]. Center: *Fermi-LAT* photon count map of the same region in the 10-100 GeV band. The 50-pc-wide excess coincident with the bubble signals a cocoon of freshly accelerated CRs [2]. Right: Energy spectrum of the Cygnus cocoon emission as detected by *Fermi LAT* (crosses), *ARGO-YBG* (squares), and MILAGRO (dashed lines). The curves show model expectations from Galactic CRs spreading the ionized gas (green band) or up-scattering the stellar and interstellar light fields (green curve). The sensitivity of *e-ASTROGAM* (red curve) is given for one year of effective exposure in the Galactic disc. Adapted from [1, 2].

stars and the ISM. X-ray observations can probe the diffuse synchrotron emission from the highest-energy (>TeV) electrons if they don't rapidly cool or escape the superbubble. The large magnetic fields ($\sim 20\mu$G in the Cygnus X cocoon [2]) yield detectable fluxes for the current X-ray telescopes, but the detection of diffuse non-thermal X rays is challenging toward these hot and complex regions and the small fields of view of the instruments are ill adapted. Gamma-ray observations are the only means to measure CR nuclei. While GeV-TeV observations inform us on the maximum CR energy and on the acceleration efficiency, observations below 1 GeV are essential to reveal the bulk of the CR population filling the bubble and to measure their diffusion lengths inside the bubble.

Expected results with e-ASTROGAM – The Cygnus X region, located at an estimated distance of 1.4 kpc [11], is a prime target for resolving details of the high-energy activity of superbubbles. The extended region, about 4° in size, contains several thousand OB stars and it holds a few million solar masses of gas for collisions with CR nuclei [2]. The flux of $(5.8 \pm 0.9) \times 10^{-8}$ γcm^{-2} s^{-1} detected from the hard cocoon in the 1 to 100 GeV band corresponds to a luminosity of $(9 \pm 2) \times 10^{34} (D/1.4\,\mathrm{pc})^2$ erg s^{-1} which is below one per cent of the kinetic power of the stellar winds in Cygnus OB2. Figure 1 shows that the cocoon emission is easily detectable by *e-ASTROGAM*. Yet, several other GeV and TeV sources have been found in this crowded direction as we look tangentially down the Local spiral Arm. One has been identified with the pulsar PSR J2032+4127 and its wind nebula, another with the extended γCygni supernova remnant and its associated pulsar PSR J2021+4026. The improved angular resolution of *e-ASTROGAM* will therefore be crucial to separate the diffuse cocoon emission from these sources and from the rest of the interstellar Galactic background. Spatial confusion prevented the cocoon detection below 1 GeV with *Fermi LAT*, despite its brightness. The performance of *e-ASTROGAM* will be key to reliably extend the cocoon spectrum below 1 GeV in order to estimate the energy distribution of the bulk of the CR nuclei, to estimate the CR pressure inside the bubble, to separate the emissions from CR electrons and nuclei, and to search for spectral variations across the bubble that would serve to test possible acceleration scenarios, by individual sources or by the collective action of wind and supernova shock waves. A refined morphology of the GeV cocoon will help capture its diffuse counterpart at TeV energies to study the cut-off energy of the particles since the extension of the cocoon spectrum beyond 100 GeV (shown in Figure 1) is still unclear in the latest data [12, 13].

Recently, an extended *Fermi LAT* source with a hard $E^{-2.1\pm0.2}$ spectrum toward G25.0+0.0 has been proposed as a possible second case of a γ-ray detection from a star-forming region in the Milky Way [14]. It may be associated with a candidate OB association G25.18+0.26, comparable to Cygnus OB2 in mass, but at a larger distance of 6 to 8 kpc. If so, the γ-ray luminosity would be about 10 times larger than that of the Cygnus cocoon, reflecting the 9 times larger volume and/or mass of the emitting region. There again, severe confusion limits the identification of the origin of the extended emission and the improved performance of *e-ASTROGAM* will open new avenues for studies.

Younger OB associations, where no supernova explosion has occurred yet, may also impart a fraction of the kinetic energy of their strong supersonic stellar winds to CR acceleration. Nearby OB associations, such as NGC 2244 in the Rosette nebula and NGC 1976 in the Orion nebula, have been proposed as test beds [15]. They can be detected by *e-ASTROGAM* below 3 GeV if a few per cent of the stellar-wind powers are supplied to CRs.

Despite the long observational and theoretical efforts to identify and study CR acceleration in supernova remnants, a number of fundamental questions remain unanswered about the acceleration efficiency and the time-dependent spectrum of the escaping particles. The detection of the high-energy activity of turbulent bubbles blown by stellar clusters adds another level of complexity between the individual CR sources and the large-scale distribution of CRs in the Galaxy. It needs to be addressed by resolving the MeV to TeV emission of active star-forming regions, by comparing them at different stages of evolution and for different cluster masses, and by uncovering new examples in the Galaxy (e.g. Westerlund 1 or 2) or in the Large Magellanic Cloud (e.g. 30 Doradus). An instrument such as *e-ASTROGAM*, in synergy with HAWC and CTA at TeV energies and with e-ROSITA in X rays, will be pivotal to make progress.

References

[1] I. A. Grenier, J. H. Black, and A. W. Strong, Annual Rev. Astron. Astroph. **53**, 199 (2015).
[2] M. Ackermann *et al.*, Science **334**, 1103 (2011).
[3] Murphy, R. P., Sasaki, M., Binns, W. R., et al., ApJ, 831, 148 (2016)
[4] Grenier, I. A., A&A, 364, L93 (2000)
[5] Binns, W. R., et al. APS April Meeting, abstract M4.009 (2017).
[6] C. J. Cesarsky and T. Montmerle, Space Science Reviews **36**, 173 (1983).
[7] A. M. Bykov, Astronomy Astrophys. Reviews, **22**, 77 (2014).
[8] A. M. Bykov, Space Science Reviews **99**, 317 (2001).
[9] G. Ferrand and A. Marcowith, Astron. Astroph. **510**, A101 (2010).
[10] T. M. Yoast-Hull *et al.*, Physical Rev. D, **96**, 043011 (2017).
[11] K. L. J. Rygl *et al.*, Astronomy Astrophys. **539**, A79 (2012).
[12] Bird, R., & for the VERITAS Collaboration 2017, arXiv:1708.04719.
[13] Hona, B., Robare, A., Fleischhack, H., Huentemeyer, P., & for the HAWC collaboration 2017, arXiv:1708.03575
[14] Katsuta, J., Uchiyama, Y., & Funk, S. 2017, ApJ, 839, 129
[15] Maurin, G., Marcowith, A., Komin, N., Krayzel, F., & Lamanna, G. 2016, A&A, 591, A71

Understanding the nature of gamma-ray emission of the *Fermi* bubbles with e-ASTROGAM

Dmitry Malyshev[1], *Anna Franckowiak*[2]

[1] *Erlangen Centre for Astroparticle Physics, Erwin-Rommel-Str. 1, Erlangen, Germany*
[2] *DESY, Platanenallee 6, D-15738, Zeuthen, Germany*

Science questions – The *Fermi* bubbles (FB) are one of the most spectacular and unexpected discoveries based on the *Fermi* LAT data [1, 2]. The FB extend to 55° above and below the Galactic center. Lobes in Seyfert galaxies have similar shape and size as the FB. The origin of lobes in these galaxies is attributed either to an emission from the supermassive black holes at the centers of the galaxies (AGN scenario) or a period of starburst activity which results in a combined wind from SNe explosions of massive stars (starburst scenario) [3]. The lobes in other galaxies are usually too distant to be resolved by gamma-ray telescopes. Thus, the study of the FB provides a unique opportunity to test, using gamma-ray data, predictions of computer simulations of the evolution of jets from supermassive black holes [4, 5], winds from supernova explosions, or CR-driven winds [6].

Although there exists a tentative association of the FB with the microwave haze at low latitudes and some features in X-ray data at low and at high latitudes [1], it is still an open question whether the microwave haze and the X-ray features are counterparts of the FB. As a result, the gamma-ray emission from the FB remains one of the main tools to study the properties and the origin of the bubbles.

Importance of gamma-ray observations – Gamma-ray emission at energies above a few tens of GeV can be produced either by inverse Compton (IC) scattering (leptonic scenario) or interactions of hadronic cosmic rays (CR) with gas (hadronic scenario). The two emission processes can be usually distinguished at energies below 100 MeV by a characteristic cutoff in the hadronic gamma-ray spectrum due to non-zero mass of the π^0 meson. In case of the FB, the secondary IC emission from electrons and positrons produced in hadronic interactions can dominate the spectrum below 100 MeV (Figure 1), which results in the absence of the π^0 cutoff [2]. In this case, one can try to separate the leptonic and hadronic scenarios of the gamma-ray emission using indirect signatures, such as the associated radio emission or the dependence of the gamma-ray spectrum on latitude. On the one hand, the microwave haze emission can be explained by the same population of electrons that produce the gamma-ray emission via IC scattering, which supports the leptonic origin of the gamma-ray emission [1, 2]. On the other hand, the absence of a softening of the gamma-ray emission as a function of latitudes is more naturally explained by the hadronic scenario (however, a hard spectrum of gamma rays at high latitudes in the leptonic scenario can be explained by re-acceleration of electrons [7]).

As one can see from Figure 1, it is very hard to distinguish the leptonic and the hadronic scenarios based on observations above 10 MeV. This is due to a contribution from the IC emission of the secondary electrons and positrons produced in the hadronic interactions. However, the secondary leptons have a spectrum that is softer by E^{-1} than the spectrum of the primary protons due to cooling. As a result, the secondary IC spectrum is softer than the primary IC spectrum in the leptonic scenario or the primary proton spectrum in the hadronic scenario. Below a few tens of MeV, the soft IC component dominates the gamma-ray emission in the hadronic scenario which results in a break in the gamma-ray spectrum around 30 MeV, while in the leptonic scenario the spectrum is expected to be featureless. The presence (absence) of the break can be used to confirm the hadronic (leptonic) scenario of the gamma-ray emission.

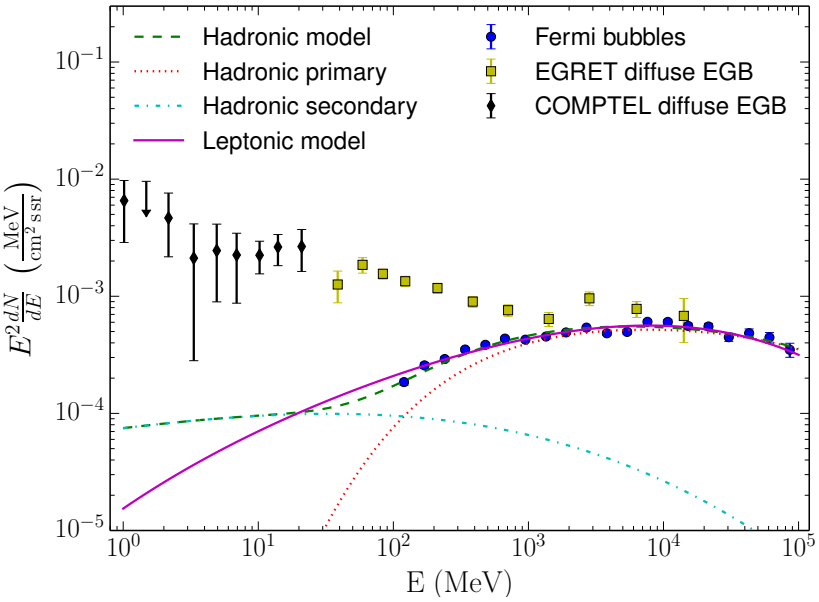

Figure 1: *Fermi* bubbles spectrum compared to the leptonic (solid purple line) and hadronic (dashed green line) models of the gamma-ray emission [2]. The hadronic model includes the primary emission (dotted red line) of gamma rays and the gamma rays produced in IC interactions of secondary electrons and positrons (dash-dotted cyan line). The secondary component of gamma-ray emission in the hadronic model is significantly softer than the primary component which results in a break around 30 MeV and a significant difference between the hadronic and leptonic models of gamma-ray emission around a few MeV. For comparison, we also plot the diffuse extragalactic gamma-ray background (EGB) fluxes measured by EGRET [8] and COMPTEL [9] experiments.

Expected results with e-ASTROGAM – The total gamma-ray flux in the hadronic model and the leptonic model are very similar to each other at energies above ~ 10 MeV (Figure 1). As a result, the two spectra are very difficult to distinguish with the existing gamma-ray data from *Fermi* LAT, especially if one takes into account modeling uncertainties. The difference between the two models becomes appreciable only at energies much smaller than 10 MeV, e.g., it is about a factor of 3 at 2 MeV.

In order to estimate the e-ASTROGAM sensitivity to distinguish the leptonic and hadronic models of gamma-ray emission in the FB, we estimate the signal to noise ratio at 2 MeV. The expected e-ASTROGAM effective area at this energy in the Compton regime is ≈ 117 cm^2 [13]. If we take into account that the effective coverage is expected to be about 23%, then the exposure after one year of observations can be estimated as $\approx 8.5 \times 10^8$ cm^2. The area of the bubbles is ≈ 1 sr [2]. For an energy bin with a width of 1 MeV, the number of signal counts around 2 MeV in the hadronic scenario after one year of observations is $\sim 3 \times 10^4$, while the number of background photons from the diffuse EGB is expected at a level of 10^6. Thus, the signal to noise ratio is expected to be at the level of 10 or more while the fractional signal is about 3%. Consequently, e-ASTROGAM will be sensitive to detect the difference between the leptonic and hadronic models of gamma-ray emission in the FB already after one year of observations. The main challenge will be to model the diffuse emission components at a few percent level.

References

[1] M. Su, T. R. Slatyer and D. P. Finkbeiner, Astrophys. J. **724**, 1044 (2010)
[2] M. Ackermann *et al.* [Fermi-LAT Collaboration], Astrophys. J. **793**, no. 1, 64 (2014)
[3] R. G. Sharp and J. Bland-Hawthorn, Astrophys. J. **711**, 818 (2010)
[4] F. Guo and W. G. Mathews, Astrophys. J. **756**, 181 (2012)
[5] H.-Y. K. Yang, M. Ruszkowski, P. M. Ricker, E. Zweibel and D. Lee, Astrophys. J. **761**, 185 (2012)

[6] J. Wiener, C. Pfrommer and P. Oh, Mon. Not. Roy. Astron. Soc. **467**, no. 1, 906 (2017)
[7] P. Mertsch and S. Sarkar, Phys. Rev. Lett. **107**, 091101 (2011)
[8] A. W. Strong, I. V. Moskalenko and O. Reimer, Astrophys. J. **613**, 956 (2004)
[9] G. Weidenspointner *et al.*, AIP Conf. Proc. **510**, 467 (2000) doi:10.1063/1.1307028
[10] A. De Angelis *et al.* [e-ASTROGAM Collaboration], Exper. Astron. **44**, no. 1, 25 (2017)

De-excitation nuclear gamma-ray line emission from low-energy cosmic rays

Vincent Tatischeff[1], *Jürgen Kiener*[1], *Isabelle A. Grenier*[2], *Andrew Strong*[3]

[1] *CSNSM, IN2P3-CNRS/Univ. Paris-Sud, Université Paris-Saclay, F-91405 Orsay Campus, France*
[2] *Laboratoire AIM, CEA-IRFU/CNRS/Université Paris Diderot, C.E.A. Saclay, France*
[3] *Max Planck Institut für extraterrestrische Physik, D-85748 Garching, Germany*

Science questions – Low-energy cosmic rays (LECRs) of kinetic energies $\lesssim 1$ GeV nucleon^{-1} are thought to be a major player in the process of star formation. They are a primary source of ionization of heavily shielded, dense molecular clouds and the resulting ionization fraction conditions the coupling of the gas with the ambient magnetic field in these regions. LECRs also represent an important source of heating that contribute to hold molecular cores in equilibrium against gravitational forces. In addition, LECRs play a central role in astrochemistry by iniating a rich ion-neutral chemistry within the cold neutral medium of the interstellar medium (ISM). Furthermore, LECRs are thought to drive large-scale magnetohydrodynamic turbulence and cause amplification of magnetic field in the ISM, and also provide critical pressure support in starburst regions to launch Galactic winds into the halo (see [7] and references therein).

Despite LECRs being thought to be a fundamental component of the ISM – the energy density of these nonthermal particles is estimated to be comparable to that of the interstellar gas, magnetic field and stellar radiation – their composition and flux are poorly known. The *Voyager 1* spacecraft has recently provided valuable measurements of the local interstellar energy spectra of Galactic CR nuclei down to 3 MeV nucleon^{-1} and electrons down to 2.7 MeV nucleon^{-1} beyond the heliopause (LECRs cannot be detected in the solar system near Earth due to the solar modulation effect). But the total CR ionization rate of atomic hydrogen resulting from the measured spectra, $\zeta_{\rm H} = (1.51 - 1.64) \times 10^{-17}$ s^{-1}, is a factor > 10 lower than the average CR ionization rate measured in diffuse interstellar clouds using astrochemistry methods, $\zeta_{\rm H} = 1.78 \times 10^{-16}$ s^{-1} [11] (see also [13]), suggesting that LECRs are relatively less abundant in the local ISM than elsewhere in the Galaxy. Observations of H_3^+ in diffuse molecular clouds show indeed that the density of LECRs can strongly vary from one region to another in the Galactic disk, and, in particular, it can be significantly higher than the average value in diffuse molecular gas residing near a site of CR acceleration such as a supernova remnant (SNR) [9, 10]. Measurements of the DCO^+/HCO^+ abundance ratio have shown that the CR ionization rate can also be very high ($\gtrsim 100$ times the standard value) in dense molecular clouds close to SNRS [5, 20].

Various astrophysical sources could produce significant amounts of LECRs in the Galaxy besides supernova remnants (SNRs), e.g., OB associations [12, 14], compact objects such as microquasars [8], and normal stars producing astropheric anomalous CRs [16]. The observed quasi-linear increase of the Be abundances measured in stellar atmospheres with the star metallicity provides an independent argument for the existence of a significant component of LECR nuclei in the Galaxy, in addition to the standard CRs thought to be produced by diffusive shock acceleration in SNRs (see [19] and references therein). Obviously, our knowledge of the production pathways and transport properties of LECRs in our Galaxy is very rudimentary.

Importance of gamma-ray observations – MeV gamma-ray astronomy is the only direct way of studying the various effects of sub-GeV hadronic CRs in the ISM. In the GeV range, the diffuse Galactic emission is dominated by π^0-decay gamma-rays from the interaction of CR nuclei (mostly protons) with interstellar matter, and observations in this domain probe CR spectra above about 1 GeV per nucleon only. Nevertheless, *Fermi*-LAT observations of the diffuse Galactic

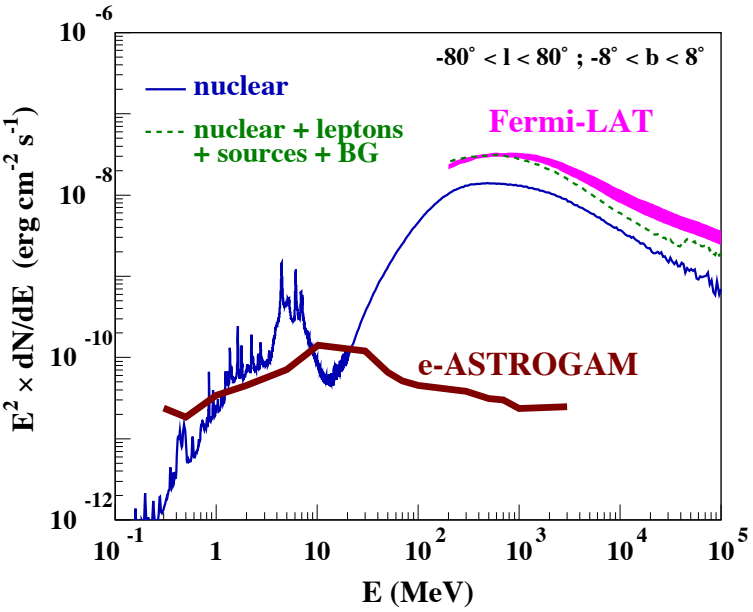

Figure 1: Predicted gamma-ray emission due to nuclear interactions of CRs in the inner Galaxy (longitude $-80° \leq l \leq 80°$ and latitude $-8° \leq b \leq 8°$). The gamma-ray line emission below 10 MeV is due to LECRs, whose properties in the ISM have been adjusted such that the mean CR ionization rate deduced from H_3^+ observations and the *Fermi*-LAT data (magenta band) at 1 GeV are simultaneously reproduced (adapted from [4]). The dashed green line shows the total calculated emission when adding leptonic contributions, point sources and extragalactic gamma-ray background that were taken from [3].The 1-year sensitivity of e-ASTROGAM (for Galactic background) is superimposed.

emission above $E_\gamma = 100$ MeV put stringent constraints on the CR origin and propagation (see, e.g., [1, 2, 3, 6]). See contribution "Gamma rays from interstellar space and cosmic rays" in this White Book for more details on the CR contributions to the multiwavelength spectrum of the inner Galaxy.

A very promising way to study hadronic CRs below the kinetic energy threshold for production of neutral pions would be to detect characteristic gamma-ray lines in the $0.1 - 10$ MeV range produced by nuclear collisions of CRs with interstellar matter. The most intense lines are expected to be the same as those frequently observed from strong solar flares, i.e. lines from the de-excitation of the first nuclear levels in ^{12}C, ^{16}O, ^{20}Ne, ^{24}Mg, ^{28}Si, and ^{56}Fe [15]. Besides strong narrow lines from excitation of abundant heavy nuclei in the ISM, the nuclear line emission is composed of broad lines produced by interaction of CR heavy ions with ambient H and He, and of thousands of weaker lines that together form a quasi-continuum in the range $E_\gamma \sim 0.1 - 10$ MeV [4]. Some of the prominent narrow lines may exhibit a very narrow component from interactions in interstellar dust grains, where the recoiling excited nucleus can be stopped before the γ-ray emission [18]. The most promising of such lines are from ^{56}Fe, ^{24}Mg, ^{28}Si and ^{16}O.

Expected results with e-ASTROGAM – Figure 1 shows a calculated gamma-ray emission spectrum from CRs in the inner Galaxy containing a low-energy component that would account for the observed mean ionization rate of diffuse molecular clouds. A future observation of this emission would be the clearest proof of an important LECR component in the Galaxy and probably the only possible means to determine its composition, spectral and spatial distribution. A particularly promising feature of the predicted gamma-ray spectrum is the characteristic bump in the range $E_\gamma = 3 - 10$ MeV, which is produced by several strong lines of ^{12}C and ^{16}O. The calculated flux in this band integrated over the inner Galaxy ($|l| \leq 80°$; $|b| \leq 8°$) amounts to 7×10^{-5} cm^{-2} s^{-1}, which is well above the predicted sensitivity of e-ASTROGAM after one year of effective exposure of such a spatially extended emission, $S_{3\sigma} = 1.1 \times 10^{-5}$ cm^{-2} s^{-1}.

References

[1] Ackermann, M., Ajello, M., Allafort, A., et al. 2011, Science, 334, 1103
[2] Ackermann, M., Ajello, M., Allafort, A., et al. 2012a, ApJ, 755, 22
[3] Ackermann, M., Ajello, M., Atwood, W. B., et al. 2012b, ApJ, 750, 3
[4] Benhabiles-Mezhoud, H., Kiener, J., Tatischeff, V., & Strong, A. W. 2013, ApJ, 763, 98. Erratum: ApJ, 766, 139
[5] Ceccarelli, C., Hily-Blant, P., Montmerle, T., et al. 2011, ApJ, 740, L4
[6] Casandjian, J.-M. 2015, ApJ, 806, 240
[7] Grenier, I. A., Black, J. H., & Strong, A. W. 2015, ARA&A, 53, 199
[8] Heinz, S., & Sunyaev, R. 2002, A&A, 390, 751
[9] Indriolo, N., Blake, G. A., Goto, M., et al. 2010, ApJ, 724, 1357
[10] Indriolo, N., & McCall, B. J. 2012, ApJ, 745, 91
[11] Indriolo, N., Neufeld, D. A., Gerin, M., et al. 2015, ApJ, 800, 40
[12] Montmerle, T. 1979, ApJ, 231, 95
[13] Neufeld, D. A., & Wolfire, M. G. 2017, ApJ in press, arXiv:1704.03877
[14] Parizot, E., Marcowith, A., van der Swaluw, E., Bykov, A. M., & Tatischeff, V. 2004, A&A, 424, 747
[15] Ramaty, R., Kozlovsky, B., & Lingenfelter, R. E. 1979, ApJS, 40, 487
[16] Scherer, K., Fichtner, H., Ferreira, S. E. S., Büsching, I., & Potgieter, M. S. 2008, ApJ, 680, L105
[17] Spitzer, L., Jr., & Tomasko, M. G. 1968, ApJ, 152, 971
[18] Tatischeff, V., & Kiener, J. 2004, New Astronomy Reviews, 48, 99
[19] Tatischeff, V., & Kiener, J. 2011, MmSAI, 82, 903
[20] Vaupré, S., Hily-Blant, P., Ceccarelli, C., et al. 2014, A&A, 568, A50

Gamma rays from the interstellar medium: probing cosmic rays throughout the Galaxy

Elena Orlando [1], *Andrew Strong* [2], *Isabelle A. Grenier* [3], *Andrei Bykov* [4]

[1] *W.W. Hansen Experimental Physics Laboratory, Kavli Institute for Particle Astrophysics and Cosmology, Stanford University, Stanford, CA, 94305, USA*
[2] *Max Planck Institut für extraterrestrische Physik, D-85748 Garching, Germany*
[3] *Laboratoire AIM, CEA-IRFU/CNRS/Université Paris Diderot, C.E.A. Saclay, France*
[4] *Ioffe Institute, St.Petersburg, Russia, 194021*

Science questions – The Milky Way is an intense source of gamma rays. These photons originate mainly from the interactions of cosmic rays (CRs) with the gas in the interstellar medium and with the interstellar radiation field, via leptonic (bremsstrahlung and inverse Compton scattering) and hadronic (pion decay) processes. Observations of this gamma-ray interstellar emission have been widely used to study the large-scale distribution and spectrum of CRs, and to understand CR propagation and interactions in the Galaxy. This is often done by comparing gamma-ray observations with propagation models and direct CR measurements. A recent extensive review of this topic can be found in [4], where it is underlined how CRs is a piece of the puzzle to understand Galaxy formation and evolution. Indeed CRs are promising candidate for explaining the driving of Galactic winds, which bring to the Galaxy formation. Our knowledge regarding the distribution of the CRs in the Galaxy, if it is more clumping along the spiral arms or in the central molecular zone, regarding the presence and the influence of Galactic winds, and regarding the possible anisotropy of the diffusion coefficient are still very limited. Recent Galaxy formation simulations [11] showed that the diffusion has important consequences on the interstellar gas. While with an isotropic diffusion CRs are allowed to quickly diffuse out of the disk, with an anisotropic diffusion most CRs remain in the disk having important consequences for the gas dynamics in the disk. Hence dynamical effects of CRs on the interstellar medium should be investigated. Over the past decade many detailed studies on CRs and on the induced interstellar gamma-ray emission have been performed thanks to the Fermi LAT and AGILE missions, and to the improved precision of the direct CR measurements. However, these data are deeply challenging our knowledge of CRs, requiring a broader energy coverage and a better angular resolution for gamma-ray instruments in order to distinguish the different emission processes and solve the open questions. Among the open questions left by Fermi LAT there are many model-dependent structures still unclear (e.g., Fermi bubbles, Loop I, outer Galaxy, the Galactic center excess) that show up as excesses over the adopted models (extensive references can be found for example in [15, 6, 3, 5, 4]). Moreover, there is the lack of a best propagation model that provides the description of the whole sky. This is likely due to fact that some models parameters are degenerate while Fermi-LAT uncertainties are relatively large. However, Fermi-LAT data show hints for a large propagation halo size, additional gas in the outer Galaxy, and/or a flat CR source distribution (e.g [1, 3]). Most of the difficulty in the study of the interstellar emission with Fermi LAT and AGILE comes from the limited angular resolution of the instruments that does not allow a clear resolution of the faintest sources, and from the confusion among the different emission mechanisms of the interstellar emission.
The main science questions e-Astrogam will address are: investigating the distribution of CR sources, understanding CR propagation in the Galaxy, and describing their density and spectral variation over the Galaxy.

Importance of gamma-ray observations – While direct CR measurements with balloons and satellites inform us about the local CR spectrum in great detail, only observations of the interstellar emission in gamma rays reveal the large-scale distribution and spectrum of CRs, and

help in understanding CR propagation and interactions in the Galaxy.
Fermi-LAT and AGILE have provided a very detailed view of the gamma-ray sky in the range above 100 MeV, which in future might extend down to about 30 MeV with the latest Fermi-LAT event reconstruction 'Pass 8'. Meanwhile our overall view of the diffuse emission from the Galaxy at the MeV energies is very limited[1] [9], and of the few thousand sources at GeV energies, only about 20 are detected in the 1-30 MeV range from GRO/COMPTEL.
While the gamma-ray diffuse emission has been extensively studied by many authors with Fermi LAT, the hard-X-ray spectrum up to MeV ranges has been derived in [7] with the SPI coded-mask telescope on board INTEGRAL mission and COMPTEL. The results from this study show that the measured diffuse intensity of the Galactic ridge is a factor of 5 above the baseline inverse Compton models. However, an increased electron density or interstellar radiation field could explain the entire emission by diffuse inverse Compton. Unfortunately the degeneracy among electrons and radiation field could not be solved. Another explanation could be a possible contamination to the measured diffuse emission by unresolved point-like sources, which e-ASTROGAM would be able to resolve. Estimates of the interstellar emission in the energy range e-ASTROGAM have been recently obtained in [17]. Figure 1 shows the multiwavelength spectrum from [10, 4] combining SPI, COMPTEL, and Fermi LAT data. The figure shows also the spectrum of the separate components of the interstellar emission. In addition to the hadronic gas-related emission, which peaks at GeV energies, below 100 MeV most of the interstellar emission comes from the Inverse Compton scattering of CR electrons on the interstellar radiation field and cosmic microwave background, and from the bremsstrahlung emission due by CR electrons interactions with gas, i.e. the leptonic-related component of the interstellar emission. The inverse Compton emission is also a significant component above 100 MeV energies, which acts as confusing foreground for many studies due to its large uncertainties. As shown in the figure the inverse Compton component is believed to be the dominant interstellar diffuse component below few tens of MeV.

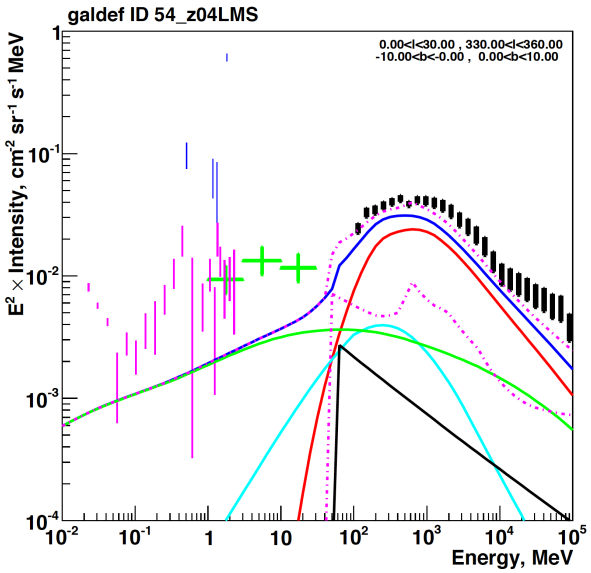

Figure 1: Spectrum of the inner Galaxy from [10, 4], including data from INTEGRAL/SPI (magenta and blue bars), COMPTEL (green crosses) and Fermi-LAT (black bars). The components are: pion decay (red line), inverse Compton (green line), bremsstrahlung (cyan line), total (blue line), isotropic (black line), detected sources (magenta lower dashed line), detected sources plus total (magenta upper dashed line). The e-ASTROGAM extended-source sensitivity for one year of observations based on simulations for the inner Galaxy is below the plotted intensity, being of the order of a few 10^{-5} cm^{-2}s^{-1}sr^{-1}MeV below a few MeV, increasing to 10^{-4} cm^{-2}s^{-1}sr^{-1}MeV around 10 MeV, and decreasing again to few 10^{-5} cm^{-2}s^{-1}sr^{-1}MeV above 30 MeV. This is a factor of $\sim 30 - 10^3$ below the predicted intensity depending on the energy.

[1] See the contribution 'COMPTEL Heritage Data Project' in this White Book for more details on the COMPTEL MeV sky

Expected results with e-ASTROGAM – Since e-ASTROGAM will extend below the maximum of the hadronic pion-decay peak at 67.5 MeV, it will for the first time allow the full pion-decay signature to be fully resolved. Hence CR protons and Helium will be better understood, as well as leptons. In fact, the energy coverage of e-ASTROGAM is well suited to probe for the first time the inverse Compton component and to help in separating also the other foreground components that are degenerate with the inverse Compton component (e.g. the extragalactic diffuse emission and the dark matter emission in the Galactic center). e-ASTROGAM would also allow for the first time to obtain, from the bremsstrahlung and the inverse Compton emission, the distribution of CR electrons in the Galaxy down to below GeV energies. Additional model constraints on the leptonic component and CR electrons will come from studies on the interstellar radio synchrotron emission produced by the same electrons that produce inverse Compton at MeV energies, in line with [13, 15, 17]. Because electrons are affected by energy losses more strongly than protons and heavier nuclei, they remain much closer to their sources and they better sample CR inhomogeneities. For here the importance of mapping the CR electrons. The difficulty of extending Fermi LAT analyses below 100 MeV where the leptonic component dominates is due to the relatively large PSF and energy dispersion at those energies. With its improved PSF and energy resolution e-ASTROGAM will be finally able to access those energies that have never been studied after the COMPTEL era. e-ASTROGAM will provide high-quality spectral imaging of the entire sky and will enable the extension of the Fermi-LAT breakthroughs on interstellar emission into the MeV range. E-Astrogam will discover the origin of the excesses over present propagation models seen by past and present gamma-ray missions. It will be also able to provide essential information on CRs and their propagation in the Galaxy, also important for the evolution of our Galaxy.

References

[1] Ackermann, M., Ajello, M., Baldini, L., et al. 2011, ApJ, 726, 81
[2] Ackermann, M., Ajello, M., Atwood, W. B., et al. 2012, ApJ, 750, 3
[3] Ackermann, M., Albert, A., Atwood, W. B., et al. 2014, ApJ, 793, 64
[4] Acero, F., Ackermann, M., Ajello, M., et al. 2016, ApJS, 223, 26
[5] Ajello, M., Albert, A., Atwood, W. B., et al. 2016, ApJ, 819, 44
[6] Barkov, M. V., & Bosch-Ramon, V. 2014, A&A, 565, A65
[7] Bouchet, L., Strong, A. W., Porter, T. A., et al. 2011, ApJ, 739, 29
[8] Grenier, I.A., Black. J.H, Strong A.W., 2015, ARA&A, 53, 199
[9] Orlando, E., et al. 2017, Proc. 35th International Cosmic Ray Conference, PoS(ICRC2017)692
[10] Orlando, E., & Strong, A. 2013, MNRAS, 436, 2127
[11] Pakmor, R., Pfrommer, C., Simpson, C. M., & Springel, V. 2016, ApJL, 824, L30
[12] Strong, A.W., et al., 1999, Astrophysical Letters and Communications, 39, 209.
[13] Strong, A. W., Orlando, E., & Jaffe, T. R. 2011, A&A, 534, A54
[14] Strong, A.W., 2011, World Scientific, ISBN: 978-981-4462-40-2, page 473.
[15] Su, M., Slatyer, T. R., & Finkbeiner, D. P. 2010, ApJ, 724, 1044

Probing the interplay between cosmic rays and the interstellar medium

Isabelle A. Grenier

Laboratoire AIM, CEA-IRFU/CNRS/Université Paris Diderot, C.E.A. Saclay, France

Science questions – The interstellar medium (ISM) is filled with gas, magnetic fields, dust, light, and cosmic rays (CRs). This medium is very dynamic and its ever-changing structure controls the efficiency of star formation and the evolution of galaxies. CRs play a key role in this evolution [1] as they heat the dense star-forming clouds, they ionize the gas and initiate a rich network of chemical reactions (and production of gas coolants), they provide pressure support to launch strong galactic winds and regulate the gas transfer in and out of a galaxy [2, 3], and they influence the growth of magnetic fields by supporting gas outflows [3]. These stimuli are driven by low-energy CRs, at GeV and sub-GeV energies. Such CRs abound, but they are poorly known. *Voyager 1* has measured their spectrum just outside the heliosphere [4], but little is known on their spatial and spectral distributions elsewhere in the Milky Way. We lack observational constraints on the degree of anisotropy in their diffusion, on the heterogeneity of their properties on the scale of star-forming regions, on their penetration inside the dense gas, and on their feedback on the multi-phase structure of clouds. These are central questions to be answered primarily in γrays in order to better understand the CR feedback on galaxy evolution.

Accurate measurements of the gas mass at all scales are also pivotal in understanding galaxy evolution and in connecting the mass distributions of stars and of their parental clouds. The gas exists in several phases according to the conditions of pressure, heating, cooling, ionization, and screening from stellar UV radiation. The phases are interleaved in turbulent, fractal structures [5]. By producing γrays in their interactions with the gas, CRs expose the total gas to view, regardless of its thermodynamical and chemical state. The full γ-ray census of the gas mass provides important insight into the use of other gas tracers. Most of the mass resides in the neutral gas at medium densities (0.1-10^3 cm^{-3}), in atomic and molecular forms that are commonly traced by HI (21 cm) and CO (2.6 mm) lines. One critical challenge in the field is to detect the "Dark" Neutral Medium (DNM) that lies at the H-H_2 interface. Gathering optically-thick HI and CO-dark H_2, the DNM easily escapes observations even though it is ubiquitous and massive [6, 7, 8]. A second challenge is to evaluate H_2 masses as we cannot directly detect cold H_2 molecules. The X_{CO} factor relates integrated CO line intensities to H_2 column densities and the challenge is to estimate the X_{CO} ratios in a variety of molecular clouds more or less susceptible to UV radiation [9]. A third challenge is to quantify how dust grains evolve across gas phases. The grains are well mixed with all forms of gas, but their emission cross section and, to a lesser extent, their specific reddening, have been found to gradually, but markedly change with increasing gas density (see [10, 11] for review). Infrared dust emission being the prime gas tracer in distant galaxies, quantifying how dust properties vary per gas nucleon in the ISM is of paramount importance to interpret galaxy evolution. The total-gas tracing capability of CRs provides decisive information to progress on these three fronts.

Importance of gamma-ray observations Gamma rays directly inform us on the interplay between CRs and the ISM. Some are produced by CR nuclei in inelastic collisions with gas nuclei, others by CR electrons in bremsstrahlung radiation in the gas. Characterizing the "pion bump" near 70 MeV gives access to the low-energy turnover in CR momentum spectrum near and below one GeV, with the advantage over direct nuclear line detections of a larger continuum emissivity which allows detection throughout the Milky Way and for a large range of cloud masses ($> 10^3$ M$_\odot$) depending on distance. Observations at energies below the pion bump give access to the lowest energy CR electrons that heat and ionize the gas, to complement the higher-energy observations of the bulk of the CRs that provide pressure support.

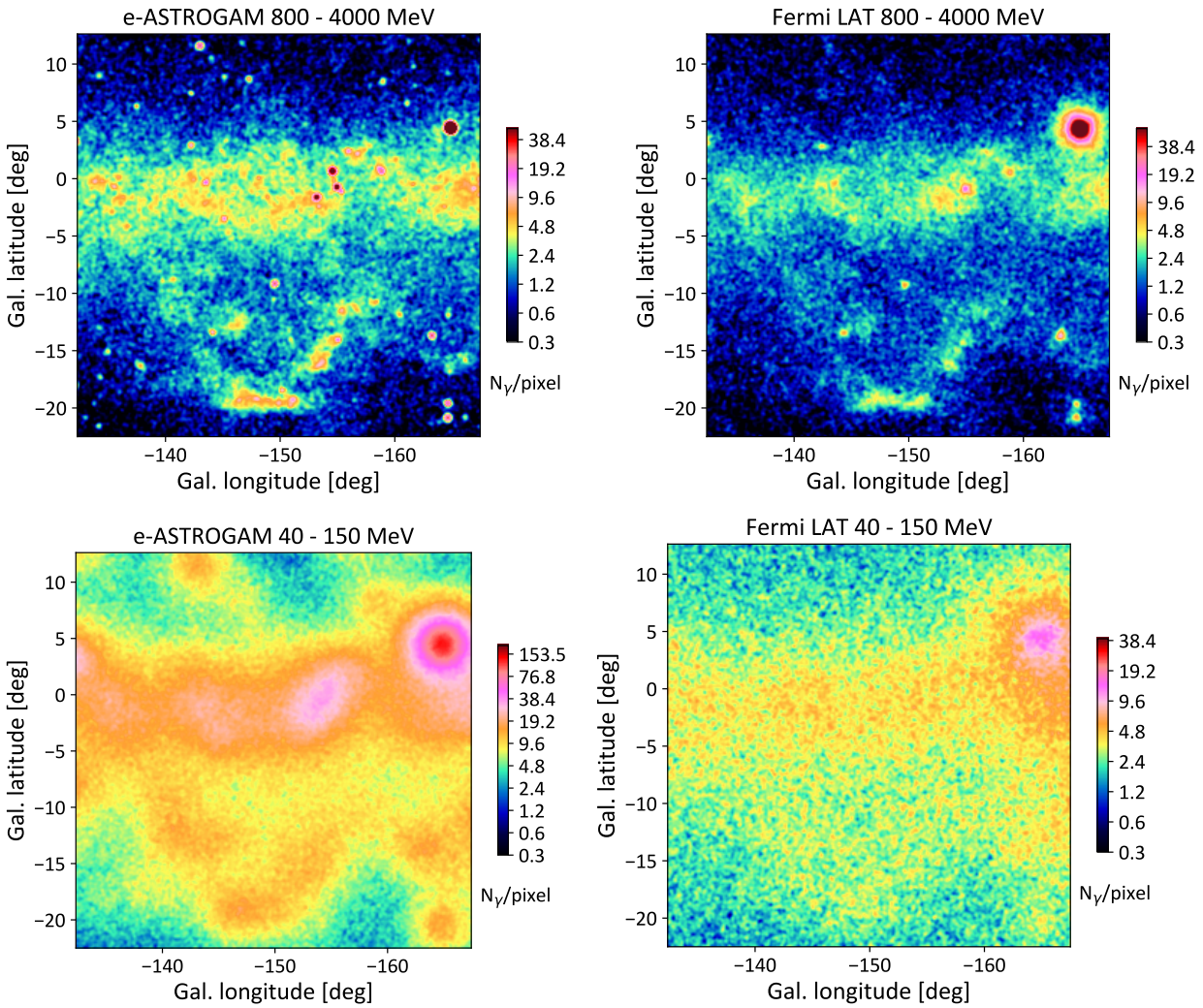

Figure 1: Photon count maps of the Galactic disc and Orion clouds in the 0.8-4 GeV (upper panels) and 40-150 MeV (lower panels) energy bands, simulated for e-ASTROGAM for one year of effective exposure (left panels) and compared to three years of *Fermi* LAT data in scanning mode (right panels)

Tracing the gas with CRs relies on the assumption of a uniform CR flux through the phases of a given cloud complex, and on the measurement of the γ-ray emissivity spectrum per gas nucleon in the atomic envelope where the gas mass can be inferred from HI line emission. Since CR concentration or exclusion processes in a cloud become significant at momenta below 1 GeV [13], higher-energy CR nuclei emitting above the pion bump can be used to estimate X_{CO} ratios, to reveal DNM envelopes of clouds, and to measure dust properties per gas nucleon. The large CR diffusion lengths in the ISM [2] and the uniformity of the GeV γ-ray spectra seen across the gas phases of nearby clouds [1] give strong weight to this method.

Expected results with e-ASTROGAM – Figure 1 illustrates that e-ASTROGAM can easily detect and resolve the 10 MeV to GeV emission from the Galactic ISM. The benefits over the current *Fermi* LAT observations are evident. One can better resolve local cloud structures to probe the penetration and pressure of GeV CRs down to the 0.5-pc scale of dense molecular cores, and to evaluate the flux of low-energy CRs at the 10-pc scale of the DNM envelopes and CO-bright edges where CRs take over other sources of heating and ionization. Measurements of the bremsstrahlung intensity below 50 MeV will enable firmer derivations of the spectrum of CR nuclei at low momenta. The improved sensitivity will allow the detection of faint cirrus clouds to compare their CR content with that of more massive clouds where the magnetic fields are stronger and more entangled.

The gain in sensitivity and in spatial separation of the different gas phases will enable the

first estimation of X_{CO} gradients across molecular clouds to shed light on the relative efficiency of the formation and photodissociation of CO molecules as the H_2 gas becomes denser [14]. These gradients cannot be explored with dust emission because of the change in grain emissivity with gas density. Because of these gradients, translucent CO clouds tend to have larger average X_{CO} factors than compact clouds [10]. Gauging the evolution of this average with the CO emission characteristics of a cloud is essential to determine reliable H_2 masses in Galactic clouds and in external galaxies. e-ASTROGAM will enable studies of a variety of clouds within a couple of kiloparsecs to shed light on this calibration and on the recurrent discrepancy, by a factor of 2 to 3, found between the X_{CO} measures at parsec scale locally and at kiloparsec scale in spiral arms [10]. It will constrain the evolution of the mass hidden in the DNM interface, to confirm and understand why it may scale with the H_2 mass revealed by CO observations[6, 12]. It will open the way to observe differences in X_{CO} ratios and in DNM abundances between clouds compressed in spiral arms and clouds sheared after their passage through an arm [9].

The recent finding of a gradual, but marked (4−6-fold) rise in dust emission cross section with increasing gas density (see [10] for review) limits the use of dust emission as a linear gas tracer to the atomic phase of clouds ($<$ few 10^{21} cm^{-2}). A moderate change in specific dust reddening has also been found [11]. The improved angular resolution of e-ASTROGAM will allow to follow dust evolution per gas nucleon to the densest, coldest molecular cores where grain evolution is strongest.

As with dust, the γrays have the disadvantage of integrating emissions across the whole Galaxy. The superior resolving power of e-ASTROGAM will be central to study remote clouds in a variety of environments in order to explore metallicity changes across the Milky Way and the resulting large-scale gradients in X_{CO} ratios, DNM abundances, and in dust properties. Explorations of clouds in extreme environments will leap forward, for instance in the Central Molecular Zone or in starburst regions where the enhanced magnetic fields, intense stellar radiation fields, high levels of turbulence and shearing, and large CR fluxes should modify the cloud states.

Difficulties rest in that all gas tracers are non-linear and suffer from spatial confusion inside a cloud complex and along the line of sight. The improved angular resolution of e-ASTROGAM at GeV energies and its coverage extending down to MeV energies will thus provide a wealth of new information on the subtle interplay between cosmic rays and the interstellar medium.

References

[1] Grenier, I. A., Black, J., & Strong, A. 2015, ARAA, 53, 199.
[2] Zweibel, E. G. 2013, Physics of plasma, 20, 055501.
[3] Pakmor, R., Pfrommer, C., Simpson, C. M., & Springel, V. 2016, ApJ, 824, L30
[4] Stone, E., et al. 2013, Science, 341, 150
[5] Hennebelle, P., Falgarone, E. 2012, Astron Astrophys Rev, 20, 55
[6] Grenier, I. A., Casandjian, J. M., & Terrier, R. 2005, Science, 307, 1292
[7] Planck Collaboration, Fermi Collaboration, 2015, A&A, 582, A31
[8] Pineda, J. L., et al. 2013, A&A, 554, A103
[9] Smith, R. J., et al. 2014, MNRAS, 441, 1628
[10] Remy, Q., Grenier, I. A., Marshall, D. J., & Casandjian, J. M. 2017, A&A, 601, A78
[11] Remy, Q., Grenier, I. A., Marshall, D. J., & Casandjian, J. M. 2017, submitted to A&A
[12] Remy, Q., Grenier, I. A., Marshall, D. J., & Casandjian, J. M. 2018, submitted to A&A
[13] Schlickeiser, R., Caglar, M., & Lazarian, A. 2016, ApJ, 824, 89.
[14] Bertram, E., et al.,. 2016, MNRAS, 455, 3763.

Fundamental physics

Conveners: Jan Conrad
Manel Martinez
Uwe Oberlack

Limiting Mev-ish dark matter decays from e-ASTROGAM: light WIMPs, dark photons, Majorons

Andrea Addazi [1], *Denis Bastieri* [2,3,4], *Antonino Marcianò* [1]

[1] *Center for Field Theory and Particle Physics & Department of Physics, Fudan University, 200433 Shanghai, China*
[2] *Dipartimento di Fisica e Astronomia* "G. Galilei", *Università di Padova, I-35131 Padova, Italy*
[3] *Istituto Nazionale di Fisica Nucleare, Sezione di Padova, I-35131 Padova, Italy*
[4] *Center for Astrophysics, Guangzhou University, Guangzhou 510006, China*

Science questions – The presence of dark matter was confirmed by many indirect gravitational observations, including galactic rotational curves and CMB. Nonetheless current observations did not shed light yet on the fundamental particle that should be the constituents of the dark halos. For instance, underground direct detection experiments, cosmic rays and colliders have not provided any definitive conclusion on the dark matter problem. This strongly motivates the individuation of new experimental constraints in order to test non-standard candidates of dark matter. For example, in stead of considering masses of $10\,\mathrm{GeV} \div 1\,\mathrm{TeV}$, it is still an open and viable possibility to have lighter dark matter particles composing the halo. For example the mass window $1 \div 100\,\mathrm{MeV}$ suggests new kind of direct and indirect detection experiments with respect to the current ones.

Here we suggest to test MeV-ish dark matter decays from e-ASTROGAM. The idea is not only to use the e-ASTROGAM data to probe standard astrophysical objects, but also to obtain useful information in understanding particle physics. The presence of MeV-ish dark matter is highly motivated within the context of many different extensions of the standard model. For instance, within the WIMP paradigm one can consider mechanisms for the genesis of non-thermal dark matter that favor lighter WIMP candidates than the thermal WIMP miracle ones. If WIMP particles are indeed MeV-ish, they can decay into light SM particles, and in particular into photons. Another possible model which may be tested is the massive Dark Photon model. We also mention here the possibility to test Majoron dark matter, which naturally favors light particles while explaining neutrino mass generation. Finally, the presence of MeV-ish dark matter can be related to dark first order phase transitions that produce a stochastic gravitational waves background. This is a novel multi-messenger approach to address new physics by comparing gamma-rays observations with gravitational radiation [11, 12, 13].

Importance of gamma-ray observations – Depending by the mass of dark matter particle, the WIMPs can annihilate into several different channels: a photon pair $\chi\chi \to \gamma\gamma$, a neutral pion and photon $\chi\chi \to \pi^0\gamma$, a neutral pions pair $\chi\chi \to \pi^0\pi^0$, light lepton-antilepton pairs (electron, muons, neutrinos) $\chi\chi \to l\bar{l}$ and more complicated cascade annihilations. In principle light WIMPs' annihilation can then be detected. The expected flux grows as the square of the energy density, i.e. a higher signal is expected in places where the dark halo is accumulated. For instance, in the galactic center the density profile roughly grows as a power law $\rho(r) \sim r^{-\gamma}$, with γ a fit parameter.

The primary component is constituted by all the photons in the final state directly arising from annihilation of WIMPs [1, 2, 7, 4]. The differential γ-ray flux reads

$$\frac{d\Phi}{dEd\Omega} = \frac{c\langle\sigma v\rangle J}{4\pi m_\chi^2}\frac{dN_\gamma}{dE_\gamma}\,,$$

where $\langle\sigma v\rangle$ is the annihilation cross section averaged on the local relative velocity, J is a factor parametrizing the astrophysical DM distributions, a denotes a numerical prefactor that equals either $= 1/2$ if χ is a Majorana particle or $= 1/4$ if χ is a Dirac particle, m_χ denotes the dark particle mass, and finally dN_γ/dE_γ stands for flux spectrum. The greatest uncertainty is contained

in the J-factor, defined as $J = \int_{l.o.s} ds\, \rho^2(s,\theta)$, which is the integration on the line of sight (l.o.s.) of the squared DM mass density profile, where s is the distance along the line of sight and θ is the l.o.s. angle — this is defined in turn by the relation $r^2 = s^2 + R_0^2 - 2sR_0\cos\theta$, in which $R_0 \sim 8\,\mathrm{kpc}$ represents the solar distance from the galactic center.

The density profile is affected by many astrophysical uncertainties, and is usually parametrized in an analytic form as

$$\rho(r) = \frac{\rho_0}{(r/R)^\gamma[1+(r/R)^\alpha]^{(\beta-\gamma)/\alpha}}\,,$$

where α, β, γ are model parameters, R is the characteristic length scale and ρ_0 is the local DM density, approximately $0.4\,\mathrm{GeV\,cm^{-3}}$. For instance, possible models are the Navarro-Frenk-White (NFW) model ($\alpha = 1.0, \beta = 3.0, \gamma = 1.0, R = 20\,\mathrm{kpc}$), the Moore model ($\alpha = 1.5, \beta = 3.0, \gamma = 1.5, R = 28\,\mathrm{kpc}$) and the isothermal halo model ($\alpha = 2.0, \beta = 2.0, \gamma = 0, R = 3.5\,\mathrm{kpc}$).

For primary $\chi\chi \to \gamma\gamma$ annihilation, the photon spectrum is expected to be a spike in the flux spectrum, namely $dN_\gamma/dE = 2\delta(E - m_\chi)$. For primary $\chi\chi \to \pi^0\pi^0$, the chiral anomaly induces the subsequent decays $\pi^0 \to \gamma\gamma$, i.e. the flux spectrum can be modeled as a box-like distribution [4],

$$\frac{dN_\gamma}{dE} = \frac{4}{E_+ - E_-}\Theta(E_+ - E)\Theta(E - E_-)\,, \qquad \text{with} \qquad E_\pm = \frac{m_\chi}{2}\left(1 \pm \sqrt{1 - \frac{m_\pi^2}{m_\chi^2}}\right).$$

The $\chi\chi \to \pi_0\gamma$ decay's contribution has to appear out of the spectrum as a spike that is over-imposed on the box spectrum contribution [4] to the photons flux spectrum, namely

$$\frac{dN_\gamma}{dE} = \delta(E - E_0) + \frac{2}{\Delta E}\Theta(E'_+ - E)\Theta(E - E'_-)\,,$$

where

$$E_0 = m_\chi - \frac{m_{\pi_0}^2}{4m_\chi},\ \ \Delta E' = m_\chi - \frac{m_{\pi_0}^2}{4m_\chi} \qquad \text{and} \qquad E'_\pm = \frac{m_\chi}{2}\left[\left(1 + \frac{m_{\pi^0}^2}{4m_\chi^2}\right) \pm \left(1 - \frac{m_{\pi^0}^2}{4m_\chi^2}\right)\right].$$

The estimate of the secondary emission processes requires a much more involved numerical analysis. This is the case of $\chi\chi \to e^+e^-$ processes, in which we can have a large contribution from Bremsstrahlung emission.

Expected results with e-ASTROGAM – The *dark photon* model extends the Standard Model (SM) so to encode an extra dark gauge sector. In the minimal model, just an extra $U(1)_X$ gauge group is added $G_{SM} \times U_X(1)$ [5, 6]. An interesting case consists in a minimal particle spectrum (s, χ, A'_μ), where s is a scalar singlet, χ is a fermion charged with respect to the extra $U(1)_X$, while A' is the dark photon. The dark photon can become massive thatnks to a spontaneous symmetry breaking induced by the scalar singlet [7]. In this scenario, fermions are thought as dark matter particles and their masses can be generated by Yukawa terms involving the singlet. A renormalizable gauge portal among dark matter and the standard model particles is the so dubbed *kinetic mixing term*, $-\epsilon F^{\mu\nu}_{(Y)} F^{(X)}_{\mu\nu}$, which mixes the SM hypercharge with the dark photon. This allows an electromagnetic-like annihilation process of dark fermions into SM particles. For instance, if we assume dark particles to be lighter than the electrons, the cross-section for this kind of precesses reads

$$\sigma(\chi\chi \to \gamma\gamma)\, v = \frac{\pi\alpha'^2}{m_\chi^2} = \left(6.5 \times 10^{-4}\,\mathrm{pb}\right)\frac{\epsilon_5^4}{m_{keV}^2}\,,$$

where $m_{keV} = m_X/keV$, $\alpha' = e'^2/4\pi = \epsilon^2\alpha$ and $\epsilon_5 = 10^5\epsilon$. Other more complicated processes from Bremsstrahlung emissions can be envisaged, involving a more sophisticated analysis, which is in preparation.

The *Majoron* is the Nambu-Goldstone boson of a global lepton symmetry that generates a Majorana mass for the neutrino. It can be very long-living, if in KeV-MeV mass spectrum range, hence

providing a natural candidate for dark matter. In various model of neutrino mass generated with a spontaneous symmetry breaking of the global lepton number symmetry, Majorons are coupled with photons with a dimension 5 operator like

$$g_{J\gamma\gamma} J \epsilon^{\nu\mu\rho\sigma} F_{\nu\mu} F_{\rho\sigma} \, ,$$

in which $[g_{J\gamma\gamma}] = M^{-1}$ is a negative dimensional coupling and J the Majorons' field. This means that Majorons have to decay radiatively into two photons, each one carrying an energy $E_\gamma \simeq m_J/2$ — the decay can be studied as it were happening in the DM rest frame with very good approximation. In order to recover the CMB constrains, the decay rate of the Majoron must be $\Gamma_J < \zeta \times 2.4 \times 10^{-25}\,\mathrm{s}^{-1}$, where ζ is the inverse efficiency factor that describes how much decay energy is deposited on baryons. This opens a pathway to test long-living metastable Majorons from indirect detection in the KeV-MeV region.

References

[1] C. Boehm, T. A. Ensslin and J. Silk, J. Phys. G**30** (2004) 279-286, [astro-ph/0208458].

[2] R. T. D'Agnolo and J. T. Ruderman, Phys. Rev. Lett. **115** (2015) 061301, [1505.07107].

[3] R. Bartels, D. Gaggero and C. Weniger, JCAP **1705** (2017) no.05, 001 [arXiv:1703.02546 [astro-ph.HE]].

[4] K. K. Boddy and J. Kumar, Phys. Rev. D**92** (2015) 023533, [1504.04024].

[5] B. Holdom, Phys. Lett. **166**B (1986) 196.

[6] S.L. Glashow, Phys. Lett. B **167** (1986) 36.

[7] N. Arkani-Hamed, D. P. Finkbeiner, T. R. Slatyer and N. Weiner, Phys. Rev. D **79** (2009) 015014 [arXiv:0810.0713 [hep-ph]].

[8] Y. Chikashige, R. N. Mohapatra and R. D. Peccei, Phys. Lett. B**98**, 26 (1981).

[9] J. Schechter and J. W. F. Valle, Phys. Rev. D**25**, 774 (1982).

[10] V. Berezinsky and J. W. F. Valle, Phys. Lett. B **318** 360 (1993) [arXiv:hep-ph/9309214].

[11] A. Addazi, Mod. Phys. Lett. A **32** (2017) no.08, 1750049 [arXiv:1607.08057 [hep-ph]].

[12] A. Addazi and A. Marciano, arXiv:1703.03248 [hep-ph].

[13] A. Addazi and A. Marciano, arXiv:1705.08346 [hep-ph].

[14] J.F. Navarro, C.S. Frenk and S.D.M. White, Astrophys. J. **490** (1997) 493 [astro-ph/9611107].

[15] J. I. Read, J. Phys. **G41** (2014) 063101, [1404.1938].

[16] R. Catena and P. Ullio, JCAP **1008** (2010) 004, [0907.0018].

[17] M. Weber and W. de Boer, Astron. Astrophys. **509** (2010) A25, [0910.4272].

[18] F. Iocco, M. Pato, G. Bertone and P. Jetzer, JCAP **1111** (2011) 029, [1107.5810].

Decay or Annihilation of Non-thermally Produced Dark Matter

Vedran Brdar[1], *Joachim Kopp*[2], *Jia Liu*[3], *Alexander Merle*[4] *Xiaoping Wang*[5]

[1] *Max Planck Institut für Kernphysik, 69117 Heidelberg, Germany*
[2] *Johannes Gutenberg-Universität Mainz, 55099 Mainz, Germany*
[3] *Enrico Fermi Institute, University of Chicago, Chicago, IL 60637, USA*
[4] *Max-Planck-Institut für Physik, 80805 Munich, Germany*
[5] *High Energy Physics Division, Argonne National Laboratory, Argonne, IL 60439, USA*

Science questions – Searches for dark matter (DM) have traditionally focused on particles around the electroweak scale, where many theoretically well motivated DM candidates have been proposed. As these scenarios are coming under pressure from the LHC and from direct and indirect DM searches, scenarios with much lighter DM are entering the spotlight. Of particular interest is the mass range from $\sim 100\,\mathrm{keV}$ to $1\,\mathrm{GeV}$. DM particles in this range are still heavy enough to act as Cold DM, even if the original production mechanism was non-thermal.[1] However, unfortunately their masses are below the detection threshold of typical searches for DM–nucleus scattering.

In the early Universe, sub-GeV DM particles could in principle be produced via thermal freeze-out. However, in many scenarios of this type, in particular those with s-wave annihilation, the required DM annihilation cross sections of order few$\times 10^{-26}\,\mathrm{cm}^3/\mathrm{sec}$ [3] is in conflict with gamma ray limits [2] and with limits on additional energy injection into the primordial plasma around the time of recombination [7]. This leaves out-of-equilibrium freeze-in as a viable production mechanism [6]. In the following, we will focus on scenarios of the latter type. Freeze-in can occur for instance through a "Higgs portal" coupling of the form

$$\mathcal{L}_{\text{Higgs-portal}} = \lambda(\phi\phi)(H^\dagger H) \tag{1}$$

between a new scalar ϕ and the Standard Model Higgs field H. Here, λ is a small coupling constant. ϕ can either be the DM particle itself or a heavier dark sector particle that decays or annihilates to DM at a later time (see for instance [8]). Alternative freeze-in scenarios include ϕ couplings to additional new particles, or freeze-in through a higher-dimensional coupling such as

$$\mathcal{L}_{5\text{d}} = \tfrac{\alpha}{4\pi\Lambda}\phi F_{\mu\nu}F^{\mu\nu}\,, \tag{2}$$

where $F^{\mu\nu}$ is the photon field strength tensor and α is the electromagnetic fine structure constant.

All production mechanisms of MeV–GeV scale DM require the couplings between the dark and visible sectors to be extremely weak to explain the observed DM abundance, making direct detection and production of DM particles in experiments at particle accelerators challenging. It is therefore likely that such DM particles would have escaped detection so far, and it is crucial to close this gap.

Importance of gamma-ray observations – Due to the difficulty of detecting DM particles at the MeV–GeV scale using other means, indirect astrophysical searches are of primary interest for them, even more so than for heavier DM. When MeV–GeV scale DM particles decay or annihilate to Standard Model particles, they typically leave signatures in the gamma ray sky at precisely the right energies for e-ASTROGAM to play out its stengths. Only few decay or annihilation channels are available for such light DM particles: below the electron threshold at $\sim 1\,\mathrm{MeV}$, only decay or annihilation to photons or neutrinos is possible. Given the small neutrino interaction rate, searches in gamma rays are most promising in practice. At somewhat larger masses, the secondary gamma

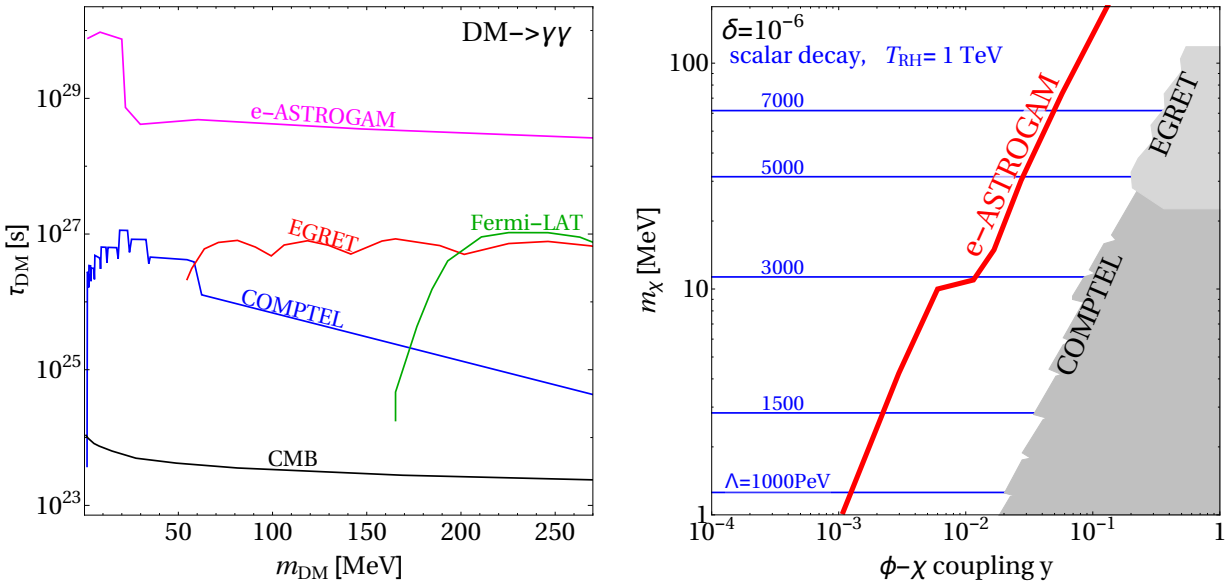

Figure 1: Left: Expected sensitivity of e-ASTROGAM to dark matter decay to photons (obtained by converting the limits on DM annihilation presented in [7]), compared to existing constraints (based on [2]). Right: Expected e-ASTROGAM constraints on the parameter space of the DM model from Ref. [3].

rays radiated in decay or annihilation to electrons/positrons, muons, or light mesons offer the most promising target for indirect searches [7, 14].

The three main classes of gamma ray signatures expected from MeV–GeV scale DM are

1. **Continuum photons from final state radiation.** If DM decays or annihilates to charged final state particles, the radiative production of photons from the final state leads to peaked spectra at energies somewhat below the DM mass [7].

2. **Mono-energetic photons.** There is a multitude of particle physics scenarios predicting this signature. The simplest example is perhaps a fermionic DM candidate χ ("sterile neutrino") mixing with neutrinos. If DM is a fermion that does not carry gauge charges, the corresponding coupling $y\bar{L}(i\sigma_2 H^*)\chi$ (with L a SM lepton doublet and σ_2 a Pauli matrix) is not forbidden by any symmetry. It is therefore generically expected to be present and leads to the decay $\chi \to \nu\gamma$ via a W–charged lepton loop. For scalar or pseudoscalar DM ϕ, direct decay to photons may be possible via an effective coupling of the form $\frac{\alpha}{4\pi\Lambda}\phi F_{\mu\nu}F^{\mu\nu}$. Such a coupling will be induced for instance if DM couples to super-heavy charged particles. In fact, the decay rate

$$\Gamma_{\phi\to\gamma\gamma} = 2.4\times 10^{24}\,\text{sec}\times\left(\frac{\text{MeV}}{m_\phi}\right)^3\left(\frac{\Lambda}{10^{16}\,\text{GeV}}\right)^2 \tag{3}$$

   suggests that in particular DM couplings to particles around the Grand Unification Scale — where we would generically expect such couplings — are of interest here.

3. **Box-shaped spectra.** If DM decays or annihilates to neutral pions, or to new intermediate particles that decay onward to photon, the expected gamma ray spectrum is box-shaped. For instance, in Ref. [3], a simple and successful scenario has been presented in which fermionic DM χ annihilates to a scalar ϕ that is long-lived, but eventually decays to photons. Note that, if χ and ϕ are nearly degenerate in this scenario, the box-shaped spectrum reduces again to a monochromatic one. Near mass-degeneracy of χ and ϕ could be understood for instance

[1]The intuitive picture is that, independent of the shape of the initial velocity spectrum, sufficiently heavy DM particles will cool down fast, thereby shifting all particle velocities to a value close to zero. Thus, no matter what the shape of the spectrum was originally, these DM particles could always be approximated as being essentially at rest.

if nature is fundamentally supersymmetric and the two particles are members of the same supermultiplet. An interesting aspect of scenarios with long-lived intermediate particles, which travel over astrophysical distance scales before decaying, is that the morphology of the gamma ray signal may not directly trace the DM distribution in the observation target. Rather, it will be smeared out compared to the DM distribution.

Expected results with e-ASTROGAM – With its superior sensitivity to gamma ray signals at MeV–GeV energies, e-ASTROGAM will significantly extend the sensitivity to DM particles at this mass scale. The mission thus has the potential to play a similarly transformative role as Fermi has played for DM at larger mass scales. Across all decay or annihilation final states, an improvement of the sensitivity by several orders of magnitude is expected compared to current constraints (see also Ref. [7]). In Fig. 1, we illustrate this for two test cases: decaying scalar DM (left panel) and two-step annihilation $\overline{\chi}\chi \to \phi\phi \to 4\gamma$ in the context of the model presented in Ref. [3].

References

[1] R. Bartels, D. Gaggero and C. Weniger, JCAP **1705**, no. 05, 001 (2017) [arXiv:1703.02546, and contribution to this White Book.

[2] K. K. Boddy and J. Kumar, Phys. Rev. D **92**, no. 2, 023533 (2015) [arXiv:1504.04024.

[3] V. Brdar, J. Kopp, J. Liu and X. P. Wang, [arXiv:1710.02146.

[4] T. Bringmann, A. Galea, A. Hryczuk and C. Weniger, Phys. Rev. D **95**, no. 4, 043002 (2017) [arXiv:1610.04613], and contribution to this White Book.

[5] R. Essig, E. Kuflik, S. D. McDermott, T. Volansky and K. M. Zurek, JHEP **1311**, 193 (2013) [arXiv:1309.4091.

[6] L. J. Hall, K. Jedamzik, J. March-Russell and S. M. West, JHEP **1003**, 080 (2010) [arXiv:0911.1120.

[7] M. S. Madhavacheril, N. Sehgal and T. R. Slatyer, Phys. Rev. D **89**, 103508 (2014) [arXiv:1310.3815.

[8] A. Merle, V. Niro and D. Schmidt, JCAP **1403**, 028 (2014) [arXiv:1306.3996]

[9] A. Merle and M. Totzauer, JCAP **1506**, 011 (2015) [arXiv:1502.01011]

[10] J. König, A. Merle and M. Totzauer, JCAP **1611**, no. 11, 038 (2016) [arXiv:1609.01289]

[11] G. Steigman, B. Dasgupta and J. F. Beacom, Phys. Rev. D **86**, 023506 (2012) [arXiv:1204.3622.

Smoking gun dark matter signatures in the MeV range

Torsten Bringmann[1], *Andrzej Hryczuk*[1], *Are Raklev*[1], *Inga Strümke*[2], *Jeriek Van den Abeele*[1],

[1] *Department of Physics, University of Oslo, Box 1048, NO-0371 Oslo, Norway*
[2] *University of Bergen, Institute for Physics and Technology, Postboks 7803, N-5020 Bergen, Norway*

Science questions – The nature of the astrophysically and cosmologically observed dark matter (DM) in the universe [1] is one of the big open scientific questions today. While it is clear that DM must be non-baryonic, the list of possible explanations in terms of a new particle is long [2]. Given that all evidence for DM so far is of gravitational origin, any non-gravitational DM signal would be a major breakthrough towards determining the identity of those DM particles.

Among the most favourite DM candidates are weakly interacting massive particles (WIMPs), with masses and coupling strengths at the electroweak scale. Besides the fact that many of these are theoretically very well motivated, such as the supersymmetric neutralino [3], an attractive feature of this class of candidates is that the observed DM abundance today can straight-forwardly be explained by the thermal production of WIMPs in the early universe. In recent years however – triggered not the least by the lasting absence of any undisputed WIMP signals, despite immense experimental efforts – the focus of the community has started to shift beyond WIMPs as the main DM paradigm.

For example, it was pointed out that thermal production is also an attractive option for smaller DM masses [4]. Other relevant DM models with (sub-)GeV masses include light gravitino DM [5], inelastic DM [6], light scalar DM [7] or secluded DM [8]. Models in this mass range have received significant interest because they could have easily escaped the ever more stringent constraints from direct DM detection experiments (for a suggestion of how to overcome the lack of sensitivity of traditional methods in this mass range, see e.g. Ref. [10]). From the indirect detection perspective, an intriguing feature of such models is furthermore that the center-of-mass energy, and hence the energy of final state quarks, is at the same mass scale as standard model hadronic states. As we argue in this contribution, this can lead to a potentially rich phenomenology in MeV gamma rays that may allow to draw far-reaching conclusions about the nature of the DM particles and the underlying theory.

Importance of gamma-ray observations – Gamma rays from both decaying and annihilating DM have sometimes been argued to be the *golden channel* of indirect DM searches [9] because they directly point back to their sources and hence provide the potentially most accurate way to probe the astronomically observed DM distribution *in situ*. Furthermore, they may carry distinct spectral features that can both act as 'smoking gun' signals for the particle nature of DM and convey further detailed information about the nature of these particles.

Motivated by the WIMP case, the main focus has traditionally been on spectral features in the 100 GeV – TeV range, with relevant limits presented e.g. in Ref. [2]; also exotic line contributions in the keV range have been scrutinized in detail, where a signal could be expected from decaying sterile neutrino DM [12]. Here, we point out that also the largely neglected MeV range is very well motivated in this respect (for earlier work, see Refs. [13, 14]), and hence ideally suited for searches with e-ASTROGAM.

In fact, gamma-ray and cosmic microwave background observations already put significant constraints on light DM candidates, and e-ASTROGAM would imply an additional boost in sensitivity [15]. As we show here, hadronic final states from DM decay or annihilation could furthermore lead to a plethora of potential smoking-gun signatures for a DM signal in MeV gamma rays that only a dedicated mission like e-ASTROGAM may be able to detect.

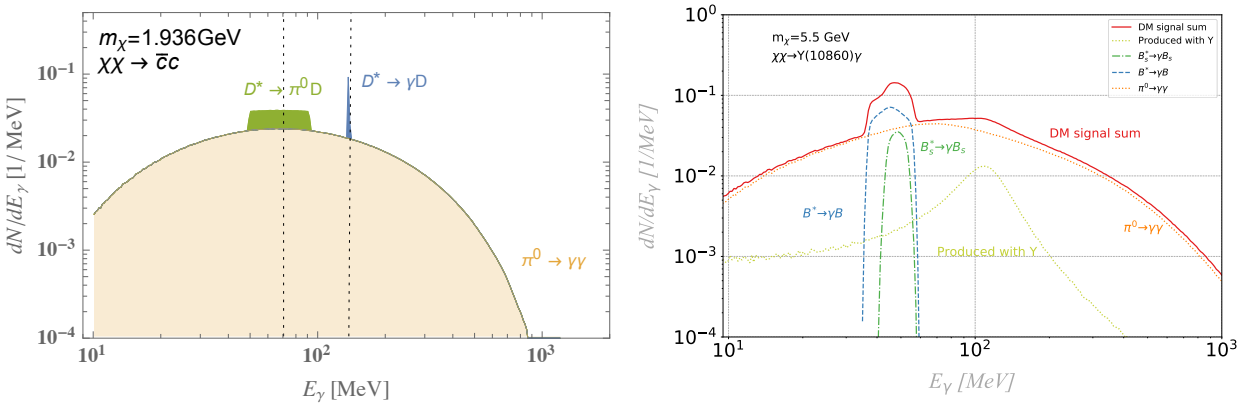

Figure 1: Left: Example of the expected gamma-ray spectrum for DM annihilation into charm quarks, with a DM mass m_χ just above the kinematic threshold to produce D-mesons. The sharp spectral features result from the indicated meson transitions, while the background is mostly due to $\pi^0 \to \gamma\gamma$. For more details, see Ref. [14]. Right: Gamma-ray spectrum from DM annihilation through the quarkonium channel $\chi\chi \to \Upsilon(10860)\gamma$. The three visible spectral features are due to two different meson transitions and the photon produced in conjunction with the quarkonium. For more details, see Ref. [18].

Expected results with e-ASTROGAM – Among the various processes that could potentially lead to spectral features in MeV gamma rays (see also Ref. [14] for an overview, and Ref. [16] for further examples), we will focus here on standard model meson transitions and quarkonium resonances. We consider a center-of-mass energy of the annihilating DM pair, or DM mass in the case of decaying DM, that is close to the threshold for the production of (excited) heavy mesons. The de-excitation of excited meson states in the final state, via the emission of a photon or neutral pion, will then generate box-like signatures (which in the case of photon emission can be almost monochromatic).

For illustration, we show in Fig. 1 an example where DM is assumed to annihilate dominantly into $\bar{c}c$ pairs. In this example, both types of de-excitation processes lead to spectral features that are clearly visible above the standard 'background' part of the signal, resulting from decaying neutral pions that are copiously produced in fragmentations and decays of heavier mesons. Implementing a realistic modelling of the expected astrophysical background, we have shown that the sensitivity of e-ASTROGAM to this DM annihilation channel improves by a factor of up to about 2 by taking into account these spectral features, compared to using the standard pion bump as a signal template [14]. For $\bar{b}b$ final states, the effect can be twice as large. We note that the exact form and location of these spectral features are very specific for each final state. This allows, in principle, a highly accurate reconstruction not only of the DM mass but also of the branching ratios for the DM decay or annihilation channels.

The possibility of MeV gamma-ray features from annihilation into heavy meson pairs also raises the issue of contributions from quarkonia. Either through the process $\chi\chi \to (\overline{Q}Q)\gamma$, where gamma-rays are produced both directly and through subsequent decay into (excited) heavy mesons, or heavy-meson production enhanced by a quarkonium resonance $\chi\chi \to (\overline{Q}Q) \to M_A M_B$, where M_A and M_B are two heavy mesons with radiative decays. An example of the resulting expected spectrum for a DM mass $m_\chi = 5.5$ GeV and the channel $\chi\chi \to \Upsilon(10860)\gamma$ is shown in Fig. 1 (right). Here structures from three processes, $B^* \to \gamma B$, $B_s^* \to \gamma B_s$, and direct production in the annihilation, can all be identified. Notably, such a signal would also exist in the annihilation of *sub*-GeV DM into light quarkonium states, e.g. $\chi\chi \to \eta^{(\prime)}\gamma$, with subsequent decay of the $\eta^{(\prime)}$ into photon pairs.

Furthermore, it is well known experimentally that for heavy-meson production at e^+e^- colliders, quarkonium resonances can be dominant near threshold [17]. We have explored dark matter annihilation through the related vector currents $\chi\Gamma^\mu\chi\overline{Q}\gamma_\mu Q$. Using collider data as input to our model we observe significant enhancement of the MeV features [18] due to these resonances. We

also find that the existence and dominance of different processes is highly dependent on the structure of the DM-quark interaction and the nature of the DM particle, e.g. as seen in the well-known suppression of the vector current for Majorana or scalar DM [13].

In conclusion, the sensitivity gap in the MeV range explored by e-ASTROGAM is a window of opportunity to detect new physics – not only by confirming the particle nature of DM, but with the additional potential of closing in on some of its detailed properties, like the DM particle's mass, its branching ratios to quark final states and, to some degree, its underlying interaction structure.

References

[1] P. A. R. Ade *et al.* [Planck Collaboration], Astron. Astrophys. **594**, A13 (2016) [arXiv:1502.01589 [astro-ph.CO]].

[2] J. L. Feng, Ann. Rev. Astron. Astrophys. **48**, 495 (2010) [arXiv:1003.0904 [astro-ph.CO]].

[3] G. Jungman, M. Kamionkowski and K. Griest, Phys. Rept. **267**, 195 (1996) [hep-ph/9506380].

[4] J. L. Feng and J. Kumar, Phys. Rev. Lett. **101**, 231301 (2008) [arXiv:0803.4196 [hep-ph]].

[5] F. Takayama and M. Yamaguchi, Phys. Lett. B **485** (2000) 388 doi:10.1016/S0370-2693(00)00726-7 [hep-ph/0005214].

[6] D. Tucker-Smith and N. Weiner, Phys. Rev. D **64** (2001) 043502 doi:10.1103/PhysRevD.64.043502 [hep-ph/0101138].

[7] C. Boehm and P. Fayet, Nucl. Phys. B **683** (2004) 219 doi:10.1016/j.nuclphysb.2004.01.015 [hep-ph/0305261].

[8] M. Pospelov, A. Ritz and M. B. Voloshin, Phys. Lett. B **662** (2008) 53 doi:10.1016/j.physletb.2008.02.052 [arXiv:0711.4866 [hep-ph]].

[9] T. Bringmann and C. Weniger, Phys. Dark Univ. **1**, 194 (2012) [arXiv:1208.5481 [hep-ph]].

[10] R. Essig, J. Mardon and T. Volansky, Phys. Rev. D **85**, 076007 (2012) [arXiv:1108.5383 [hep-ph]].

[11] M. Ackermann *et al.* [Fermi-LAT Collaboration], Phys. Rev. D **91**, no. 12, 122002 (2015) [arXiv:1506.00013 [astro-ph.HE]]; A. Abramowski *et al.* [H.E.S.S. Collaboration], Phys. Rev. Lett. **110**, 041301 (2013) [arXiv:1301.1173 [astro-ph.HE]].

[12] For the much discussed potential discovery of such a line, see E. Bulbul, M. Markevitch, A. Foster, R. K. Smith, M. Loewenstein and S. W. Randall, Astrophys. J. **789**, 13 (2014) [arXiv:1402.2301 [astro-ph.CO]]; A. Boyarsky, O. Ruchayskiy, D. Iakubovskyi and J. Franse, Phys. Rev. Lett. **113**, 251301 (2014) [arXiv:1402.4119 [astro-ph.CO]].

[13] M. Srednicki, S. Theisen and J. Silk, Phys. Rev. Lett. **56**, 263 (1986) Erratum: [Phys. Rev. Lett. **56**, 1883 (1986)]; S. Rudaz, Phys. Rev. Lett. **56**, 2128 (1986); L. Bergstrom, Nucl. Phys. B **325**, 647 (1989).

[14] T. Bringmann, A. Galea, A. Hryczuk and C. Weniger, Phys. Rev. D **95**, no. 4, 043002 (2017) [arXiv:1610.04613 [hep-ph]].

[15] See, e.g., I. A. Antonelli *et al.* and R. Bartels *et al.* (this contribution).

[16] V. Brdar, J. Kopp, J. Liu, A. Merle and X. Wang (this contribution).

[17] B. Aubert *et al.* [BaBar Collaboration], Phys. Rev. Lett. **102** (2009) 012001 [arXiv:0809.4120 [hep-ex]].

[18] A. Raklev, I. Strümke, J. Van den Abeele, *in progress* (2017).

Sub-GeV dark matter searches in the Galactic Center

Richard Bartels[1], *Daniele Gaggero*[1], *Christoph Weniger*[1], *Javier Rico*[2], *Manel Martinez*[2]

[1] *GRAPPA and Institute of Physics, University of Amsterdam, Science Park 904, 1098XH Amsterdam, The Netherlands*
[2] *Institut de Física d'Altes Energies (IFAE), The Barcelona Institut of Science and Technology (BIST), Bellaterra (Barcelona), Spain*

Science questions – There is overwhelming evidence that a large component of the matter in the Universe is non-baryonic [1]. So far, all evidence for this dark matter (DM) component is gravitational in origin. Identifying the nature of DM is one of the unsolved puzzles in modern physics.

Over the past decade, a lot of attention has gone to so-called Weakly Interacting Massive Particles (WIMPs) as a DM candidate. The main search strategies for WIMPs are collider searches, direct detection and indirect detection [10]. WIMPs typically are expected to have masses $\gtrsim$ 1 GeV. However, due to non-detection of any signal in various experiments, the attention of the community is shifting beyond the WIMP paradigm. As such, MeV (or sub-GeV) DM models have increasingly attracted attention [12]. Examples of MeV DM models include self-interacting DM [13, 22], 'cannibal' DM [21] and strongly-interacting DM [20]. Further models in the context of e-ASTROGAM are discussed in [3].

Importance of gamma-ray observations – Indirect detection of DM includes the search for gamma-rays from decaying or annihilating DM. In particular, DM could potentially produce sharp spectral features (see below for further details) that are considered to be a smoking gun of DM. A particularly sensitive target in case of annihilating DM is the Galactic Center (GC), since the annihilation luminosity scales with the DM density squared, which is expected to be highest at the center of galaxies [16]. Searches for monochromatic lines from DM towards the GC have been performed by the Fermi–LAT (> 200 MeV) and HESS (> 200 GeV) [2, 1]. On the other hand, dwarf spheroidal (dSph) satellite galaxies of the Milky Way provide clean observational targets, devoid of any astrophysical background that could potentially outshine a DM-induced signal. Considered individually, each dSph would be much less luminous than the GC, but this is partially overcome by the fact that dSphs are numerous (and still being discovered by running optical surveys [9]). Analyzed collectivelly, dSphs provide competitive and robust sensitivity for DM searches. Searches for monochromatic lines and other spectral features from DM towards the Segue 1 dSph have been perfomed by MAGIC (> 100 GeV) [7].

The sensitivity of current gamma–ray experiments in the MeV regime, and therefore the constraint on DM with masses $\lesssim 1$ GeV, is lacking. Current bounds from diffuse gamma-rays are given in [18, 11]. In addition, MeV–DM is difficult to detect via other probes: detecting DM through the measurement of the local cosmic–ray flux is impaired by solar modulation and underground direct detection experiments are insensitive due to the small recoil energies. But, gamma-rays are expected for most of the annihilation channels and can provide a potentially powerful probe.

Expected results with e-ASTROGAM – e-ASTROGAM will be particularly sensitive to spectral features due to the annihilation of sub-GeV DM. In addition, Ref. [15] showed that annihilation of slightly heavier DM can produce excited meson states which also lead to spectral features in MeV γ–rays. For the DM with MeV masses only a limited number of kinematically-allowed final states exist. For large enough masses, DM can potentially annihilate into pions or muons. Below the mass of the muon and pion, the only possible final states are into electrons or photons. Neutrinos are also possible, but this does not lead to a gamma-ray signal. In Fig. 1 we show the

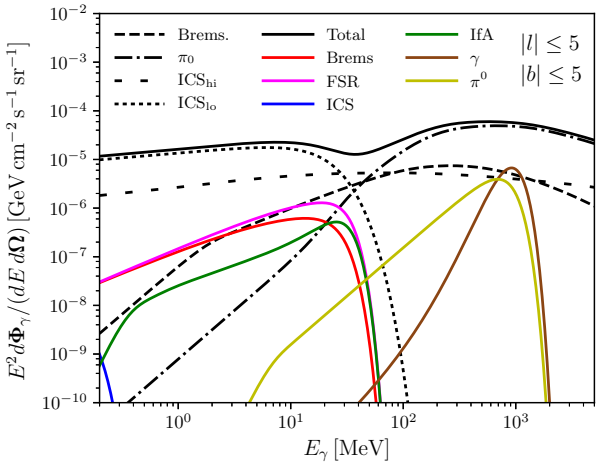

Figure 1: Total background emission in the inner $10^\circ \times 10^\circ$ (black, solid) and broken down into subcomponents (interrupted). Colored lines show spectral features from primary and secondary emission due to DM annihilation, convolved with an energy resolution of $\Delta E/E = 0.3$. The yellow (box) and brown lines (monochromatic photon) are for $\chi\chi \to \pi^0\gamma$ with $m_\chi = 800\,\mathrm{MeV}$. The red, magenta, blue and green line correspond to the emission for an $m_\chi = 30\,\mathrm{MeV}$ DM particle annihilating to e^+e^-. In both cases $\langle\sigma v\rangle = 10^{-28}\,\mathrm{cm^3\,s^{-1}}$. See Ref. [8] for details.

gamma-ray signal from the inner-Galaxy for two characteristic annihilation channels. The yellow and brown line are due to DM with a mass ($m_\chi = 800\,\mathrm{MeV}$) annihilating into a pion and a photon, $\chi\chi \to \pi^0\gamma$, leading to a box feature and a monochromatic line, respectively. This emission is prompt, and thus traces the DM distribution exactly. In addition, we show the spectrum resulting from a $m_\chi = 30\,\mathrm{MeV}$ DM particle annihilating through $\chi\chi \to e^+e^-$. This leads to a prompt signal from final-state radiation (FSR), and additional secondary signals from the injected electrons and positrons, which can have a characteristic spectrum as well. Only prompt emission is expected for dSphs, however, for low DM masses secondaries can be important in the GC.

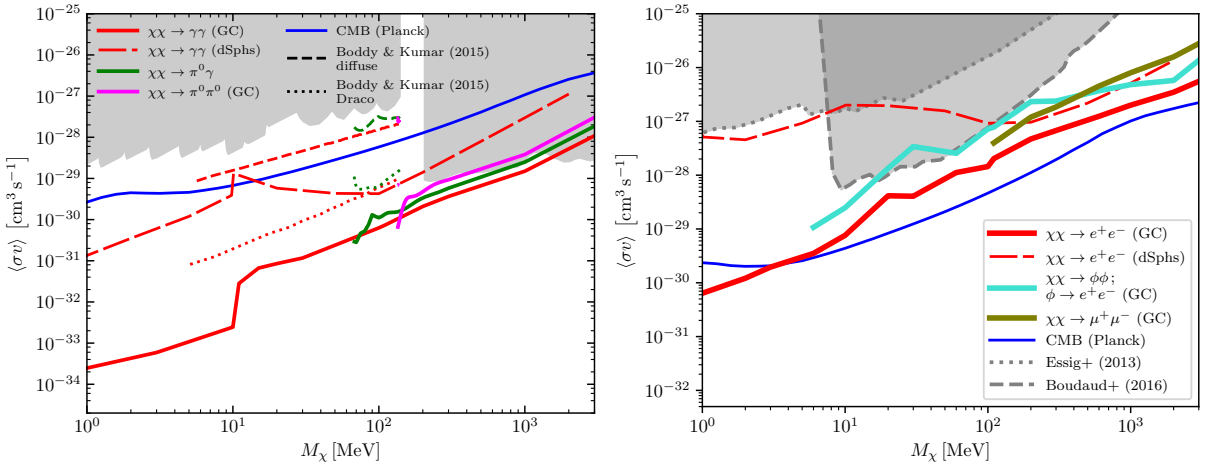

Figure 2: Projected 95% CL upper-limits on DM annihilating to various final states. Adapted from Ref. [8]. Projections are compared to current limits from the CMB (blue, [1]. Left: Projections from [8] DM annihilation into $\gamma\gamma$ (red, solid=GC, long-dashed=dSphs), $\pi^0\gamma$ (green) and $\pi^0\pi^0$ (magenta). The CMB constraints are for $\chi\chi \to \gamma\gamma$ [1, 23]. For the same channel we show γ–ray limits derived [11] and [2] in grey. Right: Projected 95% CL upper-limit on γ-ray emission from DM annihilating to $\mathrm{e^+e^-}$. Results are for the total DM spectrum from the three reference leptonic cases: direct annihilation (red, solid=GC, long-dashed=dSphs)), cascade channel (turquoise) and the muon channel (olive). The blue solid line shows the CMB limits on DM s-wave annihilation into e^+e^- from Planck [1, 23]. In addition we show in light-grey the limits for $\chi\chi \to e^+e^-$ from Voyager [14] and current limits from diffuse emission γ–rays [18].

We study e-ASTROGAM detectability of sub-GeV DM-induced gamma-ray signals from the GC and dSphs (see [19] for another recent study). For the GC we include prompt and secondary emissions from annihilation into photons, neutral pions, muons or electrons (for the latter, either directly or via a cascade) [8]. Projected limits on the annihilation cross-section are derived using Fisher forecasting [17], taking into account astrophysical backgrounds and both long– and short–range systematics in energy. For dSphs, only prompt emission from annihilation into photons and electrons are included at this stage, which already provides a useful comparison between the results expected from the two types of targets. In this case, limits are obtained from a maximum likelihood

analysis [6] and include all dSphs listed in Table 1 of Ref. [5], taking into account the uncertainty in the gamma-ray luminosity from each of them.

The results are shown in Fig. 2. In the left panel projected-limits are shown for final states involving neutral pions and/or monochromatic photons. Existing constraints from diffuse gamma-rays and the CMB are shown as shaded grey areas and a blue line respectively. e-ASTROGAM observations of the inner-Galaxy can produce significantly stronger constraints below $\mathcal{O}(\text{few} \times 100\,\text{MeV})$. Probing cross-sections close to what is expected for thermal DM with a p–wave cross-section. The right panel displays the limits that can be obtained for final states involving leptons. Again, e-ASTROGAM will improve on current bounds, both from diffuse gamma-rays and measurements of the local electron and positron flux. Current CMB limits for the e^+e^- state are stronger, but only apply to s–wave annihilating DM. In case of p–wave annihilating DM e-ASTROGAM will provide the best constraints.

In conclusion, e-ASTROGAM will be able to place very competitive, and sometimes the strongest, constraints on the DM self-annihilation cross-section for sub-GeV DM by observing the inner-Galaxy and dSph satellites of the Milky Way.

References

[1] Abdalla H. and others, 2016, Phys. Rev. Lett., 117, 151302
[2] Ackermann M. and others, 2015, Phys. Rev., D91, 122002
[3] Addazi, A., Bastieri, D. and Marcianò, A., This work.
[4] Ade P. A. R. and others, 2016, Astron. Astrophys., 594, A13
[5] Ahnen M. L. et al., 2016, JCAP, 1602, 039
[6] Aleksić J., Rico J. and Martinez M., 2012, JCAP, 1210, 032
[7] Aleksić J. et al., 2014, JCAP, 1402, 008
[8] Bartels R., Gaggero D. and Weniger C., 2017, JCAP, 1705, 001
[9] Bechtol K., et al., 2015, Astrophys. J., 807, 50
[10] Bertone G., Hooper D. and Silk J., 2005, Phys. Rept., 405, 279-390
[11] Boddy K. K. and Kumar J., 2015, Phys. Rev., D92, 023533
[12] Boehm C., Ensslin T. A. and Silk J., 2004, J. Phys., G30, 279-286
[13] Boehm C. and Fayet P., 2004, Nucl. Phys., B683, 219-263
[14] Boudaud M., Lavalle J. and Salati P., 2016
[15] Bringmann T., Galea A., Hryczuk A. and Weniger C., 2017, Phys. Rev., D95, 043002
[16] Bringmann T. and Weniger C., 2012, Phys. Dark Univ., 1, 194-217
[17] Edwards T. D. P. and Weniger C., 2017
[18] Essig R.et al., 2013, JHEP, 11, 193
[19] Gonzalez-Morales A. X., Profumo S. and Reynoso-Córdova J., 2017
[20] Hochberg Y., Kuflik E., Volansky T. and Wacker J. G., 2014, Phys. Rev. Lett., 113, 171301
[21] Pappadopulo D., Ruderman J. T. and Trevisan G., 2016, Phys. Rev., D94, 035005
[22] Pospelov M., Ritz A. and Voloshin M. B., 2008, Phys. Lett., B662, 53-61
[23] Slatyer T. R., 2016, Phys. Rev., D93, 023527

Synergy between e-ASTROGAM and optical observations for indirect Dark Matter searches

Lucio Angelo Antonelli[1], *Michele Fabrizio*[1,2], *Paola Giammaria*[2], *Saverio Lombardi*[1,2]

[1] *Space Science Data Center (SSDC) ASI, Via del Politecnico snc, 00133, Rome, Italy*
[2] *INAF-OAR, Via Frascati n. 33, 00078, Monte Porzio Catone (RM), Italy*

Science questions – Dark Matter (DM) is an unknown, as yet unidentified type of matter, which accounts for about 85% of the total mass content in the Universe. We infer its existence from the observations of its gravitational effects on galaxies, galaxy clusters, and the anisotropies of the Cosmic Microwave Background [1]. DM should consist of electrically neutral particles beyond the Standard Model (SM), likely relic from the Big Bang and stable within cosmological time scales. Furthermore, in order to produce a relic density in agreement with cosmological observations and be compatible with Big Bang nucleosynthesis [2], these particles must be "cold" (i.e. non relativistic) at the onset of structure formation (assuming the thermal production scenario).

Among different cold DM particle candidates, a particularly well-motivated and widely considered class is the so-called Weakly Interacting Massive Particles (WIMPS [3]). WIMPs naturally arise in many SM extensions, have mass in the range between $\mathcal{O}(1)$ GeV and tens of TeV, interaction cross-sections typical of the weak scale, and naturally provide the needed relic density. WIMPs are expected to self-annihilate and/or decay, producing a flux of gamma rays up to the DM mass, and potentially sharp spectral features, which could be accessible by space- and ground-based gamma-ray instruments.

In the last years, due to the lack of clear evidence of DM signal in all current complementary experiments (i.e. colliders, direct and indirect searches [4]), other scenarios beyond the WIMP paradigm are also getting increasing attention. Among them, MeV (or sub-GeV) DM models, such as self-interacting DM, "cannibal" DM, and strongly-interacting DM (see [5, 6] for further models and details in the context of e-ASTROGAM) are currently widely considered. In all these scenarios, gamma rays in the energy range where e-ASTROGAM will operate are expected to be produced.

In the local Universe, the Galactic Center (GC) and the dwarf spheroidal satellite galaxies (dSphs) are among the most promising targets for the indirect DM searches. The dSphs are believed to be the smallest (size $\sim$1 kpc) and faintest (10^2 – 10^8 $L_\odot$) astronomical objects whose dynamic is dominated by DM (mass–to–light ratios $\frac{M}{L}$ $\sim$1000 $\frac{M_\odot}{L_\odot}$ for the ultra-faint (UF) ones). Despite a typically lower DM gamma-ray induced flux with respect to the expected one from the GC, the dSphs satellite of the Milky Way (MW), due to their proximity (from few tens of kpc up to few hundreds of kpc) and intrinsic gamma-ray emission from standard astrophysical sources generally negligible [7], represent clean targets for DM searches in the gamma-ray energy domain. At the same time, most dSphs are located at intermediate or high galactic latitudes where Galactic foregrounds are suppressed, thus they are particularly interesting to be observed by gamma-ray detectors for indirect DM searches.

In addition, it has become increasingly clear over the last two years that the census of Local Group satellites is very incomplete. Moreover, the history itself of dSphs discovery has already shown amazing big steps thanks to the employment of instruments able to realize more and more deep photometric and astrometric scan of the sky [8]. Hence, the new generation of sky surveys (Pan-STARRS [9], DES [10], GAIA [11], LSST [12], etc.) – already operating and/or incoming – are bringing new discoveries[1]. These surveys are indeed extending the knowledge of possible sites of large DM concentrations and a detailed study should be made to continuously select the best targets.

[1] In 2015, they enabled the discovery of more than 20 new Milky Way satellites having morphological characteristics similar to the known DM-dominated dSphs.

Importance of gamma-ray observations – Satellite dSphs have been under the eyepiece of many telescopes of different telescope classes for the last twenty years. Optical telescopes are devoted to investigate their dynamics. However, to probe their dark matter content, instruments working in the high-energy (from MeV up to TeV) band are believed to be well suited to shed light. The reason is directly related to the mass of the DM particles expected within well-motivated theoretical scenarios. In this regard, the MeV-GeV band could be the crucial regime to understand the low energy continuum spectrum expected from DM annihilation/decay processes.

In addition to this, the sensitivity of e-ASTROGAM in the MeV-GeV domain could enable a further characterization of dSphs, allowing for possible discovery of a new class of gamma-ray emitters such as millisecond pulsars, still undetected in these galaxies at higher energy (GeV-TeV domain). Studies to estimate the GeV emission of millisecond pulsars in dSphs have been recently performed in order to valuate the impact of their emission in the DM search [13].

Importance of optical observations – The DM density profile of the target of interest is a crucial point in the indirect DM search. Mass models are most commonly derived by exploiting the stellar population as a dynamical tracer of the underlying gravitational potential well (and hence of the dominant mass component, namely the DM mass profile). The dynamical mass of a dSph is estimated by quantifying the stellar velocity dispersion (σ_v). Due to the lack of deep photometric and spectroscopic data of several ultra-faint dSphs – the most promising DM search target among satellite galaxies – current studies suffer from great uncertainties in M/L estimation, and even in target selection. In order to identify the best targets among MW dSphs' population multi-epoch photometric and spectroscopic observations have to be performed. These studies allow a better constraining of the astrophysical properties required to infer the DM content estimation (total luminosity, presence of binary systems, kinematics of member stars, ...). Optical studies devoted to dSphs have been already carried out e.g. with the Large Binocular Telescope (LBT) [14] and the Very Large Telescope (VLT) [15]. In addition, new GAIA releases are expected to both discover new dSph candidates and improve the dSphs' luminosity estimation.

Expected results with e-ASTROGAM – In [5, 16], preliminary prospects for e-ASTROGAM observations of the inner Galaxy and dSphs are provided. In particular, in [5] it is shown that e-ASTROGAM will be particularly sensitive to spectral features due to the annihilation of sub-GeV DM and be able to place for those models very competitive constraints on the DM self-annihilation cross-section. Similar conclusions are also achieved in [16], considering the observations of two dSphs, Draco and Ursa Minor.

In order to reduce systematics associated to already-known DM targets and establish new ones, optical observations are of major importance. Therefore, a synergy between gamma-ray observations with e-ASTROGAM and optical surveys is expected to strengthen the overall DM scientific case.

References

[1] G. Bertone (ed.) Particle Dark Matter. Cambridge University Press. Cambridge (2010).

[2] Plank Collaboration, Ade P.A.R. et al., Planck 2015 results, XIII. Cosmological parameters [arXiv:1502.0158].

[3] J. L. Feng, Ann. Rev. Astron. Astrophys. 48 (2010) 495.

[4] Cahill-Rowley M. et al., , Complementarity of Dark Matter Searches in the pMSSM, Phys. Rev. D 91, 055011 (2015) [arXiv:1405.6716].

[5] Bartels, R., Gaggero, D., Weniger, C., Rico, J. and Martinez, M., This work.

[6] Addazi, A., Bastieri, D. and Marciano, A., This work.

[7] Bergstrom L. (2012), Annalen der Physik, vol 524 issue 9-10, pp479-496.

[8] Walker M. G., Vol. 5 of the book 'Planets, Stars, and Stellar Systems', published by Springer, [arXiv:1205.0311].

[9] Chambers K. C., et al., The PAN-STARRS1 surveys, [arXiv:1612.05560].

[10] Drlica-Wagner A., et al.,DES Collaboration, ApJ 813 109 (2015) [arXiv:1508.03622].

[11] Antoja T., et al., Mon.Not.Roy.Astron.Soc., 453(2015)541560 [arXiv:1507.04353].

[12] Jurić M., et al., Proceedings of ADASS XXV [arXiv:1512.07914].
[13] Winter M., et al., The Astrophysical Journal letters Vol 832, N1 [arXiv:1607.06390].
[14] Fabrizio M., et al., 2014 A&A 570, 61.
[15] Fabrizio, M., et al., 2016, ApJ, 830, 126.
[16] Morselli, A., Rodriguez Fernandez, G., This work.

e-ASTROGAM and Dwarf spheroidal galaxies

Aldo Morselli, Gonzalo Rodriguez Fernandez

Istituto Nazionale di Fisica Nucleare, Sezione di Tor Vergata, Rome, Italy

Science questions – The existence of dark matter (DM) in our Universe (27% of the total energy) is well established, but its nature is still unknown. Among the most promising particle candidates are Weakly Interacting Massive Particles (WIMPs), which typically can self-annihilate and generate gamma rays [1, 7]. If WIMPs particles are produces thermally in the early Universe then the self-annihilation cross-section has a natural value of approximately $3 \times 10^{-26}\mathrm{cm}^3\mathrm{s}^{-1}$ [3]. WIMPs models, such as the supersymmetric neutralino give prediction the for gamma-ray energy spectra from the annihilations, which are crucial inputs, together with the DM distribution in the observed target, to achieve prospects for the sensitivity of indirect searches [4]. The goal of the present study is to provide preliminary comparative expectations on indirect DM searches with the planned mission e-ASTROGAM [13], taking into account continuum gamma-ray signatures coming from typical DM annihilation channels. The indirect dark matter search with e-ASTROGAM has many possible astrophysical targets with different advantages and disadvantages.

The total mass of dark matter in the Galactic halo together with its proximity to Earth make it the most promising source for dark matter searches and the perspective for e-ASTROGAM is described in [6]. However its proximity means that the source is diffuse and signal and background separation is problematic. The limits from the Galactic Center in principle are stronger but the limits from spheroidal galaxies are much less dependent from uncertainties like the halo distribution, other astrophysical signals and backgrounds. A detection from spheroidal galaxies will be a smoking gun for the discovery of Dark Matter.

Importance of gamma-ray observations – Indirect detection of dark matter annihilations through gamma rays has attracted much interest due to several unique properties of gamma rays. First of all, they do not scatter appreciably during their travel through the Galaxy, but rather point back to the site where the annihilation took place. Also, absorption can generally be neglected, as the cross-section for scattering on electrons and nuclei for MeV to TeV photons is small. This means that one may use properties of the energy distribution resulting from these processes to separate a signal from astrophysical foreground or backgrounds. And, as the electromagnetic cross-section of gamma rays is so much higher than the weak interaction cross-section for neutrinos, they are relatively easy to detect.

This is particulary true for the possible signals coming from dwarf spheroidal galaxies because it could give a clear and unambiguous detection of dark matter. Neither astrophysical gamma-ray sources (supernova remnants, pulsar wind nebulae,...) nor gas acting as target material for cosmic rays have been observed in these systems.

Expected results with e-ASTROGAM – The indirect detection experiments aim at searching for a flux of annihilation products created in astrophysical environments where DM annihilation may be occurring at an appreciable rate [7]. In particular, the indirect DM searches carried out by e-ASTROGAM look for photons from WIMPS in the mass range ∼0.3 MeV up to ∼3000 MeV. The flux expected from a DM-dominated region depends respectively on the so-called particle physics and astrophysical (or J) factors:

$$\Phi_s(\Delta\Omega) = \frac{1}{4\pi}\frac{<\sigma v>}{2m_{DM}^2}\int_{E_{min}}^{E_{max}}\frac{dN_\gamma}{dE_\gamma}dE_\gamma \times J(\Delta\Omega), \quad (1)$$

where $<\sigma v>$ is thermally averaged self-annihilation cross-section times velocity, m_{DM} is the dark matter particle mass, E_{min} and E_{max} are the energy limits for the measurement and $\frac{dN_\gamma}{dE_\gamma}$ is

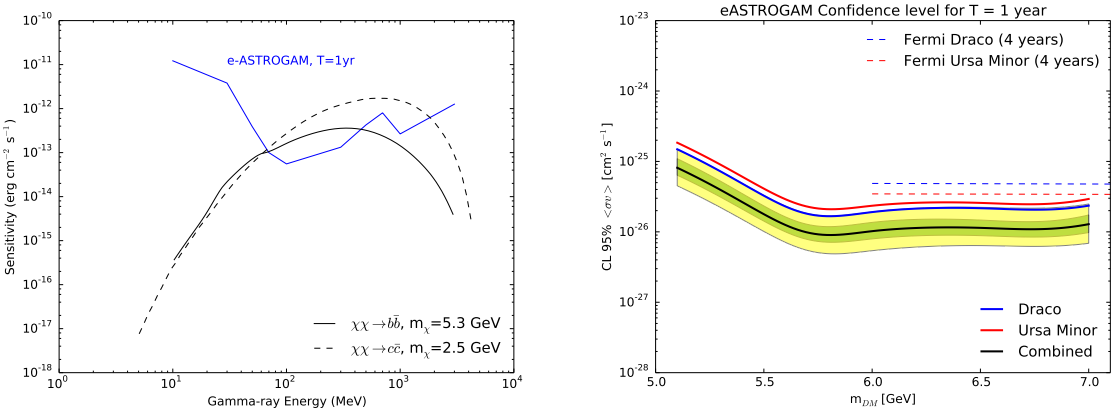

Figure 1: Left: Point source continuum sensitivity for e-ASTROGAM for an effective exposure of 1 year for a source at high Galatic latitude. Solid and dashed black lines represents the expected flux from Draco for J=1.7e19 GeV^2 cm^{-5}, $<\sigma v>$ = 3e-26 cm^3 s^{-1}, m$_\chi$= 2.5 and 5.3 GeV and two self-annihilation channels. Right: Sensitivity for $<\sigma v>$ from observation of the classical dwarf galaxy Draco and Ursa Minor for self-annihilation channel $b\bar{b}$.

the energy spectrum of the gammas produced in the annihilation (as, e.g., from [8]). The J-factor is the integral along the line of sight of the squared DM density profile of the given target integrated within an aperture angle, $\int_{\Delta\Omega} d\Omega \int_{l.o.s.} \rho^2_{DM}(r) dl d\Omega'$. The products of DM annihilation are thought to come from decay and/or hadronization of the primary Standard Model (SM) particles: quark-antiquark, lepton and boson, and each channel is expected to have its own branching ratio. In figure 1, as an example, we show the expected flux for two self-annihilation channels in comparison with the e-ASTROGAM sensitivity for 1 year.

References

[1] Lars Bergstrom, 2000, Reports on Progress in Physics, 63(5), 793

[2] G. Bertone, D. Hooper, J. Silk, 2005, Phys. Rept. 405, 279-390

[3] G. Steigman, B. Dasgupta, J. F. Beacom, Phys. Rev. D86 (2012) 023506

[4] S.P.Martin, A Supersymmetry Primer, in: G. L. Kane(Ed.),Perspectives on Supersymmetry, 1998. arXiv:hep-ph/9709356.

[5] A. DeAngelis, et al.,The e-ASTROGAM mission(exploring the extreme Universe with gamma rays in the MeV-GeV range) Experimental Astronomy 44 (2017) 25-82 [arXiv:1611.02232].

[6] Bartels, R., Gaggero, D., Weniger, C., Rico, J. and Martinez, M., This work

[7] M. Ackermann, et al., Phys. Rev. D89 (2014) 042001

[8] M. Cirelli, G. Corcella, A. Hektor, G. Hutsi, M. Kadastik, et al., PPPC 4 DM ID: A Poor Particle Physicist Cookbook for Dark Matter Indirect Detection, JCAP 1103 051.

High Galactic latitude, unassociated gamma-ray sources: uncovering dark matter subhalos in the MeV band

Daniel Nieto[1], *Juan A. Barrio*[1], *Miguel A. Sánchez-Conde* [2]

[1] *Unidad de Partículas y Cosmología (UPARCOS), Universidad Complutense, E-28040 Madrid, Spain*
[2] *Instituto de Física Teórica (IFT UAM-CSIC) and Departamento de Física Teórica, Universidad Autónoma de Madrid, ES-28049 Madrid, Spain*

Science questions – The standard model of cosmology requires around 84% of the total amount of matter in our Universe to be dark matter [1]. The existence of dark matter has been proved from its gravitational effects, yet the real nature of its constituent (or constituents) has not been unveiled and remains one of the major open questions in physics. N-body high-resolution cosmological simulations of Milky-Way-like galaxies have revealed that the distribution of dark matter in this type of objects is far from smooth, rather exhibiting a wealth of substructures, or subhalos, at all spatially-resolved mass scales [2, 3, 4]. It is believed that the most massive of these subhalos host the satellite galaxies we observe today, while there should be a large population of subhalos not massive enough to capture gas and/or stars at all. The effective lack of baryonic gas renders star formation unlikely in these small subhalos, making them virtually invisible. Yet, in models where the dark matter particle self-annihilates or decays into standard model products, some of these dark matter subhalos might be located sufficiently close to Earth so to produce detectable signals. Indeed, these objects are expected to possess very dense dark matter cores. Therefore, they are probably not only resilient to the strong tidal forces they are subject to in the inner Galactic regions, but also potentially yielding very high annihilation fluxes.

Importance of gamma-ray observations – If the dark matter particle mass is located in the MeV [5, 7] or GeV range [7], annihilation or decay signals from dark matter subhalos could be potentially detected by telescopes sensitive to these energies. Since dark-matter-induced gamma-ray emission is expected to be constant, subhalos could then appear in all-sky surveys sensitive at gamma-ray energies. Depending on the proximity of those subhalos to Earth, they might show up as point-like or extended sources in such surveys.

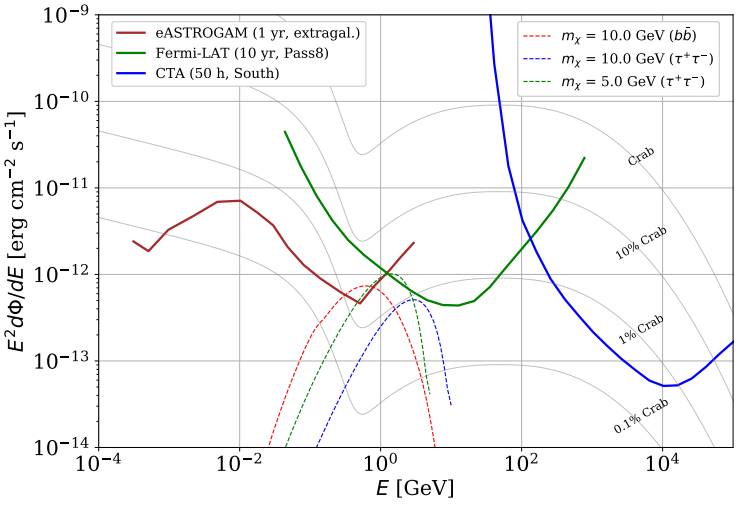

Figure 1: e-ASTROGAM sensitivity, in a spectral energy distribution form, to point-like WIMP-based dark matter subhalos. Full lines represent the sensitivity of several instruments (with e-ASTROGAM one in brown), while dash lines represent the dark matter subhalo energy flux for several dark matter models. See text for further details.

The search for dark matter subhalos in the GeV gamma-ray band has a long record: the Fermi-LAT Collaboration has thoroughly searched their data for potential point-like subhalos [8], and searches for candidates among the unassociated sources in the different LAT catalogs have been conducted, e.g., [9, 10]. Currently, there are two intriguing candidates, not only showing a lack of counterparts at other wavelengths and spectra compatible with the hypothesis of annihilating dark matter, but also showing spatial

extension in LAT data [11, 12]. Higher angular resolution experiments sensitive to gamma rays may be able to shed light on the actual morphology of the sources, resolving the standing ambiguity between the hypothesis of an extension originated by unresolved multiple sources or by the distribution of dark matter in a nearby subhalo [13].

These searches for subhalo candidates in the GeV band have also been complemented by searches in the TeV energy regime by the current generation of imaging atmospheric Cherenkov telescopes. TeV subhalo searches base their strategy on follow up observations of subhalo candidates in Fermi-LAT catalogs that are spectrally compatible with dark matter particle masses in the several hundred GeV to multi TeV range [14]. Dedicated observations of dark matter subhalo candidates have been reported by both MAGIC [15] and VERITAS [16] Cherenkov telescopes.

Expected results with e-ASTROGAM – e-ASTROGAM will be able to contribute to the search of both point-like and extended dark matter subhalos. Regarding the former, its exceptional sensitivity in all the MeV range will naturally allow to put to the test dark matter models with particle masses in the MeV range [5, 7], as well as WIMP-based models [7] in the *low-mass* GeV range (around ∼1-20 GeV). Fig.1 shows the expected e-ASTROGAM sensitivity, in a spectral energy distribution (SED) form, to point-like WIMP-based dark matter subhalos. Also shown are the SEDs corresponding to several dark matter models, obtained following Eq. 1 for the annihilation flux.

$$\frac{d\Phi}{dE} = J(\Omega) \times \frac{d\Phi^{PP}}{dE} = \int_{l.o.s} \rho^2_{DM}(l) d\Omega dl \times \frac{1}{4\pi} \frac{< \sigma_{ann} v >}{2m^2_{DM}} \sum_i B_i \frac{dN_i}{dE} \quad (1)$$

It is worth noting that WIMP-based dark matter models with particle masses beyond the e-ASTROGAM upper energy threshold can be within the reach of the instrument, since a substantial fraction of the annihilation photon yield for GeV-mass dark matter particles would be deposited in the MeV range. In the Eq. 1 above, $J(\Omega)$ is the so-called *Astrophysical Factor*. It includes the contributions of the distance to the source and its dark matter content. For the present calculation a value of 1.5×10^{19} GeV^2 cm^{-5} is assumed, which corresponds to that of *Segue 1* dSph [18]. $d\Phi^{PP}/dE$ corresponds to the dark matter particle model, for which we have used the value of the dark matter *relic density* ($< \sigma_{ann} v >= 2.2 \times 10^{-16}$ cm^3 s^{-1}). In Fig.1 we present three different models in which the WIMP dark matter particle completely annihilates either to a $\tau^+\tau^-$ pair or to a $b\bar{b}$ pair. The corresponding $d\Phi^{PP}/dE$ fluxes are obtained from [19].

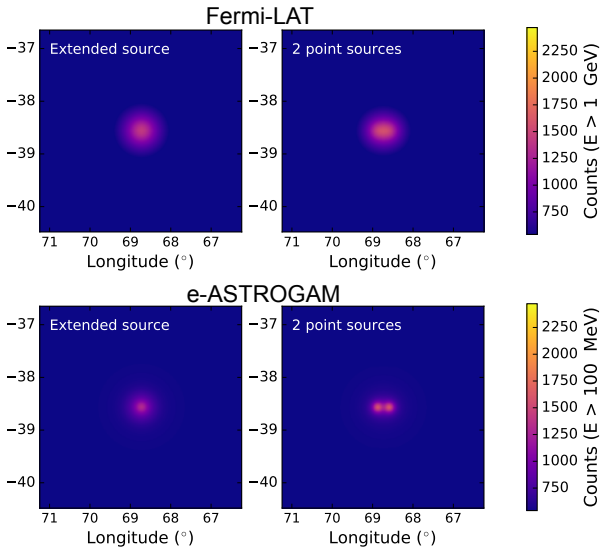

Figure 2: Compared *Fermi*-LAT and e-ASTROGAM ability to resolve between an extended source and two nearby point sources. See text for details.

Additionally, e-ASTROGAM's improved angular resolution with respect to past gamma-ray missions is of remarkable importance to search for dark matter subhalos. There are at least two strong arguments supporting the latter statement: first, a more precise source localization and a smaller containment region will help with source association, especially for those cases where multiple counterparts currently coexist within the source containment region derived from previous missions. This will allow a cleaner sample of unassociated sources for point-like dark matter subhalo search studies. Second, as previously mentioned, a better definition of source spatial morphology can be used as a handle to tell extended dark matter subhalos from conventional unresolved multiple sources. Fig. 2 depicts a simulation result extracted from [13]

showing how e-ASTROGAM can successfully resolve a dark matter subhalo-like extended source (with $\sigma_{68} = 0.25^\circ$) from a pair of point sources (separated by 0.28°), as opposed to *Fermi*-LAT. As a conclusion, e-ASTROGAM all-sky mapping will surely enlarge the population of high Galactic latitude, unassociated sources in the gamma-ray band, thus increasing the likelihood of discovery of dark matter subhalos.

Finally, it is worth mentioning that the synergy in this field between current generation space-borne and ground-based gamma-ray telescopes mentioned above could be extended in the future through the complementarity between the incoming Cherenkov Telescope Array [17] and the e-ASTROGAM mission.

References

[1] **Planck** Collaboration, P. A. R. Ade et al., *Planck 2015 results. XIII. Cosmological parameters*, *Astron. Astrophys.* **594** (2016) A13, [arXiv:1502.01589].

[2] V. Springel, J. Wang, M. Vogelsberger, A. Ludlow, A. Jenkins, A. Helmi, J. F. Navarro, C. S. Frenk, and S. D. M. White, *The Aquarius Project: the subhaloes of galactic haloes*, *MNRAS* **391** (Dec., 2008) 1685–1711, [arXiv:0809.0898].

[3] J. Diemand and B. Moore, *The Structure and Evolution of Cold Dark Matter Halos*, *Advanced Science Letters* **4** (Feb., 2011) 297–310, [arXiv:0906.4340].

[4] S. Garrison-Kimmel, M. Boylan-Kolchin, J. Bullock, and K. Lee, *ELVIS: Exploring the Local Volume in Simulations*, *Mon. Not. Roy. Astron. Soc.* **438** (2014), no. 3 2578–2596, [arXiv:1310.6746].

[5] A. X. Gonzalez-Morales, S. Profumo, and J. Reynoso-Córdova, *Prospects for indirect MeV Dark Matter detection with Gamma Rays in light of Cosmic Microwave Background Constraints*, arXiv:1705.00777.

[6] R. Bartels, D. Gaggero, and C. Weniger, *Prospects for indirect dark matter searches with MeV photons*, *JCAP* **1705** (2017), no. 05 001, [arXiv:1703.02546].

[7] G. Bertone, D. Hooper, and J. Silk, *Particle dark matter: Evidence, candidates and constraints*, *Phys.Rept.* **405** (2005) 279–390, [hep-ph/0404175].

[8] **Fermi-LAT** Collaboration, M. Ackermann et al., *Search for Dark Matter Satellites Using Fermi-LAT*, *ApJ* **747** (Mar., 2012) 121, [arXiv:1201.2691].

[9] H.-S. Zechlin and D. Horns, *Unidentified sources in the Fermi-LAT second source catalog: the case for DM subhalos*, *JCAP* **11** (Nov., 2012) 50, [arXiv:1210.3852].

[10] B. Bertoni, D. Hooper, and T. Linden, *Examining The Fermi-LAT Third Source Catalog In Search Of Dark Matter Subhalos*, *JCAP* **1512** (Apr., 2015) 035, [arXiv:1504.02087].

[11] B. Bertoni, D. Hooper, and T. Linden, *Is The Gamma-Ray Source 3FGL J2212.5+0703 A Dark Matter Subhalo?*, *JCAP* **1605** (2016) 049, [arXiv:1602.07303].

[12] Z.-Q. Xia, K.-K. Duan, S. Li, Y.-F. Liang, Z.-Q. Shen, C. Yue, Y.-P. Wang, Q. Yuan, Y.-Z. Fan, J. Wu, and J. Chang, *3fgl j1924.8-1034: A spatially extended stable unidentified gev source?*, *Phys. Rev. D* **95** (May, 2017) 102001.

[13] T.-L. Chou, D. Tanoglidis, and D. Hooper, *Resolving Dark Matter Subhalos With Future Sub-GeV Gamma-Ray Telescopes*, arXiv:1709.08562.

[14] **MAGIC** Collaboration, D. Nieto, V. Martínez, N. Mirabal, J. A. Barrio, K. Satalecka, S. Pardo, and I. Lozano, *A search for possible dark matter subhalos as IACT targets in the First Fermi-LAT Source Catalog*, 3^{rd} *Fermi Symposium, Rome* (Oct., 2011) [arXiv:1110.4744].

[15] **MAGIC** Collaboration, D. Nieto et al., *The search for galactic dark matter clump candidates with Fermi and MAGIC*, 32^{nd} *International Cosmic Ray Conference, Beijing* (Aug., 2011) [arXiv:1109.5935].

[16] **VERITAS** Collaboration, D. Nieto, *Hunting for dark matter subhalos among the Fermi-LAT sources with VERITAS*, in *Proceedings, 34th International Cosmic Ray Conference (ICRC 2015)*, 2015. arXiv:1509.00085.

[17] M. Doro et al., *Dark matter and fundamental physics with the Cherenkov Telescope Array*, *Astroparticle Physics* **43** (Mar., 2013) 189–214, [arXiv:1208.5356].

[18] V. Bonnivard et al., *Contamination of stellar-kinematic samples and uncertainty about dark matter annihilation profiles in ultra-faint dwarf galaxies: the example of Segue I*, *MNRAS* **462** (2016) 223,, [arXiv:1506.08209].

[19] M. Cirelli et al., *PPPC 4 DM ID: a poor particle physicist cookbook for dark matter indirect detection*, *JCAP* **03** (2011) 051, [arXiv:1012.4515].

All-sky mapping in the 100 MeV region in search for point-like Dark Matter sources

G. Vankova-Kirilovai, Vladimir Bozhilov, V. Kozhuharov, Stefan Lalkovski

Faculty of Physics, University of Sofia "St. Kl. Ohridski"*, Sofia 1164, Bulgaria*

Science question – The nature of Dark matter (DM) and the mechanisms leading to its creation is one of the biggest open questions in modern physics. Currently, it is estimated that about 27% of our Universe consists of Dark matter. To address this question, we propose to perform an all-sky survey in the 100 MeV region in search for discrete lines and point-like sources. The working assumption is that Dark Matter may annihilate, or decay, via emission of leptons, including particles other than electrons. The advantage of having the e-ASTROGAM is that it will have an unprecedented sensitivity exactly in the energy range where lines originating from $\mu^+\mu^-$ annihilation are expected to emerge.

Importance of gamma ray observation – Previously, it was suggested that the dark matter (DM) consists of weakly interacting massive particle (WIMP) that naturally emerge from the supersymmetric extension of the Standard model. Such a WIMP particle was predicted to have a mass of the order of 100 GeV. However, no such particle was experimentally found and the search for dark matter candidates is now being carried out in other directions. Recently, the idea of involving a complete hidden sector of new particles, was revitalized. This hidden sector naturally incorporates the DM and interacts only through a limitted number of processes with the visible sector, usually through the so-called mediator, as shown in fig. 1.

Even though, neither the nature of the DM particle(s) (χ) nor the mechanism that generates it are known, there are indirect experimental evidences suggesting that χ is indeed a weakly interacting particle. Given that, it is natural to assume that the annihilation, and/or its decay, will involve leptons, as shown in fig. 2. These can be electrons and positrons, but also muons, which can be generated via annihilation $\chi + \chi \rightarrow \mu^+ + \mu^-$ and/or decay $\chi \rightarrow \mu^+ + \mu^-$. It should be noted, however, that similar scenario is not forbidden for the τ particles either, but the cross-section for formation of two-tauon bound state is negligible, and hence, the observation of a signature of true taonium is considered to be less likely [1]. The advantage of using muonium annihilation lines for searching of Dark Matter particles is that muon mass is much larger than the $e^{\pm}$ and, hence, the expected signal will be cleaner.

The simplest effective interaction that can be used to describe the process is:

$$L \sim g' q' \overline{\psi}(\gamma_\mu + \alpha' \gamma_\mu \gamma^5)\psi A'^\mu \ , \tag{1}$$

where A' is the mediator between the Dark and Visible sectors. Here ψ is the leptonic field and g' is the new interaction coupling constant. Usually $\alpha'_a = 0$. The charges, q_i, are in general free parameters and for the some of the flavours might vanish - $q_i \rightarrow 0$. The branching ratios for $A' \rightarrow e^+ + e^-$, $A' \rightarrow \mu^+ + \mu^-$, and other competitive at higher energies processes are given in ref. [2]. There is a threshold of 1022 keV for $e^{\pm}$ creation and a 210 MeV for the $\mu^{\pm}$ creation. At higher energies other channels are enabled. In most of the studied scenarios, it is assumed also that the mediator decays with the same strength to different lepton-anti-lepton pairs. But this may prove not to be true due to the lepton non-universality, which may lead to an enhancement of creation (μ^+, μ^-) pairs via the annihilation reaction $\chi + \chi \rightarrow \mu^+ + \mu^-$. New experimental results on the muon magnetic moment [3] and the proton radius[4, 5, 6], indeed, seems to support the different behavior of the electrons and muons with respect to the weak interaction. The $g_\mu - 2$ anomaly may be, indeed, related to a new weakly interacting particle, which lies outside the Standard model, and which would be the best candidate for the DM χ particle.

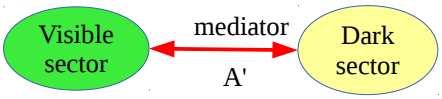

Figure 1: A connection between the visible and the hidden sector through a vector mediator.

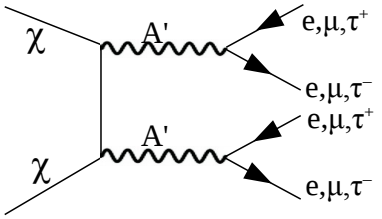

Figure 2: Feynman diagram for Dark matter annihilation into lepton final states.

An all-sky mapping of the 511-keV line was already performed and it is considered to be among the major achievements in the γ-ray astronomy. But the origin of the positrons in the Galaxy is still debated. They can be generated in different process – from nuclear reactions and decays, through black hole evaporation, to decay and/or annihilation of Dark Matter particles. Hence, it is difficult to disentangle the processes leading to DM creation. The key to the problem may lie in the possible complementary channels. The other two types of electrically charged leptons in the Standard model, which can annihilate into photons, are the muons μ and tauons τ with masses M_μ = 105.6 MeV and M_τ=1777 MeV, respectively [7]. It is worth noting that in contrast to the electrons and positrons, the muons and the tauons can not be produced in radioactive decays of atomic nuclei, owing to their superior masses. As such, the maps based on the $\mu^+ + \mu^-$ and/or $\tau^+ + \tau^-$ annihilation peaks can provide a cleaner signal and a new information about the sites of enhanced DM concentration which would be complementary to the data obtained from the 511-keV surveys.

Further, the leptons can be created not only via processes involving DM particles such as $\chi + \chi \rightarrow l^+ + l^-$, but in high energy astrophysical environments a significant numbers of them can be also produced via the $\gamma + \gamma \rightarrow l^- + l^+$ and $e^- + e^+ \rightarrow l^- + l^+$ reactions. However, the muons created in these high-energy environments have energies much higher than the ionization energy (E_{ion} ≈1.4 keV) of the true muonium [1] and, hence, only a small fraction of pairs with energies less then E_{ion} will form a bound system. The muonium has two states, depending on the particles spin orientation. These are para- and orto-muonium. The para-muonioum predominantly decays via two-photon annihilation, while the orto-muonium – via electron-positron annihilation. The energy released in the two-photon annihilation is E=105.66 MeV [1]. This is well inside the energy range of e-ASTROGAM optimal sensitivity. The detection of the muonium annihilation gamma rays will provide an opportunity to study their production mechanism or at least to put constraints to the model predictions.

Expected results with e-ASTROGAM – The advantage of using unstable leptons, rather than using electrons, for allocation of DM particles is in their finite lifetime. The tauons have a lifetime of 2.9×10^{-13} s., while the muons have lifetimes of 2.2μs. Their finite lifetimes provide an unique opportunity for mapping of DM regions with an enhanced precision. Thus, for example, DM particles with masses higher than M_χ = 100 MeV will either annihilate or decay into muons. Estimated mean free path of the muons, before they decay, is of the order of 1000 km, which provides an excellent instrument for mapping of regions of DM particles. Given that, the $\mu^+\mu^-$ annihilation could happen only close to their production site, such processes could provide a higher

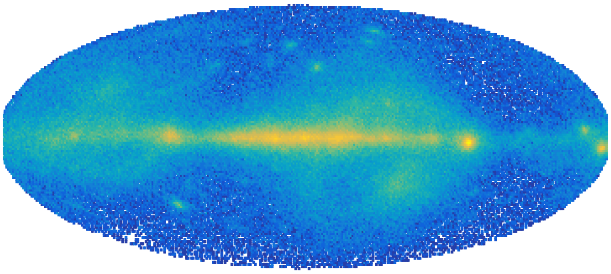

Figure 3: A map of the emission in the range between 100 MeV and 110 MeV obtained from the early FERMI data.

precision all-sky maps of the DM distribution in our Galaxy/Universe.

A preliminary map of the emission in the 100 MeV - 110 MeV region is shown in fig. 3. Although the Galactic plane, Vela, Crab, and Geminga pulsars are clearly visible, the angular resolution limits the possible observation of weak point-like sources. The e-ASTROGAM will have 3 to 5-fold better angular resolution which will enhance the signal to noise ratio significantly. This study will also allow to estimate the $\chi + \chi \rightarrow \mu^+ + \mu^-$ branching ratio which would also have an impact on the understanding of the $g_\mu - 2$ anomaly and the nature of the weak interaction(s).

Due to low cross-section, the process of muon annihilation into two photons has not been observed experimentally so far. On the other side, some astrophysical environments where regions with large abundance of Dark Matter can provide unique opportunity for the observation of such exotic channels. e-ASTROGAM, being superior than its predecessors in the O(100 MeV) region [8], will be capable of addressing these long standing questions by directly detecting some of the most exotic particle reactions, or at least to put constrains on some of the production rates.

References

[1] S. C. Ellis and J. Bland-Hawthorn, Phys. Rev. D **91** (2015) no.12, 123004

[2] M. Raggi and V. Kozhuharov Riv. Nuovo Cim. **38 no. 10** (2015) 449.

[3] G. W. Benett *et al.* (The g-2 Collaboration), Phys. Rev. **D73** (2006) 072003.

[4] C. E. Carlson, Prog. Part. Nucl. Phys. **82** (2015) 59

[5] A. Bayer *et al.*, Science **358** (2017) 79

[6] 2014 CODATA recommended values

[7] K.A. Olive *et al.* (Particle Data Group), Chin. Phys. **C38** (2014) 090001

[8] A. De Angelis *et al.* [e-ASTROGAM Collaboration], Exper. Astron. **44** (2017) no.1, 25 doi:10.1007/s10686-017-9533-6 [arXiv:1611.02232 [astro-ph.HE]].

Particle dark matter searches via angular cross-correlations

Stefano Camera[1,2,3,4], *Nicolao Fornengo*[1,2] *Marco Regis*[1,2]

[1]*Dipartimento di Fisica, Università degli Studi di Torino, Via P. Giuria 1, 10125 Torino, Italy*
[2]*Istituto Nazionale di Fisica Nucleare, Sezione di Torino, Via P. Giuria 1, 10125 Torino, Italy*
[3]*Istituto Nazionale di Astrofisica, Osservatorio Astrofisico di Torino, Strada Osservatorio 20, 10025 Pino Torinese, Italy*
[4]*Department of Physics & Astronomy, University of the Western Cape, Cape Town 7535, South Africa*

Science questions – The nature of dark matter (DM) is still an unsolved mystery: its particle physics interpretation is a quite natural option, but a clear and unequivocal signal due to its particle physics nature is nonetheless missing. From the host of investigations of the last two decades, it is now clear that the expected signals have to be extremely weak. Moreover, they need to be isolated from overwhelming and complex astrophysical backgrounds that mask the expected DM signal both morphologically and in terms of spectral features. This makes individual DM targets (clusters, galaxies, galaxy satellites or subhaloes) difficult to be detected, although contributing to a (possibly) large cumulative unresolved component. DM constitutes the backbone of all cosmic structures and DM haloes represent, collectively, a potential source of DM decay or annihilation signals. While isotropic at first order, this signal emission reflects the fluctuations of the underlying DM distribution: statistical investigations of maps of large portions of the sky can therefore be a powerful technique that can potentially help in separating the DM signal from the astrophysical backgrounds. Even if the radiation originating from DM annihilations or decays in a single halo is too faint to be detected, their cumulative signal and its spatial coherence could be.

The non-gravitational signal associated to decay is proportional to the DM density, while the DM annihilation signal is proportional to the density squared; in both cases the emission is peaked at low redshift, say $z < 0.3$. The redshift distribution gives a handle to separate DM signals from more mundane astrophysical processes that typically trace the star formation history and peak at higher redshifts. An effective way to filter out any γ-ray signal that is not associated to DM-dominated structures or that is originated at high redshift is to cross-correlate the γ-ray radiation field with *bona fide* low-redshift DM tracers [1, 2, 3, 4, 5, 9,]. Note that this technique has the potential to bring redshift information to the γ signal, otherwise not available. To perform a measurement of the angular cross-correlation between the γ-ray background and the large scale structure distribution in the Universe with significant statistics, we need surveys with large sky coverage and (at least) sub-degree angular resolution for both the gravitational and γ-ray measurements.

Importance of γ-ray observations – The e-ASTROGAM mission offers intriguing prospects for the identification of γ-ray signals induced by particle DM. This is true in particular for DM candidates having the peak of the γ-ray emission in the range from sub-MeV up to about 1 GeV. In this range of energy, e-ASTROGAM is superior to the Fermi-LAT satellite in performing the cross-correlation analysis mentioned above. Indeed, not only e-ASTROGAM increases sensitivity and extends the energy range covered by Fermi-LAT, but it also improves the angular resolution, a property of the detector which is very relevant when performing angular correlation studies.

In the following, we illustrate the e-ASTROGAM capability in the specific and yet very relevant framework of light weakly interacting massive particles (WIMP). Indeed, for a WIMP DM candidate annihilating into quarks, the peak of the γ-ray emission occurs at about 1/20 of the DM mass. Therefore, a candidate with mass below $\lesssim 20$ GeV can be efficiently constrained (or detected) with observations of sub-GeV photons.

On the other hand, the cross-correlation analysis is not limited to WIMPs. A similar approach can be adopted with e-ASTROGAM to study MeV DM (emitting γ-rays in the MeV range), such

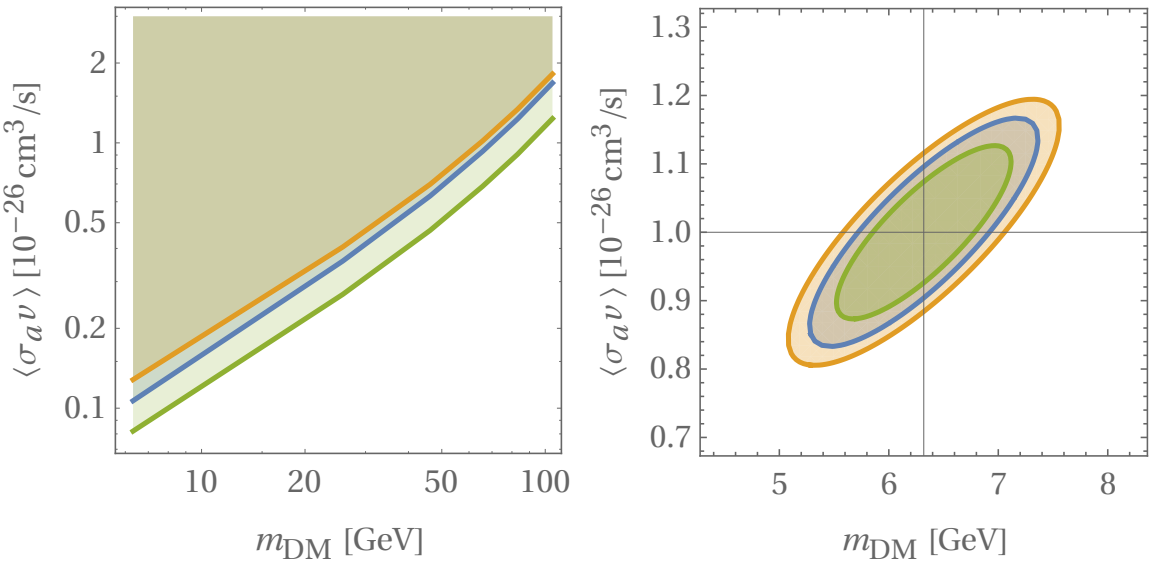

Figure 1: Left: 2σ bounds on the DM annihilation cross section versus its mass for a DM candidate annihilating into bottom quarks. The blue line is derived from the cross-correlation of e-ASTROGAM with Euclid cosmic shear, the yellow instead considers the Euclid galaxy clustering, and green line is their combination. Right: 1σ joint marginal error contours on WIMP parameters for e-ASTROGAM γ-ray data cross-correlated with Euclid (same colour code as in left panel). We chose a WIMP candidate with fiducial DM mass of $\sim$6 GeV and annihilation cross section of $10^{-26}\,\mathrm{cm}^3/\mathrm{s}$.

as self-interacting DM, 'cannibal' DM , strongly-interacting DM, and axion-like-particles. DM candidates annihilating into leptonic final states or charged pions through s-waves can be strongly constrained by CMB experiments [6]. For p-wave annihilation and, in general, for DM candidates with prompt γ-ray emission, the constraints derived from γ-rays are instead found to be the strongest [7]. The technique proposed here, involving angular cross-correlation of extragalactic DM, have been already proven to provide bounds comparable to local probes (such as dwarf spheroidal galaxies and the Galactic center) for WIMP DM [8]. This applies also to MeV DM since the term dependent from particle properties can be (roughly, at first approximation) factorized in the computation of the signals. Note also that the capability of the cross-correlation analysis will especially benefit from the tremendous improvement expected from cosmological surveys in the next decade, and thus not only from the progresses on gamma-ray detectors.

Expected results with e-ASTROGAM – In order to assess the potential of e-ASTROGAM for the cross-correlation studies, we adopt a Fisher matrix technique to obtain forecasts for the angular cross-correlation signal of DM γ-ray emission with two gravitational tracers of the DM distribution in the Universe, namely cosmic shear and galaxy number counts, as they will be measured by a Stage IV DETF experiment such as, for instance, the Euclid-like satellite [see e.g.[10],[11],[12]].

The γ-ray background used for this analysis is assumed to be dominated by blazars and is modeled by extrapolating the γ-ray luminosity function that fit Fermi-LAT observations, cross-checking that the derived emission in the sub-GeV range can accommodate Comptel measurements. For details about the computation of the angular power spectrum, the choice of the cosmological parameters, and the DM properties, see Ref. [9]. The performance of e-ASTROGAM is taken from Table IV in Ref. [13]. For the sake of simplicity and to be definite, we focus here on the pair production regime for DM annihilation and we consider γ-ray energies above 50 MeV. The Compton domain is very relevant for MeV DM and will be considered in future extensions of this forecast. For the specifications of the Stage IV DETF Euclid-like experiment, we follow Ref. [3].

Bounds on the DM annihilation cross section versus its mass are reported in Fig. 1 (left panel) for a DM candidate annihilating into bottom quarks. The blue line shows the constraint considering

cross-correlation of e-ASTROGAM with Euclid cosmic shear, yellow with Euclid galaxy clustering, while green is their combination. In Fig. 1 (right panel) we show the capability of e-ASTROGAM in reconstructing the microphysics properties of the DM particle in the case of a positive detection of the cross-correlation signal, under the hypothesis that the fiducial DM mass is about 6 GeV and the annihilation cross section is $10^{-26}\,\mathrm{cm}^3/\mathrm{s}$, i.e. a factor of three below the so-called natural scale for a thermal relic. Fig. 1 shows that prospects for e-ASTROGAM in the cross-correlation channel are quite interesting and could lead to relevant limits in a wide portion of the DM parameter space, especially for light DM particles.

References

[1] Stefano Camera, Mattia Fornasa, Nicolao Fornengo, and Marco Regis. A Novel Approach in the Weakly Interacting Massive Particle Quest: Cross-correlation of Gamma-Ray Anisotropies and Cosmic Shear. *Astrophys. J.*, 771:L5, 2013.

[2] Nicolao Fornengo, Laurence Perotto, Marco Regis, and Stefano Camera. Evidence of cross-correlation between the CMB lensing and the γ-ray sky. *Astrophys. J.*, 802(1):L1, 2015.

[3] Stefano Camera, Mattia Fornasa, Nicolao Fornengo, and Marco Regis. Tomographic-spectral approach for dark matter detection in the cross-correlation between cosmic shear and diffuse γ-ray emission. *JCAP*, 1506(06):029, 2015.

[4] Jun-Qing Xia, Alessandro Cuoco, Enzo Branchini, and Matteo Viel. Tomography of the Fermi-LAT γ-Ray Diffuse Extragalactic Signal via Cross Correlations with Galaxy Catalogs. *Astrophys. J.s*, 217:15, March 2015.

[5] Enzo Branchini, Stefano Camera, Alessandro Cuoco, Nicolao Fornengo, Marco Regis, Matteo Viel, and Jun-Qing Xia. Cross-correlating the γ-ray sky with Catalogs of Galaxy Clusters. *Astrophys. J. Suppl.*, 228(1):8, 2017.

[6] T. R. Slatyer. Indirect dark matter signatures in the cosmic dark ages. I. Generalizing the bound on s-wave dark matter annihilation from Planck results. *Phys. Rev. D* **93** (2016) no.2, 023527.

[7] R. Bartels, D. Gaggero and C. Weniger. Prospects for indirect dark matter searches with MeV photons. *JCAP* **1705** (2017) no.05, 001.

[8] M. Regis, J. Q. Xia, A. Cuoco, E. Branchini, N. Fornengo, and M. Viel. Particle dark matter searches outside the Local Group. *Phys. Rev. Lett.* **114** (2015) no.24, 241301.

[9] Tilman Tröster et al. Cross-correlation of weak lensing and gamma rays: implications for the nature of dark matter. *Mon. Not. Roy. Astron. Soc.*, 467:2706, 2017.

[10] R. Laureijs et al. Euclid Definition Study Report. *ESA-SRE*, 12, 2011.

[11] Luca Amendola et al. Cosmology and fundamental physics with the Euclid satellite. *Living Rev. Rel.*, 16:6, 2013.

[12] Luca Amendola et al. Cosmology and Fundamental Physics with the Euclid Satellite. 2016.

[13] A. De Angelis et al. The e-ASTROGAM mission. *Exper. Astron.*, 44(1):25–82, 2017.

Axion-like particles (ALPs) and MeV space gamma-ray detectors

Alessandro De Angelis [1], *Giorgio Galanti*[2], *Marco Roncadelli*[3], *Fabrizio Tavecchio*[4]

[1] *INFN and INAF Padova, Italy; LIP/IST Lisboa, Portugal*
[2] *Dipartimento di Fisica, Università dell'Insubria,Via Valleggio 11, I-22100 Como, Italy*
[3] *INFN, Sezione di Pavia, Via A. Bassi 6, I-27100 Pavia, Italy, and INAF*
[4] *INAF – Osservatorio Astronomico di Brera, via E. Bianchi 46, I–23807 Merate, Italy*

Science questions – ALPs are neutral and very light pseudo-scalar bosons a [1]. They are predicted by many extensions of the Standard Model, especially by those based on superstrings. They couple to two photons and their interaction Lagrangian is

$$\mathcal{L}_{\rm ALP} = \frac{1}{2}\,\partial^\mu a\,\partial_\mu a - \frac{1}{2}\,m^2\,a^2 + g_{a\gamma}\,a\,\mathbf{E}\cdot\mathbf{B}\ , \qquad (1)$$

where $\mathbf{E}$ and $\mathbf{B}$ are the electric and magnetic components of the field strength $F^{\mu\nu}$. They are similar to axions but at variance with them the 2-photon coupling $g_{a\gamma}$ is *unrelated* to the ALP mass m. The Feynman diagram of the 2-photon ALP interaction is shown in the left panel of Fig. 1.

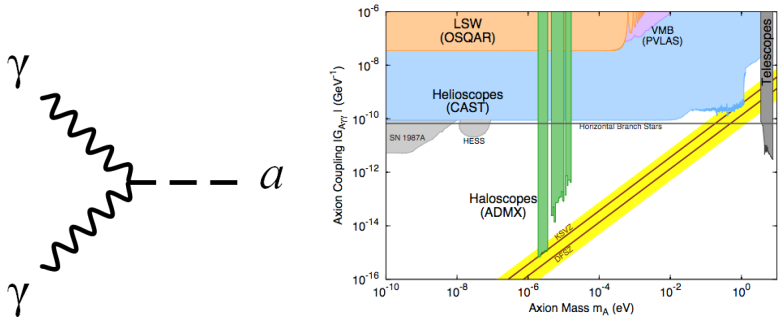

Figure 1: Left: Photon-photon-ALP vertex. Right: experimental limits on ALPs – the yellow line indicates standard axions.

Present limits (Fig. 1, right) come mostly from the (indirect) non-observation of ALPs produced in the core of stars (like the Sun) through the Primakoff process in the Coulomb field $\mathbf{E}$ of ionized matter, illustrated in the left part of Fig. 2. The CAST experiment at CERN was looking at the Sun and found nothing, thereby deriving $g_{a\gamma} < 0.66 \times 10^{-10}\,{\rm GeV}^{-1}$ for $m < 0.02\,{\rm eV}$ [2].

Importance of gamma-ray observations – Let us consider a monochromatic photon beam and assume that an external magnetic field $\mathbf{B}$ is present (in stars the rôle of $\mathbf{E}$ and $\mathbf{B}$ is interchanged). Then $\gamma \to a$ conversions occur, as shown in the left part of Fig. 2, but also the process $a \to \gamma$ takes place, as in right part of Fig. 2: hence photon-ALP *oscillations* $\gamma \leftrightarrow a$ can occur. They can change the intensity of a gamma-ray signal, both increasing and decreasing it [3].

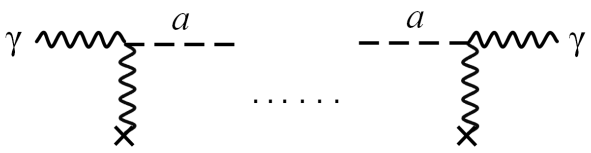

Figure 2: Left: $\gamma \to a$ conversion in the external magnetic field $\mathbf{B}$ (in stars the rôle of $\mathbf{E}$ and $\mathbf{B}$ is interchanged). Right: inverse process $a \to \gamma$.

Expected results with e-ASTROGAM: Evidencing the distortion of a gamma-ray signal – Suppose that a distant source emits a γ/a beam of energy E in the range $0.3\,\mathrm{MeV} - 3\,\mathrm{GeV}$ which propagates along the y direction reaching us. Consider now the simplest possible case, where no photon absorption takes place and $\mathbf{B}$ is homogeneous. Taking $\mathbf{B}$ along the z-axis, we have (see for example [3] for a review of the assumptions and the details of the calculations)

$$P_{\gamma\to a}(E;0,y) = \left(\frac{g_{a\gamma}\,B}{\Delta_{\rm osc}}\right)^2 \sin^2\left(\frac{\Delta_{\rm osc}\,y}{2}\right)\,, \qquad \Delta_{\rm osc} \equiv \left[\left(\frac{m^2-\omega_{\rm pl}^2}{2E}\right)^2 + \left(g_{a\gamma}\,B\right)^2\right]^{1/2}\,, \tag{2}$$

where $\omega_{\rm pl}$ is the plasma frequency of the medium. Defining $E_* \equiv |m^2 - \omega_{\rm pl}^2|/(2\,g_{a\gamma}\,B)$, one has $P_{\gamma\to a}(E;0,y) = 0$ for $E \ll E_*$, $P_{\gamma\to a}(E;0,y)$ rapidly oscillates with E for $E \sim E_*$ – this is the *weak-mixing regime* – while $P_{\gamma\to a}(E;0,y)$ is maximal and independent of m and E for $E \gg E_*$ (*strong-mixing regime*). The extragalactic magnetic field $\mathbf{B}$ is usually modeled as a domain-like structure with coherence length $L_{\rm dom} = (1-10)\,\mathrm{Mpc}$, $B = (0.1-1)\,\mathrm{nG}$, and the $\mathbf{B}$ direction changing randomly among domains. The $\mathbf{B}$ structure enhances oscillations around E_* (Fig. 3).

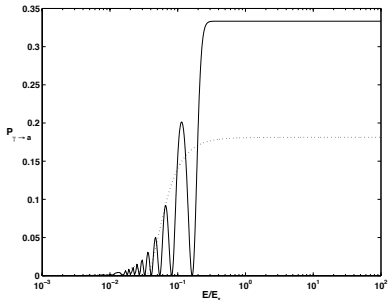

Figure 3: Oscillatory behavior around E_* for $g_{a\gamma} = 0.33\times10^{-10}\,\mathrm{GeV}^{-1}$, B = 0.5 nG and $N = 200$ magnetic domains.

On top of the oscillatory behavior we also have a feature in the energy spectrum followed by a dimming of the signal al lower energies [4]: the production of ALPs implies a reduced photon flux. It can be shown that for $N \gg 1$ magnetic domains, the two photon polarization states and the single ALP state undergo equipartition, so that the signal becomes dimmer by a factor of 2/3.

In addition, the coupling $g_{a\gamma}\,a\,\mathbf{E}\cdot\mathbf{B}$ acts as a *polarizer*. Photons $\gamma_\perp$ with linear polarization orthogonal to the plane defined by $\mathbf{k}$ and $\mathbf{B}$ do not mix with a, but only photons $\gamma_\parallel$ with linear polarization parallel to that plane do [5]. Two distinct phenomena come about: *birefringence*, namely the change of a linear polarization into an elliptical one with the major axis parallel to the initial polarization, and *dichroism*, namely a selective conversion $\gamma \to a$ which causes the ellipse's major axis to be misaligned with respect to the initial polarization. Thus, the measure of the polarization of radiation with known initial polarization provides additional information to discriminate an ALP from other possible effects. Actually, we do *not need* to know the initial polarization by employing a simple trick. Because when one does not measure the polarization one has to sum over the two final photon polarizations – while when one does measure it no sum is performed – the signal has to be *twice as large* when the polarization is not measure as compared with the case in which the polarization is measured.

What is the mass range of the ALP that can be probed by e-ASTROGAM? As far as the polarization effect is concerned it is of course maximal in the strong mixing regime ($E \gg E_*$) but it is present also in the weak mixing regime ($E \sim E_*$), while the spectral feature shows up only in the weak mixing regime. So, what is required is that E_* falls inside the energy range of e-ASTROGAM. Neglecting $\omega_{\rm pl}$ and recalling the definition of E_* we get (regardless of N)

$$0.3\,\mathrm{MeV} < \frac{m^2}{2\,g_{a\gamma}\,B} < 3\,\mathrm{GeV} \tag{3}$$

and by employing the parametrizations $g_{a\gamma} = \alpha\, 10^{-10}\,\mathrm{GeV}^{-1}$ and $B = \beta\,\mathrm{nG}$, Eq. (3) becomes

$$1.08 \times 10^{-12}\,(\alpha\beta)^{1/2}\,\mathrm{eV} < m < 1.08 \times 10^{-10}\,(\alpha\beta)^{1/2}\,\mathrm{eV} \tag{4}$$

By taking e.g. $g_{a\gamma} = 0.33 \times 10^{-10}\,\mathrm{GeV}^{-1}$ and $B = 0.5\,\mathrm{nG}$ one has $0.44 \times 10^{-12}\,\mathrm{eV} < m < 0.44 \times 10^{-10}\,\mathrm{eV}$.

Expected results with e-ASTROGAM: Prompt gamma-ray signal from Type II supernovae – ALPs can be produced at the centre of core-collapse (Type II) supernovae soon after the bounce (when also the neutrino burst is produced) by the Primakoff effect and reconverted to photons of the same energy during their travel in the Milky Way. The arrival time of these photons would be the same as for neutrinos, thus providing a clear-cut signature.

Integrating over the explosion time, which is of the order of 10 s, the Authors of [6] find that the ALP spectrum can be parametrized by a power law with exponential cutoff,

$$\frac{dN_a}{dE} = C \left(\frac{g_{a\gamma}}{10^{-11}\mathrm{GeV}^{-1}} \right)^2 \left(\frac{E}{E_0} \right)^{\beta} \exp\left(-\frac{(\beta+1)E}{E_0} \right) \tag{5}$$

where for a progenitor mass of $10\,M_\odot$, C, E_0 and β are $5.32 \times 10^{50}\,\mathrm{MeV}^{-1}$, 94 MeV, and 2.12, respectively, while for a progenitor mass of $18\,M_\odot$ they are $9.31 \times 10^{50}\,\mathrm{MeV}^{-1}$, 102 MeV, and 2.25, respectively.

The ALP energy spectrum – which corresponds to the γ-ray energy spectrum after reconversion – is shown in Fig. 4. The bulk is below $\sim 100\,\mathrm{MeV}$, which shows the potential of e-ASTROGAM for a possible detection. Indeed, e-ASTROGAM has a sensitivity better than Fermi/LAT and can access to much smaller mass/coupling values than dedicated laboratory experiments.

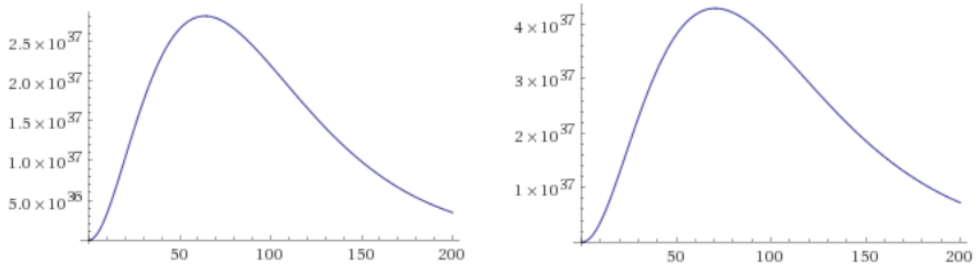

Figure 4: The differential axion rate from the supernova, $dN_a/dE\,(\mathrm{GeV}^{-1})$, for a SN of 10 (left) and 18 (right) solar masses. The abscissa is in MeV.

References

[1] Jaeckel J. and Ringwald A., Ann. Rev. Nucl. Part. Sci. **60**, 405 (2010)

[2] Anastassopoulos V. *et al.* Nature Physics **13**, 584 (2017)

[3] De Angelis A., Galanti G., and Roncadelli M., Phys. Rev. D **84**, 105030 (2011); *erratum,* Phys. Rev. D **87**, 109903 (2013)

[4] De Angelis A., Mansutti O. and Roncadelli M., Phys. Lett. B **659**, 847 (2008)

[5] Maiani L., Petronzio R. and Zavattini E., Phys. Lett. B **175**, 359 (1986)

[6] Meyer M., et al., Phys. Rev. Lett. **118**, 011103 (2017)

Search for Primordial Black Holes Signatures with e-ASTROGAM

Michele Doro [1,2], *Javier Rico* [3], *Dmitry Malyshev* [4]

[1] *Dipartimento di Fisica e Astronomia* "G. Galilei", *Università di Padova, I-35131 Padova, Italy*
[2] *Istituto Nazionale di Fisica Nucleare, Sezione di Padova, I-35131 Padova, Italy*
[3] *Institut de Física d'Altes Energies (IFAE), The Barcelona Institute of Science and Technology (BIST), E-08193 Bellaterra (Barcelona), Spain*
[4] *Erlangen Centre for Astroparticle Physics, Erwin-Rommel-Str. 1, Erlangen, Germany*

Science questions – A large number of theories predict the formation of black holes in the primordial Universe, according to diverse mechanisms: from the collapse of local overdensities, to that of domain walls, cosmic strings, etc. Such formation scenarios are reviewed in [1]. Many of these theories predict Primodial Black Holes (PBH) to have formed in a narrow time period, and therefore having practically a very narrow mass distribution[1]. Depending on the formation epoch the mass may vary from few grams to millions of solar masses. Non-observation of PBHs of particular masses can constrain cosmological models on small angular scales, which are not accessible in CMB observations [4, 5].

PBHs radiate particles via the Hawking mechanism [2], thus losing mass over time, and accordingly increasing their temperature following the law $T_{BH} = (8\pi\, G\, M_{BH})^{-1}$. However, specially for larger mass BH, the possibility of accretion of material could have altered the above simple evolution formula. In the non-accretion scenario, the Hawking mechanisms predict that, as the temperature increases, BHs will finally evaporate, where the lapse time to evaporation is given by: $\tau \sim G^2\, M_{BH}^3 \hbar^{-1} c^{-4}$. This allows to make the straightforward estimation that all PBH of mass smaller than 10^{14} g (10^{-19} $M_\odot$) would be evaporated today. Small mass PBHs can affect the cosmological observables, such as CBM spectrum or BBN, while larger mass PBHs can be observable with current observations.

The instantaneous gamma-ray rate for different BH temperatures is shown in Figure 1. The spectra have two components: the primary component from direct Hawking mechanism, and the secondary component from the decay of hadrons produced by fragmentation of primary quarks and gluons, and by the decay of gauge bosons. The spectrum of secondary photons [6] peaks around $E_\gamma = 68$ MeV, independent of the BH temperature, because it is dominated by the 2γ-decay of soft neutral pions. It is thus clear that instruments sensitive to the gamma-ray energy band in the $\sim$10 MeV–1GeV range such as e-Astrogam, can provide very deep insights into the questions, in some scenarios providing the strongest bounds for PBH in the mass range around 10^{14-15} g.

It should also be noted that for $M_{PBH} > 10^{15}$ g, their lifetime exceeds that of the Universe, and therefore PBH could constitute part of the DM (lighter PBH may still have a cosmological role, e.g. in altering BBN, being involved in baryogenesis, etc.). When particles from the Hawing radiation are injected into the Universe, they are normally too scarce to significantly alter the energy budget of the Universe or the CMB number of photons, however, they heat up and ionize the gas, therefore altering the optical depth of the CMB photons. This provides strong cosmological bounds [7, 8]. Competitive or stronger bounds can be found from the MeV diffuse component of the extragalactic gamma-ray background (EGB) [9] and from the Galactic diffuse emission [10].

Not only PBH could constitute part of the DM component, but their detection could be of utmost interest to understand the presence and distribution of such elusive objects in the Universe. PBHs are one of the predictions of general relativity and detection of PBHs would be a spectacular confirmation of quantum field theory in vicinity of BH. The radio telescopes are also approaching the resolution to be able to observe directly the horizon of nearest SMBHs and specific instruments to observe it are also utilized [11].

[1] However, wider mass distributions is not completely ruled out, see e.g. [3]

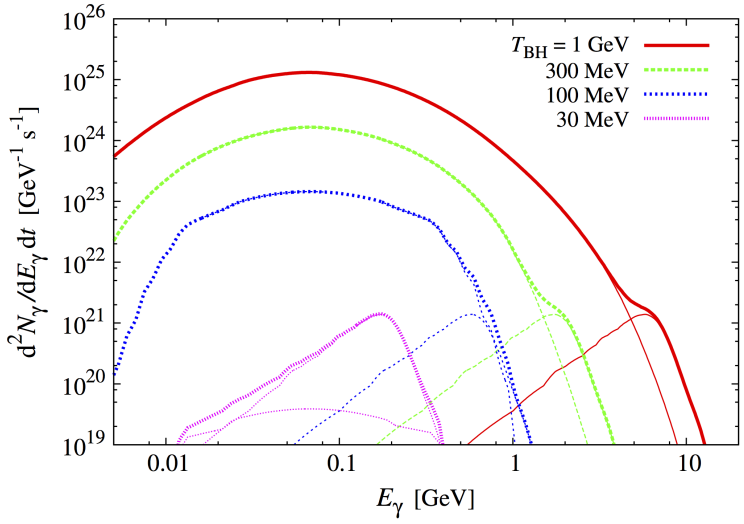

Figure 1: Gamma-ray instantaneous rate for BH at different temperatures. For each temperature, the curve with the peak to the right (left) represents the primary (secondary) component and the thick curve denotes their sum. The figure is a reproduction of Fig. 1 of Ref. [9].

Importance of gamma-ray observations – Photons (and other particles) are radiated from BH at any time in its history, following the Hawking mechanism. In this section, we concentrate on high energy photon emission. The photon emission is computed in [9]. For PBHs in the mass range 10^{15-17}g, the peak intensity occurs at 130 MeV. This means that all PBHs of those mass, either already evaporated, or close to evaporation, could have injected a large amount of MeV radiation into the Universe. This would now be seen as an unresolved contribution into the MeV component of the EGB, in which the e-Astrogam satellite would be uniquely competitive.

Besides the continuous (in time) emission from the radiating BH, there is also the possibility to directly observe the very last final phase of the BH life, when the BH explodes and vanishes. All non-accreting BH are expected to go into this final destiny, and the energy and time scales of this phase is governed only by the mass (or temperature) scale. During the last phases, a small loss of mass reduces rapidly the BH lifetime. In comparison to indirect searches like those performed using the EGB, direct searches of the PBHs evaporation bursts are sensitive to the local (sub-kpc scale) PBH distribution. It has been appreciated for a long time [9] that by strictly considering Standard Model processes, the likelihood of detecting the final explosive phase of PBH evaporations is very low. However, the physics of the QCD phase transition is still uncertain and the prospects of detecting explosions would be improved in less conventional particle physics models [12]. For instance, it has been argued that the formation of a fireball at the QCD temperature could explain some of the short-period gamma-ray bursts (i.e. those with duration less than 100 ms) [13].

Expected results with e-Astrogam – Previous constraints COMPTEL and EGRET experimental data on the PBH density using EGB were computed in Ref. [12, 14]. Some of these are shown in Figure 2, together with Planck limits [8] and femtolensing [15]. Planck provides the strongest constraint on the abundance of PBHs for masses 10^{15-16} g, while the EGB dominates for smaller masses. These studies used the EGB as bound the contribution of PBHs, i.e. they were requiring the integrated MeV contribution not to be larger than that of the measured EGB. However, the authors themselves claim the interest of actually considering (fractions of) the EGB as a signal of PBHs. This is an exciting possibility because the origin of this MeV gamma-ray background is yet uncertain [16]. In Ref. [17], the authors claims that standard astrophysical contributions cannot explain the whole diffuse MeV contribution, see in particular their figure 13. There is therefore space for additional contribution, and PBHs could contribute to some of this missing flux.

In conclusion, the improved sensitivity of e-Astrogam in the MeV range will allow to use the diffuse MeV component of the EGB to put possibly the strongest constraints on the PBH number

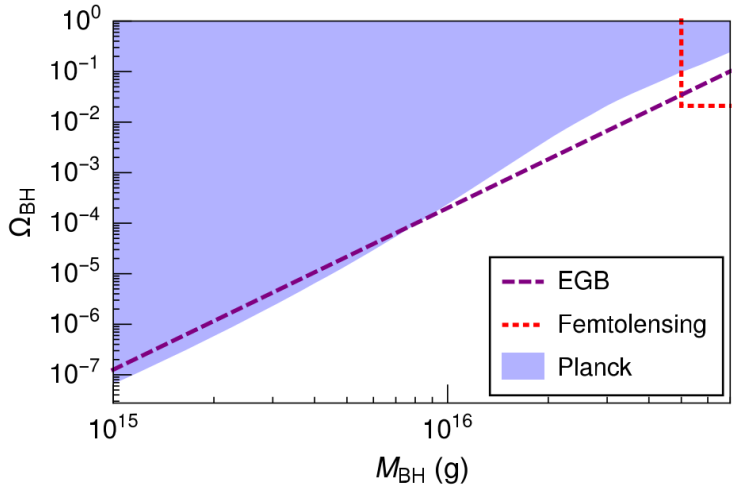

Figure 2: Compilation of PBH density bounds ni the range 10^{15-17}g. The figure is a reproduction of Fig. 6 of [8].

density for masses in the range of 10^{15-17}g. Considering the EGB limits in Figure 2 are obtained assuming 100% of the background produced by PBHs, e-Astrogam bounds are expected to improve these results.

References

[1] B. J. Carr, in Inflating Horizons in Particle Astrophysics and Cosmology, edited by H. Susuki et al. (Universal Academy Press, Tokyo, Japan, 2005), p. 119.

[2] S.W. Hawking, Nature (London) 248, 30 (1974).

[3] J. García-Bellido, In Proceedings of 11th LISA Symposium, Zurich (2016) (p. 25). (2017)

[4] A. S. Josan and A. M. Green, Phys. Rev. D **82**, 047303 (2010)

[5] A. Linde, S. Mooij and E. Pajer, Phys. Rev. D **87**, no. 10, 103506 (2013)

[6] J. H. MacGibbon and B. R. Webber, Phys. Rev. D 41, 3052 (1990).

[7] V. Poulin, J. Lesgourgues, and P. D. Serpico, J. Cosmol. Astropart. Phys. 03 (2017) 043.

[8] S. J. Clark, B. Dutta, Y. Gao, L. E. Strigari, & S. Watson (2017). Planck constraint on relic primordial black holes. PRD, 95(8), 110.

[9] B. J. Carr, K. Kohri, Y. Sendouda, and J. Yokoyama, Phys. Rev. D 81, 104019 (2010).

[10] R. Lehoucq, M. Casse, J.-M. Casandjian and I. Grenier, Astron. Astrophys. **502**, 37 (2009)

[11] `http://eventhorizontelescope.org/`

[12] C. E. Fichel et al. Astroph. J., **434** no. 2 557-559 (1994)

[13] D. B. Cline and W. Hong, Astrophys. J. 401, L57 (1992).

[14] G. Weidenspointner, Ph.D. thesis, Technical University of Munich, Munich, http://mediatum.ub.tum.de.

[15] B. Carr, F. Kuhnel, and M. Sandstad, Phys. Rev. D 94, 083504 (2016).

[16] M. Fornasa and M. A. Snchez-Conde, Phys. Rept. **598** (2015) 1

[17] P. Ruiz-Lapuente, L.-S. The, D. H. Hartmann, M. Ajello, R. Canal, F. K. Röpke, W. Hillebrandt, The Astrophysical Journal, 820(2), 142. (2016).

Search for matter-antimatter annihilation for testing baryogenesis models

Cosimo Bambi[1,2], *Alexander D. Dolgov*[3,4]

[1] *Fudan University, 200433 Shanghai, China*
[2] *Eberhard-Karls Universität Tübingen, 72076 Tübingen, Germany*
[3] *Novosibirsk State University, 630090 Novosibirsk, Russia*
[4] *ITEP, 117259 Moscow, Russia*

Science questions – The local Universe is clearly matter dominated and the small amount of observed antimatter can be explained as of secondary origin, produced in space by collisions of high energy particles. However, we do not know the origin of this matter-antimatter asymmetry. Matter and antimatter have quite similar properties. The observed asymmetry cannot be explained as due to the Universe initial conditions, because any initial asymmetry would be washed out during inflation and therefore the observed asymmetry today had to be generated by some mechanism after inflation [8]. The matter-antimatter asymmetry cannot be explained within the Standard model of particle physics, and it is thus one of the cosmological indications of new physics.

We can distinguish three possible scenarios of matter-antimatter asymmetry [7]:

1. The asymmetry is spatially constant and the Universe is matter dominated.
2. The Universe is globally baryo-symmetric and there are domains of matter and antimatter.
3. The Universe has a non-vanishing baryonic charge, but the asymmetry is not spatially constant. In particular, there may exist lumps of antimatter in a matter dominated Universe.

Different baryogengesis models can predict any of the scenarios 1-3. Most models proposed in the literature belong to the first class [8], but at present there is neither experimental nor observational evidence in favor of one model over another, because they operate at so high energies that it is difficult or impossible to test them in laboratories on Earth. The scenario 2 seems to be observationally excluded, or at least the size of the domain where we live should be larger than the visible Universe [6]. The scenario 3 can have interesting phenomenological implications, in particular the existence of antimatter objects in our neighborhood and the observation of matter-antimatter annihilation [1, 4].

Importance of gamma-ray observations – An unambiguous proof of the existence of primordial antimatter would be the observation of sufficiently heavy anti-nuclei, starting from helium-4 (*direct search*). Indeed anti-deuterium can be created in energetic cosmic ray reactions, while the probability of production of heavier anti-nuclei is negligible. For example the expected flux of the secondary produced anti-helium-4 is $10^{-15}/\mathrm{m}^2/\mathrm{s}/\mathrm{sr}/(\mathrm{GeV/n})$ [11, 2], i.e. 17 orders of magnitude below the observed flux of normal helium. For the time being, there are only upper bounds on the flux of cosmic anti-helium-4. The best published limit is by BESS, $\overline{\mathrm{He}}^4/\mathrm{He}^4 < 3 \times 10^{-7}$, though an order of magnitude more stringent bound is expected from PAMELA and another order of magnitude improvement may be achieved by AMS. None of that is yet reported.

A complementary direction for the search of primordial antimatter in the Universe is through the identification of electromagnetic radiation produced by matter-antimatter annihilation (*indirect search*). In particular, we may expect an excess of ~ 100 MeV photons from proton-antiproton annihilation and a 0.511 MeV line from electron-positron annihilation at low energies. Current data provide an upper bound on the possible antimatter abundance in galaxies. If we consider the possibility of the existence of anti-stars, observations require that the ratio between the number of anti-stars and stars is not more than about 10^{-6} [14].

The current constraints on the abundance of antimatter become much weaker in the case of antimatter compact objects [4]. Efficient mechanisms of cosmological production of antimatter lumps were studied in Refs. [10, 9]. Such antimatter objects would be compact and distributed over large volume (e.g. galactic halos) rather than concentrated in galactic disks, two ingredients that make antimatter objects much more difficult to observe. The phenomenology of such baryogengesis scenarios is discussed in Refs. [1, 4], where bounds from current observations are also derived. These antimatter objects may also represent the cosmological dark matter and therefore baryogengesis models predicting lumps of antimatter can potentially explain both the matter-antimatter asymmetry in the Universe and the origin of dark matter [9, 10], especially if such antimatter objects predominantly form primordial black holes [3].

The model of antimatter formation considered in Refs. [1, 4] allows for abundant antimatter in the Galaxy but it is difficult to present a reasonable limit on its density because it strongly depends upon the types of the antimatter objects. Some other scenarios of cosmological antimatter creation are discussed in [12] and references therein.

Expected results with e-ASTROGAM – Indirect search for antimatter requires the observation of γ-rays from 0.5 to about 100 MeV, corresponding to the energy range between the electron and the pion masses. Current data at 0.5-1 MeV are from INTEGRAL, at 1-30 MeV from COMPTEL/CGRO, and at 30-100 MeV from EGRET/CGRO and Fermi-LAT. Generally speaking, e-ASTROGAM will be able to measure lower fluxes and thus improve current bounds on the abundance of anti-objects in our Galaxy and in the whole Universe. e-ASTROGAM can measure fluxes two orders of magnitude smaller than previous missions at energies below 30 MeV, and about an orders of magnitude smaller than EGRET and Fermi-LAT at 30-100 MeV. Recently, the AMS experiment has detected 4-5 candidate anti-helium-3 particles [13]. If confirmed, this would strongly suggest the existence of lumps of primordial antimatter in the contemporary Universe. e-ASTROGAM could investigate such a possibility with a complementary approach, looking for the annihilation signal of such antimatter lumps.

References

[1] C. Bambi and A. D. Dolgov, NPB 784, 132 (2007).

[2] B. Baret *et al.*, AIP Conf. Proc. 842, 1004 (2006).

[3] S. Blinnikov, A. Dolgov, N. K. Porayko and K. Postnov, JCAP 1611, 036 (2016).

[4] S. I. Blinnikov, A. D. Dolgov and K. A. Postnov, PRD 92, 023516 (2015).

[5] L. Canetti, M. Drewes and M. Shaposhnikov, New J. Phys. 14, 095012 (2012).

[6] A. G. Cohen, A. De Rujula and S. L. Glashow, ApJ 495, 539 (1998).

[7] A. D. Dolgov, hep-ph/0211260.

[8] A. D. Dolgov, hep-ph/0511213.

[9] A. D. Dolgov, M. Kawasaki and N. Kevlishvili, NPB 807, 229 (2009).

[10] A. Dolgov and J. Silk, PRD 47, 4244 (1993).

[11] R. Duperray, B. Baret, D. Maurin, G. Boudoul, A. Barrau, L. Derome, K. Protasov and M. Buenerd, PRD 71, 083013 (2005).

[12] M. Y. Khlopov, S. G. Rubin and A. S. Sakharov, PRD 62, 083505 (2000).

[13] J. Sokol, Science **356**, 240 (2017)

[14] G. Steigman, JCAP 0810, 001 (2008).

Nucleosynthesis and chemical evolution of the Galaxy

Conveners: Jordi Isern
Mark Leising
Vincent Tatischeff

Thermonuclear supernovae (SN Ia)

Eugene Churazov [1,2], *Roland Diehl* [3], *Jordi Isern* [4], *Vincent Tatischeff* [5]

[1] *MPI für Astrophysik, Garching D-85741, Germany*
[2] *Space Research Institute, Moscow 117997, Russia*
[3] *Max Planck Institut für extraterrestrische Physik, D-85748 Garching, Germany*
[4] *ICE-CSIC/IEEC, Ed. Nexus-201, c/Gran Capità 2-4, E-08034 Barcelona, Spain*
[5] *CSNSM, IN2P3-CNRS/Univ. Paris-Sud, Université Paris-Saclay, F-91405 Orsay Campus, France*

Science questions – SN Ia are the outcome of a thermonuclear burning front that sweeps a carbon/oxygen white dwarf (WD) in a close binary system. But exactly how the ignition conditions are obtained, and on which WDs, and more so how the thermonuclear runaway proceeds through the WD and turns it into a variety of isotopes that are ejected, all this is subject to considerable debate (see, e.g., [7, 6] and references therein). It seems that several candidate evolutionary channels may all contribute, from the *double degenerate* variant of merging WD binaries disrupting one of the dwarfs through tidal forces or a hard collision, to a variety of *single degenerate* models where accretion of material from a companion star may lead to either the WD reaching the critical Chandrasekhar mass stability limit, or be ignited earlier through a surface explosion from a helium flash.

Such uncertainties are troublesome for cosmology since the use of SN Ia as standard candles depends on an empirical relationship between the shape and the maximum of the light curve [13]. Although useful up to now, in view of the development of *precision cosmology*, a better, astrophysically supported understanding of thermonuclear SNe, as well as their evolutionary effects at large distances and low metallicities, are mandatory. The brightness-decline relation [13] is closely related to the mass of synthesized ^{56}Ni, and factors like the progenitor evolution, ignition density, flame propagation, mixing during the burning, completeness of burning in outer, expanding regions, all lead to different amounts of ^{56}Ni.

Furthermore, SNIa are the main producers of iron peak elements and understanding the rate at which these elements are injected into the interstellar medium is fundamental to understand the chemical evolution of the Galaxy.

Importance of gamma-ray observations – The mass of ^{56}Ni synthesized in the explosion is measured directly through gamma-ray lines. On the other hand, radiation transport from radioactivity to optical light and their spectra depend on complex atomic line transitions in the expanding SN, as well as on the total mass burned, the amount and distribution of radioactive nickel and intermediate mass elements, all of which must combine in quite a tight way to reproduce the observations [15, 10].

With SN 2014J, for the first time a SN Ia occurred close enough for current generation gamma-ray telescopes, at 3.5 Mpc in the starburst galaxy M82. INTEGRAL data could detect the long awaited gamma-ray signatures of the thermonuclear runaway. The lines of ^{56}Co (life time of ∼111 days) at 847 and 1238 keV, consistent in flux and broadening with the predictions of a canonical Chandrasekhar WD explosion model, have been unambiguously detected [1, 2, 5], as well as a Thomson-scattered continuum and positron annihilation emission. Even although overall significance of the signal was just above $10\,\sigma$, good constraints were obtained on the mass of radioactive material and the expansion velocity of the ejecta. Moreover, possible signatures of the radioactive ^{56}Ni (mean lifetime ∼8.8 days) lines have been reported [4, 8], albeit at lower statistical significance. The presence of such lines in the spectrum, if confirmed, would suggest either a surface explosion or very special morphology of the runaway in contrast to the conventional model. Clearly, the glimpse offered by SN 2014J observations with INTEGRAL underline the importance of gamma-ray line

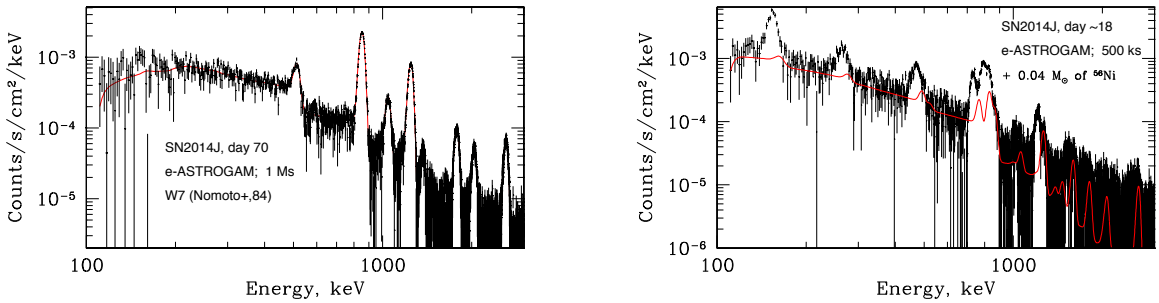

Figure 1: Left: Simulated background-subtracted spectrum of a SN event like SN 2014J (distance of 3.5 Mpc; 70 days after explosion; 1 Ms exposure). The spectrum is dominated by ^{56}Co lines, scattered continuum and annihilation emission. The W7 model [12] is used in the simulations [1]. Such event would be detected at $\sim 300\,\sigma$ by e-ASTROGAM. Right: Simulated spectrum for a model with 0.04 $M_\odot$ of radioactive ^{56}Ni located outside the main ejecta (3.5 Mpc; 500 ks exposure centered at day 17.5 after explosion; 3Dball model from [8]). Extremely bright lines of ^{56}Ni at 158 and 810 keV are clearly detected. Such lines would not be seen if all ^{56}Ni is confined within the ejecta (see red curve that shows a canonical model).

diagnostics in these systems and emphasize that more and better observations hold the key to a deeper understanding of how the thermonuclear explosion of a WD star unfolds.

The presence of a bump in the early light curve of SN2016jhr, as recently reported by [9], provides additional support to the idea that supernovae triggered by the ignition of an outer helium layer or cap do occur in nature. However, such lightcurve bumps remain ambiguous in their nature, as they can also be produced by other mechanisms like the interaction of supernova ejecta with circumstellar material or internal shocks [11], while characteristic gamma-ray lines from the ^{56}Ni decay chain are unambiguous tracers of the underlying physical process.

Expected results with e-ASTROGAM – e-ASTROGAM will achieve a major gain in sensitivity compared to INTEGRAL for the main gamma-ray lines arising from ^{56}Ni and ^{56}Co decays (see Figs. 1 and 2) allowing for events like SN 2014J the exquisitely accurate (at percent level) measurements of the Ni mass, the mass of the progenitor and the expansion velocity, easily differentiating between major astrophysical scenarios. For instance, the presence of an envelope of 0.2 $M_\odot$ around a canonical Chandrasekhar WD (such envelope might appear due to the merger of WDs), would be detected at $50\,\sigma$ level in 1 Ms observation. Moreover, e-ASTROGAM will be able to i) detect gamma-rays up to 600-700 days after the explosion, when ejecta are essentially transparent to gamma-rays, ii) measure with 3-10% accuracy the annihilation rate of positrons produced during ^{56}Co decay up to 300 days, iii) verify the presence of even very small ($\sim 2\times10^{-3}$ $M_\odot$) amount of ^{56}Ni at the surface of the remnant (see Fig.1, right panel) and iv) monitor the emergence of scattered continuum during early phase of the ejecta expansion (Fig.2).

These data will allow us to probe the explosion mechanism in detail, and compare with astrophysical models for each event to better understand the progenitor system(s) and the thermonuclear explosion process. We also note that for a truly nearby type Ia SN, e.g., in M31 or in the Milky Way, even more ambitious diagnostics will be possible, including a search for asymmetry in the ejecta by using e-ASTROGAM polarization capabilities or measuring the rate of positrons escape [3].

Events like SN 2014J are, of course, rare. However, with the e-ASTROGAM sensitivity, the observatory will be able to detect such SN up to a distance of 35 Mpc at $10\,\sigma$ level, i.e., corresponding to the INTEGRAL detection of SN 2014J at 3.5 Mpc after few Ms integration time. In this volume, that includes, in particular, the Virgo cluster of galaxies, one can expect about 10 type Ia SN explosions in 3 years of nominal mission lifetime. Such sample would allow for a clean and fundamental test of the Phillips relation for a dominant population of Branch Normal type Ia SNe. Moreover, about 30% of SN Ia's are peculiar and e-ASTROGAM has an excellent chance to detect few of those, especially bright ones, like SN 1991T, due to the Malmquist bias. Therefore, even without relying on "lucky" events like SN 2014J, e-ASTROGAM will be able not only to elucidate

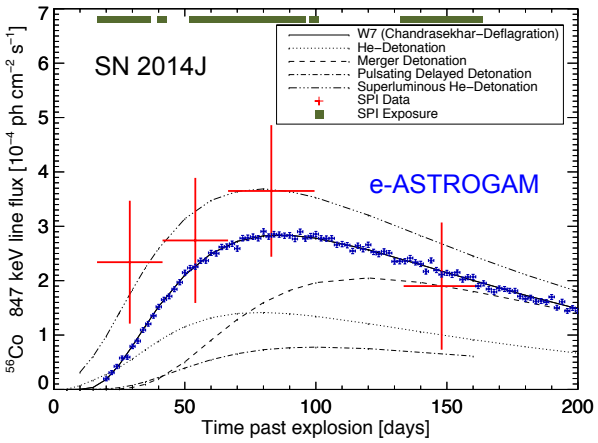

Figure 2: Light curve of the 847 keV line from ^{56}Co decay in SN 2014J. INTEGRAL data (adapted from Fig. 4 in Ref. [5], red data points) are compared to various models of Type Ia SN [14]. A simulation of the e-ASTROGAM response to a time evolution of the 847 keV line such as in the W7 model [12] shows that the sensitivity improvement by e-ASTROGAM (blue points) will lead to a much better understanding of the SN progenitor system and explosion mechanism.

the nature of the Phillips relation, but also to study the departures from it.

Overall, e-ASTROGAM will provide a decisive reference set of data on type Ia SNe, addressing questions ranging from the progenitor system(s) and the physics of thermonuclear runaway in WDs to the use of type Ia SNe for cosmology.

References

[1] Churazov E., Sunyaev R., Isern J., et al., 2014, Nature, 512, 406
[2] Churazov E., Sunyaev R., Isern J., et al., 2015, ApJ, 812, 62
[3] Churazov E., 2017 (in preparation)
[4] Diehl R., Siegert T., Hillebrandt W., et al., 2014, Sci, 345, 1162
[5] Diehl R., Siegert T., Hillebrandt W., et al., 2015, A&A, 574, A72
[6] Hillebrandt, W., Kromer, M., Röpke, F., & Ruiter, A., 2013, Front. Phys. 8, 116
[7] Hillebrandt, W., & Niemeyer, J. C. 2000, ARA&A, 38, 191
[8] Isern J., Jean P., Bravo E., et al., 2016, A&A, 588, A67
[9] Jiang, J.-A., Doi, M., Maeda, K., et al. 2017, Nature, 550, 80
[10] Kerzendorf, W. & Sim, S., 2014, MNRAS, 440, 387
[11] Noebauer U.M., Kromer M., Taubenberger S., et al., 2017, MNRAS, 472, 2787
[12] Nomoto K., Thielemann F.-K., Yokoi K., 1984, ApJ, 286, 644
[13] Phillips, M. M. 1993, ApJ, 413, L105
[14] The, L.-S., & Burrows, A. 2014, ApJ, 786, 141
[15] Woosley, S. E., Kasen, D., Blinnikov, S., & Sorokina, E. 2007, ApJ, 662, 487

Core collapse supernovae

Jordi Isern [1], *Mark Leising* [2], *Roland Diehl* [3], *Vincent Tatischeff* [4]

[1] *Institute of Space Science -CSIC/IEEC, Ed. Nexus-201, c/Gran Capità 2-4, E-08034 Barcelona, Spain*
[2] *Clemson University, Clemson, SC 29634-0978, USA*
[3] *Max Planck Institut für extraterrestrische Physik, D-85748 Garching, Germany*
[4] *CSNSM, IN2P3-CNRS/Univ. Paris-Sud, Université Paris-Saclay, F-91405 Orsay Campus, France*

Science questions – Stars more massive than 11–12 $M_\odot$ develop a massive Si–Fe core that progressively grows until it becomes unstable and collapses to form a compact object (a neutron star or a black hole), giving rise to a gravitational supernova (a core collapse supernova – CCSN). Stars in the mass-range 10–11 $M_\odot$ develop an O–Ne core that grows until it collapses to form a neutron star as a consequence of the electron captures on oxygen (an electron capture supernova –ECSN) [6]. The outcome of such instability is the formation of a proto-neutron star that can lead to the formation of a neutron star or a back hole after accretion of enough matter. The phenomenological properties of the explosion not only depend on the amount of the energy deposited but also on the structure and chemical composition of the envelope at the moment of the explosion which, in turn, depends on the initial mass and metallicity of the star, and the presence of a companion in the case of close binary systems. To these factors it is necessary to add the influence of rotation and magnetic fields. Just as an example of the existing uncertainties, it is necessary to mention the presence of residual amounts of C in the inner regions of ONe degenerate cores that could completely change the present picture of ECSN [6].

The theory of core collapse, which involves hydrodynamics and shock physics, radiative transfer, nuclear physics, neutrino physics, particle physics, statistical physics and thermodynamics, gravitational physics, and convection theory, is still not well understood in terms of an astrophysical model (e.g. Refs. [18, 12, 3]). The main goal is to explain a tremendous variety of core collapse events, e.g. the peculiarities of the Crab nebula and pulsar, the distribution of the elements in events like Cassiopeia A (Cas A), collapsars that appear as gamma-ray burst sources and produce stellar mass black holes, superluminous supernovae that may be powered entirely differently by magnetar rotational energy, or pair instability supernovae that create huge amounts of radioactive ^{56}Ni. This requires quantitative explanations of a number of observation facts, such as [3] (i) the relative proportions of stellar black holes and neutron stars, (ii) the mass distribution of the residual neutron stars, (iii) the high average proper motion speeds of radio pulsars (the fastest population of stars in the Galaxy), (iv) the observed morphologies of supernova explosions and spatial distributions of the ejecta, as well as (v) the measured nucleosynthetic yields as a function of stellar progenitor.

The different scenarios and models that have been advanced to account for these explosive events predict the synthesis of many radioactive isotopes that can be used as a diagnostic tool and can provide key information to understand the phenomenon.

Importance of gamma-ray observations – The main detectable gamma-ray line emissions from radioactive nucleosynthesis products of CCSNe result from the decay chains (i) ^{56}Ni ($T_{1/2}$ = 6.075 d) $\rightarrow$ ^{56}Co ($T_{1/2}$ = 77.2 d) $\rightarrow$ ^{56}Fe, (ii) ^{57}Ni ($T_{1/2}$ = 35.6 h) $\rightarrow$ ^{57}Co ($T_{1/2}$ = 271.7 d) $\rightarrow$ ^{57}Fe, and (iii) ^{44}Ti ($T_{1/2}$ = 60.0 y) $\rightarrow$ ^{44}Sc ($T_{1/2}$ = 3.97 h) $\rightarrow$ ^{44}Ca, as well as from the long-lived radioisotopes ^{26}Al ($T_{1/2} = 7.17 \times 10^5$ y) and ^{60}Fe ($T_{1/2} = 2.62 \times 10^6$ y). While these two last radioactive isotopes have half-lives that are much longer than the characteristic timescale between two explosive events, $\sim$ 75 y for CCSNe [4, 5], such that they produce diffuse gamma-ray line emissions resulting from the superposition of numerous Galactic sources (see contribution "Diffuse gamma-ray line emissions" in this White Book), they can also be measured in individual nearby

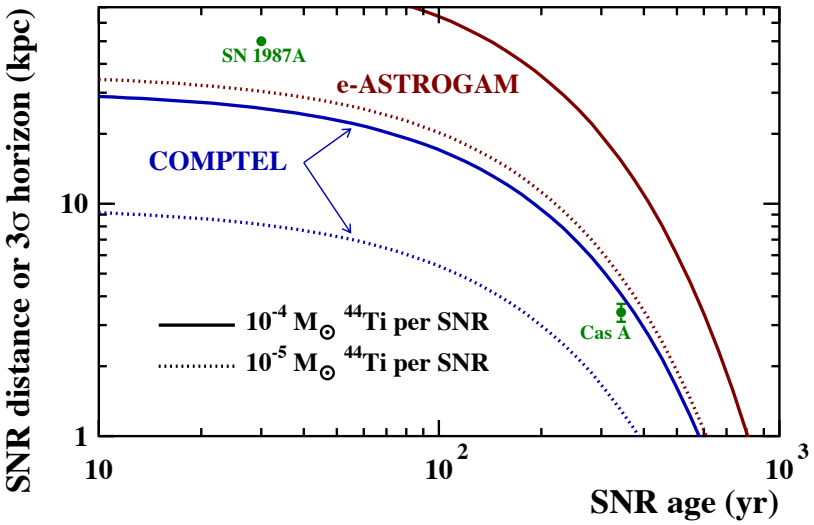

Figure 1: Horizon of detectability of the ^{44}Ti line at 1157 keV as a function of SNR age for CGRO/COMPTEL (blue lines) and e-ASTROGAM (red lines). The plotted sensitivities are for an effective source exposure of 1 year (COMPTEL: 9.0×10^{-6} ph cm^{-2} s^{-1}; e-ASTROGAM: 6.4×10^{-7} ph cm^{-2} s^{-1}), assuming two different yields of ^{44}Ti production per SNR: 10^{-5} $M_\odot$ (common events; dotted lines) and 10^{-4} $M_\odot$ (Cas A-like events; solid lines). Also shown are the age and distance of the two CCSNe with detected ^{44}Ti: SN 1987A and Cas A.

sources, such as the Vela supernova remnant. Isotopes like ^{44}Ti, ^{56}Co, and ^{56}Ni can be detected in individual CCSNe, and this is one of the more direct ways to extract information on the inner processes triggering the explosion near the newly forming compact stellar remnant (e.g., [10]). Other observables, such as the optical light curve and thermal X-ray emission from shocked-heated gas, are more indirect, and mostly reflect interactions within the envelope, or with circumstellar, pre-explosively ejected, or ambient gas.

The power of gamma-ray observations to study the physics of core collapse is exemplified with the observations of SN 1987A and Cas A. Thus, the early appearance and measured profiles of ^{56}Co gamma-ray lines in SN 1987A [14] provided key indications for an asymmetric explosion and the rapid mixing of ^{56}Ni in the outer ejecta (e.g. [13, 17]). The spatial distribution of ^{44}Ti in the remnant of Cas A as revealed by NuSTAR's observations provides strong evidence of explosion asymmetries caused by the development of low-mode convective instabilities in CCSNe [9, 10].

Expected results with e-ASTROGAM – e-ASTROGAM will achieve a gain in sensitivity for the ^{44}Ti line at 1157 keV by a factor of 14 compared to CGRO/COMPTEL and 27 compared to INTEGRAL/SPI (for the same effective time exposure). As illustrated in Fig. 1, the proposed observatory should detect the radioactive emission from ^{44}Ti from most of the young (age $\lesssim$ 500 yr) supernova remnants (SNRs) in the Milky Way, thus uncovering about 10 new, young SNRs in the Galaxy presently hidden in highly obscured clouds. e-ASTROGAM should also detect the youngest SNRs in the Large Magellanic Cloud and will measure precisely the amount of ^{44}Ti in the remnant of SN 1987A, which is currently disputed in the literature ([8, 2, 16]). These observations will give new insights on the physical conditions of nucleosynthesis in the innermost layers of a supernova explosion and the dynamics of core collapse near the mass cut. e-ASTROGAM could measure ^{60}Fe yields in individual supernova remnants, and should not only measure ^{26}Al, but also possibly map it in the Vela remnant, discerning whether a fraction of the ^{26}Al is present in the X-ray emitting shrapnel [1].

e-ASTROGAM should also detect the signatures of ^{56}Ni and ^{56}Co decay from several CCSNe in nearby galaxies. The gain in sensitivity for the 847 keV line from ^{56}Co decay amounts to a factor ranging from 30 to 70 compared to INTEGRAL/SPI, depending on the width of the gamma-ray line (i.e. the velocity dispersion of the ejected radioactive cobalt). The comparison with e-ASTROGAM of gamma-ray characteristics of different classes of CCSNe, possibly including

the pair instability SNe with their order of magnitude higher ^{56}Ni production (e.g., [7]), will probe potentially large variations in their progenitors and offer a direct view of their central engines. Asymmetries in ejected radioactivity might be reflected in 3–5 times higher line fluxes [11]. Rare core collapse events are predicted to have gamma-ray line brightnesses orders of magnitude above typical supernovae: pair instability and magnetar-powered jet explosions will reveal much larger amounts of ^{56}Ni. e-ASTROGAM will reach out to a larger part of the nearby universe to constrain the rate of such events, if not detect them.

Is is also possible that e-ASTROGAM could identify the long sought site of the r-process production of heavy nuclei. Given the possible very long integration times, relatively long-lived isotopes, such as ^{126}Sn, in nearby supernova remnants are the most promising targets [15].

References

[1] Aschenbach, B., Egger, R., & Trümper, J. 1995, Nature, 373, 587
[2] Boggs, S. E., Harrison, F. A., Miyasaka, H., et al. 2015, Science, 348, 670
[3] Burrows, A. 2013, Reviews of Modern Physics, 85, 245
[4] Diehl, R., Halloin, H., Kretschmer, K., et al. 2006, Nature, 439, 45
[5] Diehl, R. 2016, Journal of Physics Conference Series, 703, 012001
[6] Doherty, C.I., Gil-Pons, P., Siess, L., et al. 2017, Pub. Astron. Soc. Austr. in press, arXiv: 1703.06895
[7] Gal-Yam, A., Mazzali, P., Ofek, E. O., et al. 2009, Nature, 462, 624
[8] Grebenev, S. A., Lutovinov, A. A., Tsygankov, S. S., & Winkler, C. 2012, Nature, 490, 373
[9] Grefenstette, B. W., Fryer, C. L., Harrison, F. A., et al. 2017, ApJ, 834, 19
[10] Grefenstette, B. W., Harrison, F. A., Boggs, S. E., et al. 2014, Nature, 506, 339
[11] Hungerford, A. L., Fryer, C. L., & Warren, M. S. 2003, ApJ, 594, 390
[12] Janka, H.-T. 2012, Annual Review of Nuclear and Particle Science, 62, 407
[13] Mahoney, W. A., Varnell, L. S., Jacobson, A. S., et al. 1988, ApJ, 334, L81
[14] Matz, S. M., Share, G. H., Leising, M. D., Chupp, E. L., & Vestrand, W. T. 1988, Nature, 331, 416
[15] Qian, Y.-Z., Vogel, P., & Wasserburg, G. J. 1998, ApJ, 506, 868
[16] Tsygankov, S. S., Krivonos, R. A., Lutovinov, A. A., et al. 2016, MNRAS, 458, 3411
[17] Tueller, J., Barthelmy, S., Gehrels, N., et al. 1990, ApJ, 351, L41
[18] Woosley, S., & Janka, T. 2005, Nature Physics, 1, 147

Nova explosions

Margarita Hernanz[1], *Jordi José* [2], *Pierre Jean*[3], *Alain Coc*[4], *Vincent Tatischeff* [4], *Laura Delgado*[1], *Gloria Sala*[2], *Sumner Starrfield* [5], *Robert Gehrz*[6], *Marina Orio*[7,8], *Domitilla de Martino*[9], *Solen Balman*[10]

[1] *Institute of Space Sciences (CSIC-IEEC), Campus UAB, C/ Can Magrans s/n, 08193 Cerdanyola del Vallés (Barcelona), Spain*
[2] *Departament de Física, EEBE, UPC, 08019 Barcelona, Spain*
[3] *IRAP, 9 av. colonel Roche, BP 44 346, 31028 Toulouse Cedex 4, France*
[4] *CSNSM, IN2P3-CNRS/Univ. Paris-Sud and Paris-Saclay, F-91405 Orsay Campus, France*
[5] *Arizona State University, Tempe, AZ 85287-1504, USA*
[6] *University of Minnesota, Minneapolis, MN 55455, USA*
[7] *Department of Astronomy, University of Wisconsin, Madison WI 53704, USA*
[8] *INAF - Osservatorio di Padova, I-35122 Padova, Italy*
[9] *INAF - Osservatorio Astronomico di Capodimonte, I-80131 Napoli, Italy*
[10] *Department of Physics, Middle East Technical University, Ankara, Turkey*

Science questions – Accreting white dwarfs in close binary systems can explode as novae and/or as thermonuclear supernovae (SNe Ia). Novae are responsible for the enrichment of the Galaxy in some species and for the peculiar isotopic signatures found in some presolar grains [12]. Understanding the origin of the elements in the Galaxy and in the whole Universe is an important topic, intimately related to explosive nucleosynthesis and emission of γ-rays. In fact, γ-rays directly trace isotopes, whereas observations at other wavelengths give only elemental abundances, except some measurements of CO molecular bands in the infrared, where ^{12}CO and ^{13}CO can be distinguished, thus giving the ^{13}C/^{12}C ratio.

Nova ejecta are enriched in CNO nuclei, as well as in Ne, Na, Mg and even S in some cases (see [11] and reviews [6, 10, 16, 17]). They also produce ^{7}Be, which through electron-capture becomes ^{7}Li; the role of novae in the origin of ^{7}Li in the Galaxy and the Universe is a hot scientific topic. Also the contribution of novae to the galactic content of ^{26}Al - traced by 1809 keV γ-rays detected since long ago - is still not well known.

There are two main types of binary systems where white dwarfs can accrete matter and subsequently explode as novae. The most common case is a cataclysmic variable, where the companion is a main sequence star transferring H-rich matter. In this system, mass transfer occurs via Roche lobe overflow, and typical orbital periods range from hours to days. As a consequence of accretion, hydrogen burning in degenerate conditions on top of the white dwarf leads to a thermonuclear runaway and a classical nova explosion occurs, ejecting $10^{-3} - 10^{-7}$M$_\odot$ with speeds $10^2 - 10^3$ km/s and reaching luminosities 10^5L$_\odot$. The nova explosion does not disrupt the white dwarf (as occurs in SNe Ia explosions); therefore, after enough mass is accreted again from the companion star, a new explosion will occur. The typical recurrence time is 10^4–10^5 years, although a broader range is not ruled out. Another scenario where a white dwarf can explode as a nova is a symbiotic binary, where the white dwarf accretes H-rich matter from the stellar wind of a red giant companion. Typical orbital periods for these systems are a few 100 days, much larger than in cataclysmic variables. This scenario leads to more frequent nova explosions than in cataclysmic variables, because of larger accretion rates, with typical recurrence periods smaller than 100 years, and therefore more than one outburst can be recorded. Recurrent novae are indeed interesting objects, since the mass of the white dwarf is expected to increase after each eruption - at least in some cases - and thereof they can explode as SNe Ia, when the white dwarf reaches the Chandrasekhar mass.

The symbiotic recurrent nova RS Oph had its last eruption in 2006. It has been identified - based on the analysis of its early X-ray, IR and radio emission - as a site of particle acceleration, in the shocks between the ejecta and the circumstellar matter (red giant companion wind), making

it and other novae of this class responsible for a fraction of the Galactic cosmic rays [19]. These "miniature supernova remnants" are key systems to study the time dependence of diffusive shock acceleration of cosmic rays, since their evolution is scaled-down with respect to standard supernova remnants. An important consequence of the production of high-energy particles is that photons with energies higher than about 100 MeV are emitted, both via neutral pion decay and inverse Compton processes [9]. Importantly enough, five to eight classical and two symbiotic recurrent novae have been detected by Fermi-LAT at E>100 MeV, since its launch in 2008, confirming theoretical expectations (for symbiotic recurrent novae RS Oph-like), but being challenging to interpret for classical novae, where there's not a red giant wind with which the ejecta can interact. Recent studies of internal shocks in the ejecta have started to explain this phenomenon (see for instance [14]). In most cases, this emission has been observed early after the explosion, around the optical maximum, and for a short period of time [1, 2, 3].

Importance of gamma-ray observations – γ-rays emitted by novae have two very different origins: radioactivity and high energy particle accelerated in diffusive shocks.

- First of all, radioactive isotopes in the ejecta release photons with energies E$\sim$1 MeV. This emission has not been detected yet by any space observatory, e.g. CGRO and INTEGRAL. The potential role of novae as γ-ray emitters related to radioactive nuclei was already pointed out in the 70's [5], referring to electron-positron annihilation and ^{22}Na decays. Seven years later, Clayton [4] noticed that another γ-ray line could be expected from novae, when ^{7}Be transforms (through an electron capture) to an excited state of ^{7}Li, which de-excites by emitting a photon of 478 keV. Thus, two types of gamma-ray emission related to radioactive nuclei are expected in novae: prompt emission, from electron-positron annihilation (with positrons coming from the short-lived β^{+}-unstable isotopes ^{13}N and ^{18}F), and long-lasting emission, from the medium-lived radioactive isotopes ^{7}Be and ^{22}Na decays. The prompt emission has very short duration (less than 1 day), appears very early (before optical maximum) and consists of a continuum (between 20 and 511 keV) and a line at 511 keV [13, 7]. The origin of this emission is $e^{+}e^{-}$ annihilation and its Comptonization. The long-lasting emission consists of lines at 478 keV (mainly CO novae) and 1275 keV (mainly ONe novae), lasting around 2 months or 3 years, respectively (CO and ONe refer to the chemical composition of the white dwarf). See Table 1, [7] and review [8] for details.

  Recent detections of radioactive ^{7}Be in a few novae in the ultraviolet (see [18, 15]), yield an amount of ejected ^{7}Be larger than the most optimistic theoretical values from [11], but anyway, the detectability distances of all the γ-ray lines from novae are still very short, around 0.5 kpc with INTEGRAL/SPI.

- Another way to produce γ-rays in novae is through particle acceleration (p and e^{-}), in strong shocks between the ejecta and the surrounding medium - recurrent symbiotic novae - and internal shocks in the ejecta itself - in classical novae (see previous section). The high-energy γ-rays originated mainly by neutral pions decay (hadronic origin) and Inverse Compton scattering (leptonic origin) have been detected by Fermi-LAT in a handful of novae [1, 2, 3]. High-energy γ-rays give unique insights on the mass ejection processes in novae.

Expected results with e-ASTROGAM – If the sensitivity of e-ASTROGAM for the nova broad lines at 1275 keV and 478 keV (ΔE (FWHM)$\sim$20 keV and 8 keV, respectively) is 25 (13 for 478 keV, if we adopt the value for 511 keV) times better than INTEGRAL/SPI's, then detectability distances would be 5 (3.6) times larger, reaching 3 kpc and 2 kpc. Then it could be expected to detect one nova per year. Detectability distances correspond to model fluxes 1.2×10^{-5} and 10^{-5} ph/cm^2/s, for the 478 and 1275 keV lines of typical CO and ONe novae, respectively, at d=1 kpc.

In addition to the direct and unambigous detection for the first time of the radioactive nuclei ^{22}Na and ^{7}Be-^{7}Li in novae (with ^{7}Be and ^{7}Li now already detected from ground in the near UV and optical, respectively), e-ASTROGAM observations would help to answer some key questions about

nova explosions. For instance, the mixing between accreted matter (expected to be solar-like) and white dwarf core (CO or ONe) is crucial to understand nova explosions, and the amount of ^{7}Be and ^{22}Na directly detected through γ-rays strongly depends on it. The contribution of novae to the galactic content of ^{7}Li is by itself very relevant and a hot topic; detection of radioactive ^{7}Be with e-ASTROGAM would directly lead to the determination of ^{7}Li ejected mass: the amount of ^{7}Be - and thus ^{7}Li - can only be measured unambiguously in the γ-ray range.

e-ASTROGAM will also help to disentangle the origin of the high-energy γ-ray emission of novae, hadronic or leptonic, thanks to its unprecedented sensitivity in the energy range between 10 MeV and 100 MeV (not accessible to Fermi-LAT), together with its excellent coverage of the GeV energy range. It is crucial that e-ASTROGAM will be able to observe and detect novae promptly, since this emission appears very early and has relatively short duration.

Table 1: List of main radioactive isotopes in nova ejecta.

Isotope	Lifetime	Main process	Type of emission	Nova type
^{13}N	862 s	β^{+}-decay	511 keV line and continuum	CO and ONe
^{18}F	158 min	β^{+}-decay	511 keV line and continuum	CO and ONe
^{7}Be	77 days	e^{-}-capture	478 keV line	CO
^{22}Na	3.75 years	β^{+}-decay	1275 and 511 keV lines	ONe
^{26}Al	10^{6} years	β^{+}-decay	1809 and 511 keV lines	ONe

References

[1] Abdo, A.A., Ackermann, M., Ajello, M., et al. 2010, Science, 329, 817

[2] Ackermann, M., Ajello, M., et al. 2014, Science, 345, 554

[3] Cheung, C.C., Jean, P., Shore, S.N. et al. 2016, ApJ, 826, 142

[4] Clayton, D.D. 1981, ApJ, 244, L97

[5] Clayton, D.D., & Hoyle, F. 1974, ApJ, 187, L101

[6] Gehrz, R.D., Truran, J.W., Williams, R.E., & Starrfield, S.E. 1998, PASP, 110, 3

[7] Gómez-Gomar, J., Hernanz, M., José, J., & Isern, J. 2004, MNRAS, 296, 913

[8] Hernanz, M. 2008, in Classical Novae, Second Edition, eds. M.F. Bode and A. Evans, Cambridge Astrophysics Series 43, CUP, Cambridge, 252

[9] Hernanz, M. & Tatischeff, V. 2012, Baltic Astronomy, 21, 62 (arXiv:1111.4129v1; astro-ph-HE)

[10] José, J. 2016, Stellar Explosions: Hydrodynamics and Nucleosynthesis (Boca Raton, FL, London: CRC/Taylor and Francis)

[11] José, J., & Hernanz, M. 1998, ApJ, 494, 680

[12] José, J., & Hernanz, M. 2007, J. Phys. G: Nucl. Phys., 34, R431

[13] Leising, M.D., & Clayton, D.D. 1987, ApJ, 323, 159

[14] Metzger, B.D. et al. 2015, MNRAS 450, 2739; Li, K. et al. 2017, Nature Astronomy, 1, 697

[15] Molaro, P., Izzo, L., Mason, E., Bonifacio, P., & Della Valle, M. 2016, MNRAS, 463, L117

[16] Starrfield, S., Iliadis, C., & Hix, W. R. 2008, in Classical Novae, Second Edition, eds. M. F. Bode and A. Evans, Cambridge Astrophysics Series 43, CUP, Cambridge, 77

[17] Starrfield, S., Iliadis, C., & Hix, W. R. 2016, PASP, 128, 051001

[18] Tajitsu, A. et al. 2015, Nature, 518, 381; Tajitsu, A. et al. 2016, ApJ, 818, 191

[19] Tatischeff, V., & Hernanz, M. 2007, ApJ, 663, L101

Diffuse gamma-ray line emissions

Roland Diehl[1], *Nikos Prantzos*[2], *Vincent Tatischeff* [3]

[1] *Max Planck Institut für extraterrestrische Physik, D-85748 Garching, Germany*
[2] *Institut d'Astrophysique de Paris, F-75014, Paris, France*
[3] *CSNSM, IN2P3-CNRS/Univ. Paris-Sud and Paris-Saclay, F-91405 Orsay Campus, France*

Science questions – Starting from the synthesis of new nuclei by nuclear fusion reactions within stars and their explosions, the cycle of matter proceeds towards the ejection of metal-enriched and processed stellar gas into interstellar space. After cooling on the further trajectory, such metal-enriched gas mixes with interstellar gas from other origins and trajectories, to eventually partly ending up in newly-forming stars, closing and starting the cycle of cosmic matter again. This cycle includes at least two phases where gamma rays can provide astrophysical and rather direct diagnostics of aspects of cosmic nucleosynthesis: (1) The ejected yields of radioactive by-products of stellar and explosive nucleosynthesis tell us about the conditions of nuclear fusion reactions in those sites, and (2) the tracing of the flow of ejecta over their radioactive lifetimes, which is made possible from radioactive decay gamma rays from longer-lived nuclei because these are independent of thermodynamic conditions or density of gas. Further diagnostics arise (3) from positrons emitted in radioactive decays through their annihilation gamma-rays, and (4) from nuclear de-excitation gamma rays caused by cosmic-ray collisions with ambient-gas nuclei.

1. The yield in specific isotopes from stars and stellar explosions is an important diagnostic of the environmental conditions within such sites. These are occulted and not directly accessible, due to absorption of radiation in massive overlying envelopes. Even gamma rays rarely escape, except for some explosion scenarios. Nuclear reactions with their steep temperature sensitivities are excellent probes of the conditions in the nuclear burning regions of cosmic nucleosynthesis. Isotopic yields are the outcome of all nuclear reactions as they are determined by conditions in those inner regions. Candidate sources are novae from explosive hydrogen burning on the surfaces of white dwarfs composed of C and O or a further-enriched C-O-Ne mixture, the latter from more massive progenitors, supernovae in all their variants, and massive stars which experience major mass loss and thus may release nuclearly-processed interior gas (Asymptotic Giant Branch stars and Wolf-Rayet stars). When point sources cannot be observed, either due to low individual source yields, or due to superposition from multiple events occurring during a radioactive lifetime span, a diffuse glow of characteristic gamma rays provides a useful signal. Specifically, this could be the case for nova-produced ^{22}Na from sources within our Galaxy (event rate 30–50 per year in our Galaxy, ^{22}Na lifetime 3.8 years), and for supernova-produced ^{44}Ti from nearby galaxies (event rate few per century in M31, ^{44}Ti lifetime 85 years). It has been seen already for long-lived gamma-ray emitters ^{26}Al (τ 1.0 10^6 yr) and ^{60}Fe (τ 3.8 10^6 yr), where many sources along the disk of the Galaxy contribute.

   Specific science questions include [6]: Mixing in regions outside of the stellar core; here, stellar rotation, convection, and diffusion from compositional gradients, all interplay in complex ways. The structure of stars in their outer regions is a result of these processes, as they affect the nuclear burning in shell burning regions, which release nuclear binding energy. Further questions address the dynamic environments in stellar explosions. These bear the same mixing issues, and in addition non-equilibrium effects such as nuclear-burning fronts and their propagation, the properties of degenerate gas, and neutrino interactions further complicate the burning conditions. Again, nuclear-reaction products and their radioactive trace isotopes store such conditions through their production amounts, and carry them outside through the explosion into optically-thin regimes, where decay gamma rays can be observed.

In nova explosions, science questions are the compositional mix of accreted and underlying white dwarf material within the hydrogen burning region and the propagation of the ignition flame. In thermonuclear supernovae [5], the ignition of carbon fusion and its flame dynamics is a fundamental issue, then again the flame propagation and how nuclear burning in degenerate cores might be frozen out from nuclear statistical equilibrium as the flame reaches lower-density regions further outside, and lifts degeneracy. In the case of core collapses [2], electron capture in hot massive cores of massive stars removes pressure and initiates core collapse for the less-massive of the massive stars, while more massive cores collapse under gravity once the nuclear fuel has all been processed to its most stable form of iron. The collapse then leads to formation of a neutron star, and the intense neutrino emission upon its formation and neutronisation of matter may trigger the supernova explosion, or not. Further collapse towards a black hole may occur. In all collapses, vigorous convective flows onto and away from the central compact object include nuclear statistical equilibrium and freezing out from that. The resulting isotopic compositions carry the conditions of such nuclear processing as a memory into the ejecta, specifically for the long-lived ^{44}Ti, ^{26}Al and ^{60}Fe.

Neutrino-induced processing of ^{26}Al and ^{60}Fe, in addition to some modest explosive-burning amounts, reflect the conditions within the supernova explosion. These two isotopes are plausibly assumed to be mainly produced by the same sources, by massive stars [3]. Therefore, in the measurement of the isotopic ratio ^{60}Fe/^{26}Al any unknowns about source distances and location will cancel: This ratio is a valuable diagnostic for the internal structure of massive stars. Although integrated over a large population of such sources, it serves to test our overall validity of models for the internal structure of massive stars as it evolves over their lifetime, ending in a core collapse supernova. ^{26}Al is mainly produced in the hydrogen burning stages, i.e. the main sequence phase, and O-Ne shell burning in the late evolution. ^{60}Fe, on the other hand, is produced in shell He and C burning phases, in the later evolution. Each of these late shell burning regions is expelled only in the final supernova. ^{26}Al from the main sequence phase may be ejected also by Wolf Rayet winds for very massive stars that evolve rather rapidly within several million years. As massive stars occur in groups, the integrated radioactive emission from such regions and these two isotopes provides a global test of models of massive star evolution. Additionally, for individual massive star groups where a steady state has not been reached, this isotopic ratio encodes the age of the group, as the Wolf-Rayet wind and supernova contributions relate to different stellar masses and ages.

2. The cyle of matter includes a phase where the how hot nucleosynthesis ejecta cool down and are propagated towards new star formation. This is often ignored, as it is particularly hard to constrain through observations. This recycling time scale depends on the structure of the dynamic interstellar medium. It could be rather long, up to 10^7–10^8 years, and thus exceed stellar evolution times which are of the order of tens of Myr, SNRs can be seen over time scales of few 10^5 yr at most. Long-lived radioactive gamma-ray emitters ^{26}Al (τ 1.0 10^6 yr) and ^{60}Fe (τ 3.8 10^6 yr) can trace mixing processes of ejecta into the next generation of star formation over much longer time. Among others, this provides observational constraints on molecular-cloud lifetime and models for stimulated/triggered star formation. On the global, Galactic scale, superbubbles have been proposed to be key structures in the transport of fresh ejecta towards new star forming regions, from INTEGRAL/SPI data for the ^{26}Al line. Mapping Galactic ^{26}Al gamma-ray emission can thus trace ejecta flows into and through such superbubbles, and compare their connections to specific star forming regions with their massive-star groups at their respective ages.

3. Radioactivity from proton-rich nuclei generally produces positrons, and contributions from many such nucleosynthesis sources would integrate to a diffuse emission from annihilation gamma rays with the 511 keV line being most prominent. Novae and supernovae contribute through ^{13}N, ^{18}F, ^{56}Ni, ^{44}Ti, for example, with characteristic radioactive lifetimes from hours to a century, and also other positron sources are known to exist and add to such diffuse emission. The science question here is a discrimination among the different candidate sources.

4. Nuclear de-excitation gamma rays reflect cosmic ray fluxes as they collide with ambient interstellar gas and are energetic enough to excite nuclear levels [1]. The characteristic gamma-ray lines provide most-direct measurements of the flux of cosmic rays at several tens of MeVs, which cannot be observed in direct cosmic ray measurements as they are deflected by interstellar magnetic fields. One of the unsolved science questions on the origin of cosmic rays could thus be answered by a first observation of characteristic gamma-ray lines from young supernova remnants, which generally are considered plausible cosmic-ray acceleration environments.

Expected results with e-ASTROGAM – With its huge increase in sensitivity, e-ASTROGAM will provide a detailed view of the morphology of this emission, with high precision measurements of the line flux from many regions of the Galaxy. This will advance the current state of such observational constraints [4]. For example, e-ASTROGAM will observe the ^{26}Al radioactivity from dozens of nearby ($\leq$kpc) stellar objects and associations. In particular, it will measure precisely the amount of ^{26}Al ejected by the Wolf-Rayet star WR11 in the γ^2-Velorum binary system (expected line flux is $\sim 10^{-5}$ ph cm^{-2}s-1), thus providing a unique calibration of the ^{26}Al production during the Wolf-Rayet phase of a massive star. e-ASTROGAM has also the capability of detecting ^{26}Al emission from the LMC (expected line flux of $\sim 10^{-6}$ ph cm^{-2}s-1), thus providing new insight into stellar nucleosynthesis outside the Milky Way. For the first time, e-ASTROGAM will provide the sensitivity needed to establish the Galactic ^{60}Fe emission and build an accurate map of the ^{60}Fe flux in the Milky Way, enabling its comparison with the ^{26}Al map to gain insight into the stellar progenitors of both radioisotopes. In particular, measuring gamma-ray line ratios for specific massive-star groups will constrain ^{60}Fe production in massive stars beyond 25–40 M$_\odot$, which directly relates to stellar rotation and uncertain convective-layer evolution in massive star interiors. Marginally-bright diffuse radioactivity may arise from nova explosions, due to their higher frequency of occurrence at about 30 yr^{-1} in the Galaxy, ejecting into their surroundings β^+ emitters such as ^{13}N, ^{18}F, and long-lived ^{22}Na. These β^+ decays inject positrons into interstellar space. e-ASTROGAM will provide a detailed map of annihilation gamma rays, also imaging faint regions near candidate sources along the disk of the Galaxy and in star forming regions. This will allow discrimination of nucleosynthesis contribution of positrons from several other types of sources that are expected to contribute positrons as well, from a variety of electron-positron pair plasma creation scenarios as well as from cosmic-ray hadronic interactions. Sources of cosmic ray accelerations will be directly probed with e-ASTROGAM through interactions with ambient interstellar gas, which leads to characteristic nuclear lines, such as from ^{12*}C at 4430 keV.

References

[1] H. Benhabiles-Mezhoud, H., Kiener, J., Tatischeff, V., and Strong A.W., 2013, ApJ 763, 98
[2] Burrows, A., 2013, Rev. Mod. Phys. 85, 245
[3] Chieffi, A., Limongi, M., 2013, ApJ, 764, 21
[4] Diehl R., 2013, Rep. Prog. Phys. 76, 026301
[5] Hillebrandt, W., Kromer, M., Röpke, F., & Ruiter, A., 2013, Front. Phys. 8, 116
[6] Meynet, G., Maeder, A., Georgy, C., *et al.*, 2017, Proc. IAU, arXiv:1704.04616

Galactic positron annihilation radiation

Nikos Prantzos [1], *Pierre Jean* [2], *Jürgen Knödlseder* [2], *Peter von Ballmoos* [2], *Thomas Siegert* [3], *Roland Diehl* [3], *Jordi Isern* [4], *Vincent Tatischeff* [5]

[1] *IAP, CNRS/Univ. P. & M. Curie, 98bis Bd. Arago, 75104, Paris*
[2] *IRAP, 9 av. colonel Roche, BP 44 346, 31028 Toulouse Cedex 4, France*
[3] *Max Planck Institut für extraterrestrische Physik, D-85748 Garching, Germany*
[4] *ICE-CSIC/IEEC, Ed. Nexus-201, c/Gran Capità 2-4, E-08034 Barcelona, Spain*
[5] *CSNSM, CNRS/Univ. Paris-Sud, F-91405 Orsay Campus, France*

Science questions – The 511 keV emission from electron-positron annihilation in the Galaxy is the brightest gamma-ray line in the sky, and the first ever detected from outside the solar system [6, 8]. It is produced by the annihilation of a few 10^{43} positrons with electrons of the interstellar medium (ISM) every second (flaring stars could also contribute to the observed annihilation radiation from the Galactic bulge, according to Ref. [2]). Despite more than 40 years of intense observational and theoretical investigation, the origin of annihilating positrons remains a mystery. The emission is strongly concentrated toward the Galactic bulge. The bulge/disk ratio appeared higher than observed in any other wavelength [7, 14], but with increasing sensitivity the disk emission emerges more clearly, perhaps as an extended, low brightness thick disk [12]. This bulge/disk ratio is believed to point towards source types, hence requires better observations.

High-resolution spectroscopy of the annihilation radiation provides information on the nature of the environment in which the positrons annihilate. Measurements with INTEGRAL/SPI of the shape of the 511 keV line and positronium fraction in the bulge are consistent with positron annihilation in a mixture of warm ($T \sim 8000$ K) neutral and ionized phases of the interstellar medium [3, 5].

It remains unclear what are the main sources of positrons: supernovae of gravitational and thermonuclear types, or pulsars, X-ray binaries and microquasars, or more "exotic", such as self-interacting dark matter particles or the Galactic supermassive black hole - which, appears inactive today but may have been a transient positron injector. The latest proposed positron source is a rare type of thermonuclear supernovae known as SN 1991bg-like (resulting from the merger of a CO white dwarf and a He white dwarf) that could cause both the strength and morphology of the Galactic positron annihilation signal as well as the origin of ^{44}Ca [4]. However, a major issue in all studies is that positrons may propagate for several 10^5 yr far away from their sources before annihilating – depending on still poorly understood properties of Galactic ISM and magnetic fields – making it difficult to infer positron sources from the observed gamma-ray emission (see Ref. [9] and references therein). Understanding the Galactic 511 keV emission constitutes a major challenge for modern astro-particle and astro-physics.
Progress in the field requires advances in several directions:

- *Observations of 511 keV emission*: What is the true spatial distribution of the emission? How far do the spheroid and disk extend? Can we find support for transport physics or galactic outflows from an extended disk? Is there a distinct central point source, and how concentrated is it [12]? Is the recently-reported [11] broadened positron annihilation emission from the flaring microquasar V404 Cyg really proof of pair plasma near accreting black holes, and can it be confirmed (see dispute by [10])? Does the morphology of 511 keV disk emission differ from the one observed at 1.8 MeV, resulting from the decay of radioactive ^{26}Al, which is a major positron provider in the disk? (Similarity would imply dominance of this source in the disk and that positrons do not travel far away from their sources.)

- *Physics of positron sources*: What is the escaping fraction of positrons from SN Ia? What is the production yield of ^{44}Ti in normal, and in SN 1991bg-like thermonuclear supernovae?

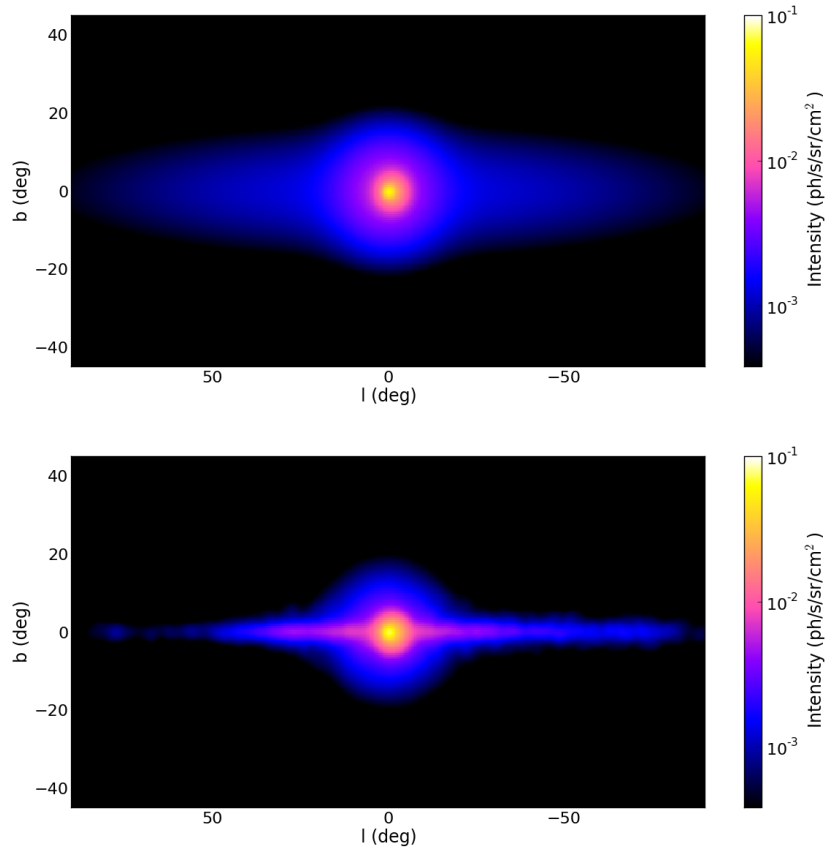

Figure 1: Simulated e-ASTROGAM observations of the 511 keV emission, obtained for an exposure of 1 year of the inner Galactic region, assuming (top) the model proposed by [12] with a thick disk and (bottom) a model with the disk of [1] and the point source and bulge components of [13].

Could these, with ^{26}Al, explain the Galactic positron production rate? What is the SN Ia rate in the inner (star forming) and in the outer (inactive) bulge? What are the positron yields, activity time scales, and spatial distribution in the inner Galaxy of X-ray binaries, microquasars and millisecond pulsars? How can the past level of activity of the central supermassive black hole be reliably constrained?

- *Studies of positron propagation*: What is the multi-scale morphology of the interstellar medium near positron sources, and how may interstellar turbulences affect the positron transport? What is the large-scale configuration of the Galactic magnetic field? What is the role of particle reacceleration?

Those issues are of great interest to a broad community, including researchers in nucleosynthesis and supernova physics, compact and accreting objects, the Galactic supermassive black hole, as well as cosmic-ray physics, particle transport in turbulent interstellar plasmas, the large scale galactic magnetic field, and even dark matter research.

Expected results with e-ASTROGAM – Figure 1 shows two simulated sky maps of the 511 keV intensity distribution observed with e-ASTROGAM: one with a thick Galactic disk as suggested by [12] and another with the disk component of [1], which results from a Monte Carlo modeling of the Galactic propagation of nucleosynthesis positrons produced by the β^+-decay of ^{26}Al, ^{44}Ti, and ^{56}Ni, and the bulge components of [13]. With its large field of view of 46° half width at half maximum (HWHM) at 511 keV, corresponding to a fraction-of-sky coverage in zenith pointing mode of 23% at any time, e-ASTROGAM will perform a deep Galactic survey of the positron annihilation radiation to search for potential point-like sources, and study in detail the

morphology and spectral characteristics (e.g. positronium fraction) of the disk, bulge, and central source emissions. With a predicted point-source sensitivity of 4.1×10^{-6} ph cm^{-2} s^{-1} for the 511 keV line in 1 Ms of integration time, e-ASTROGAM will be able to detect low surface brightness regions outside the Galactic plane and enhanced emission from the inner Bulge, as well as individual star forming regions in the disk, such as the Cygnus region.

References

[1] Alexis, A., Jean, P., Martin, P., et al. 2014, A&A, 564, 108
[2] Bisnovatyi-Kogan, G. S., & Pozanenko, A. S. 2017, Astrophysics, 60, 223
[3] Churazov, E., Sunyaev, R., Sazonov, S., Revnivtsev, M., & Varshalovich, D. 2005, MNRAS, 357, 1377
[4] Crocker, R. M., Ruiter, A. J., Seitenzahl, I. R., et al. 2017, Nature Astronomy, 1, 0135
[5] Jean, P., Knödlseder, J., Gillard, W., et al. 2006, A&A, 445, 579
[6] Johnson, W. N., III, Harnden, F. R., Jr., & Haymes, R. C. 1972, ApJ, 172, L1
[7] Knödlseder, J., Jean, P., Lonjou, V., et al. 2005, A&A, 441, 513
[8] Leventhal, M., MacCallum, C. J., & Stang, P. D. 1978, ApJ, 225, L11
[9] Prantzos, N., Boehm, C., Bykov, A. M., et al. 2011, Reviews of Modern Physics, 83, 1001
[10] Roques, J.P., Jourdain, E., Bazzano, A. et al. 2015, ApJL, 813, 22
[11] Siegert, T., Diehl, R., Greiner, J., et al. 2016a, Nature, 531, 341
[12] Siegert, T., Diehl, R., Khachatryan, G., et al. 2016b, A&A, 586, A84
[13] Skinner, G. K., Diehl, R., Zhang, X., et al. 2014, INTEGRAL workshop proceedings, 054
[14] Weidenspointner, G., Skinner, G., Jean, P., et al. 2008, Nature, 451, 159

Compact objects physics

Conveners: Alice Harding
Josep M. Paredes

Isolated Neutron Stars and Pulsars

Christian Gouiffés [1], *Isabelle A. Grenier* [2], *Alice Harding* [3], *Philippe Laurent* [4], *Roberto Mignani* [5,6], *Marcos López Moya* [7], *Pablo Saz Parkinson* [8,9], *Andy Shearer* [8], *Luca Zampieri* [9], *Silvia Zane* [10]

[1] *Laboratoire AIM, UMR 7158, CEA/DRF, CNRS, Université Paris Diderot, IRFU/SAp, F-91191 Gif-sur-Yvette, France* [2] *Laboratoire AIM, CEA-IRFU/CNRS/Université Paris Diderot, C.E.A. Saclay, France*
[3] *NASA/Goddard Space Flight Center, Greenbelt, MD 20771, USA*
[4] *Laboratoire APC, UMR 7164, CEA/DRF CNRS, Université Paris Diderot, Paris, France*
[5] *INAF - Istituto di Astrofisica Spaziale, Milano, Italy*
[6] *University of Zielona Gora, Poland*
[7] *Unidad de Partículas y Cosmología (UPARCOS), Universidad Complutense, E-28040 Madrid, Spain*
[8] *Santa Cruz Institute for Particle Physics, University of California, Santa Cruz, CA, USA*
[9] *Dept. of Physics & Laboratory for Space Research, University of Hong Kong, Hong Kong*
[10] *Centre for Astronomy, NUI Galway, Ireland*
[11] *INAF - Osservatorio Astronomico di Padova, I-35122, Padova, Italy*
[12] *Mullard Space Science Laboratory, University College London, Holmbury St. Mary, Dorking, Surrey, RH5 6NT, UK*

Science questions – *Fermi* revolutionized γ-ray pulsar studies increasing the number of pulsars detected above 100 MeV from 7 with *CGRO/EGRET* to about 200[1] today. However in the soft γ-ray region there are only 18 detections above 20 keV and only four have been detected with pulsed emission in the range 1-10 MeV [9]. e-ASTROGAM's sensitivity at 10 MeV is 100 times better than *CGRO/COMPTEL*, consequently we would expect a significant number of new pulsar detections at this energy. At lower energy, e-ASTROGAM will study the pulsars and magnetars detected in hard X-rays with INTEGRAL. This will allow filling the gap in the electromagnetic spectrum of these compact objects. Spatial, spectral and temporal data in the e-ASTROGAM energy range will be crucial to better understand the physics, still poorly known, of these sources. Furthermore e-ASTROGAM's polarization sensitivity will enable a unique contribution to pulsar studies. For the first time it should be possible to have a 0.1-10 MeV survey with both pulse shape determination and measurements of phase resolved polarization, both of which will constrain current pulsar emission models and mechanisms. This mission can play a major role as an alert monitor for the variable sky survey in coordination with all the future radio, infrared, optical and X-rays facilities for the electromagnetic domain and the coming neutrino and gravitational observatories.

Importance of gamma-ray observations – The *Fermi* Large Area Telescope (LAT) has detected many types of γ-ray pulsars: young radio-loud and radio-quiet pulsars [2, 3], millisecond pulsars [4], etc. The measured spectral shapes of most *Fermi* γ-ray pulsars exhibit exponential cut-offs in the GeV range. This has favoured high-altitude models in which the emission originates in the outer magnetosphere, in the so-called outer gaps (e.g. [5, 6]), over polar cap models, in which super-exponential cut-offs were predicted (e.g. [7, 8]). However, one class of pulsars that has hitherto remained relatively elusive are the so-called soft γ-ray pulsars. Our understanding of soft γ-ray pulsars is in its infancy and limited by the small sample of objects (see [9] for a recent review).The majority of these soft γ-ray pulsars exhibit broad, structured single pulse profiles, and

[1] https://confluence.slac.stanford.edu/display/GLAMCOG/Public+List+of+LAT-Detected+Gamma-Ray+Pulsars

only six have double (or even multiple, in the case of Vela) pulses. Soft γ-ray pulsars typically have hard power-law spectra in the hard X-ray band, reaching their maximum luminosities in the MeV range, as opposed to the GeV range (see Figure 1). They tend to be younger and more luminous ($L_{sd} > 4 \times 10^{36}$ ergs/s) than the overall LAT pulsar population [9]. Only seven soft γ-ray pulsars (as defined by [9]) have so far shown pulsed emission detected by the LAT. In fact, PSR B1509-58, the prototypical soft γ-ray pulsar, detected in the 1–10 MeV range by COMPTEL [10] and confirmed by AGILE [11], was particularly challenging to detect with *Fermi* [12] due to its soft spectrum. Other soft γ-ray pulsars remain undetected by *Fermi* (see Table 13 of [13]), despite pre-launch expectations of their detection based on their large spin-down power.

Any soft γ-ray pulsar model must explain why most of them are not seen at GeV energies by *Fermi*. A possible explanation can be found in [14, 15]. According to this model, charges of the pairs created in the outer gap move in opposite directions due to the electric field: one in the inflow direction, towards the surface of the neutron star, and another in the outflow direction. In both cases the charges are accelerated emitting GeV photons, but whereas the outflow radiation can escape from the star, most of the high-energy inflow curvature photons interact with the high magnetic field and are converted into pairs, which then emit lower energy synchrotron radiation. Soft γ-ray pulsars may therefore simply be standard pulsars for which the GeV part of the beam is not visible and the line of sight is in the direction of the incoming beam instead [14]. Increasing the population of GeV-quiet soft γ-ray pulsars is crucial to test models over a range of spin-down parameters and viewing geometries.

e-ASTROGAM will enable the detection of new pulsars in the MeV band by carrying out measurements that are difficult or impossible to conduct with current instruments. *Fermi*-LAT has detected over 200 pulsars with only 7 out of the 18 known soft γ-ray pulsars in this sample. This soft γ-ray population represents younger pulsars whose spectrum peaks below 100 MeV so they would be undetected by *Fermi*-LAT. From [9] it is reasonable to expect the number of detected soft γ-ray to at least double with e-ASTROGAM.

Expected results with e-ASTROGAM – Conversely to traditional γ-ray telescopes, which have relied exclusively on spectroscopy and timing, e-ASTROGAM will also be able to measure the polarization characteristics of the γ-ray emission from pulsars. Model predictions depend on the pulsar inclination and viewing angles, which in the best cases are only poorly known. In contrast, the expected polarization signature differs significantly from one model to another because it is very sensitive to the electromagnetic geometry, and hence to the location of the emitting zones [16]. Nearly all high-energy emission mechanisms can give rise to linearly polarized emission, though the polarization angle and degree of polarization are highly dependent on the source physics and geometry. Both synchrotron and curvature radiation produce linearly polarized radiation in which the angle traces the field direction and the degree of polarization is independent of energy. On the other hand, inverse Compton scattering produces scattered radiation whose polarization degree depends on energy and scattering angle[17]. γ-ray polarimetry observations with e-ASTROGAM will thus be crucial to deliver information on the neutron star magnetic field and locate the region in the magnetosphere where the acceleration of particles takes place, as well as identifying different emission mechanisms. From [18] e-ASTROGAM will be able to detect 0.7% polarization from a Crab like source in 1 Msec; it will be about 100 times more sensitive than INTEGRAL.

Polarimetry observations in the soft γ-ray regimes will be complemented by X-ray (2-10 keV) fluxes detected by the new generation of X-ray polarimetry missions, which are due to fly in the e-ASTROGAM mission time frame. These include the Chinese mission eXTP (enhanced X-ray Timing Polarimetry) a multi-facility X-ray observatory [19] with a polarimeter with a time resolution of 100 μs, ESA's XIPE (X-ray Imaging Polarimeter Explorer)[20], and NASA's IXPE mission [21], which will be XIPE's precursor. XIPE's time resolution (8μs), would make it an ideal instrument to measure phase-resolved polarization from young and bright X-ray pulsars, decoupling the emission from their surrounding and bright Pulsar Wind Nebulae (PWN). Together with a new generation of optical/infrared polarization instruments designed for the forthcoming 30 m-class telescopes, we will then, for the first time, be able to carry out multi-wavelength polarization

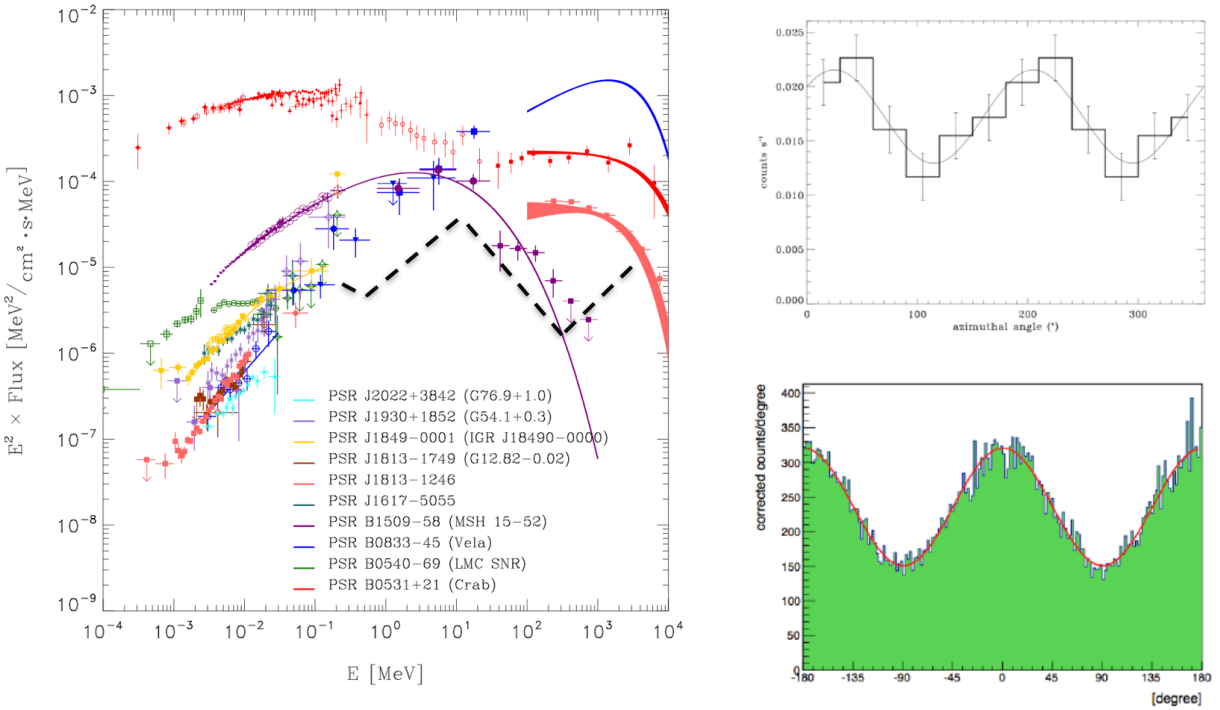

Figure 1: Left : SED for a number of soft $\gamma - ray$ pulsars taken from Kuiper & Hermsen[9] with the expected sensitivity for 1 Msec e-ASTROGAM exposure shown (black dashed line). Right: Comparison of the polarization sensitivity of INTEGRAL-IBIS (top) - observed Crab polarisation from 1 MSec observation (unpublished) vs e-ASTROGAM (bottom) for 1 Msec observation of a 100% polarised 10mCrab source in the 0.2 – 2 MeV range[18]. The spectral fit to the archetypal pulsar PSR B1509-58 is depicted by the purple curve.

studies of pulsars across the entire electromagnetic spectrum, from radio to soft γ-rays, including the mm/sub-mm range with ALMA, providing us with unprecedented diagnostic tools to determine the characteristics of pulsar magnetospheres from a synoptic, and synergistic, point of view.

References

[1] A. A. Abdo et al. (*Fermi* LAT Coll.), ApJ Supplement Series 187 (2010) 460
[2] A. A. Abdo et al. (*Fermi* LAT Coll.), Science 325 (2009) 840
[3] P. M. Saz Parkinson et al., ApJ 725 (2010) 571
[4] A. A. Abdo et al. (*Fermi* LAT Coll.), Science 325 (2009) 845
[5] K. S. Cheng, C. Ho & M. Ruderman, ApJ 300 (1986) 500
[6] K. S. Cheng, M. Ruderman, and L. Zhang, ApJ 537 (2000) 964
[7] M. A. Ruderman et al., ApJ 196 (1975) 51
[8] A. K. Harding, J. V. Stern, J, Dyks, & M. Frackowiak, ApJ, 680 (2008) 1378
[9] L. Kuiper & W. Hermsen, Mon Not R Astron Soc 449 (2015) 3827
[10] L. Kuiper et al., Astron. Astrophys 351 (1999) 119
[11] A. Pellizzoni et al. (AGILE Coll.), ApJ Letters 695 (2009) 115
[12] A. A. Abdo et al. (*Fermi* LAT Coll.), ApJ 714 (2010) 927
[13] A. A. Abdo et al. (*Fermi* LAT Coll.), ApJ Supplement Series 208 (2013) 17
[14] Y. Wang, J. Takata, and K. S. Cheng, ApJ 764 (2013) 51
[15] Y. Wang et al, Mon Not R Astron Soc 445 (2014) 604
[16] B. Cerutti et al., Mon. Not. R. Astron. Soc. (2016) 16
[17] A. Harding & C. Kalapotharakos, ApJ (2017), 840, 73
[18] A. de Angelis et al, arXiv:1611.02232, v5
[19] S. N. Zhang, M. Feroci, A. Santangelo, 2016, Proceedings of the SPIE, Volume 9905
[20] P. Soffitta et al., 2016, Proceedings of the SPIE, Volume 9905
[21] M. Weisskopf et al, 2016, Proceedings of the SPIE, Volume 9905

Transitional Millisecond Pulsars

Tyrel Johnson[1], *J. Eric Grove*[2] *Alessandro Papitto*[3], *Domitilla de Martino*[4]

[1] *College of Science, George Mason University, Fairfax, VA 22030, USA, resident at Naval Research Laboratory, Washington, DC 20375, USA*
[2] *Space Science Division, Naval Research Laboratory, Washington, DC 20375-5352, USA*
[3] *INAF, Osservatorio Astronomico di Roma, via di Frascati 33, I-00044, Monte Porzio Catone (Roma), Italy*
[4] *INAF, Osservatorio Astronomico di Capodimonte, Salita Moiariello 16, I-80131 Naples,Italy*

Science questions – Millisecond pulsars (MSPs) are thought to be old, "recycled" pulsars, spun up by the transfer of mass and angular momentum from a binary companion [1]. The detection of ms pulsations in accretion-powered low-mass X-ray binaries (LMXBs) [2] provided early observational support for this scenario. Dramatic new supporting evidence has come from the recent observation of three MSPs to switch in both directions, between rotation-powered pulsar (RPP) and accreting (LMXB) states [3, 4, 5, 6]. All three transitional MSPs (tMSPs) belong to the class of MSPs known as "redbacks," binary MSPs with low-mass ($\sim$0.2 to 0.5 $M_\odot$), non-degenerate companions (typically G-type stars) and short orbital periods ($\lesssim$ 1 day) [7].

Transitions to (from) the LMXB state are accompanied by the disappearance (reappearance) of radio pulsations, a drastic increase (decrease) in high-energy emission – more than an order of magnitude in X-rays and a factor of a few in gamma rays – and the appearance (disappearance) of a disk around the pulsar. Intermittent, accretion-powered X-ray pulsations are detectable in the LMXB state of the three known tMSPs [3, 8, 9] suggesting episodic accretion. X-ray emission is detected out to 100 keV with no high or low energy cutoff [11]. The $\geq$ 100 MeV emission displays significant spectral curvature, well-described with an exponentially cutoff power-law shape. The emission mechanism responsible for the enhanced HE emission in the LMXB state is uncertain, and it is unclear what conditions must be met for a system to transition. Can only redbacks transition? Can all redbacks transition?

Importance of gamma-ray observations – One of the primary differentiators between models explaining the enhanced HE emission from tMSPs in the LMXB state is whether or not the disk penetrates the pulsar magnetosphere, quenching the RPP emission. If it does not, the enhanced HE emission is synchrotron X-ray and inverse Compton (IC) off UV disk photons $>$ 100 MeV [10]. If it does, a propeller system is created, and energized electrons emit synchrotron X-rays that then interact with the same electrons to create synchrotron self Compton (SSC) $>$ 100 MeV gamma rays [11]. Both models can match the X-ray and $>$ 100 MeV spectra reasonably well. An alternate scenario, discussed in the contribution by Zdziarski et al., is that the enhanced HE emission during the LMXB state originates from a jet, based on similarities in the X-ray emission properties with microquasars.

Measuring the shape of the spectrum in the MeV range would constrain the physics and conditions in the binary system. If the disk is outside of the magnetosphere, a slow roll over after a few hundred keV is predicted, turning up at a few tens of MeV as the IC dominates. In contrast, the propeller model predicts a more gradual transition from synchrotron to SSC dominance. In the propeller model, the electron energy distribution power-law index can be derived from the X-rays, the maximum Lorentz factor from the $>$ 100 MeV spectrum, and the electron acceleration parameter from the cutoff energy in the few MeV range. Measuring the spectrum in the MeV range would then leave only the magnetic field strength at the disk-magnetosphere interface not directly constrained in the propeller model.

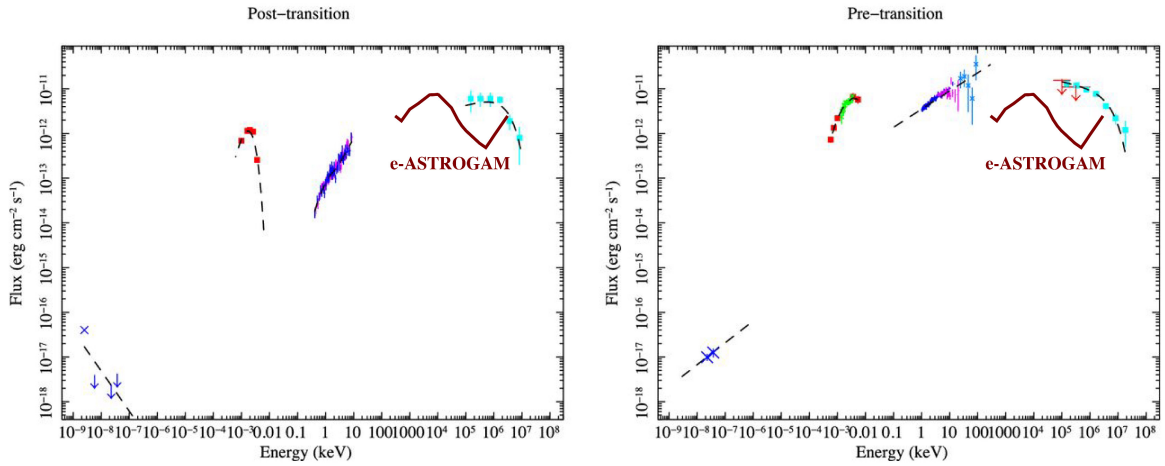

Figure 1: Broadband SED of XSS J122704859/PSR J1227−4853 during RPP state (left) and LMXB state (right), taken from [14]. One-year sensitivity of *e-ASTROGAM* is added to each panel. This tMSP would be detected quite significantly by *e-ASTROGAM* in either state, and in particular the spectrum from a long-lasting LMXB phase might be detectable across the full science range.

Expected results with *e-ASTROGAM* – Theoretical predictions of an energy flux in the MeV domain of few 10^{-12} to few 10^{-11} erg cm^{-2} s^{-1} from tMSPs are within reach of *e-ASTROGAM* (see Figure 1). While one tMSP transitioned from RPP to LMXB and back over the course of one month [3], historical observations of the other two suggests transition time scales of order 10 years. Thus, tMSPs in the LMXB state may remain there long enough to allow for multiple observations, which can then be stacked.

During the LMXB state, the X-ray emission also varies between low and high "modes" with periods of intense flaring, lasting as long as ∼45 minutes, in which the luminosity increases by a factor of ∼3 [3, 12, 13]. It is likely that these changes in X-ray flux state, not transitions, are due to changes in which emission mechanism dominates. If so, the MeV emission could also be variable and at times enhanced above the model predictions discussed previously, and MeV observations triggered by X-ray monitoring could provide a detection on shorter timescales.

References

[1] Alpar, M. A., Cheng, A. F., Ruderman, M. A., & Shaham, J. 1982, *Nature*, 300, 728
[2] Wijnands, R. & van der Klis, M. 1998, *Nature* 394, 344
[3] Papitto, A., Ferrigno, C., Bozzo, E., et al. 2013, *Nature*, 501, 517
[4] Stappers, B. W., Archibald, A. M., Hessels, J. W. T., et al. 2014, ApJ, 790, 39
[5] Bassa, C. G., Patruno, A., Hessels, J. W. T., et al. 2014, MNRAS, 441, 1825
[6] Roy, J., Ray, P. S., Bhattacharyya, B., et a.. 2015, ApJ, 800, L12
[7] Roberts, M. S. E. 2011, in AIP Conf. Series, Vol. 1357, ed. M. Burgay, N. D'Amico, P. Esposito, A. Pellizzoni, & A. Possenti, 127-130
[8] Papitto, A., de Martino, D., Belloni, T. M., et al. 2015, MNRAS 449, L26
[9] Archibald, A. M., Bogdanov, S., Patruno, A., et al. 2015, ApJ, 807, 62
[10] Takata, J., Li, K. L., Leung, G. C. K., et al. 2014, ApJ, 785, 131
[11] Papitto, A., Torres, D. F., & Li, J. 2014, MNRAS, 438, 2105
[12] de Martino, D., Belloni, T., Falanga, M., et al. 2013, A&A, 550, A89
[13] Bogdanov, S., Archibald, A. M., Bassa, C., et al. 2015, ApJ, 806, 148
[14] de Martino, D., Papitto, A., Belloni, T., et al. 2015, MNRAS, 454, 2190

Magnetars

Roberto Turolla[1], *Roberto Taverna*[1], *Silvia Zane*[2]

[1] *Department of Physics and Astronomy, University of Padova, via Marzolo 8, 35131 Padova, Italy*
[2] *Mullard Space Science Laboratory, University College London, Holmbury St. Mary, Dorking, Surrey, RH5 6NT, UK*

Science questions – Magnetars are ultra-magnetized neutron stars ($B \approx 10^{13}$–10^{15} G) which, at variance with ordinary radio-pulsars, are powered by their own magnetic energy (see e.g [6], for a review). Observationally identified with two peculiar classes of X-ray pulsars, the soft gamma repeaters (SGRs) and the anomalous X-ray pulsars (AXPs), their persistent emission has been detected from the IR/optical range up to the hard X-rays ($\approx$ 200 keV) with the Integral satellite (see fig. 1, left). Up to now, only upper limits at higher energies ($\approx$ 1–10 MeV) are available, thanks to old CGRO Comptel observations (see again fig. 1, left).

The basic picture for the high-energy magnetar emission involves the reprocessing of thermal photons emitted by the star surface through resonant Compton scattering (RCS) onto charges, moving in a "twisted" magnetosphere [5, 4]. Many crucial details of the model are however still unclear. The distribution of the scattering particles in the velocity space is not completely understood as yet, nor is the geometry of the region where currents flow (the "j-bundle" [1]). Moreover, a substantial hard X-ray energy emission is expected from curvature radiation from ultra relativistic charges accelerated in the external magnetosphere.

Importance of gamma-ray observations – Observations in the gamma-ray range, as those e-ASTROGAM will allow, are key in addressing the previous issues. Fig. 1 (right) and fig. 2 clearly show how theoretical spectral predictions (here based on the RCS scenario) are substantially different above $\sim$ 0.5 MeV, according to the assumed velocity distribution of the charges, the geometry of the twisted region (either localized or global) and the viewing angle.

SGRs and AXPs show somewhat different behaviours at high energies ($\approx$ 10–100 keV). While the spectrum of the former steepens, the latter exhibit a spectral upturn. Extrapolating the hard X-ray flux to the 0.3–0.5 MeV energy band, bright, persistent magnetar sources are expected to reach fluxes up to $\sim 10^{-4}$ cts/s/cm^2, as in the case of the AXPs 1RXS J1708849-4009, 4U 0142+616, 1E 1841-045 and the SGRs 1806-20, 1900+14. At energies > 1 MeV, theoretical calculations predict a steep decline of the flux, in agreement with the upper limits set by Comptel (see fig. 1 left).

Expected results with e-ASTROGAM – A flux in the range 10^{-4}–10^{-5} cts/s/cm^2 is well above e-ASTROGAM sensitivity limit, $< 2.8 \times 10^{-5}$ cts/s/cm^2 above 0.3 MeV for an exposure time of 1 Ms. A preliminary assessment of the detectability with e-ASTROGAM of bright magnetar sources is reported in the table. With the exception of SGR 1900+14, which falls below the sensitivity threshold by a factor $\sim$ 3, all the other objects should be easily detectable with an exposure time of 1 Ms. We stress that even the absence of a positive detection would be extremely valuable in constraining magnetar physics.

Polarization studies of magnetars in the 0.3–1 MeV range will be also extremely important and ideally complement those carried out by X-ray polarimetric missions, like IXPE, XIPE and e-XTP. Magnetars flux in the 2–10 keV range does not exceed a few mCrab. e-ASTROGAM MDP is 10% at a flux level of 10 mCrab with an exposure time of 30 Ms. Despite large polarization fractions are expected from these sources ($\gtrsim$ 50%; [3]), quite long exposure times are needed to obtain a significant measure of the polarization properties.

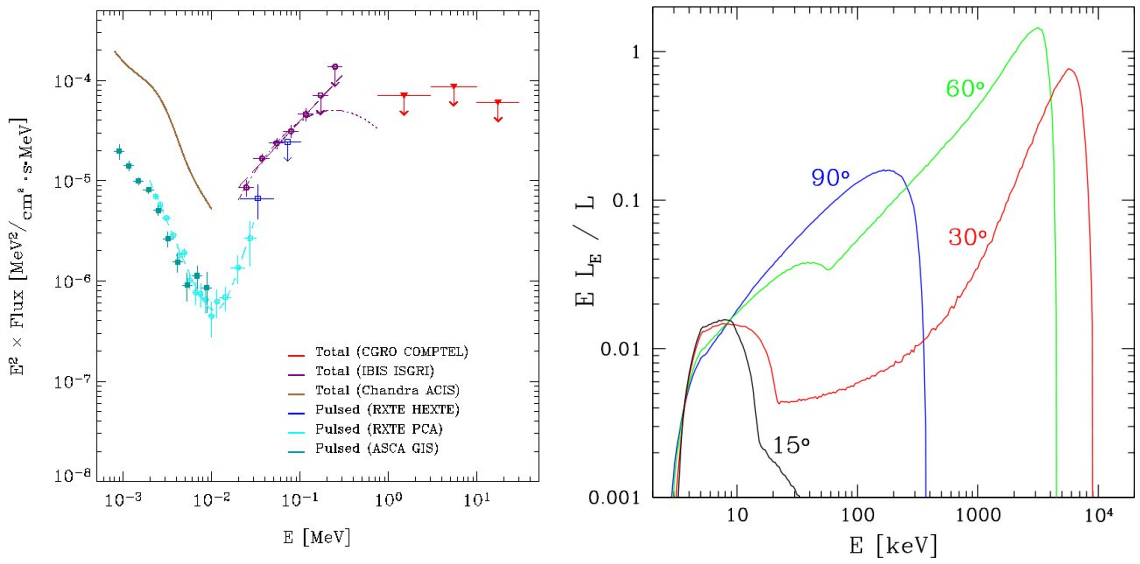

Figure 1: Left: The observed SED of the AXP 4U 0142+614 [2]. Right: RCS model spectra from a localized j-bundle at different viewing angles with respect to the magnetic axis [1].

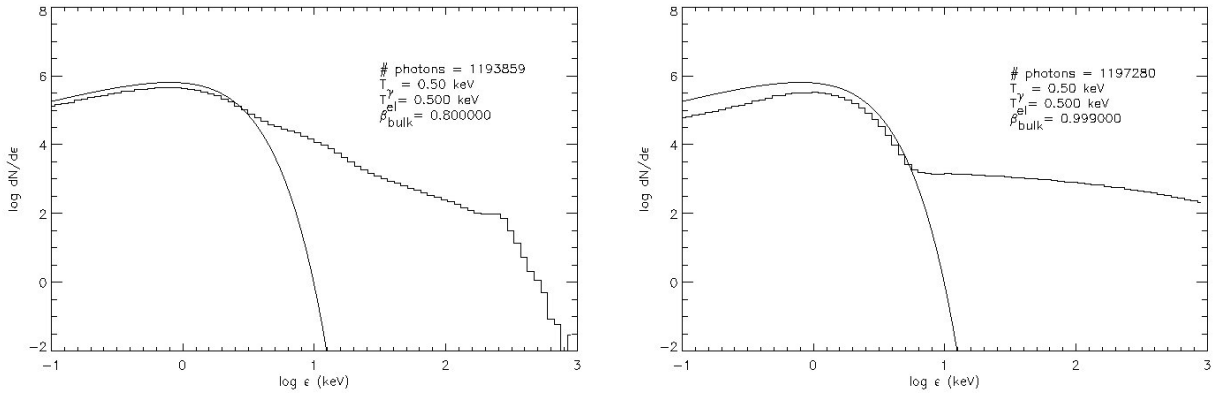

Figure 2: Montecarlo simulations of RCS spectra emerging from a globally twisted magnetosphere for different values of the bulk electron velocity, $\beta = 0.8$, left, and $\beta = 0.999$, right [7].

Source	Estimated flux @0.3 MeV (cts/s/cm^2)	e-Astrogam sensitivity @0.3 MeV (cts/s/cm^2)	Estimated flux @0.5 MeV (cts/s/cm^2)	e-Astrogam sensitivity @0.5 MeV (cts/s/cm^2)
RXS J1708	12×10^{-5}	2.8×10^{-5}	7×10^{-5}	1.3×10^{-5}
4U 0142	23×10^{-5}	2.8×10^{-5}	14×10^{-5}	1.3×10^{-5}
1E 1841	8×10^{-5}	2.8×10^{-5}	5×10^{-5}	1.3×10^{-5}
1806-20	8×10^{-5}	2.8×10^{-5}	5×10^{-5}	1.3×10^{-5}
1900+14	10^{-5}	2.8×10^{-5}	0.7×10^{-5}	1.3×10^{-5}

References

[1] Beloborodov A.M., 2013, ApJ, 762, 13

[2] Kuiper, L., Hermsen, W., den Hartog, P.R., Collmar, W., 2006, ApJ, 645, 556

[3] Taverna, R., Muleri, F., Turolla, R., Soffitta, P., Fabiani, F., Nobili, L., 2014, MNRAS, 438, 1686

[4] Nobili, L., Turolla R., Zane S., 2008, MNRAS, 386, 1527

[5] Thompson C., Lyutikov M., Kulkarni S.R., 2002, ApJ, 574, 332

[6] Turolla R., Zane S., Watts, A.L., 2015, RPPh, 78, 116901

[7] Zane S., Turolla R., Nobili L., Rea, N., 2011, Adv. Space Sci., 47, 1298

Probing the plasma origin in pulsar magnetospheres

Alice Harding [1], *Isabelle A. Grenier* [2], *Pablo Saz Parkinson* [3,4]

[1] *NASA/Goddard Space Flight Center, Greenbelt, MD 20771, USA*
[2] *Laboratoire AIM, CEA-IRFU/CNRS/Université Paris Diderot, C.E.A. Saclay, France*
[3] *Santa Cruz Institute for Particle Physics, University of California, Santa Cruz, CA, USA*
[4] *Dept. of Physics & Laboratory for Space Research, University of Hong Kong, Hong Kong*

Science questions – Neutron stars develop rich magnetospheres, filled with plasma pulled out of the star by the large electric fields induced by the fast rotation of the stellar magnetic field. Large-scale currents flow out of the stellar polar caps and return back to them in a thin sheet flowing along the separatrix between the open and closed magnetic field lines (Figure 1). When the magnetic dipole is inclined relative to the rotation axis, the thin sheet undulates around the star. It is stable up to a distance of order ten times the size of the co-rotating part of the magnetosphere (i.e. the so-called light-cylinder radius) [1]. Young pulsars and, surprisingly, old recycled millisecond pulsars emit most of their radiated power in the γ-ray band and the Fermi Large Area Telescope (LAT) has transformed our views on the electrodynamical environment of neutron stars by detecting more than 200 γ-ray pulsars [2]. Their sharp γ-ray pulses and their spectral energy distributions (SEDs) and cut-offs at high energy have revealed that the pulses are produced in thin accelerators in the outer regions of the magnetosphere. These characteristics imply that most of the open magnetosphere is filled with a dense plasma that can efficiently screen the electric fields and tend to be force free.

The modelling of the MHD structure and of the global current circulation has rapidly progressed in the last few years, thanks to sophisticated MHD [3, 4] and PIC simulations [5, 6, 7], and to the interpretation of GeV observations. Yet our understanding of the structure of real, dissipative, pulsar magnetospheres and of their potential acceleration sites remains uncertain. The central question that challenges current theories is the origin of the large space densities of charges that support the magnetospheric currents. Specific regions can retain large electric fields along the magnetic field lines to accelerate primary particles to TeV energies. The latter initiate rich cascades of secondary electron-positron pairs, but where are the primary accelerators? Where do the cascades take place? How far do they develop? Can they supply the large charge flows that power the pulsar wind nebulae? What are the dominant radiation mechanisms for the primary and secondary particles? The comparison of the data recorded at MeV and GeV energies is essential to progress.

Importance of gamma-ray observations – Our current knowledge of primary and secondary pairs suggests that the pulsed GeV emission emanates from particles accelerated in the current sheet, more or less near or beyond the light cylinder. On the other hand, pulsed emission in the MeV band should relate to 'polar' pairs produced at various altitudes above the polar caps on field lines that do not connect to the current sheet. The spectrum and number density of the bulk of the

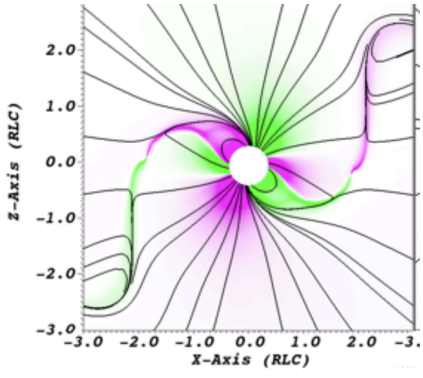

Figure 1: Current $J \cdot B$ in a near-force-free magnetosphere. The pink/green color indicates current along/opposite the local magnetic field direction. Current flows out of the polar regions and in from the current sheet. From [8].

cascading pairs can be inferred from the SED of the pulsed synchrotron radiation at MeV energies. The peak energy of the SED also yields the maximum energy of the pairs in the cascades. The MeV data is therefore crucial to constrain how the open magnetosphere manages to be near force free and to massively produce the outward currents.

The combination of MeV and GeV information for a population of pulsars with different spin-down powers and different magnetic field strengths near the polar caps and in the current sheet, and with different magnetic obliquities and viewing inclinations, is pivotal to constrain the relative geometries of the primary accelerators and secondary cascades and the beam widths of their respective radiations. In particular, the light curve shapes and the relative phases of the MeV and GeV pulses can inform us on the location of the emission sites and on whether the line-of-sight crosses the thin accelerating regions along the last open field lines.

The polarization data in γrays also hold key diagnostics on the radiation processes (synchrotron? curvature? inverse-Compton?) responsible for the pulsed emissions borne in the current sheet and in the open magnetosphere. The polarization fraction and polarization angle also bear information on the location of the emitting regions with respect to the light cylinder.

Expected results with e-ASTROGAM – The Fermi LAT data show that the pulsars with the largest spin-down powers or largest magnetic-field strengths tend to be very soft, with SEDs peaking in the 100 keV- 100 MeV band. This trend applies to young and millisecond pulsars indifferently. Eighteen such pulsars are known to exhibit hard X-ray emission that keeps brightening toward the MeV band, but steeply dims down or disappears above 100 MeV [9]. Figure 2 illustrates that the sensitivity of e-ASTROGAM allows us to easily detect the SED peaks of such energetic young and millisecond pulsars. We also expect the MeV beam produced by the pairs from cascades on a broad range of field lines to remain detectable over a wide range of viewing angles. *The MeV observations therefore provide the means to uncover a large fraction of the most energetic pulsars present in the Milky Way.* These objects are rare in the radio because the radio beams cover a much smaller solid angle in the sky than the γrays, hence the importance of an MeV survey for energetic pulsars.

A key diagnostic of the origin of the cascade pairs resides in the peak energy, E_{pk}, of the synchrotron component seen at MeV energies. It scales as $\gamma_{\pm}^2 B_{\pm}$, where $\gamma_{\pm}$ is the maximum Lorentz factor of the pairs and $B_{\pm}$ is the ambient magnetic field strength. Since the bulk of the cascade pairs should radiate at high altitudes, a characteristic value for the ambient field is the strength B_{LC} at the light cylinder. Primary particles accelerated above the polar caps can produce pairs that acquire pitch angles as they move out to the outer regions through resonant absorption of radio emission [11]. In this case, the maximum energy of the pairs relate to the magnetic field strength near the stellar surface, B_{NS}, so the SED peak energy should scale as $E_{pk} \propto B_{NS}\, B_{LC}$. Pair production can also occur in the outer-gap regions [10]. In this case, the SED peak energy depends more strongly on the outer field strength as $E_{pk} \propto B_{LC}^{7/2}$. *Measuring MeV peak energies for a significant sample of pulsars can therefore discriminate between different models and locate the origin of the pair cascades that populate the open magnetosphere. Moreover, because the MeV luminosity directly relates to the multiplicity of secondary pairs in the cascade, it directly informs us on the amount of plasma that eventually flows into the pulsar wind and termination shock.*

The comparison of the radio-loud and radio-quiet populations of MeV pulsars, as well as the possible correlation between the MeV and radio luminosities, can constrain the origin of the pitch angle of the synchrotron radiating plasma. For instance, these data can discriminate whether polar pairs or current-sheet pairs absorb radio photons as they move out, or whether current-sheet pairs acquire a pitch angle in the reconnecting magnetic field lines inside the current sheet, of if the pitch angles are produced and radiated away in the cascading process itself.

The sensitivity of e-ASTROGAM should allow the detection of large enough samples of MeV and GeV pulsars to perform population studies and explore trends in luminosity, SED shape, and SED peak energy. Based on the latest LAT 4FGL data, we expect to detect over 170 γ-ray pulsars, of which about 50 should be seen below 100 MeV; 20-40% of them should be millisecond pulsars, depending on energy. The population studies can also bring clues to the origin, possibly geometrical, of the puzzling dichotomy between pulsars seen only at GeV energies (emission from primaries) or

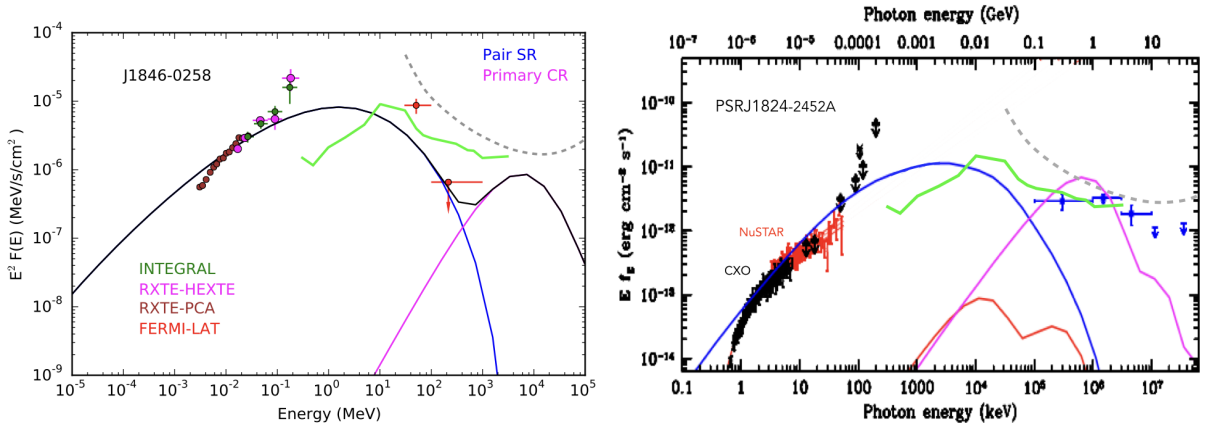

Figure 2: Spectral energy distributions of the young pulsar J1846-0258 (left) and of the millisecond pulsar J1824-2452A (right). The model curves show the expected curvature radiation (magenta) and synchrotron radiation (red) from the primary particles accelerated in the current sheet, and the synchrotron radiation (blue) from the secondary pairs produced in cascades and radiating in the open magnetosphere. Adapted from [13] and [11]. The sensitivities of e-ASTROGAM (solid green) and of Fermi LAT (dashed gray) are given for one year of effective exposure in the Galactic disc.

only at MeV energies (emission from secondary cascades).

Finally, we expect curvature radiation from accelerated particles [12] to be much more polarized than synchrotron emission from accelerated particles [6] and/or secondaries. An abrupt rise in polarization fraction in the whole pulsed emission, in coincidence with the rise of the GeV emission component, would establish the curvature-radiation origin of the latter. The polarization data can also constrain the altitude of the GeV emission site with respect to the light cylinder and the altitude of the emission zone for polar pairs in the open magnetosphere. Observations of rotation-powered pulsars with e-ASTROGAM thus holds the promise of constraining the origin(s) and spectrum of the pair plasma that shapes the pulsar magnetosphere, as well as the GeV emission mechanism.

References

[1] Kalapotharakos, C., Kazanas, D., Harding, A., & Contopoulos, I. 2012, ApJ, 749, 2

[2] https://confluence.slac.stanford.edu/display/GLAMCOG/Public+List+of+LAT-Detected+Gamma-Ray+Pulsars

[3] Kalapotharakos, C., Contopoulos, I., & Kazanas, D. 2012, MNRAS, 420, 2793

[4] Li, J., Spitkovsky, A., & Tchekhovskoy, A. 2012, ApJ, 746, 60

[5] Philippov, A., & Spitkovsky, A. 2014, ApJL, 785, L33

[6] Cerutti, B., Philippov, A., & Spitkovsky, A. 2016, MNRAS, 457, 2401

[7] Kalapotharakos, C., Brambilla, G, Timokhin, A., Harding, A. K., Kazanas, D., & . 2017, ApJ, submitted, ArXiv:1710.03170

[8] Brambilla, G., Kalapotharakos, C., Timokhin, A., Harding, A. K., & Kazanas, D. 2017, submitted, ArXiv:1710.03536

[9] L. Kuiper & W. Hermsen, Mon Not R Astron Soc 449 (2015) 3827

[10] Takata, J., Chang, H. K. & Shibata, S. 2008, MNRAS, 386, 748.

[11] Harding, A. & Kalapotharakos, C., 2015, ApJ, 811, 63.

[12] Harding, A. & Kalapotharakos, C., 2017, ApJ, submitted.

[13] Gotthelf, E. V., & Bogdanov, S. 2017, ApJ, 845, 159

Probing the maximum particle energies in pulsar wind nebulae

Alice Harding [1], *Isabelle A. Grenier* [2], *Pablo Saz Parkinson* [3,4]

[1] *NASA/Goddard Space Flight Center, Greenbelt, MD 20771, USA*
[2] *Laboratoire AIM, CEA-IRFU/CNRS/Université Paris Diderot, C.E.A. Saclay, France*
[3] *Santa Cruz Institute for Particle Physics, University of California, Santa Cruz, CA, USA*
[4] *Dept. of Physics & Laboratory for Space Research, University of Hong Kong, Hong Kong*

Science questions – Pulsar wind nebulae (PWNe) are the manifestation of the particle production by pulsars. The electron-positron pairs that are produced in cascades in the magnetosphere flow outward and form the pulsar wind that dissipates the spin-down luminosity of the pulsar. These pairs are accelerated near or in the termination shock, the reverse shock that reacts to the contact outer discontinuity of the nebula with the interstellar medium through pressure balance [1]. Although PWNe are the most numerous Galactic sources detected at TeV energies by Air Cherenkov telescopes, *Fermi* has detected relatively few at GeV energies. PWNe have a multicomponent spectrum consisting of a synchrotron (SR) component in soft gamma-rays and an inverse Compton (IC) component at higher energies. The Crab PWN is the brightest and most powerful, its SR component extending to 100 MeV, with the IC component extending to at least 50 TeV. The Crab nebula differs from the others because the IC emission is synchrotron-self Compton. The IC components of most other known PWNe are produced by up-scattering of the ambient soft photon fields. The *Fermi* sensitivity falls in the valley between the SR and IC components for most other PWNe whose SR spectra extend to lower energies. The maximum SR photon energy of the Crab PWN, together with the IC spectrum, tells us that the pairs are continuously accelerated to a PeV [2]. A major science question that will be answered by e-ASTROGAM is: What is the maximum energy of the particles accelerated in PWNe and how does it depend on properties of the pulsar?

Fermi and AGILE discovered surprising flares from the Crab PWN [2, 4] with SR photon energies reaching up to 500 MeV (see Figure 1). They require transient particle acceleration to several PeV and violate the 140 MeV diffusive shock acceleration limit [5]. The *Fermi* GBM and *Swift* detected much slower flux variations on year timescales that may be caused by the GeV flares [6]. e-ASTROGAM, with its wide field of view, will be able to detect possible flares from PWNe with SR cutoffs in the MeV band. It will also be able to detect flux variations in the Crab to determine whether the GeV flares produce variability at energies below 100 MeV, with the timescales giving information on the flare location and geometry. A key question is what is the very rapid acceleration mechanism that produces the high-energy flare particles?

Importance of gamma-ray observations – Since the transition between SR and IC components in PWNe spectra fall in the hard X-ray to GeV γ-ray band, γ-ray observations can catch both components. The maximum steady-state (non-flaring) energy to which particles can be accelerated in a PWN is equal to the voltage across the open field lines, $V_{\rm open} = 6 \times 10^{12}\, B_{12} P^{-2}$ eV, where B_{12} is the pulsar surface magnetic field strength and P is the period. For the Crab PWN, $V_{\rm open}$ reaches the maximum SR photon energy where SR losses balance acceleration gains (assuming $E < B$. For most other middle-aged PWNe, $V_{\rm open}$ is much lower and the expected maximum of the SR spectrum, $\epsilon_{SR} \propto V_{\rm open}^2 B_s \sim 0.14\,{\rm MeV}\, L_{36}^{6/5}\, [\sigma/(1+\sigma)]^{1/2}\, \tau_{kyr}^{-3/10}$, where B_s is the field strength at the termination shock, L_{36} is the pulsar spin-down luminosity in units of $10^{36}\,{\rm erg\,s^{-1}}$, σ is the wind magnetization and τ_{kyr} is the pulsar age in kyr. Therefore, these PWNe should have SR cutoffs visible in the energy range of e-ASTROGAM.

The detected Crab flares occur near the high-energy cutoff of the SR spectrum, since the maximum-energy particles producing this emission have the fastest SR timescales. Similarly, flares on longer timescales of months may be expected for other PWNe with SR spectral cutoffs in the

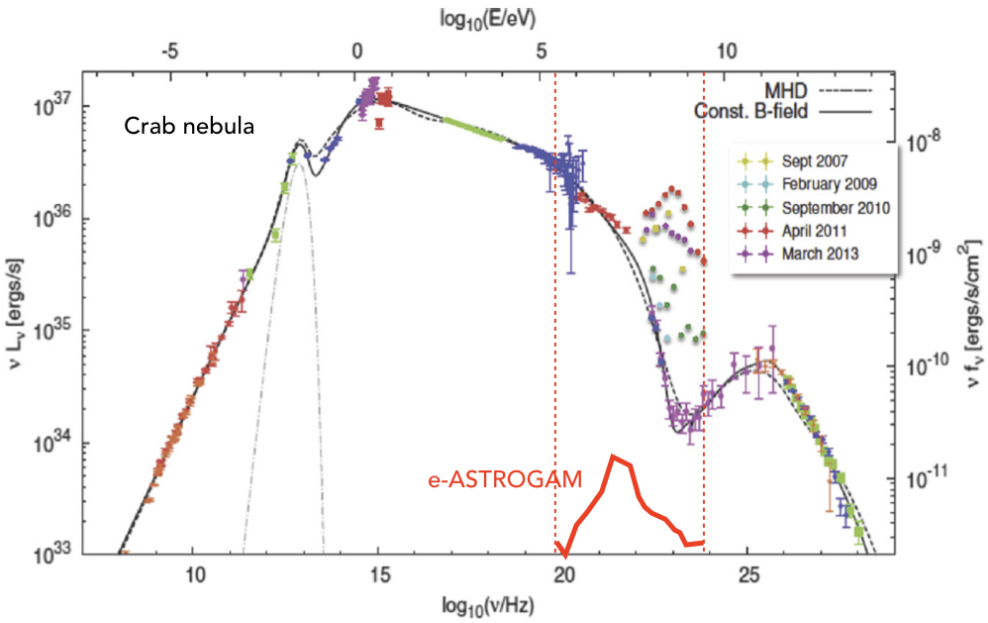

Figure 1: Spectral energy distribution of the Crab nebula from the radio to very high energy rays, also showing the flares. The sensitivity of e-ASTROGAM (red curve) is given for one year of effective exposure in the Galactic disc. Adapted from [4, 7]

MeV band. If the same processes, such as magnetic reconnection [8], that are proposed to cause flaring in the Crab PWN are occurring in other PWNe, then we might expect to see flares near the high end of their SR spectra that is not accessible with current telescopes. Whether the Crab GeV flares are connected with the slower flux variations in the hard X-ray band is currently not clear. An e-ASTROGAM detection of flux variations of the Crab, which would be on month timescales, would confirm whether the variations are due to radiation of flare particles as they lose energy to SR.

Expected results with e-ASTROGAM – Figure 2 shows examples of two PWNe with measured X-ray and GeV spectra, where the SR cutoff should fall around 1-10 MeV. It is expected that e-ASTROGAM will detect the SR cutoff in these and other PWNe. Together with a detected IC component from either e-ASTROGAM or *Fermi*, the maximum particle energy can be deduced since the IC spectrum constrains B_s, as well as the magnetization of the wind, σ. Since most PWNe will have SR spectra with cutoffs in the 100 keV - 10 MeV band, e-ASTROGAM will greatly increase the number of PWN detections at γ-ray energies over the number that *Fermi* detected, and will be able constrain the maximum particle energy in a large number of PWN.

Synergy between e-ASTROGAM, Athena and CTA will allow significant progress in understanding how the pulsar spin-down power is transferred to the wind and also how the radiating electron-positron pairs diffuse into the ISM, important in explaining the observed cosmic-ray positron excess [9]. Athena and e-ASTROGAM give information on the maximum particle energy and rapid SR losses in or near the accelerator site. CTA can image the spatial variations of the spectral losses of the pairs in the wind at tens of pc from the pulsar, thereby mapping the MHD structure of a PWNe.

Finally, detection of flares in older PWNe by e-ASTROGAM would provide valuable information of relativistic reconnection physics, a field still in its infancy [10].

References

[1] Rees, M. J. & Gunn, J. E. 1974, MNRAS, 167, 1.
[2] De Jager, O. C. & Harding, A. K. 1992, ApJ, 296, 161.
[3] Abdo, A .A. et al., 2011, Science, 331, 739.

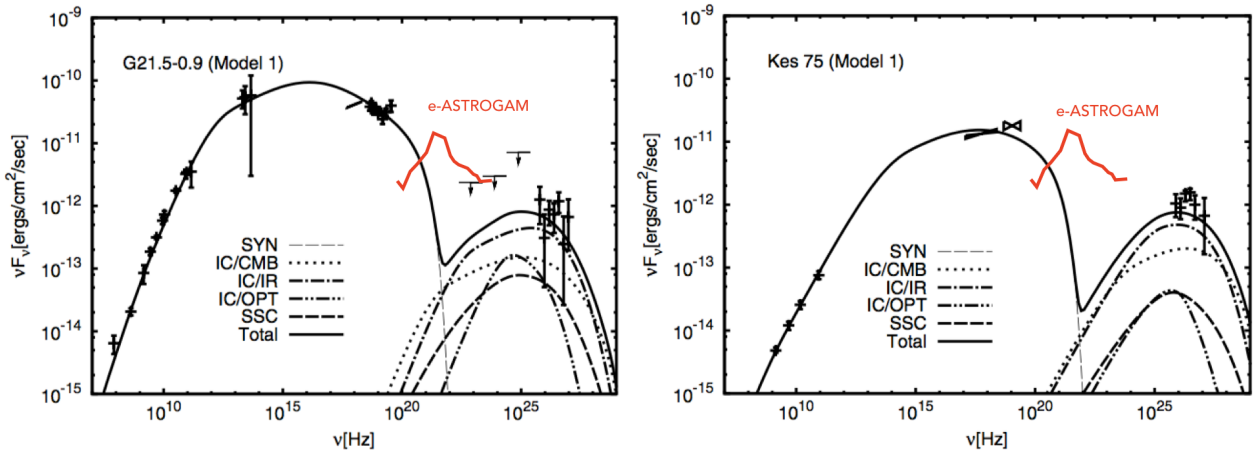

Figure 2: Spectra and models for PWN G21.5-0.9 and Kes75 from [11]. The sensitivity of e-ASTROGAM (red curve) is given for one year of effective exposure in the Galactic disc.

[4] Beuhler, R. & Blandford, R. 2014, Rep. Prog. Phys., 77, 066901
[5] De Jager, O. C. et al. 1996, ApJ, 457, 253.
[6] Wilson-Hodge, C. et al. 2016, American Astronomical Society, HEAD meeting, 15, id.118.09
[7] Meyer, M., Horns, D., Zechlin, H.S. 2010, A&A 523, 2.
[8] Cerutti, B., Werner, G. R., Uzensky, D. A. & Begelman, M. C. 2014, Phys. Plasmas, 21, 056501
[9] Accardo, L. et al. 2014, Phys. Rev. Letters, 113, 121101.
[10] Sironi, L.; Giannios, D.; Petropoulou, M. 2016, MNRAS, 462, 48.
[11] Tanaka, S. J. & Takahara, F. 2011, ApJ, 741, 40.

Gamma-ray binaries

Josep M. Paredes[1], *Valenti Bosch-Ramon*[1] *Domitilla de Martino*[2], *Alessandro Papitto*[3], *Roland Walter*[4], *Andrzej A. Zdziarski*[5]

[1]*Departament de Física Quàntica i Astrofísica, Institut de Ciències del Cosmos (ICCUB), Universitat de Barcelona, IEEC-UB, Martí i Franquès 1, E08028 Barcelona, Spain*
[2]*INAF, Osservatorio Astronomico di Capodimonte, Salita Moiariello 16, I-80131 Naples,Italy*
[3]*INAF, Osservatorio Astronomico di Roma, via di Frascati 33, I-00044, Monte Porzio Catone (Roma), Italy*
[4]*ISDC Data Centre for Astrophysics, Chemin d'Ecogia 16, CH-1290 Versoix, Switzerland*
[5]*Nicolaus Copernicus Astronomical Center, Polish Academy of Sciences, Bartycka 18, PL-00-716 Warsaw, Poland*

Science questions – The nature of γ-ray emission from X-ray binaries presents a number of major puzzles. Generally, that emission can be either powered by accretion onto a compact object or be due to collisions between winds from the binary components [7, 8]. Among those sources, the most prominent γ-ray emission is seen from the so-called gamma-ray binaries, consisting of a massive star and a compact object, and where γ-rays dominate the spectral energy distribution (SED, defined as EF_E), peaking above 1 MeV, see Fig. 1. There are six γ-ray binaries detected in high (HE, 0.1-100 GeV) or very high energy (VHE, >100 GeV) γ-rays. In one case, PSR B1259–63, radio pulsations are detected [11], showing that the compact object is a rotation-powered pulsar, and thus the γ-rays, emitted close to periastron, are likely to be due to interaction between the pulsar and stellar winds [6], where particles are accelerated at the shock between the winds. No radio pulsations have been found in other cases; although this can be explained by free-free absorption in the stellar wind, no definite proofs of the nature of the other sources exist [6]. *Fermi*-LAT detected PSR J2032+4127, a new γ-ray binary that shares many similar characteristics with the previously unique TeV binary PSR B1259-63. This new source is a long period ($\sim$ 40 years) Be binary system hosting a pulsar [12] located in the vicinity of the first (and yet) unidentified TeV source discovered by HEGRA, TeV J2032+4130. At present, it is not known whether PSR J2032+4127 can produce γ-rays in the star-pulsar wind colliding region. Observations with e-ASTROGAM will be crucial to fully characterize the gamma-ray spectrum of the source, and identify a potential non-magnetospheric component in the MeV-GeV energy band. Perhaps, the best studied gamma-ray binary is LS 5039 [13, 1], which presents, in addition to HE and VHE γ-rays, very strong MeV radiation that is modulated along the orbit. The soft γ-rays seem to naturally follow a synchrotron component coming from $\lesssim 1$ keV and peaking around 30 MeV [3]. Generally, satisfactory detailed models explaining both the spectra and orbital modulation of these objects are still missing, largely due to the lack of observations in the MeV range.

Importance of gamma-ray observations – Although *Fermi*-LAT has opened a new discovery space for γ-ray emission from binaries, since their SED often peak below $\sim$ 100 MeV [3, 4], lack of enough coverage and sensitivity at these energies has so far hampered to assess the true nature of the γ-ray emission from these sources. Also, only upper limits were obtained in that range by *AGILE*. Thus, sensitive observations below $\sim$ 100 MeV are likely to detect many more of such objects, as the number of gamma-ray binaries in the Galaxy is expected to be between $\sim$50 and 200 [9].

Gamma-ray binaries have most likely two dominant radiation mechanisms: synchrotron emission, from radio to X-rays/soft γ-rays, and inverse Compton (IC) scattering of stellar photons, dominant in the HE and the VHE range [2]. The MeV-GeV spectral range is right between the synchrotron and the IC dominance energy ranges [14], and is very important to properly understand the physics originating the synchrotron and the IC emission from these objects. Then, γ-ray

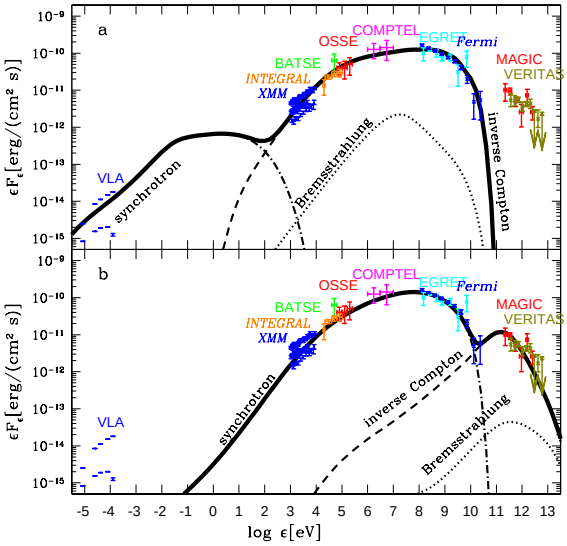

Figure 1: The broad-band spectrum of the gamma-ray binary LS I +61 303 modelled by two variants of the model of the pulsar-wind/stellar-wind interaction [15]. (a) The model in which the soft and HE γ-rays are dominated by Compton scattering. (b) The model in which the soft and HE γ-rays are dominated by the synchrotron process.

observations below $\sim$ 100 MeV will probe the intersection region, allowing us to distinguish between the two components.

If synchrotron emission is dominant, exploring the MeV-GeV range can allow probing extreme particle acceleration. Interestingly, the $\sim$100-MeV synchrotron limit can be exceeded in some cases, as observed in the Crab Nebula. In a gamma-ray binary, the observation of a synchrotron component exceeding that limit could unveil important physical information, such as highly relativistic motions, or contamination by a different radiation component.

On the other hand, if IC is dominant, the MeV-GeV range can provide important information related to how non-thermal particles propagate away from the stellar companion, as IC losses are slow for electrons producing MeV photons via IC with stellar photons. The IC process can also probe the geometry of the sources by observing its orbital modulation, related to the varying viewing angle with respect to the binary major axis, which implies changes in the IC emission.

Regardless of the dominant emission process, the MeV-GeV range also permits carefully looking for the effects of γ-ray absorption and reprocessing on the spectrum, and complements the study of different wind physical conditions in eccentric systems such as the O/Be binaries.

Finally, if gamma-ray binaries host a powerful pulsar that powers the non-thermal emission, the MeV photons can interact with the pulsar wind if the latter reaches Lorentz factors of about $10^5 - 10^6$. This would trigger electromagnetic cascades in the pulsar wind that should give rise to strong γ-ray and lower energy radiation, and also strongly modify the wind nature [5].

Expected results with e-ASTROGAM – COMPTEL data already indicated that gamma-ray binaries (in particular LS 5039 [3] but perhaps most of them [4]), are powerful MeV emitters. *e-ASTROGAM*, with its sensitivity in soft γ-rays two orders of magnitude better than that of COMPTEL, will discover many new cases of γ-ray emission of binaries. Its sensitivity will allow the characterization of the orbital lightcurve and spectral evolution of γ-ray binaries, clearly differentiating the synchrotron and the IC components, probing particle acceleration and γ-ray reprocessing, and potentially revealing pulsar wind physics that can only be probed in this kind of objects. After the expected launch of *e-ASTROGAM*, major new facilities from radio to VHE γ-rays, SKA, *Athena* and CTA, will also be operational. This will provide an unprecedented opportunity to study particle acceleration, outflows, and wind launching mechanisms in different types of binaries.

References

[1] Aharonian, F., Akhperjanian, A. G., Aye, K.-M., & et al. 2005, Science, 309, 746

[2] Bosch-Ramon, V., Khangulyan, D., 2009, IJMPD, 18, 347

[3] Collmar, W., Zhang, S. 2014, A&A, 565, 38

[4] Collmar, W. 2017, at IVth workshop on Variable Galactic Gamma-ray Sources, Tokyo, Japan
[5] Derishev, E. V., Aharonian, F. A. 2012, AIPC ,1505, 402
[6] Dubus, G. 2006, A&A, 456, 801
[7] Dubus, G. 2013, A&A Rev, 21, 64
[8] Dubus, G. 2015, CRPhy, 16, 661
[9] Dubus, G., Guillard, N., Petrucci, P.-O., & Martin, P. 2017, arXiv:1707.05744
[10] Guilbert, P. W., Fabian, A. C., Rees, M. J. 1983, MNRAS, 205, 593
[11] Johnston, S., et al. 1992, ApJ, 387, L37
[12] Lyne, A. G. et al. 2015, MNRAS, 451, 581
[13] Paredes, J. M., Martí, J., Rib; M., & Massi, M. 2000, Science, 288, 2340
[14] Paredes, J. M., Bosch-Ramon, V., Romero, G. E. 2006, A&A, 451, 259
[15] Zdziarski, A. A., Neronov, A., Chernyakova, M. 2010, MNRAS, 403, 1873

Gamma-ray emission from accretion-powered X-ray binaries

Andrzej A. Zdziarski[1], *Roland Walter*[2], *Valenti Bosch-Ramon*[3], *Pierre Jean*[4], *Domitilla de Martino*[5], *Alessandro Papitto*[6], *Josep M. Paredes*[3], *Vincent Tatischeff*[7],

[1]*Nicolaus Copernicus Astronomical Center, Polish Academy of Sciences, Bartycka 18, PL-00-716 Warsaw, Poland*
[2]*SDC Data Centre for Astrophysics, Chemin d'Ecogia 16, CH-1290 Versoix, Switzerland*
[3]*Dept. de Física Quàntica i Astrofísica, ICCUB, Universitat de Barcelona, IEEC-UB, E08028 Barcelona, Spain*
[4]*Univ. Paul Sabatier, CNRS, IRAP, F-31028, Toulouse Cedex, France*
[5]*INAF - Osservatorio Astronomico di Capodimonte, Salita Moiariello 16, I-80131 Napoli, Italy*
[6]*INAF - Osservatorio Astronomico di Roma, via di Frascati 33, I-00044, Monte Porzio Catone (Roma), Italy*
[7]*CSNSM, IN2P3-CNRS/Univ. Paris-Sud and Paris-Saclay, F-91405 Orsay Campus, France*

Science questions – We consider γ-ray emission from accretion-powered X-ray binaries, excluding the so-called gamma-ray binaries (see the contribution by Paredes et al.), where γ-rays peak above 1 MeV and dominate the spectral energy distribution (SED, defined as EF_E). γ-rays from accretion-powered binaries are usually observed from microquasars, i.e., systems featuring jets. Unambiguous detections of high-energy (HE) γ-rays have only been from high-mass X-ray binaries Cyg X-3 [8] and Cyg X-1 [22, 26]. In Cyg X-3, where the nature of the compact object still remains unknown, γ-rays are observed in its soft spectral state, and are strongly orbitally modulated. The γ-ray modulation and spectrum are interpreted by Compton scattering of the blackbody emission of the donor in the jet [7, 23]. However, the models cannot be constrained due to the lack of sensitive observations in the crucial MeV range. In Cyg X-1, HE γ-rays are observed instead only in the hard spectral state (Fig. 1), where a compact radio jet is also detected. On the other hand, excess emission below 100 MeV is observed in both hard and soft spectral states (Fig. 1), appearing to connect to the high-energy tails observed in soft γ-rays [26]. Another puzzle of Cyg X-1 is the claim of very strong polarization around 1 MeV [13, 17], at face value pointing to synchrotron emission from the jet. This interpretation, however, presents a number of problems. We note here that those detections were obtained by the instruments not designed to measure polarization.

Interestingly, no HE γ-rays have been detected from low-mass X-ray binaries (LMXBs) containing black-holes, except for a hint of transient emission from V404 Cyg [14]. This lack of emission remains not understood. V404 Cyg is also the only object in which an $e^{\pm}$ annihilation feature has been detected at a relatively high significance [18]. An important science question is how common such emission is and how it can be modelled.

A new type of γ-ray binaries are the so-called transitional ms pulsars, objects showing both rotation-powered and accretion-powered states [2, 3, 6, 15] (see the contribution by Johnson et al.). In two sources, transitions between the pulsar and weak accretion states were associated with a power-law shaped X-ray spectrum with no cut-off up to at least $\sim$100 keV and an increase by up to a factor of a few of the γ-ray flux in the latter [21]. The increase of the γ-ray flux has been explained by the interaction of the accretion disc with the pulsar wind [20] or a propellering magnetosphere [16]. However, the enhanced γ-ray emission was also associated with the appearence of a strong variable radio flux with a spectral index $\sim$0 [11, 5]. This behaviour is typical of microquasars, suggesting the possibility that both γ-ray and radio emissions originate in a jet. This would be the first case of steady γ-ray emission from LMXBs during a disc state.

Finally, the conditions in inner parts of accretion discs can allow neutrons to be produced by spallation of He, at the rate depending on the disc physical state. The neutrons produce 2.2-MeV photons when captured by protons, which can result in a broad line in black-hole accretion discs in the case of fast protons, at the estimated flux of $\sim 10^{-6}$ s^{-1} cm^{-2} at 1 kpc [1]. If neutron

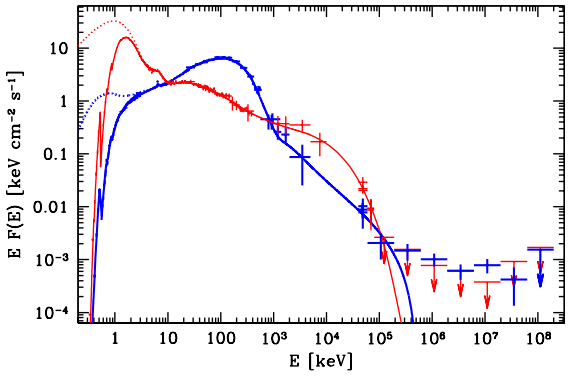

Figure 1: Broad-band X-ray/γ-ray spectra for Cyg X-1 in the hard (blue heavy symbols) and soft (red thin symbols) states compared to hybrid-Comptonization accretion-flow models [26]. The observed emission above $\sim$100 MeV in the hard state is dominated by the jet. The dotted curves at soft X-rays show the unabsorbed models.

capture takes place in the upper atmosphere of an accreting neutron star, the line will be narrow and gravitationaly redshifted, and its redshift would yield the neutron star mass to radius ratio, and thus a constraint on the equation of state [4]. Neutrons can also escape the accretion disc and hit the companion star, where they slow down and get captured by ambient protons, resulting in a narrow line [12]. The flux in this case depends on many parameters, and a rough estimate is also $\sim 10^{-6}$ s^{-1} cm^{-2} for nearby (1–2 kpc) X-ray binaries [9].

Importance of gamma-ray observations – Although *Fermi*-LAT has opened a new discovery space for γ-ray emission from binaries, the lack of adequate coverage and sensitivity below 100 MeV has so far hampered to assess the true nature of their γ-ray emission. Also, sensitive observations in that range are likely to detect many more of such objects.

Detailed modelling of the MeV-range emission will provide the first unambiguous tests of emission mechanisms and help disentangling disc-jet coupling in accretion-powered binaries. The main physical processes contributing to γ-rays in binaries are synchrotron and Compton. The former is, in usual cases, limited to the range of $\lesssim$100 MeV [10]. Then, γ-ray observations below 100 MeV will probe the intersection region, allowing us to distinguish between the two components. However, the $\sim$100-MeV limit can be exceeded in some cases, as observed in the Crab Nebula, and an observation of a synchrotron component exceeding that in a binary would be of paramount importance. We can also probe the geometry of the sources by observations of their orbital modulation.

If the MeV tail of Cyg X-1 is due to polarized jet synchrotron emission, an intersection of the synchrotron and Compton components is expected below 100 MeV [25]. If, on the other hand, the tail is from Compton scattering by nonthermal electrons in the accretion flow, the intersection will be of the accretion and jet emissions. In the case of Cyg X-3, we observe strong orbital modulation of X-rays up to 100 keV with the minimum at the superior conjunction [24], and strong orbital modulation at >100 MeV peaking at it [8]. Observations below 100 MeV will allow us to unambiguously distinguish between the jet and accretion components, and e.g., test popular models in which the tail beyond the accretion-disc blackbody peak in the soft states of X-ray binaries is due to jet synchrotron emission. Furthermore, observations of orbital modulation of γ-rays below 100 MeV due to inverse Compton scattering of stellar blackbody photons will allow us a precise determination of both the location of the γ-ray source along the jet and the jet orientation.

Then, detections of the 2.2 MeV line from X-ray binaries would be a new major discovery, allowing to set strong constraints on the physics of their accretion flows.

Expected results with e-ASTROGAM – e-ASTROGAM, with its sensitivity in the soft (<100 MeV) γ-ray range two orders of magnitude better than that of COMPTEL (and not covered by *Fermi*-LAT), will discover many new cases of accretion-powered X-ray binaries. Its sensitivity will allow the characterization of their orbital light curves and spectral evolution for the first time down to the soft γ-rays, clearly differentiating the synchrotron/IC and accretion/jet components, probing particle acceleration and γ-ray reprocessing, and potentially revealing pulsar wind physics.

Fig. 2(left) shows a simulation of a 10^5-s observation of Cyg X-1 in the hard state. The signal-to-noise ratio of the detection at $>$ 500 keV is high, 76. We have also found that e-ASTROGAM will be able to detect it in 10^3 s up to several MeV with the significance similar to that obtained by

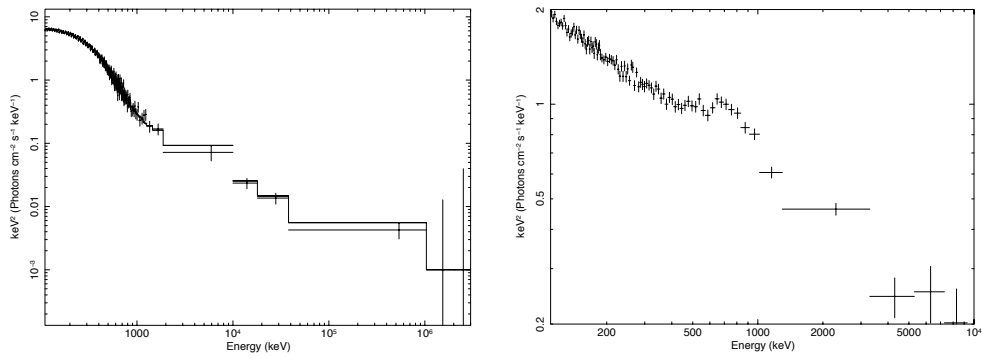

Figure 2: Left: Simulated 10^5-s e-ASTROGAM average hard-state spectrum of Cyg X-1 assuming contributions from thermal Comptonization in the accretion flow at low energies and from synchrotron emission in a jet at high energies, as in Fig. 1. Right: Simulated 10^5-s spectrum of an X-ray binary with a power law of $\Gamma = 2.5$ and a broad line from annihilation of $e^{\pm}$ [19] at the temperature of $kT \simeq 100$ keV.

INTEGRAL in 2×10^6 s [17]. This will allow us to study for the first time correlations between the thermal Comptonization and the high-energy tail components. Given its capability to detect γ-ray polarization, e-ASTROGAM will test the intriguing detection of soft γ-ray polarization in Cyg X-1. In a 10^6 s exposure, the minimal polarization measurable above 500 keV at 99% confidence level will be as low as 5%. We will also be able to search for it in other sources. Fig. 2(right) demonstrates the sensitivity of e-ASTROGAM to detect $e^{\pm}$ annihilation lines. At the line equivalent width of 106 keV and the flux an order of magnitude lower than that found in V404 Cyg [18], the signal-to-noise ratio of the line detection is 32. Finally, the time required for a detection of a broad 2.2 MeV line at the estimated flux is $\sim$4 Ms.

References

[1] Aharonian F. A., Sunyaev R.A., 1984, MNRAS, 210, 257
[2] Archibald, A. M. et al. 2009, Science, 324, 1411
[3] Bassa, C. G., et al. 2014, MNRAS, 441, 1825
[4] Bildsten L., Salpeter E. E., Wasserman I., 1993, ApJ, 408, 615
[5] Deller, A. T. et al. 2015, ApJ, 809, 13
[6] de Martino, D., et al. 2010, A&A, 515, A25
[7] Dubus, G., Cerutti, B., Henri, G., 2010, MNRAS, 404, L55
[8] Fermi LAT Collaboration, 2009, Science, 326, 1512
[9] Guessoum N., Jean P., 2002, A&A, 396, 157
[10] Guilbert, P. W., Fabian, A. C., Rees, M. J. 1983, MNRAS, 205, 593
[11] Hill, A. B., et al. 2011, MNRAS, 415, 235
[12] Jean P., Guessoum N., 2001, A&A, 378, 509
[13] Jourdain, E., Roques, J. P., Chauvin, M., Clark, D. J., 2012, ApJ, 761, 27
[14] Loh, A., et al. 2016, MNRAS, 462, L111
[15] Papitto, A., et al. 2013, Nature, 501, 517
[16] Papitto, A., Torres, D. F. 2015, ApJ, 807, 33
[17] Rodriguez J., et al., 2015, ApJ, 807, 17
[18] Siegert T., et al., 2016, Nature, 531, 341
[19] Svensson R., Larsson S., Poutanen J., 1996, A&AS, 120C, 587
[20] Takata, J., et al. 2014, ApJ, 785, 131
[21] Torres, D. F., et al. 2017, ApJ, 836, 68
[22] Zanin R., et al. 2016, A&A, 596, A55
[23] Zdziarski A. A., et al. 2012, MNRAS, 421, 2956
[24] Zdziarski, A. A., et al. 2012, MNRAS, 426, 1031
[25] Zdziarski, A. A., Pjanka, P., Sikora, M., Stawarz, L. 2014, MNRAS, 442, 3243
[26] Zdziarski A. A., Malyshev D., Chernyakova M., Pooley G. G. 2017, MNRAS, 471, 3657

Detection of Very Short Gamma-Ray Bursts in exotic stellar transitions with e-ASTROGAM

M. Ángeles Pérez-García[1], *Conrado Albertus*[1], *Marina Cermeño*[1], *José M. Álvarez*[2], *Luis Roso*[3]

[1] *Department of Fundamental Physics and IUFFyM University of Salamanca, Plaza de la Merced s/n 37008 Spain*
[2] *Spanish Center for Pulsed Lasers (CLPU), M5 Bldg. Science Park, Villamayor, Salamanca (Spain)*
[3] *University of Salamanca (USAL), Plaza de la Merced s/n, 37008, Salamanca (Spain)*

Science questions – Gamma-ray Bursts (GRBs) are highly energetic fenomena than remain without a definite explanation [1]. Its origin is believed to be triggered by cataclysmic events linked to large changes in the internal structure of stellar compact objecs of mass $M \sim 1.5 M_\odot$ and radius $R \sim 12$ km releasing gravitational energies $\Delta E \approx GM^2/R \approx 10^{53} - 10^{55}$ erg.

One of the possible situations where GRBs may be emitted involve neutron stars (NSs) transitioning to more compact stars. In particular, the possible formation of stars where the quark component has been deconfined out of the the nucleons has been studied in the literature [2]. Such an scenario is often referred to as quark stars (QS). In a NS to QS transition part of the outer stellar crust in the original star can be expelled to relativistic speeds leading to a transient episode of high-energy emission. In those cases the expected duration of the gamma-ray signal is much smaller than that typically predicted for short GRBs at about ~ 2 s. The mechanism behind the hipothesized transition is not yet clear but has been considered to be due either to a rise in the central density for slowly rotating old NS or due to the accretion of an exotic dark component [3]. This latter possibility [4, 5] links two types of matter (standard and dark) present in our Universe as experimentally determined from complementary indications [6] and constitute itself another key aspect of the Physics motivation driving the e-ASTROGAM mission.

One of the key quantities in this short GRB scenario is the isotropic equivalent energy range $E_{\gamma,iso} \simeq 10^{48} - 10^{52}$ erg [7, 8] and the gamma-ray signal peak energy expected arising in the modellization of the (possibly beamed) transient event. This type of short GRBs can occur in any type of galaxy (and location inside) and typically with a time delay above $\sim 10^3 - 10^5$ yr since the end of the stellar life. As for the local rate it is expected that only a tiny fraction of about $\sim 10^{-3}$ of the short GRBs, $R_{SGRB} \sim (400 - 1500)\,\mathrm{Gpc^{-3}yr^{-1}}$, is expected to be due to this deconfinement transition. The possible detection of the associated gamma-ray signal of these stellar transitions would be of major importance in our understanding not only of the stellar evolution but also it would affect to the Physics of the interaction of ordinary and dark matter underlaying current particle physics models.

Importance of gamma-ray observations – The expected properties of the short GRBs produced in this scenario are important in the possible identification of the specific central engine that could help discriminate the mechanism underlaying the event. The relativistic emission is due to the outer stellar crust ejection with mass $M_{\rm ej} = M_{\rm ej,-5} \times 10^{-5}\, M_\odot$ and a width $\Delta = c\Delta t$, where c is the speed of light and $\Delta t = \Delta t_{-6} \times 10^{-6}$. The initial energy is given by $E_{\rm ej} = f_{\rm ej,-3} \times 3.5 \times 10^{50}\,\mathrm{erg}$. If this energy is not deposited in a homogeneous way in the expelled crust the final Lorentz factor Γ in the ejecta may not be uniform. For a thermal acceleration the saturation to the final Lorentz factor will occur at radius $R_{\rm sat} \simeq \Gamma \times 10^7\, M_{\rm ej,-5}^{-1} f_{\rm ej,-3}\,\mathrm{cm}$. The ejecta will become transparent to its own radiation at the photospheric radius $R_{\rm ph} \simeq \sqrt{\frac{\kappa M_{\rm ej}}{4\pi}} \simeq 2 \times 10^{13}\, M_{\rm ej,-5}^{1/2}\,\mathrm{cm}$. Both radii are estimated based on the fireball theory for GRBs [9]. The internal shock dissipation will occur at a typical radius $R_{sat} \lesssim R_{is} \ll R_{ph}$. Let us mention that an initial free expansion would be followed by a deceleration process in the external medium (two episodes of emission)

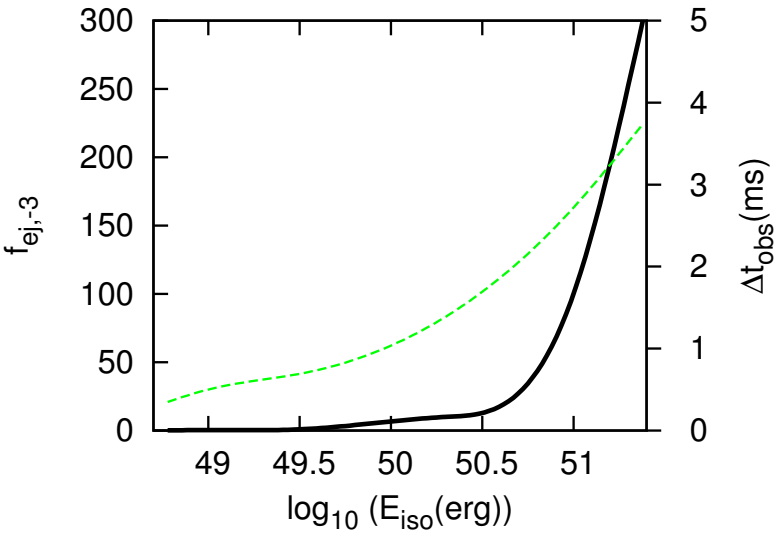

Figure 1: Expected e-ASTROGAM visibility window for vSGRBs. Lower energy bound for peak energy at $E_p \sim 300$ keV shows the upper region limit (black solid line) where detection with e-ASTROGAM is possible as a function of the logarithm of the isotropic equivalent energy released in the GRB. On the left axis the fraction of the energy ejected in the outer crust is shown while on the right axis (dashed line) the duration of the expected signal is depicted (in ms).

at a radius $R_{dec} \gg R_{ph}$. The spectrum and duration of the signal depend on the details of the complex crust ejection. However, the duration of the prompt spike, $\Delta t_{\rm obs}$, should be fixed by the intrinsic curvature of the emitting region and its lateral expansion. This can be written $\Delta t_{\rm obs} \simeq \min\left(\frac{R_{\rm ph}}{2\Gamma^2 c}; \frac{\theta_{\rm j}^2 R_{\rm ph}}{2c}\right) \simeq \min\left(M_{\rm ej,-5}^2 f_{\rm ej,-3}^{-2}; \left(\frac{\theta_{\rm j}}{3^\circ}\right)^2\right) \times 0.8\, M_{\rm ej,-5}^{1/2}\,{\rm s}$. Except if the ejection is highly beamed with a beaming angle $\theta_j \sim 2/f_b^{1/2}$, being f_b the beaming factor the minimum is usually given by the first term. Emission in the gamma-ray band require kinetic energies for the outer crust with injected fraction $f_{\rm ej,-3} \sim (1 - 10^2)$

Expected results with e-ASTROGAM – e-ASTROGAM will incorporate technology [10, 11, 12] capable of detecting signals in the energy range 0.3 MeV−3 GeV as it appears in table 1 of [13]. As an example, the effective area of e-ASTROGAM at low energies will be about two times larger than that of SPI and 7.5 times larger than that of COMPTEL (at 1 MeV).The time resolution is also expected to be at the sub-ms level. With this increased accuracy with respect to recent missions such as XMM-Newton or INTEGRAL gamma-ray photons arising from a prompt signal expected in collapse of a dense star are experimentally detectable. The emission of the relativistic outer crust mass (with Lorentz factor $\Gamma > 15$) will allow the detection of specific prompt (sharp) signals beyond the opacity limit. In Fig. 1 we show the visibility window for the very SGRBs based on the model of Pérez-García et al [3] with the expected performance of e-ASTROGAM. On the left axis the fraction of the energy ejected in the outer crust is shown (solid line) while on the right axis (dashed line) the duration of the expected signal is depicted (in ms) both as a function of the logarithm of the isotropic equivalent energy emitted in the astrophysical event. It is clearly shown that the duration of the signals is well below the ~ 1 s duration, therefore we can refer to them as very SGRBs, i.e. vSGRBs. We have considered an average beaming factor of $f_b \sim 50$. In this scenario the ejected mass $M_{\rm ej,-5} \lesssim 10$ for the event energy range considered. The region above the solid line is to be understood as that where signal peak energies $E_p > 300$ keV being thus detectable with the e-ASTROGAM capabilities.

The accuracy provided by new data in the context of this mission will allow us to probe the explosion mechanism to improved levels and compare with astrophysical models for each event to better understand the outcome of the transitioning star. In addition, a possible interest for the gravitational wave community (and more generally for the multi-messenger one) is expected to better constrain new physics [14].

These events, triggering the emission of vSGRBs, although rare in nature could allow to discover or give hints, in an astrophysical scenario, of new phases of matter like the deconfined quark matter phase claimed to be first obtained in heavy-ion physics colliders. However, a possible *indirect* discovery from the e-ASTROGAM performance seems now at hand.

References

[1] Ghirlanda G., et al., A&A, 2009, 496, 3, 585

[2] Alcock, C., Farhi, E., & Olinto, A. 1986, ApJ, 310, 261

[3] Pérez-García, M. A., Daigne, F., Silk, J., 2013, ApJ 768, 145

[4] Pérez-García, M. A., Silk, J., & Stone, J. R. 2010, Physical Review Letters, 105, 141101

[5] Cermeño, M., Pérez-García, M. A. & Silk, J., 2017, Publications of the Astronomical Society of Australia (PASA), 34, e043, arXiv:1710.06866v1 [astro-ph.HE]

[6] Bertone, G., ed., Particle Dark Matter: Observations, Models and Searches. Cambridge University Press, 2010

[7] Nakar, E. 2007, Phys. Rep. 442, 166

[8] Berger, E. 2007, ApJ 670, 1254

[9] Piran, T. 2004, Reviews of Modern Physics, 76, 1143

[10] Tasticheff, V, et al., Proc. SPIE 9905, Space Telescopes and Instrumentation 2016: Ultraviolet to Gamma Ray, 2016, 99052N

[11] von Ballmoos P., Álvarez J., et al., 2012, Experimental Astronomy. 34 , 2, 583.

[12] Feroci M., Álvarez J., et al., 2012, Experimental Astronomy, 34, 2 , 415

[13] The e-ASTROGAM Collaboration, De Angelis A. et al., Experimental Astronomy 2011 1, arXiv:1611.02232v5

[14] Ghirlanda G., et al., 2016, A&A 594, A84

Globular clusters

Wlodek Bednarek

Department of Astrophysics, University of Lodz, ul. Pomorska 149/153, 90-236 Lodz, Poland

Science questions – Globular clusters (GCs), luminous concentrations of $\sim 10^5$-10^6 low mass stars within the volume of a few parsecs, contain also a large number of compact objects (neutron stars, white dwarfs) which are products of the final evolution of stars with the masses above ~ 0.8 $M_\odot$. Several GCs have been recently discovered by *Fermi*-LAT to emit GeV γ-rays [1, 2, 3, 4]. The γ-ray emission at TeV energies has been searched with the present Cherenkov telescopes but only detected from the GC Ter 5 [5]. Ter 5 also emits non-thermal diffusive radiation in the $1-7$ keV energy range [6, 7]. The origin of the non-thermal X-ray and γ-ray emission is not clear at present.

The GeV γ-ray emission is usually interpreted as a cumulative emission produced in the inner MSP magnetospheres [8, 9]. This scenario is supported by the detection of γ-ray pulsations from two MSPs within GCs, i.e. B1821-24 [10] and J1823-3021A [11]. The GeV (and TeV) emission might also originate in the Inverse Compton Scattering process of the $e^{\pm}$ pairs which are injected from the MSP magnetospheres into a dense low energy radiation field present within (and around) GCs [12, 13, 14]. It is argued that MSPs within GCs can significantly differ from those observed in the galactic field [14]. They are expected to be frequently captured by the low mass stars in GCs. As a result, their inner magnetic field could have different structure favoring production of a low energy $e^{\pm}$ plasma. The $e^{\pm}$ pairs from MSPs have to pass through a dense radiation field from the GCs (and also from the nearby Galactic disk and the Microwave Background Radiation) producing γ-rays and possibly also diffusive synchrotron radiation [14]. Their radiation might contribute to the observed by *Fermi*-LAT γ-ray emission. This process can also produce additional emission components at lower energies due to the comptonization of the infrared or the MBR. In fact, in some cases the γ-ray spectra do not show the characteristic exponential cut-off at a few GeV typical for the MSPs, arguing against the origin within MSP magnetospheres [2].

Some MSPs within GCs are expected to occupy the ejector/accretor transition state. A few such systems have been recently discovered. They show enhanced GeV γ-ray emission in the accretor state in respect to that observed in the stationary ejector phase of the MSPs (e.g. PSR J1023+0038 [15])). Also other high energy components might appear appear in the hard X-ray to γ-ray spectrum due to the interaction of the accretion flow with the rotating pulsar magnetosphere as e.g. observed in accreting X-ray binary systems containing neutron stars.

Importance of gamma-ray observations – Observations of GCs in the hard X-ray to GeV γ-ray energy range (e.g. Ter 5) should allow to determine the extension of the diffusive, non-thermal *Chandra* X-ray spectrum to the larger energies. Discovery of the hard X-ray emission will provide constraints on: the magnetic field within the specific GC, the parameters of $e^{\pm}$ pair plasma injected by the MSPs (injection rate, maximum energies), the features of relativistic electrons accelerated in the collisions of the MSP winds between themselves or with the winds from the companions stars. The constraints on the injection rate of $e^{\pm}$ plasma from MSPs will allow to limit the models for the non-thermal processes in the inner magnetospheres of the MSPs within the GCs.

The detailed studies of the GeV γ-ray morphology of the GCs will allow to identify the nature of the discrete sources (ejecting, accreting, transitional MSPs?) or identify processes responsible for this emission. Discovery of the pulsed γ-ray emission from the many radio MSPs within GCs will support the hypothesis that the observed GeV γ-ray emission originates in this type of compact objects.

The discovery of a new hard X-ray and soft γ-ray features in the non-thermal spectra of GCs will argue for the importance of various radiation processes (or soft radiation fields) as predicted by the IC scattering model proposed in e.g. [14].

Finally, a part of $e^{\pm}$ pairs from the MSPs can be thermalized in the atmospheres of the companion stars and/or their winds. These $e^{\pm}$ pairs could annihilate producing the narrow $\sim$0.5 MeV line which intensity will allow to put independent constraints on the $e^{\pm}$ pair injection rate.

Expected results with e-ASTROGAM – Possible extension of the diffusive synchrotron X-ray emission from Ter 5, observed by *Chandra* in the energy range 1-7 keV [6], to a few hundred keV should be detectable by the e-ASTROGAM (see Fig. 1 in [16]), allowing to constrain the injection rate of $e^{\pm}$ pairs by the MSPs and indirectly the MSP models.

A factor of a few better localization of the GeV γ-ray source by e-ASTROGAM (see Fig. 19 in [16]) should allow to conclude on the morphology of the emission region, within and/or around the GC, and answer the question whether this emission is related to the distribution of the MSPs within the GC or it has a diffusive nature.

The precise time accuracy of the γ-ray events by the e-ASTROGAM telescope (see Table I in [16]) will allow to measure the light curves of the MSPs within the GCs. Thus, the fraction of the GeV γ-ray emission from GCs, which is undoubtedly linked to the MSPs, can be determined.

The e-ASTROGAM will have enough sensitivity to detect possible additional components in the γ-ray spectrum due to the comptonization of different soft radiation fields, such as the infrared emission from the Galactic disk and the MBR, by a relatively low energy $e^{\pm}$ pairs (see prediction in Fig. 3 in [14]).

Finally, the improved sensitivity of the e-ASTROGAM (see Table I in [16]) should allow to search for the $e^{\pm}$ the annihilation feature. It might be produced within a large number of the compact MSP binary systems confined within the GCs. Discovery of such annihilation line should independently constrain the injection rate of the $e^{\pm}$ pair plasma from the MSPs within GCs.

References

[1] Abdo, A.A. et al. 2009 Sci, 325, 845
[2] Abdo, A.A. et al. 2010 A&A 524, A75
[3] Kong, A.K.H., Hui, C.Y., Cheng, K.S. 2010 ApJ 712, L36
[4] Tam, P.H.T. et al. 2011 ApJ 729, 90
[5] Abramowski, A. et al 2011 A&A 524, L18
[6] Eger, P., Domainko, W., Clapson, A.-C. 2010 A&A 513, A66
[7] Clapson, A.-C., Jamrozy, M., Dyrda, M., Eger, P. 2011 A&A 532, A47
[8] Venter, C., de Jager, O.C. 2008 ApJ 680, L125
[9] Venter, C., de Jager, O.C., Clapson, A.-C. 2009 ApJ 696, L52
[10] Freire, P.C.C. et al. 2011 Science 334, 1107
[11] Johnson, T.J. et al. 2013 ApJ 778, 106
[12] Bednarek, W., Sitarek, J. 2007 MNRAS 377, 920
[13] Kopp, A., Venter, C., Büsching, I., de Jager, O.C. 2013 ApJ 779, 126
[14] Cheng, K.S., Chernyshov, D.O., Dogiel, V.A., Hui, C.Y., Kong, A.K.H. 2010 ApJ 723, 1219
[15] Archibald, A.M. et al. 2009 Science 324, 1411
[16] de Angelis, A. et al. 2017 Exp.Astron. (arXiv:1611.02232)

Solar and Earth Science

Conveners: Francesco Longo

The Sun: a giant lab for cosmic-ray studies

Elena Orlando[1], *Mario N. Mazziotta* [2], *Nicola Giglietto* [2,3], *Silvia Rainó* [2,3], *Andrew Strong* [4]

[1] *Hansen Experimental Physics Laboratory and Kavli Institute for Particle Astrophysics and Cosmology, Stanford University, Stanford, CA 94305, USA*
[2] *Istituto Nazionale di Fisica Nucleare, Sezione di Bari, I-70126 Bari, Italy*
[3] *Dipartimento di Fisica "M. Merlin" dell'Università e del Politecnico di Bari, I-70126 Bari, Italy*
[4] *Max Planck Institut für extraterrestrische Physik, D-85748 Garching, Germany*

Science questions – The Sun is a known quiescent gamma-ray source [14, 2]. Its gamma-ray steady-state, characterized by two distinct emissions, is unique for its spatially and spectrally distinct components: 1) disc emission due by pion decay of cosmic-ray (CR) hadrons interacting with the solar atmosphere [20]; 2) spatially extended emission from inverse Compton (IC) scattering of CR electrons on the solar photons of the heliosphere [11, 13]. The latter extends to the whole sky and it is above the background even at large angular distances from the Sun.
Observations of the two components of the solar emission allow to gain information on CRs very close to the Sun and on CR propagation in the heliosphere. In addition, because CRs are affected by solar modulation, the intensity of both solar emissions is expected to be inversely proportional to the solar activity. This allows to obtain information of CRs close to the Sun as a function of different periods of solar activity.
After the discovery of the quiet solar emission in gamma rays with EGRET [14], thanks to *Fermi* LAT we can now detect the solar steady state with higher sensitivity and in different periods of solar activity [2, 12]. However, at low energy *Fermi* LAT has a relatively large PSF that does not allow to disentangle the hadronic disc emission from the leptonic extended emission. This prevents from knowing the CRs and their propagation close to the Sun for those energies where the solar modulation effects are important. Present models of propagation in the inner heliosphere that work well with *Fermi* LAT data assume the force field approximation for the modulation of the CRs [9]. However reality is more sophisticated[1], and this aspect can not be investigated with the limited PSF and sensitivity of present missions. Even more challenging is that the observed integral flux from the solar disk is found [2] to be 7 times higher than predicted by the 'nominal' model of [20]. This is possibly due to difficulties on the two component separation, calling for more sensitive observations and better PSF. In addition, observations of the energy range from few hundred MeV to 100 MeV of the Sun, where the solar modulation is very significant, is crucial for understanding low-energy CRs and their propagation in the heliosphere.

Importance of gamma-ray observations – Our knowledge on CRs at Earth has substantially increased in the recent years thanks to advanced instruments. For example, PAMELA [4] launched in 2006, *Fermi* Large Area Telescope [7] in orbit since 2008, and the Alpha Magnetic Spectrometer-02 (AMS-02)[5] working since 2011 have obtained very precise measurements of CRs at Earth. Moreover, the data from *Voyager 1* [8], the first human-build instrument leaving the Solar System, made also possible to know the low-energy CRs in the interstellar space. Measurements of CRs are also obtained indirectly by looking at the interstellar emission from gamma rays (e.g. [1, 3]) to radio-microwave frequencies (e.g. [21, 16]).
On the contrary, measurements of the CRs in the inner heliosphere are very difficult, if ever possible. However, an indirect way to probe CRs and their propagation in this region is by looking at the gamma-rays from the Sun, and by monitoring its emission components during various solar

[1] e.g. see the following code for CR propagation in the heliosphere: www.helmod.org/ and https://github.com/cosmicrays/HELIOPROP

cycles. In more detail, CRs in the heliosphere are affected by the solar wind and the magnetic field, which change their spectrum at energies below few tens of GeV/n. The strength of this effect depends on the solar activity, and it is known as the solar modulation. The solar activity has a period of 22 years, when the Sun changes twice the magnetic field polarity, and it passes through two solar maxima, and two solar minima. During solar maxima the solar modulation of CRs is the largest, while during solar minima is the the lowest. As a consequence being produced by CRs, both gamma-ray emission components of the Sun vary as a function of the solar activity. Observations of the two solar components allow to obtain information of CRs at the Sun. In addition, observations of the IC emission provide information about CR electron spectra throughout the entire inner heliosphere, and allows comprehensive studies of the solar modulation in this region.
The first attempt to detect the disc emission with EGRET data was performed by the EGRET Collaboration [22] that obtained only an upper limit. An accurate analysis [14] of the EGRET data accounting also for the IC emission component and background sources lead to the first detection of the quiescence gamma-ray Sun [14], and to the separation of the disc and the extended IC components. The flux and spectrum of the two components were found in agreement with the expectations. This analysis was performed with data mainly during solar maximum. During the first two years of the *Fermi* mission the solar activity has been extremely low, resulting in a high heliospheric flux of Galactic CRs. Therefore, the CR-induced quiescent gamma-ray emission from the Sun was expected to be near its maximum. The first study with *Fermi* LAT data [2] allowed to distinguish the two components with higher statistical significance than previously achieved. This analysis was conducted using 18 month of data during low solar activity. Different IC models have been investigated, yet no best model was found. The observed integral flux from the solar disk was found to be 7 times higher than predicted by the "nominal" model of [20]. Few years ago the solar activity started to increase, allowing us to start studying the evolution of the gamma-ray emission for different solar conditions [12, 19] for energies above 100 MeV. Disentangling the different components and characterizing the sources below 100 MeV with *Fermi* LAT is very challenging due to the relatively large PSF and energy dispersion at those energies. Moreover, any analysis below 30 MeV is discouraged[2]. Besides the CR studies the solar emission need to be accurately modeled in order to properly account for its emission in other studies. Indeed being moving and extended in the sky, the solar emission acts as a confusing source and it should be included in the analyses in a dedicated software as done with the Fermi Solar Science Tools within the Fermi LAT collaboration [10] that include physically based models of the IC emission [15].

Expected results with e-ASTROGAM – The e-ASTROGAM mission will achieve a major gain in sensitivity compared to the COMPTEL missions. It will also provide improved PSF with respect to *Fermi* LAT, which will help in the component separation and angular resolution. This will enable us to study CR transport in the inner heliosphere, to improve on the models of the solar modulation and on the models of CR cascades in the solar atmosphere.
As an example we report here the expected emission due by IC, as obtained in [18], where we have updated our previous models used in [2] to account for the latest more precise AMS-02 CR electron and positrons measurements [6]. In that work [18] we have used the StellarICs code [15] to extend the predictions down to 1 MeV for various models. Figure 1 shows these predictions of the IC component for the entire range of e-ASTROGAM. Solid lines represents our intensity predictions for different solar modulation conditions (0 MV, 400 MV, 600 MV) at 0.26° from the direction of the center of the Sun. As an example, dashed lines represent the same prediction at 0.5° from the direction of the Sun. For more details on the modeling see [18]. The same figure shows also *Fermi* LAT data from [3] at intermediate latitudes and the predictions of the interstellar emission at MeV energies at intermediate latitudes from [17]. In the energy range 1-100 MeV the solar modulation effect is at its maximum, thus allowing to easily distinguish among different models. This will allow to trace for the first time the low-energy CR electrons close to the Sun.
In summary, the e-ASTROGAM mission will provide a unique opportunity to monitor the solar

[2] https://fermi.gsfc.nasa.gov/ssc/data/analysis/LAT_caveats.html

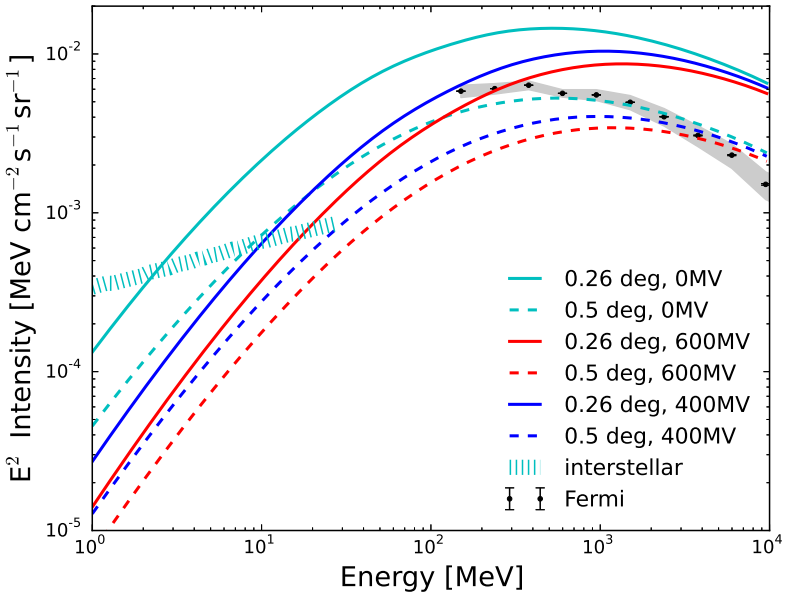

Figure 1: Predictions of the intensity of the solar IC emission for the energy range of e-ASTROGAM for various models and various angular distances from the Sun. The figure shows also the Fermi LAT data [1] and predictions of the interstellar emission at intermediate latitudes for comparison. The figure is taken from [18].

emission over the different solar cycles with changes in polarity. Moreover, covering lower energies than *Fermi* LAT, e-ASTROGAM will allow to access the energy range where the solar modulation plays the most important role.

References

[1] Abdo, A. A., Ackermann, M., Ajello, M., et al. 2009, Physical Review Letters, 103, 251101
[2] Abdo, A. A., Ackermann, M., Ajello, M., et al. 2011, ApJ, 734, 116
[3] Ackermann, M., Ajello, M., Atwood, W. B., et al. 2012, ApJ, 750, 3
[4] Adriani, O., Barbarino, G. C., Bazilevskaya, G. A., et al. 2009, Nature, 458, 607
[5] Aguilar, M., Alberti, G., Alpat, B., et al. 2013, Physical Review Letters, 110, 141102
[6] Aguilar, M., Aisa, D., Alvino, A., et al. 2014, Physical Review Letters, 113, 121102
[7] Atwood, W. B., Abdo, A. A., Ackermann, M., et al. 2009, ApJ, 697, 1071
[8] Cummings, A. C., Stone, E. C., Heikkila, B. C., et al. 2016, ApJ, 831, 18
[9] Gleeson, L. J., & Axford, W. I. 1968, ApJ, 154, 1011
[10] Johanesson, G., & Orlando, E., 2013, Proc. 33rd ICRC, p.0957 (arXiv:1307.0197)
[11] Moskalenko, I. V., Porter, T. A., & Digel, S. W. 2006, ApJL, 652, L65
[12] Ng, K. C. Y., Beacom, J. F., Peter, A. H. G., & Rott, C. 2016, Phys. Rev. D, 94, 023004
[13] Orlando, E., & Strong, A. W. 2006, arXiv:astro-ph/0607563, 2007 Ap&SS, 309, 359
[14] Orlando, E., & Strong, A. W. 2008, A&A, 480, 847
[15] Orlando, E., & Strong, A. 2013, Nuclear Physics B Proceedings Supplements, 239, 266
[16] Orlando, E., & Strong, A. 2013, MNRAS, 436, 2127
[17] Orlando, E., et al. 2017, Proc. 35th International Cosmic Ray Conference, PoS(ICRC2017)692
[18] Orlando, E., et al. 2017, Proc. 35th International Cosmic Ray Conference, PoS(ICRC2017)693
[19] Rainó, S., Giglietto, N., Moskalenko, I., Orlando, E., & Strong, A. W. 2017, European Physical Journal Web of Conferences, 136, 03007
[20] Seckel, D., Stanev, T., & Gaisser, T. K. 1991, ApJ, 382, 652
[21] Strong, A. W., Orlando, E., & Jaffe, T. R. 2011, A&A, 534, A54
[22] Thompson, D. J., Bertsch, D. L., Morris, D. J., & Mukherjee, R. 1997, JGR, 102, 14735

Gamma-ray emission from solar flares

Elisabetta Bissaldi,[1,2] *Nicola Giglietto,*[1,2] *Francesco Longo,*[3,4] *Manuela Mallamaci,*[5] *Silvia Rainó*[1,2]

[1] *Dipartimento di Fisica "M. Merlin" dell'Università e del Politecnico di Bari, I-70126 Bari, Italy*
[2] *Istituto Nazionale di Fisica Nucleare, Sezione di Bari, I-70126 Bari, Italy*
[3] *Dipartimento di Fisica, Università di Trieste, I-34127 Trieste, Italy*
[4] *Istituto Nazionale di Fisica Nucleare, Sezione di Trieste, I-34127 Trieste, Italy*
[5] *Istituto Nazionale di Fisica Nucleare, Sezione di Padova, I-35131 Padova, Italy*

Science questions – Solar flares are the most energetic phenomena in the Solar System. They appear as sudden flashes of light with time scales of minutes to hours, releasing up to 10^{32-33} ergs. These events are sometimes associated with explosive blasts of material from the solar corona, the so-called *Coronal Mass Ejections* (CMEs), even if the correlation between the two processes is not clearly established yet. The frequency of both flares and CMEs follows the 11-year solar activity cycle, the most intense ones usually occurring during the maximum.
Solar flares are mainly classified on the basis of the X-ray flux between 0.1 and 0.8 nm measured by the Geostationary Operational Satellite Server (GOES). However, during the last few decades many events have been detected by several experiments over a very wide range of energies, going from decameter radio waves to gamma-rays beyond 1 GeV, hinting at a complex underlying scenario.
What triggers the flares and how the Sun releases this energy with such high efficiency is presently not completely understood. Flare energy may be considered to result from reconnecting magnetic fields in the corona. According to the standard scenario [11], the release of energy derives from accelerating particles, which precipitate from the corona to the chromosphere, where they heat the plasma. The hot plasma expands then along the magnetic loop into the corona, a process named *evaporation*. This model explains several observations, like the soft and hard X-ray emission, but not all (see for example [12]). In addition the acceleration mechanism is not part of the model, being one of the puzzling aspects of the phenomenon.
An intriguing counterpart of the solar flares are the so-called Solar Energetic Particles (briefly SEPs), a population of charged particles observed in interplanetary space, with energies going from some keV up to GeV. SEPs can be detected after the solar flares, especially when these are followed by CMEs. A key question is whether particles producing the flare radiation and SEPs are accelerated by the same mechanism.
Phenomena similar to solar flares and CMEs are believed to occur at larger scales elsewhere in the universe, for example in stellar flares, magnetars, young circumstellar disks, supernovae shock waves, etc. These energetic phenomena from the Sun are therefore the most accessible laboratories for the study of the fundamental physics of transient energy release and efficient particle acceleration in cosmic magnetized plasmas. Furthermore, it is worth to study them since they produce the most extreme forms of space weather, like the radiation hazard from the most intense SEP fluxes, and the disruption of the heliospheric plasma environment.

Importance of gamma-ray observations – As outlined above, the solar flares emit radiation with very different energies. This results from the acceleration of charged particles which interacts with the ambient solar atmosphere and magnetic fields and typically occurs in the regions near the footpoints of magnetic field lines. In particular, accelerated electrons mainly produce X-rays via non-thermal bremsstrahlung and radio emission via synchrotron mechanism. On the other hand, accelerated protons and ions come into play emitting at higher energies: nuclear interactions produce excited and radioactive nuclei, neutrons and pi-mesons. All of these products subsequently are responsible of the gamma-ray emission via secondary processes, consisting in nuclear gamma-ray lines in the 1-10 MeV range and a continuum spectrum above 100 MeV [7]. Also accelerated

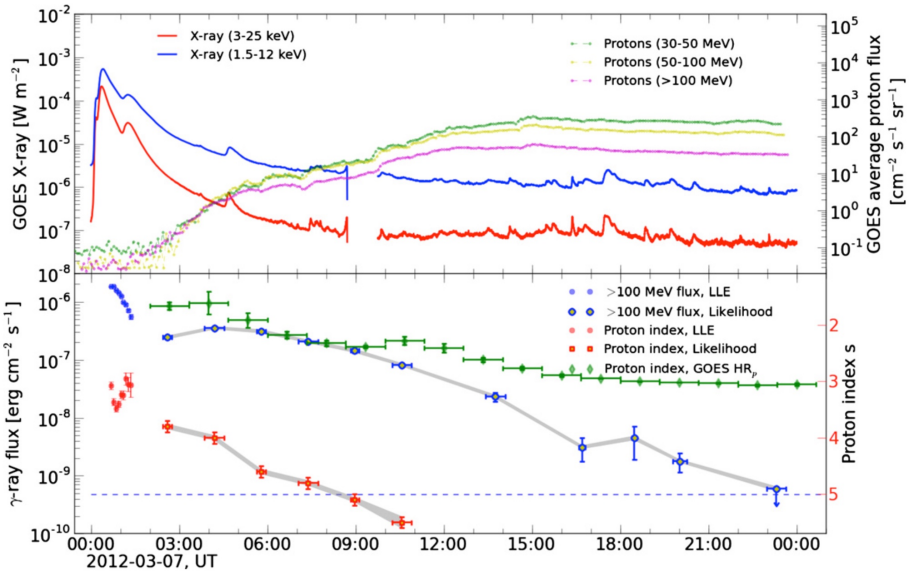

Figure 1: Temporal evolution of two bright X-class solar flares - 2012 March 7. (Top panel) X-ray emission and proton flux detected by GOES satellite. (Bottom panel) Long lasting gamma-emission detected by *Fermi*. Picture taken from [3].

primary electrons, undergoing inelastic scattering, yield bremsstrahlung radiation with a broad energy spectrum extending up to the originating electron energy.
Previous gamma-ray observations of solar flares were carried out for the first time by the gamma-ray spectrometer on board of the Solar Maximum Mission (SMM). Later on many detections were performed by the Energetic Gamma Ray Experiment Telescope (EGRET) on the Compton Gamma-ray Observatory (CGRO), and in some cases also by the Reuven Ramaty High Energy Solar Spectroscopic Imager (RHESSI), still operating but mainly designed for hard-X ray energies. A review of these gamma-ray observations can be found in [5]. Besides in [14], a compilation of SMM data for 258 gamma-ray flares detected above 300 keV is presented. Recent observations of solar flares at keV-MeV-GeV energies have been carried out by the two instruments onboard the *Fermi* satellite. The secondary instrument, the *Fermi* Gamma-Ray Burst Monitor (GBM), consists of two types of detectors, namely the NaI (8-900 keV) and BGO (250 keV - 40 MeV) detectors. GBM triggered on $>$ 1200 solar flares in the hard X-ray band over 9 years. Some of those were also detected in the 1-10 MeV band. However, the BGO energy resolution is not fine enough to perform an accurate line analysis (see next section).
The gamma-ray emission light curve can be similar to one observed in X-rays, lasting for 10-100 s and indicating the acceleration of both ions and electrons from the same solar ambient. This is referred to as "impulsive" phase of the flare. However, some events have been found to have a long-duration gamma-ray emission, lasting for several hours after the impulsive phase [10]. In this respect, a relevant number of flares detected by the primary instrument on board *Fermi* namely the Large Area Telescope (LAT), above 100 MeV shows this kind of long duration emission [1]. Fig. 1 displays the temporal evolution of the emission for one of these events. In general, during the extended phase, there does not seem to be any other associated radiation, but most of these flares are associated with fast CMEs and a significant flux of SEPs. The origin of this temporally extended events is not well understood and raised new questions, such as the type of radiative process (if hadronic or leptonic), the location of the acceleration (if at the flare site or in the proximity of the CME), the mechanisms of the acceleration [3]. Finally *Fermi* LAT has detected an intriguing class of "behind-the-limb" solar flares [2], for which one possible explanation is the gamma-ray emission by protons in the CME environment.

Expected results with e-ASTROGAM – The detections of solar flares by SMM and EGRET, in the past, and more recently by *Fermi* indicate that acceleration of particles in the gamma-ray energy range is not a so rare phenomenon, even for more modest events [1]. e-ASTROGAM will study for the first time the solar flare radiation from 300 keV to 3 GeV, covering therefore a very broad range of energies and complementing information collected by dedicated future experiments

like the ESA Solar Orbiter [6]. In the following we report the different types of measurements that e-ASTROGAM will be able to perform.

- **Temporal evolution**. During the expected 3 years of operation, e-ASTROGAM will have the opportunity to detect solar flares (the number depending on the phase of the solar cycle) and to study the evolution in time of the gamma-radiation from each event. These and other observations performed in different energy bands and channels (like SEP fluxes) will give important information about the classification of the events between impulsive and long duration events, helping in constraining model of acceleration and propagation [1].

- **Energy spectrum.** As already outlined, the gamma-ray solar flare spectrum is characterized by a bremmstrahlung continuum, nuclear lines and pion-decay components. e-ASTROGAM will have optimal sensitivity and energy resolution (much better than *Fermi* GBM) to detect the de-excitations lines from accelerated ions. This will be fundamental to gain insight about the chemical abundances and about the physical conditions where accelerated ions propagate and interact [9]. Also the 0.511 MeV and 2.223 MeV lines will be detected. It will also be interesting to compare e-ASTROGAM results with SMM spectroscopic analysis in MeV domain (see for example [8]). Going at higher energies, the spectral analysis will allow one to distinguish spectroscopically between electron bremsstrahlung and the pion-decay models.

- **Photon polarization**. The study of polarization is appealing in that the bremsstrahlung emission from solar flares will be polarized if the phase-space distribution of the emitting electrons is anisotropic. Polarization measurements therefore provide a direct handle on the extent to which the accelerated electrons are beamed, which, in turn, has important implications for particle acceleration models. These type of measurements were carried out in X band, while the first and unique measurement of gamma-ray polarimetry has been performed in [4], by exploiting RHESSI data between 0.2-1 MeV, but only for two solar flares. e-ASTROGAM can be therefore further exploited in this field, giving unprecedented polarization measurements in the MeV range by means of the Compton interactions in the instrument, and possibly also to higher energies [13].

- **Source localization**. e-ASTROGAM is designed to have an angular resolution of about 0.2° at 1 GeV (a factor 4 better than the *Fermi*/LAT instrument). Even if it will not be able to resolve the details of the gamma-ray emission, localizing the source on the solar disk and comparing this with measurements in X-rays (from which typically the source region is identified) could give additional information for constraining the emission and acceleration mechanisms.

References

[1] Ackermann M., Ajello M., Albert A., et al., 2014, Astrophysical Journal, 787, 15
[2] Ackermann M., et al., 2017, The Astrophysical Journal Letters, 805, No.2
[3] Ajello M., Albert A., Allafort A., et al., 2014, The Astrophysical Journal, 789, 20
[4] Boggs S. E., Coburn W., Kalemc E., 2006, The Astrophysical Journal, 638, 1129-1139
[5] Chupp E. L., Ryan J. M., 2009, Research in Astronomy and Astrophysics, vol. 9 No. 1, 11-40
[6] Müller D., Marsden R. G., StCyr O. C., et al., 2013, vol. 285,1-2, 25-70
[7] Murphy R. J., Dermer, C. D. Ramaty, R., 1987, The Astrophysical Journal Supplement Series, vol. 63, 721-748
[8] Murphy R. J., Ramaty R., Zozlovsky B. and Reames D. V., 1991, Astrophysical Journal, 371, 793-803
[9] Murphy R. J., Share G. H., 2005, Advances in Space Research, 35,1825-1832
[10] Kanbach et al., 1993, Astronomy and Astrophysics Supplement Series, 97, 349
[11] Kopp R. A., Pneuman G. W, 1976, Solar Physics, 50, 85-98
[12] Krucker S., Hudson H. S., Jeffrey N. L. S., et al., 2011, The Astrophysical Journal, 739, 96
[13] Tatischeff V., De Angelis A., Gouiffe' C., et al., arXiv:1706.07031 [astro-ph.HE]
[14] Vestrand W. T., Share G.H., J. Murphy R., et al., 1999, The Astrophysical Journal Supplement Series, vol. 120, 409-467

Gamma-ray spectrum of the Moon

Francesco Loparco[1,2]*, Mario N. Mazziotta* [1]

[1] *Istituto Nazionale di Fisica Nucleare, Sezione di Bari, I-70126 Bari, Italy*
[2] *Dipartimento di Fisica "M. Merlin" dell'Università e del Politecnico di Bari, I-70126 Bari, Italy*

Science questions – The Moon is one of the brightest sources of high-energy gamma rays in the Solar System. Gamma rays from the Moon are originated in the shower cascades produced by the interactions of Galactic cosmic-ray (CR) nuclei with the lunar surface [1, 2]. The lunar gamma-ray emission depends on the fluxes of the primary cosmic-ray nuclei impinging on the Moon and on the mechanisms of their hadronic interactions with the rock composing the lunar surface. The gamma-ray energy spectrum of the Moon extends in the energy interval from a few MeV up to a few GeV and it is well understood, thus making the Moon a useful standard candle for the calibration of gamma-ray telescopes [3, 1].

As mentioned above, gamma rays emitted from the Moon are produced after inelastic interactions of charged CRs with the lunar surface. Assuming that the CR flux on the lunar surface is spatially isotropic and indicating with $I_i(T)$ the intensity of CRs of the i-th species (in units of particles MeV^{-1} cm^{-2} sr^{-1} s^{-1}) as a function of kinetic energy T, the rate $\Gamma_i(T)$ of CRs of the i-th species (in units of particles MeV^{-1} s^{-1}) impinging on the lunar surface is given by:

$$\Gamma_i(T) = 4\pi R_{\leftmoon}^2 \, I_i(T) \int \cos\theta_M d\Omega_M = 4\pi^2 R_{\leftmoon}^2 \, I_i(T) \tag{1}$$

where $R_{\leftmoon} = 1737.1\,\mathrm{km}$ is the radius of the Moon. In the previous equation we set $d\Omega_M = d\cos\theta_M d\phi_M$, where (θ_M, φ_M) are the zenith and azimuth angles of CR particles with respect to the lunar surface ($0 < \cos\theta_M < 1$ and $0 < \phi_M < 2\pi$).

The differential gamma-ray luminosity of the Moon $L_\gamma(E_\gamma)$ (in units of photons MeV^{-1} s^{-1}) is given by:

$$L_\gamma(E_\gamma) = \sum_i \int Y_i(E_\gamma|T)\Gamma_i(T)dT = 4\pi^2 R_{\leftmoon}^2 \sum_i \int Y_i(E_\gamma|T) I_i(T) \, dT \tag{2}$$

where $Y_i(E_\gamma|T)$ is the differential gamma-ray yield (in units of photons $\mathrm{particle}^{-1}$ MeV^{-1}), i.e. the number of photons per unit energy produced by a primary particle of the i-th species. The yields $Y_i(E_\gamma|T)$ depend on the mechanisms of the interactions of primary CRs with the lunar surface (regolith) and on its composition.

The differential intensity of gamma rays (in units of photons MeV^{-1} cm^{-2} sr^{-1} s^{-1}) emitted from the Moon can be evaluated starting from the differential luminosity and is given by:

$$I_\gamma(E_\gamma) = \frac{L_\gamma(E_\gamma)}{4\pi^2 R_{\leftmoon}^2} = \sum_i \int Y_i(E_\gamma|T) I_i(T) \, dT \tag{3}$$

The gamma-ray flux observed by a detector at Earth (in units of photons MeV^{-1} cm^{-2} s^{-1}) can also be evaluated from the differential luminosity and is given by:

$$\phi_\gamma(E_\gamma) = \frac{L_\gamma(E_\gamma)}{4\pi d^2} = \frac{\pi R_{\leftmoon}^2}{d^2} I_\gamma(E_\gamma) = \frac{\pi R_{\leftmoon}^2}{d^2} \sum_i \int Y_i(E_\gamma|T) I_i(T) \, dT \tag{4}$$

where d is the distance between the center of the Moon and the detector.

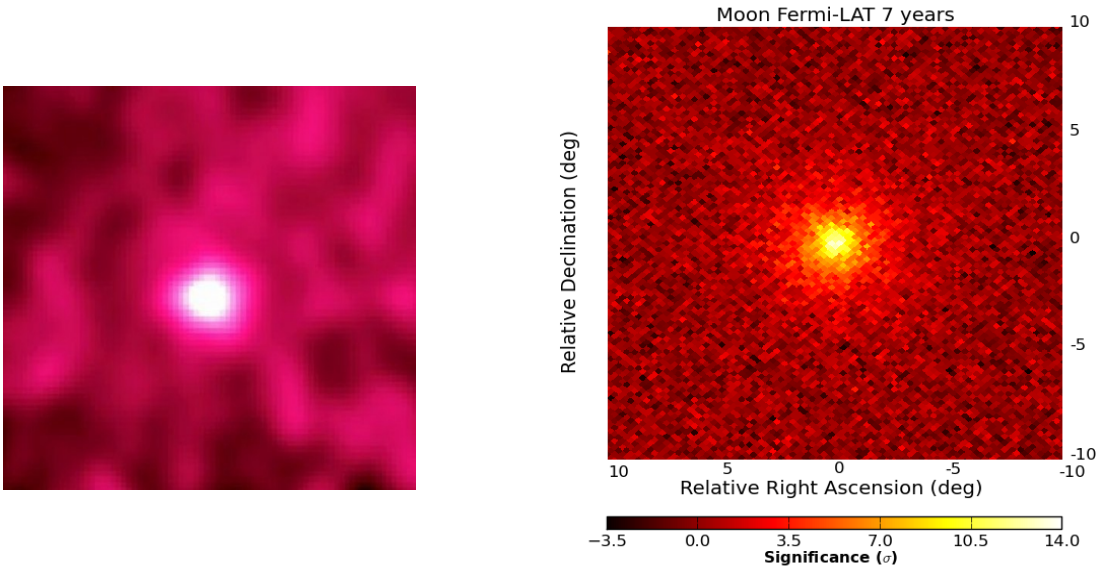

Figure 1: Images of the Moon seen by EGRET [2] (left) and by the Fermi LAT [1] (right). The EGRET plot covers a field of view of roughly 40°.

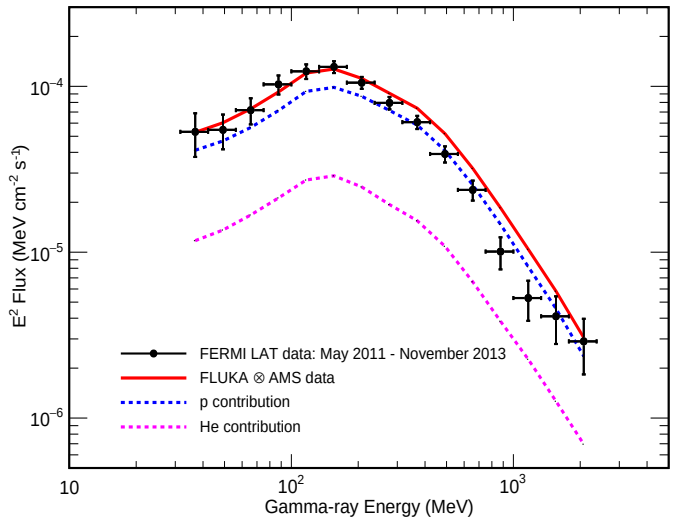

Figure 2: Comparison of the lunar gamma-ray flux measured by the Fermi LAT in the period from May 2011 to November 2013 [1] with the predictions obtained by folding the fluxes of cosmic-ray protons and helium nuclei measured by AMS-02 [10, 11].

Importance of gamma-ray observations – The emission of high-energy gamma rays from the Moon was first observed by the EGRET experiment [2], which operated from 1991 to 2000 onboard the Compton Gamma Ray Observatory. Recently, the Fermi Large Area Telescope (LAT) has performed further measurements [3, 1] of the lunar gamma-ray emission, extending the energy range down to 30 MeV with an improved energy resolution with respect to its predecessor. Figure 1 shows the images of the Moon seen by EGRET during eight exposures in the period 1991-1994 and by the LAT during its first seven years of operation [1]. In addition to the extension of the energy range with respect to its predecessor, the LAT can also observe the Moon with a better angular resolution.

The direct measurements of the primary proton and helium spectra performed by the AMS-02 experiment [10, 11] have allowed the Fermi LAT Collaboration to validate their model describing the cosmic-ray interactions with the Moon. Figure 2 shows a comparison of the lunar gamma-ray flux measured by the LAT in the same period when AMS-02 performed its measurements of the proton and helium spectra (May 2011 November 2013) with the predictions obtained with a full simulation of the interactions of primary cosmic rays with the lunar surface based on the `FLUKA` code [3, 4, 5]. The Monte Carlo predictions shown in Figure 2 have been obtained by folding the proton and helium fluxes measured by AMS-02 with the gamma-ray yields predicted by the simulation [1].

Expected results with e–ASTROGAM – The energy range of e-ASTROGAM will cover the whole gamma-ray spectrum emitted by the Moon. In addition to providing a new accurate measurement of the lunar gamma-ray spectrum in the MeV-GeV band, e-ASTROGAM data will extend the energy range observed by the Fermi LAT towards lower energies. This feature will provide the unique opportunity to explore possible gamma-ray lines in the keV-MeV region, originating from the decays of excited states produced in the interactions of CR nuclei with the lunar rock. Moreover, thanks to the better PSF, e-ASTROGAM will be able to resolve the gamma-ray emission from the lunar disc.

References

[1] D. J. Morris, J. Geophys. Res. **89** (1984), 10685.

[2] D. J. Thompson *et al.*, J. Geophys. Res. **102** (1997), 14735.

[3] A. A. Abdo *et al.*, Astrophys. J. **758** (2012), 140.

[4] M. Ackermann *et al.*, Phys. Rev. D. 93, 082001 (2016).

[5] M. Aguilar *el al.*, Phys. Rev. Lett. **114**, 171103 (2015).

[6] M. Aguilar *et al.*, Phys. Rev. Lett. **115**, 211101 (2015).

[7] G. Battistoni *et al.*, "Overview of the FLUKA code", Annals of Nuclear Energy **82** (2015), 10-18.

[8] A. Ferrari, P. R. Sala, A. Fassò and J. Ranft, *FLUKA: a multi-particle transport code* CERN-2005-10 (2005), INFN/TC_05/11, SLAC-R-773.

[9] `http://www.fluka.org`

Cosmic ray studies with the gamma-ray emission from the Moon

Fabio Gargano[1], *Francesco Loparco*[1,2], *Mario N. Mazziotta* [1]

[1] *Istituto Nazionale di Fisica Nucleare, Sezione di Bari, I-70126 Bari, Italy*
[2] *Dipartimento di Fisica "M. Merlin" dell'Università e del Politecnico di Bari, I-70126 Bari, Italy*

Science questions – The lunar gamma-ray emission is originated from the hadronic interactions of high-energy cosmic-ray (CR) nuclei with the rock composing the lunar surface. Measurements of the gamma-ray flux from the Moon provide also a useful tool to study the properties of CRs and to monitor the solar cycle, since it depends on the primary cosmic-ray nuclei fluxes, which change during the solar cycle.

Importance of gamma-ray observations – The Fermi-LAT has monitored the time evolution of the lunar gamma-ray emission on a 7-year time scale, detecting the expected correlation with the solar cycle. The left panel of Figure 2 shows the time evolution of the gamma-ray intensity from the Moon measured by the LAT above 56, 75, 100 and 178 MeV [1]. As expected, the gamma-ray intensity from the Moon follows the evolution of the solar cycle. This feature is confirmed when looking at the correlations between the lunar gamma-ray intensity and the data from the neutron monitor stations installed in various locations on the Earth. As an example, in the right panel of Figure 2 it is shown a comparison of the lunar gamma-ray intensity measured by the LAT with the count rates of the McMurdo neutron monitor [2]. Furthermore, as the gamma-ray threshold energy is increased, the correlation with the solar cycle becomes weaker, as gamma rays of higher energies are produced by more energetic cosmic rays, which are not affected by the solar modulation.

The Fermi-LAT Collaboration has developed a full simulation of the interactions of CR nuclei with the lunar surface based on the `FLUKA` code [3, 4, 5]. Starting from a model for the CR proton and ^{4}He local interstellar spectra (LIS) [6] evaluated using a customized version of the CR propagation code `DRAGON` [7, 8], the simulation has been used to derive from the lunar gamma-ray spectrum the solar modulation potential in the framework of the force field approximation [9] and consequently the intensities of CR protons and ^{4}He nuclei impinging on the Moon. The proton and ^{4}He spectra are shown in the left panel of Fig. 2, where they are also compared with the data from

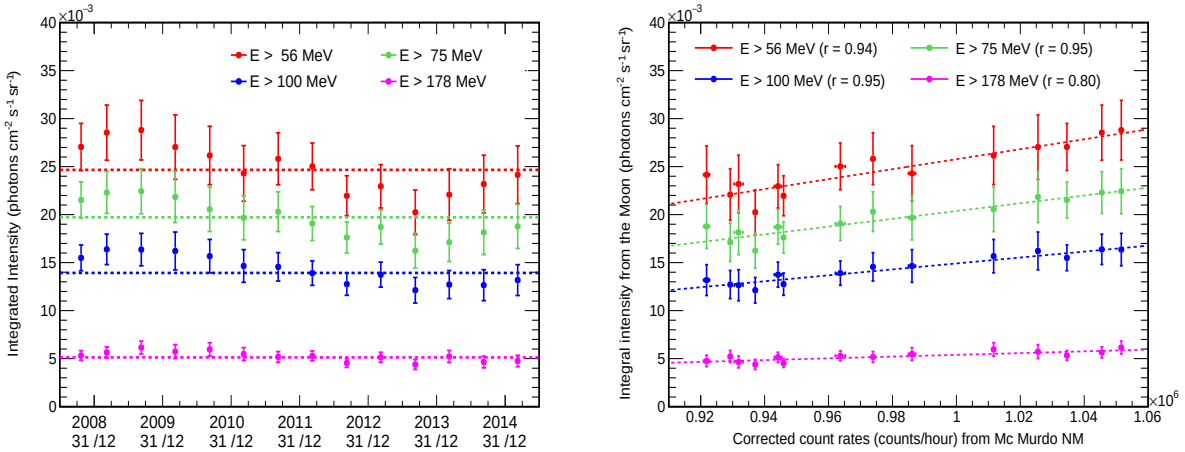

Figure 1: Left: time evolution of the lunar gamma-ray intensity above 56, 75, 100 and 178 MeV [1]. Right: study of the correlations between the lunar gamma-ray intensity [1] and the count rates of the McMurdo neutron monitor [2]. The values reported in brackets are the correlation coefficients.

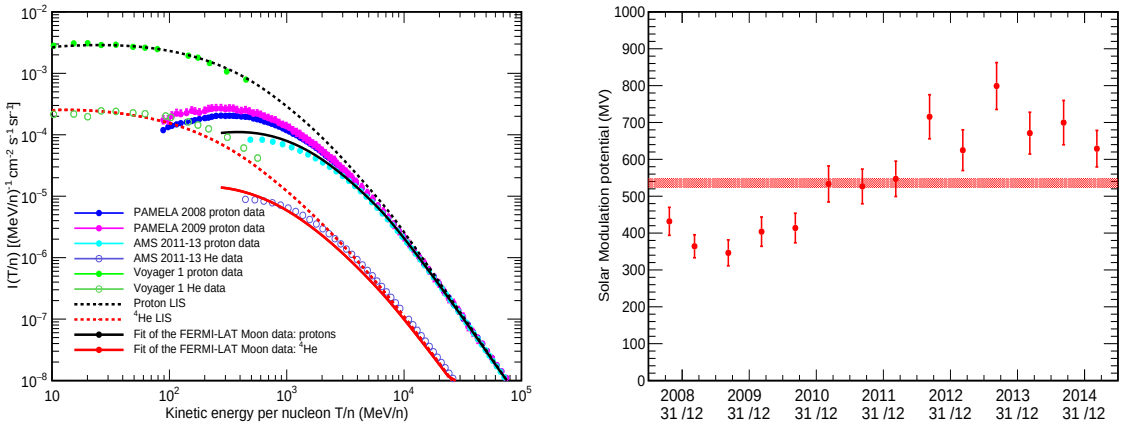

Figure 2: Left: CR proton and helium spectra obtained from the best fit of the Fermi LAT Moon gamma-ray data [1]. The results of the fit (continuous black and red lines) are compared with the proton measurements taken by PAMELA [12] in 2008 (blue points) and 2009 (purple points) and with the AMS-02 [10, 11] proton (cyan points) and helium data (violet points). The plot shows also the proton and helium LIS (dashed black and red lines) and the Voyager 1 proton (light green points) and helium (dark green) data [13]. Right: Time evolution of the solar modulation potential, evaluated from a fit of the lunar gamma-ray emission. The central band corresponds to the average value of the solar modulation potential during the whole data-taking period.

direct measurements performed by AMS-02 [10, 11] and PAMELA [12] in different epochs. This procedure has also allowed the Fermi LAT Collaboration to study the time evolution of the solar modulation potential, as shown in the right panel of Fig. 2.

Expected results with e–ASTROGAM – The energy range of e-ASTROGAM will cover the whole gamma-ray spectrum emitted by the Moon. e-ASTROGAM data will extend the energy range observed by the Fermi LAT towards lower energies. The lunar gamma-ray data at low energies will represent a powerful tool to monitor the solar modulation and to study the CR spectra impinging on the Moon surface.

References

[1] M. Ackermann *et al.*, Phys. Rev. D. 93, 082001 (2016).

[2] Home page of the University of Delaware Bartol Research Institute Neutron Monitor Program: `neutronm.bartol.udel.edu`

[3] G. Battistoni *et al.*, "Overview of the FLUKA code", Annals of Nuclear Energy **82** (2015), 10-18.

[4] A. Ferrari, P. R. Sala, A. Fassò and J. Ranft, *FLUKA: a multi-particle transport code* CERN-2005-10 (2005), INFN/TC_05/11, SLAC-R-773.

[5] `http://www.fluka.org`

[6] M. N. Mazziotta, F. Cerutti, A. Ferrari, D. Gaggero, F. Loparco and P. R. Sala, Astropart. Phys. **81**, 21 (2016) doi:10.1016/j.astropartphys.2016.04.005 [arXiv:1510.04623 [astro-ph.HE]].

[7] C. Evoli, D. Gaggero, D. Grasso and L. Maccione, JCAP **0810** (2008) 018 [arXiv:0807.4730 [astro-ph]].

[8] D. Gaggero, L. Maccione, G. Di Bernardo, C. Evoli and D. Grasso, Phys. Rev. Lett. **111** (2013) 2, 021102 [arXiv:1304.6718 [astro-ph.HE]].

[9] L. J. Gleeson and W. I. Axford, Astrophys. J. **149** (1967), L115
L. J. Gleeson and W. I. Axford, Astrophys. J. **154** (1968), 1011.

[10] M. Aguilar *el al.*, Phys. Rev. Lett. **114**, 171103 (2015).

[11] M. Aguilar *et al.*, Phys. Rev. Lett. **115**, 211101 (2015).

[12] O. Adriani *et al.*, Astrophys. J. **765**, 91 (2013) [arXiv:1301.4108 [astro-ph.HE]].

[13] E.C. Stone et al., Science **341** (2013), 150

Detection of Terrestrial Gamma-ray Flashes with e-ASTROGAM

Alessandro Ursi[1], *Marco Tavani* [1,2,3], *Martino Marisaldi*[4,5], *Fabio Fuschino*[5], *Claudio Labanti* [5], *Sébastien Celestin* [6], *Stefano Dietrich*[7]

[1] *INAF-IAPS Roma Italy*
[2] *Dipartimento di Fisica, Università di Roma "Tor Vergata", Roma, Italy*
[3] *Gran Sasso Science Institute, L'Aquila, Italy*
[4] *Birkeland Centre for Space Science, University of Bergen, Allegaten 55, 5007, Bergen, Norway*
[5] *INAF-IASF, Bologna, Italy*
[6] *LPC2E, University of Orléans, CNRS, France*
[7] *ISAC-CNR, Roma, Italy*

Science questions – Terrestrial Gamma-ray Flashes (TGFs) are brief (tens of μs – few ms) and intense gamma-ray (hundreds of keV – tens of MeV) emissions coming from the terrestrial atmosphere ($\sim 12 - 15$ km a.s.l.), strictly correlated with lightning activity representing the highest-energy natural phenomenon observed on Earth. Representing a crossover between atmospheric physics and high-energy astrophysics, TGFs constitute a really attractive challenge for both scientific fields.

TGFs take place at thundercloud tops and, despite being a completely terrestrial phenomenon, most of the studies about this phenomenon have been carried out using high-energy astrophysics satellites. After the serendipitous discovery in the early 90's by the BATSE experiment [7], wide contributions to their phenomenology have been brought by the NASA Reuven Ramaty High-Energy Solar Spectroscopic Imager (RHESSI) [14, 8], the Astrorivelatore Gamma ad Immagini LEggero (AGILE) [11] and the NASA Fermi space telescope [1]. Moreover, TGFs have also been found within the BeppoSAX (1996-2002) data [20] and have been detected by aircraft [15] and at ground level both in correlation with natural [18] and triggered lightning [3, 5, 10].

The most accepted hypothesis besides their production suggests the upper part of Earth's troposphere behaves as a particle accelerator, under thunderstorm conditions: free electrons in air, accelerated to relativistic energies by intense electric fields, may produce hard X- and gamma-rays via Bremsstrahlung processes on atoms and nuclei in the atmosphere. [9, 4, 5]. Nevertheless, TGFs have also drawn an interest, as the significant radiation dose they emit, together with the height at which they occur, have been pointed out as potentially hazardous for aircraft and possible sources of injuries for airlines crews and on-board electronics [17, 6].

To date, a wide database including thousands of TGFs for more than 10 years activity is provided by the RHESSI, AGILE and Fermi data [8, 11, 13, 1]. In particular, the AGILE satellite produced interesting breakthroughs in the field of TGF science by performing the first imaging of a TGF event exploiting the on-board silicon tracker [12], by investigating the spectrum tail at the highest energies (> 40 MeV) [16] and by detecting multiple TGFs produced by the same thunderstorm systems taking advantage of meteorological data from geostationary satellites [19] (Fig. 1(d)).

Expected results with e-ASTROGAM – Taking into consideration the heritage provided by the previous TGF-detecting satellites, especially AGILE, key points of a suitable TGF detector are represented by a wide energy range, by a high time resolution of the on-board trigger logic timescales (with the possibility of acquiring data in a photon-by-photon mode), as well as by a joint working mode with other on-board instruments (such as a gamma-ray imager). Moreover, having a nearly-equatorial satellite orbit plays an important role, in ensuring the monitoring of the tropical regions where most of the lightning activity takes place. Basic contributions and expected results of the e-ASTROGAM mission for what concerns the science of TGFs are listed below.

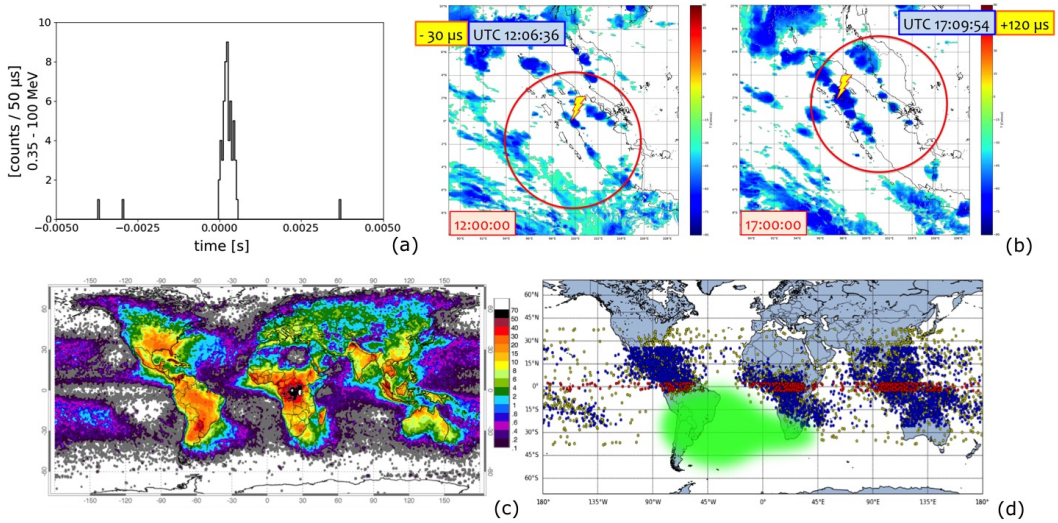

Figure 1: (a) Light curve of a TGF detected by the AGILE MCAL. (b) The annualized distribution of total lightning activity (flashes / km^2 / yr), detected by the Lightning Imaging Sensor (LIS) [2]. (c) World distribution of TGFs detected by RHESSI (yellow), Fermi (blue) and AGILE (red). The green region represents the South Atlantic Anomaly (SAA). (d) Example of two multiple TGFs, with associated WWLLN sferics, detected by the AGILE satellite at successive overpasses (within $\sim$ 3 hours), produced by the same developing storm [19].

- The strongest point of e-ASTROGAM is the calorimeter, that provides gamma-ray data in an energy range (30 keV – 200 MeV) fully including the typical TGF energies and, in particular, the Compton range (0.3 – 15 MeV) of atmospheric processes linked to TGFs. Such an energy range allows the investigation of the **TGF high-energy spectral component**, in order to shed light on the nature of the high-energy tail of the TGF spectrum discovered by AGILE and the existence of a possible higher-energy TGF population.

- The calorimeter acquires data in a photon-by-photon mode for triggered events, with a time resolution of 2 μs (at 3σ): this way, the time and energy binning is limited just by a statistical factor. Moreover, the presence of a **sub-millisecond trigger logic timescale**, just as for the AGILE MCAL, plays a leading role in the detection of very brief events such as TGFs, allowing for revealing a large number of events. Considering the current missions, the e-ASTROGAM calorimeter is expected to detect about $>$ 1000 TGFs/y, providing a wide database that can be used for scientific purposes.

- The calorimeter is an all-sky detector with no imaging capabilities and it is therefore capable of detecting events from every direction, regardless the satellite pointing. Nevertheless, the calorimeter instrument can work alone in a so-called burst mode, or together with the on-board silicon tracker, as a gamma-ray imager, in the 0.3 MeV –3 GeV energy range. This allows to perform **imaging of TGFs**, reconstructing the incoming direction and geographic position of the TGF source and constraining the gamma-ray emission cone.

- The e-ASTROGAM satellite will be delivered into **a near-equatorial orbit** ($\sim$ 2.5°) that not only guarantees a low and stable charged particle background for the on-board instruments, but also allows for the monitoring of geographic regions with the highest lightning activity on Earth. This strongly increases the chance of detecting TGFs and of revealing multiple TGFs during the same passage and throughout successive overpasses over the same region, providing interesting data for the study of the storm evolution, the associated climatological scenario, and the capability of single storms to produce several TGFs and hence, allowing to refine the production models.

References

[1] Briggs, M. S., G. J. Fishman, V. Connaughton, et al. 2010, Journal of Geophysical Research (Space Physics), 115, A07323, doi:10.1029/2009JA015242

[2] Christian, Hugh J., et al. 2003, Journal of Geophysical Research: Atmospheres, 108, D1, 2156-2202, ACL 4-1–ACL 4-15, doi:10.1029/2002JD002347

[3] Dwyer, J. R., et al. 2004, Geophys. Res. Lett., 31, L05119, doi:10.1029/2003GL018771

[4] Dwyer, J. R. 2008, J. Geophys. Res., 113, D10103, doi:10.1029/2007JD009248

[5] Dwyer, J. R. 2012, Journal of Geophysical Research (Space Physics), 117, A02308, doi:10.1029/2011JA017160

[6] Dwyer, J., N. Liu, and H. Rassoul 2013, EGU General Assembly Conference Abstracts, EGU General Assembly Conference Abstracts, vol. 15, pp. EGU2013–3231

[7] Fishman, G. J., et al. 1994, Science, 264, 1313–1316, doi:10.1126/science.264.5163.1313

[8] Grefenstette, B. W., D. M. Smith, B. J. Hazelton, and L. I. Lopez 2009, J. Geophys. Res., 114, A02314, doi:10.1029/2008JA013721

[9] Gurevich, A. V., G. M. Milikh, and R. Roussel-Dupre 1992), Physics Letters A, 165, 463–468, doi:10.1016/0375-9601(92)90348-P

[10] Hare, B. M., et al. 2016, J. Geophys. Res. Atmos., 121, 65116533, doi:10.1002/2015JD024426

[11] Marisaldi, et al. 2010a, Journal of Geophysical Research (Space Physics), 115, A00E13, doi:10.1029/2009JA014502

[12] Marisaldi, M., A. Argan, A. Trois, et al. 2010b, Physical Review Letters, 105(12), 128501, doi: 10.1103/PhysRevLett.105.128501

[13] Marisaldi, M., et al. 2014, EGU General Assembly Conference Abstracts, EGU General Assembly Conference Abstracts, vol. 16, p. 11326

[14] Smith, D. M., et al. 2005, Science, 307, 1085–1088, doi:10.1126/science.1107466

[15] Smith, D. M., et al. 2011, J. Geophys. Res., 116, D20124, doi:10.1029/2011JD016252

[16] Tavani, M., G. Barbiellini, et al. 2011, Physical Review Letters, 106, 018501, doi:10.1103/PhysRevLett.106.018501

[17] Tavani, M., et al. 2013, Natural Hazards and Earth System Sciences, 13, 1127–1133, doi:10.5194/nhess-13-1127-2013

[18] Tran, M. D., V. A. Rakov, S. Mallick, J. R. Dwyer, A. Nagc, and S. Heckman 2015, Florida, J. Atmos. Sol. Terr. Phys., 136, 8693, doi:10.1016/j.jastp.2015.10.010

[19] Ursi, A., M. Marisaldi, M. Tavani, D. Casella, P. Sanò and S. Dietrich 2016, Journal of Geophysical Research (Space Physics), 121, A10, 11, doi:10.1002/2016JA023136

[20] Ursi, A., C. Guidorzi, M. Marisaldi, D. Sarria and F. Frontera 2017b, Journal of Atmospheric and Solar-Terrestrial Physics, 156, 50-56, doi:10.1016/j.jastp.2017.02.014

Miscellanea

COMPTEL Reloaded: MeV Heritage supports e-ASTROGAM

Andrew Strong, Werner Collmar

Max Planck Institut für extraterrestrische Physik, D-85748 Garching, Germany

Science questions – Fermi-LAT and AGILE have provided a very detailed view of the gamma-ray sky in the range above 100 MeV, which in future may extend down to about 30 MeV with the latest Fermi-LAT event analysis techniques ('Pass 8'). Meanwhile we have a few thousand GeV sources but only about 20 in the 1-30 MeV range from GRO/COMPTEL. The new mission e-ASTROGAM is being proposed and the balloon experiment COSI has flown, both promising for the future; meanwhile a long-term on-going effort to exploit heritage COMPTEL data is underway at at the Max-Planck-Institut für extraterrestrische Physik and the Max-Planck-Institut für Astrophysik in Garching, Germany. The new COMPTEL analyses will be relevant to forecasting to support e-ASTROGAM science and instrumentation.

The double-Compton telescope COMPTEL flew on the NASA Compton Gamma Ray Observatory (CGRO) satellite from 1991 to 2000, and is still the basis of most of our knowledge about the 1-30 MeV sky. Pending new missions, for the next decade it will still be our most important resource for MeV continuum gamma rays [1].

COMPTEL [5] consists of an upper layer of 7 liquid-scintillators (D1) and a lower layer (D2) of 14 NaI detectors. The energy deposits in D1 and D2 are measured together with the direction of the scattered photon. Since only the Compton-scattered photon is measured, the response is basically circles on the sky centred on the true photon direction (Compton scattering formula) and broadened by direction and energy measurements. The full 9 year mission had 341 roughly 2-week observations covering the entire sky, with a field-of-view of about 30^o radius. Instrumental background discrimination is obtained with a time-of-flight (TOF) measurement and pulse-shape discrimination (PSD). Instrumental background variations are fitted using a template from high-latitudes where the celestial emission is smallest, or using a filtering technique for source detection.

The main results of COMPTEL were detections and properties of several Galactic and extra-galactic sources, the ^{44}Ti radioactive decay line from Cas A, mapping of the Galaxy in the 1.8 MeV line of ^{26}Al, and in Galactic continuum emission [9], cosmic-ray interactions in the interstellar medium [10, 1, 4], as well as GRBs and solar flares. The source results are collected in [6]. A spectrum of the Galactic plane emission from keV to TeV including COMPTEL and Fermi-LAT is in [4]. For more details on the interstellar emission and the cosmic-ray connection see the contribution to this White Book by Orlando, Strong and Grenier.

A more recent result from the continuing analysis of COMPTEL data at MPE is the definitive identification of the LS5039 binary via its light-curve [2] (still however using the earlier data processing).

Several new developments are completed or in progress for COMPTEL: The COMPTEL data analysis system ('COMPASS') was ported from Sun Solaris to Linux, removing the dependence on the Oracle database. New event processing techniques improve the background rejection, and new energy ranges are selected to avoid background lines. Time-of-flight (TOF) background rejection has been improved using intra-detector resolution instead of just per detector (TOF-VI vs previous TOF-IV), pulse-shape discrimination (PSD) is used with 2-D discrimination using TOF and PSD together. The entire COMPTEL event database has been re-processed with the new selections. A new source catalogue is being generated with the new event processing.

The maximum-entropy skymapping method for COMPTEL [9] based on the MEMSYS5 package [8] has been updated to use current state-of-the art convolution on the sphere and the HealPix

[1] The SPI instrument on ESA's INTEGRAL satellite provides more details on high-resolution line spectroscopy, in particular the 511 keV positron annihilation line, ^{26}Al and ^{60}Fe lines but is not very sensitive to continuum emission above an MeV up to now. COMPTEL does not extend down to the 511 keV line.

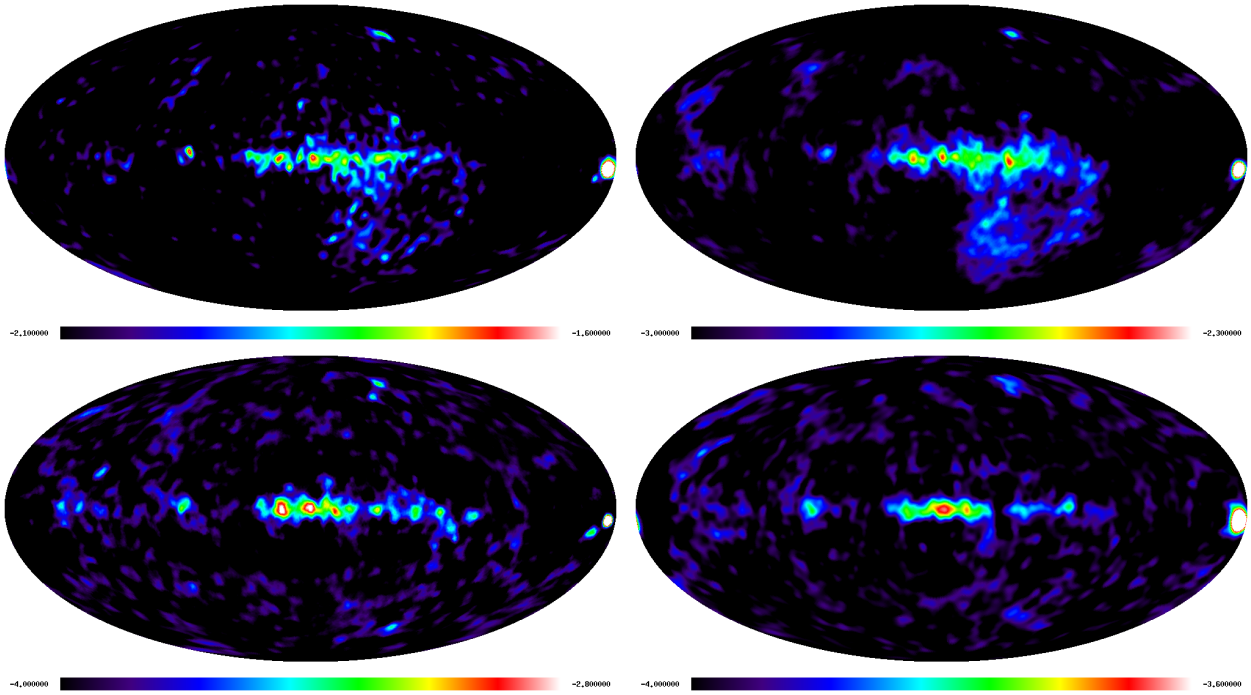

Figure 1: COMPTEL all-sky images using the current Maximum Entropy implementation. Galactic coordinates, centred on l = 0, b = 0. Left to right, top to bottom: 1-3 MeV, 3-10 MeV, 10-30 MeV, 1.8 MeV ^{26}Al line.

sky projection (uniform pixelization of the sphere), and the method has been adapted to modern parallel processing hardware so that skymaps can be produced in a short time compared to the large supercomputer requirements of 20 years ago. Fig 1 shows all-sky images in continuum 1–3, 3–10 and 10–30 MeV, and in the 1.8 MeV line of ^{26}Al. using the new maximum entropy algorithm, and data from the first 6 years of the mission and the original processed data. The Galactic plane is clearly visible (in continuum mainly interstellar emission from cosmic-ray interactions) as well as the principal sources: Crab, Vela pulsar, LS5039, Cyg X-1, 3C273, 3C279, Cen A. The extended feature below the plane at low energies is contamination from earth atmospheric emission. In future these maps will be updated with the full mission and the new data processing techniques described here. Preliminary maps using the new data processing for the full mission, with the new energy ranges, are shown in [3].

In addition, more advanced analysis using Information Field Theory and the D^{3}PO package [7] is foreseen. With D^{3}PO the Fermi gamma ray sky was reconstructed in nine separate energy bands. Spatial correlation of the gamma-ray flux was essential to discriminate the diffuse from the point-source emission and to denoise and deconvolve the former. Spectral correlations were not exploited. To also benefit from these, the D^{4}PO code is currently under development at the MPI for Astrophysics. This will detect and exploit spatio-spectral correlation structures of the diffuse emission as well as correlations in the point source spectra.

Acknowledgements – We thank Martin Reinecke for adapting the Maximum Entropy imaging software as described above, and to Torsten Enßlin and his group at MPA for supporting this project.

References

[1] Bouchet, L., Strong, A.W.., Porter T.A., Moskalenko., I.V., Jourdain, E., Roques, J.-P., 2011, 'Diffuse emission measurement with INTEGRAL/SPI as indirect probe of cosmic-ray electrons and positrons', ApJ, 739, 29

[2] Collmar, W., Zhang, S., 2014, 'LS5039 - the counterpart of the unidentified MeV source GRO J1823-12', A&A, 565, 38

[3] Collmar, W., Strong, A., 2017, 'COMPTEL Reloaded - an MeV data heritage project', Proc. 7th Fermi Symposium, October 2017, Garmisch-Partenkirchen, to appear in Proceedings of Science.

[4] Grenier, I.A., Black. J.H, Strong A.W., 2015, 'The Nine Lives of Cosmic Rays in Galaxies', Annual Review of Astronomy and Astrophysics, 53, 199

[5] Schönfelder, V., et al., 1993, 'Instrument description and performance of the Imaging Gamma-Ray Telescope COMPTEL aboard the Compton Gamma-Ray Observatory', ApJS 86, 657

[6] Schönfelder, V., et al., 2000, 'The first COMPTEL source catalogue', A&AS, 143, 145S

[7] Selig, M., et al., 2015, 'The denoised, deconvolved and decomposed Fermi $\gamma-$ray sky. An application of the D^{3}PO algorithm', A&A 581, 126

[8] Skilling J., 1989, 'Classical Maximum Entropy', in Maximum Entropy and Bayesian Methods, Kluwer:Dordrecht, ISBN 0-7923–224-9, p.45

[9] Strong, A.W., et al., 1999, 'COMPTEL Skymapping: a new approache using parallel computing', Astrophysical Letters and Communications, 39, 209. http://www.mpe.mpg.de/ aws/publications/strong_taormina_paper15.ps

[10] Strong, A.W., 2011, 'Interstellar gamma rays and cosmic rays: new insights from Fermi-LAT and INTEGRAL', World Scientific, ISBN: 978-981-4462-40-2, page 473, http://www.worldscientific.com/doi/abs/10.1142/9789814329033_0059

Cataloguing the MeV sky

Alberto Domínguez[1], *Juan A. Barrio* [1], *Marco Ajello*[2], *Marcos López Moya*[1], *Benoit Lott* [3], *Dario Gasparrini*[4,5]

[1] *Unidad de Partículas y Cosmología (UPARCOS), Universidad Complutense, E-28040 Madrid, Spain*
[2] *Department of Physics and Astronomy, Clemson University, Clemson, SC 29634, USA*
[3] *IN2P3/CNRS, Université Bordeaux 1, BP120, Gradignan Cedex, France*
[4] *Space Science Data Center, Agenzia Spaziale Italiana, I-00133, Roma, Italy*
[5] *Istituto Nazionale di Fisica Nucleare, Sezione di Perugia, I-06123, Perugia, Italy*

Science questions – The production of source catalogs is a fundamental task of any scientific mission with an instrument that benefits from large field of view (FoV) and high sensitivity such as e-Astrogam. According to the Scientific requirements [5], e-Astrogam will be designed both with pointing and surveying capabilities. The latter can be activated at any time allowing an optimized all-sky survey.

Source catalogs list sky positions and basic physical properties, which are typically integrated fluxes, photon indices, photometry, etc. Other complementary properties, such as redshifts, multiwavelength associations to other catalogs, and source classes, may be included in order to help in the source description and identification. This large collection of high-level data usually is the starting point of many science papers. As an example, the *Fermi*-LAT catalogs are at the top of the most cited works that have been published by the LAT collaboration (e.g. [3, 2]).

Importance of gamma-ray observations – In the multi-messenger multi-wavelength era that we are entering, cataloguing the sky in the whole electromagnetic spectrum turns as a indispensable condition for the astronomy community, yet the MeV Universe is still largely uncatalogued. For instance, the sensitivity in the range 100 MeV–500 MeV for the all-sky Third Catalog of Fermi Sources (3FGL, [2]) is 2-3 times worse than what is expected with e-Astrogam. The 3FGL catalog contains more than 3,000 sources from the first four years of LAT data and despite its energy threshold, the catalog is more representative of the GeV range. At lower energies of approximately 0.1 MeV and below, there is the Fourth IBIS/ISGRI Soft Gamma-Ray Survey Catalog (IBISCAT4, [6]). This catalog provides more than 700 sources both transients and faint persistent objects from the first 5.5 years of data. Also, the Swift-BAT 70 month catalog lists over 1000 sources at similar energies (about 0.1 MeV, [5]). Delivering a deep survey of the sky at about 1 MeV will be a major achievement for e-Astrogam.

Expected results with e-ASTROGAM – As a first step in the construction of an e-Astrogam catalog, we are proposing to generate simulated source catalogs based on expected performance of the instrument plus studies of source populations at the lowest energies measured by the *Fermi*-LAT, and extrapolate them down to MeV energies. This procedure will allow us to estimate the source populations that will be seen by e-Astrogam at different exposures and survey strategies. This will help in the surveys optimizations, also between pointing versus survey mode telescope time allocation. In reasonable amounts of telescope exposure, we expect to detect of the order of 1000s sources. These sources wil include blazars, radio galaxies, supernova remnants, pulsar and pulsar wind nebulae, and possibly binary systems, star forming galaxies, lobes of radio galaxies, radio quiet AGN powered by non-thermal electrons in corona, etc. A similar methodology for source population studies has been applied at higher energies to estimate TeV populations expected to be detected by the Cherenkov Telescope Array (CTA, [8]).

Catalogs will be produced from e-Astrogam observations providing high-level information to the public. Furthermore, there are plans on building association pipelines for the source identification

and classification from information at other wavelengths. It is interesting to find sources with no association or/and class identification (unIDs). The classification of these unIDs sources lead to many interesting scientific possibilities (e.g. [2]). Nuclear lines intensities will be also included in the surveys. The e-Astrogam catalogs will contain transients as well as persistent source, thus delivering the most detailed description of the MeV sky for years to come. Monitoring capabilities to constantly look for flares will be explored as well (e.g. [1]). These catalogs will be an essential legacy of the mission.

References

[1] Abdollahi et al., 2017, ApJ, 846, 34
[2] Ackermann et al., 2012, ApJ, 747, 121
[3] Ackermann et al., 2013, ApJS, 209, 34
[4] Acero et al., 2015, ApJS, 218, 23
[5] Baumgartner et al., 2013, ApJS, 207, 19
[6] Bird et al., 2010, ApJS, 186, 1
[7] de Angelis et al. 2017, Exp. Astr., 44, 1
[8] Hassan et al. 2017, ICRC 2017, arXiv:1708.07704

Galactic center gamma-ray excess: Constraining the point source contribution with e-ASTROGAM

Richard T. Bartels[1], *Katie Short*[1], *Christoph Weniger*[1], *Dmitry Malyshev*[2]

[1] *GRAPPA and Institute of Physics, University of Amsterdam, Science Park 904, 1098XH Amsterdam, Netherlands*
[2] *Erlangen Centre for Astroparticle Physics, Erwin-Rommel-Str. 1, Erlangen, Germany*

Science questions – The Galactic center (GC) is expected to be the brightest source of gamma rays from possible annihilation of dark matter (DM) particles. An excess of gamma rays, henceforth the Galactic-Center excess (GCE), consistent with DM annihilation in the vicinity of the GC was reported by several groups [1, 2, 3, 4, 5, 6, 7, 8]. Apart from DM annihilation, possible explanations of the excess include a population of CR electrons emitted near the GC and a population of faint but numerous point sources, such as millisecond pulsars (MSPs). The latter model is supported by various statistical methods, e.g., analysis based on wavelet fluctuations [9], non-Poissonian template fits [10], and Monte Carlo reconstruction of PS population near the GC [11]. Understanding the origin of the excess is difficult due to significant uncertainties in the diffuse Galactic gamma-ray emission as well as the properties of resolved point sources near the GC.

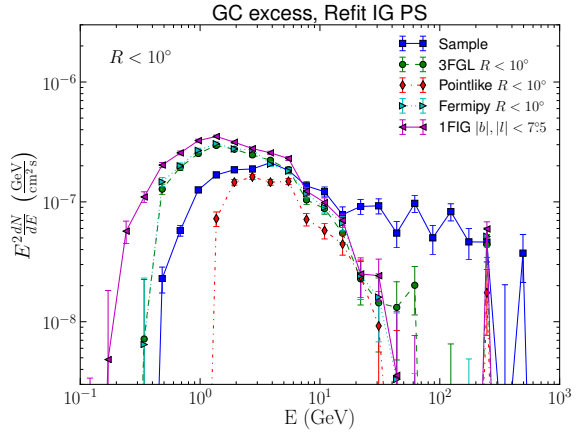

Figure 1: Effect on the spectrum of the GC excess from refitting of PS near the GC [8].

In Figure 1 we illustrate the uncertainty due to resolved PS by showing the effect of refitting PS near the GC found with different PS detection algorithms. One can notice that, at low energies, the changes in the GC excess flux are much larger than the statistical error bars. This is a manifestation of the fact that our knowledge about the GC excess spectrum is limited by the modeling uncertainties rather than lack of photon statistics. In part, this is due to relatively poor angular resolution of the *Fermi* LAT at energies below 1 GeV. Improved angular resolution of e-ASTROGAM will help to better separate individual PS and to constrain the spectrum and the morphology of the excess, which is an important step in distinguishing the MSP hypothesis of the excess from the truly diffuse emission coming from CR electrons or DM annihilation. Application of statistical methods to the e-ASTROGAM data would even further reduce the uncertainty on the interpretation of the excess.

Importance of gamma-ray observations – The gamma-ray GC excess has no clear counterparts in other frequencies, such as radio or X-ray. This lack of counterparts makes it hard to

determine the origin of the excess. Although proposed future observations with new radio telescopes such as MeerKAT, GBT, VLA, and later SKA have the potential to observe dozens of MSPs in the bulge of the MW, e.g., if the GC excess is coming from MSPs, then one can expect to detect about 200 MSPs with SKA when surveying the inner–Galaxy for $\sim$ 100h [12]. Nonetheless, the gamma-ray observations will remain our main tool to learn about the origin of the excess.

With gamma-ray observations one can either directly search for MSP candidates based on the gamma-ray spectrum [11] or use statistical methods to determine the contribution of sub-threshold point sources. Currently there are about 60 MSP candidates detected in the Fermi LAT data [11], while statistical methods show that all of the excess can be explained with a population of point sources.

Straightforward detection of MSPs in the Inner Galaxy are compromised by large diffuse foregrounds and point source confusion, along with the degrading resolution of Fermi-LAT in the inner few degrees of the GC. Challenges also arise when performing a wavelet analysis in the Inner Galaxy. In principle, there is potential for falsely induced wavelet peaks due to, e.g., mismodeled emission of CRs interacting with interstellar gas. Such concerns can be addressed by a careful analysis of the spatial distribution of peaks, comparison with the expected signal from gas sub-structure only, or a spectral analysis to distinguish between the potential signals. At sub-GeV energies, the poor angular resolution of the Fermi-LAT makes it difficult to constrain the MSP population via both a direct search or statistical analysis using, e.g., wavelet fluctuations analysis.

Expected results with e-ASTROGAM – One of the main advantages of e-ASTROGAM relative to *Fermi* LAT is a better angular resolution at energies below 1 GeV. Although the statistical sensitivity of e-ASTROGAM around 1 GeV after 5 years of observations is expected to be comparable to *Fermi* LAT statistical sensitivity after 10 years of observations, the main challenge in analyses near the GC is not the statistical uncertainty, but rather the source confusion and uncertainties in the diffuse emission modeling. Thus, it is important to take into account the signal to background ratio (SBR) together with the signal to noise ratio (SNR).

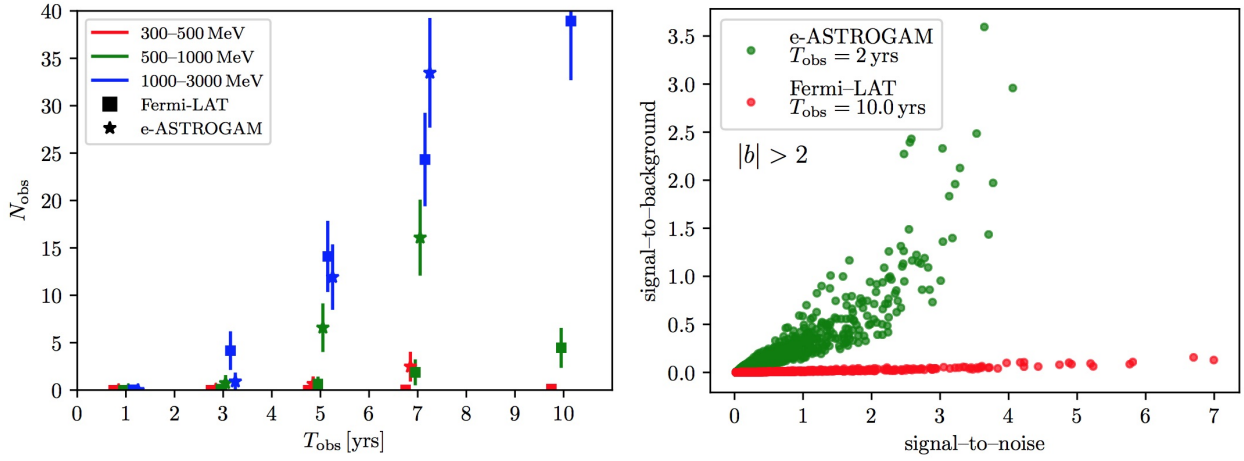

Figure 2: Projections for the detectability of the bulge MSP population. Left: Number of sources detectable with SNR > 5 as a function of total observation time in different energy ranges and for $|b| > 2°$. We show predictions for $T_{\rm obs} \in [1, 3, 5, 7]$ yrs (minor shifts away from these values are for visibility). For Fermi-LAT we also include the 10 year prediction for comparison. Right: Signal–to–noise ratio (SNR) versus signal–to–background ratio (SBR) for a random realization of an MSP population that can reproduce the GCE in the energy range 0.5–1 GeV. We compare the current Fermi–LAT sensitivity (red) to that expected for e-ASTROGAM after 2 years of total exposure (green). Due to its larger exposure, the Fermi–LAT can reach a SNR comparable to e-ASTROGAM in this energy range, however, e-ASTROGAM has a superior SBR due to better angular resolution.

To estimate the improvement in the source characterization, we simulate a population of MSP-like point sources in the bulge of the MW. For the simulation, we are using the best fit distribution of MSPs in the Galactic Bulge as described in [9], which can explain 100% of the GCE. We make

predictions for the number of sources detectable by the *Fermi* LAT and e-ASTROGAM in the energy ranges 0.3–0.5 GeV, 0.5–1 GeV and 1–3 GeV. We compute the sensitivity to a point source as a function of sky position by requiring that the signal-to-noise ratio is larger than 5 within the 68% containment radius of the PSF (Figure 2 left). In Figure 2 on the right we show the signal–to–noise and signal–to–background ratios for the sources in this population for energy range 0.5 – 1 GeV. In this range, the statistical sensitivity of *Fermi* LAT is comparable to the sensitivity of e-ASTROGAM, but the signal to background ratio is significantly better for e-ASTROGAM due to superior angular resolution, which will enable one to better separate the sources from each other and from the diffuse background. For the wavelet analysis, the number of high significance peaks is expected to be similar for *Fermi* LAT and e-ASTROGAM due to similar statistical sensitivity, but at low significance, the peaks which overlap in *Fermi* LAT will be resolved with e-ASTROGAM, which will improve the statistical power of the wavelet analysis.

The main scientific output of this study will be a better characterization of the GC excess. If the MSP scenario is disproved, i.e., the excess emission is consistent with truly diffuse component, then the DM interpretation will be still one of the possibilities. If, on the other hand, most of the GC excess emission will be explained by a population of MSPs, then one will put tighter limits on DM annihilation, which will be competitive or even more constraining for some channels of annihilation than the limits from the dwarf galaxies.

- Scientific output:
  - Characterization of low-energy component of excess;
  - Higher resolution of excess emission in individual sources;
  - Better constraints on DM annihilation.

References

[1] Goodenough, L., & Hooper, D. 2009, ArXiv:0910.2998
[2] Vitale, V., Morselli, A., & for the Fermi/LAT Collaboration. 2009, ArXiv:0912.3828
[3] Abazajian, K. N., & Kaplinghat, M. 2012, Phys. Rev. D, 86, 083511
[4] Hooper, D., & Slatyer, T. R. 2013, Physics of the Dark Universe, 2, 118
[5] Gordon, C., & Macías, O. 2013, Phys. Rev. D, 88, 083521
[6] Calore, F., Cholis, I., & Weniger, C. 2015, JCAP, 3, 038
[7] Ajello, M., Albert, A., Atwood, W. B., et al. 2016, ApJ, 819, 44
[8] M. Ackermann *et al.*, Astrophys. J. 840, no. 1, 43 (2017)
[9] Bartels R., Krishnamurthy S. and Weniger C., 2016, PRL, 116, 051102
[10] Lee, S. K., Lisanti, M., Safdi, B. R., Slatyer, T. R., & Xue, W. 2016, PRL, 116, 051103
[11] Ajello M. *et al.*, arXiv:1705.00009.
[12] Calore F., Di Mauro M., Donato F., Hessels J. W. T. and Weniger C., 2016, ApJ, 827, 143

e-ASTROGAM contribution to Unidentified gamma-ray sources

Josep M. Paredes[1], *Valenti Bosch-Ramon*[1], *Benito Marcote*[2]

[1]*Departament de Física Quàntica i Astrofísica, Institut de Ciències del Cosmos (ICCUB), Universitat de Barcelona, IEEC-UB, Martí i Franquès 1, E08028 Barcelona, Spain*
[2]*Joint Institute for VLBI ERIC, Postbus 2, 7990 AA Dwingeloo, The Netherlands*

Science questions – The third EGRET catalogue provided a list of unidentified sources (168 out 271 detected sources) [1]. The discovery of gamma-ray sources with no feasible counterpart at lower energies has been also common in more recent spatial missions such as *Fermi*-LAT, or by ground Cherenkov telescopes. Although the fraction of unidentified sources is lower than in the case of EGRET, the fraction is still significant, specially in the case of *Fermi*-LAT [2], in which a large amount of sources have been detected (see Table 1). In most of the unidentified gamma-ray sources the lower energy part of their spectrum is unknown, and thus e-Astrogam will for the first time allow the determination of this part of the spectrum, which can be fundamental for the source identification.

Importance of low-energy gamma-ray observations – Observations in the 0.3 MeV–3 GeV range of unidentified sources give valuable information about the unknown spectrum of these sources in the low energy part of the gamma-ray spectrum. On one hand, the majority of the 3FGL Catalog sources (2415 out of 3033) have a power-law spectra (at energies larger than 100 MeV) steeper than E^{-2}, and among the unidentified sources, the fraction of them steeper than E^{-2} is 898 out of 1010. This implies that the peak energy output of these sources is below 100 MeV, making them good targets for e-ASTROGAM. On the other hand, the most powerful AGNs peak in the MeV region [3], whereas gamma-ray pulsars typically have spectral peaks in the GeV energy band [4]. Therefore, the knowledge of the MeV–GeV spectrum can already allow one to find possible candidates for the unidentified sources (e.g. AGN vs pulsar), and together with multi-wavelength data, fully reveal the nature of many of them. Thus, e-ASTROGAM, working in the poorly explored energy range from 0.3 MeV to 3 GeV, can play a fundamental role in the identification of gamma-ray sources without known counterpart.

Expected results with e-ASTROGAM – With the e-ASTROGAM sensitivity for different integration times, 1 Ms (Extragalactic case) and 1 year (Galactic case), we have estimated the number of *Fermi*-LAT unassociated sources, pulsars, and AGNs that could be detected by e-ASTROGAM for each one of the 0.1–0.3, 0.3–1.0, 1–3 GeV energy ranges that are common to *Fermi*-LAT and e-ASTROGAM (see Fig. 1). In the case of the unassociated sources, we plot in Fig. 2 two histograms showing how many of them would be detected depending on its galactic latitude ($|b| < 5^\circ$ and ($|b| > 5^\circ$). Among the 335 unassociated sources with $|b| < 5^\circ$ (Galactic) in the 3FGL Catalog, 166, 276 and 194 of them (50%, 82%, and 58%) would be detected by e-ASTROGAM in the 0.1–0.3, 0.3–1.0, 1–3 GeV energy ranges, respectively. For the 675 unassociated sources with $|b| > 5^\circ$

Table 1: Fraction of unidentified sources from different gamma-ray instruments.

	Detected	Unidentified	
EGRET	271	168	62%
COMPTEL 1st cat	32	9	28%
AGILE 1st cat	47	8	17%
FERMI-LAT 3FGL	3033	1010	33%
CHERENKOV	204	44	22%

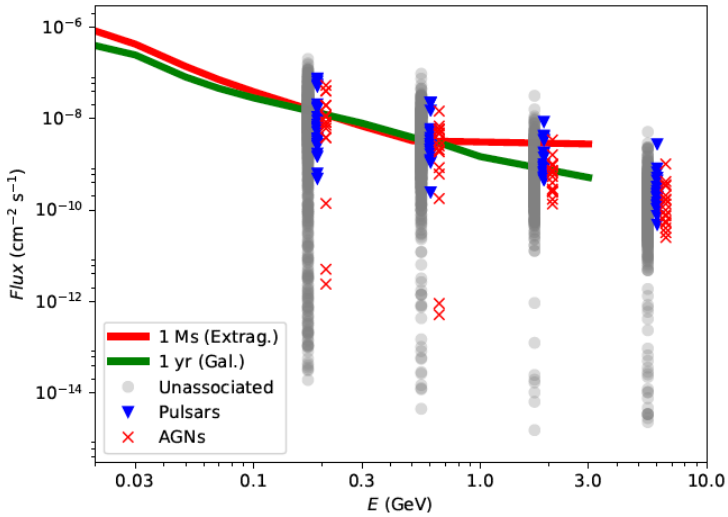

Figure 1: Flux of the unassociated sources, pulsars and AGNs detected by *Fermi*-LAT (3FGL) as a function of individual bands. The red and green curves are the e-ASTROGAM sensitivity for different integration times and for the energy range 0.03–3 GeV.

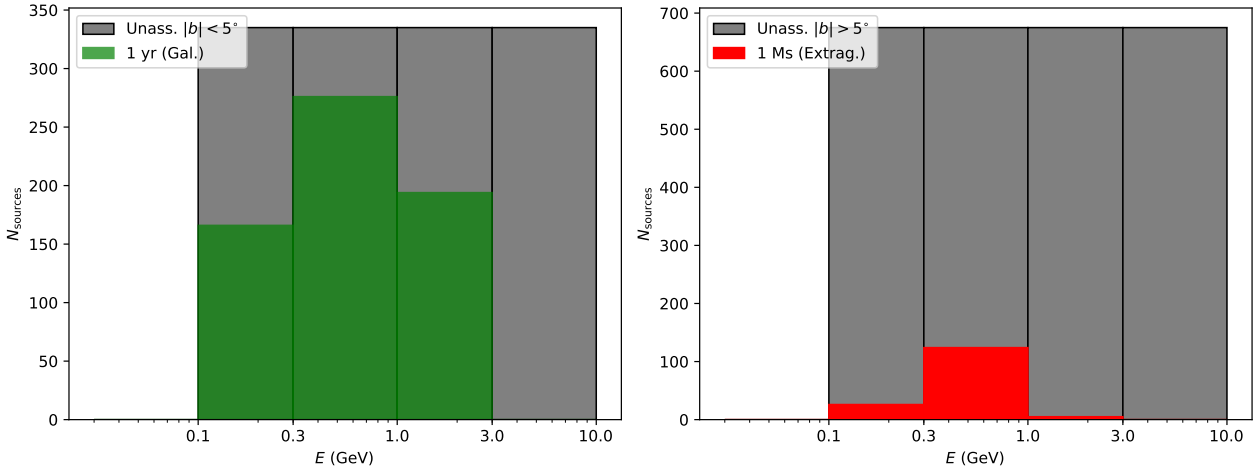

Figure 2: **Left:** Number of unidentified low galactic sources from the 3FGL Catalog that would be detected by e-ASTROGAM for different energy intervals . **Right:** The same but for high galactic latitud sources.

(Extragalactic), 26, 124 and 5 of them (4%, 18%, and 0.7%) would be detected in the respective energy ranges. Given the steep spectra of many of the sources seen by *Fermi*-LAT, crucial information at low-energy gamma-rays will be available for those sources detectable above 0.1 GeV for e-ASTROGAM.

References

[1] Hartman, R. C., Bertsch, D. L., Bloom, , S. D. et al., 1999, ApJS, 123, 79

[2] Acero, F., Ackermann, M., Ajello, M. et al., 2015, ApJS, 218, 23

[3] Ghisellini, G., Righi, C., Costamante, L. and Tavecchio, F., 2017, arXiv:1702.02571

[4] Thompson, D.J. 2004, Cosmic Gamma-Ray Sources, Volume 304 of the series Astrophysics and Space Science Library pp 149-168 (arXiv:astro-ph/0312272)

Fast MeV γ-ray flashes and perspectives on γ-SETI

Stefano Ciprini [1,2], *Chi C Cheung* [3]

[1] *Space Science Data Center, Agenzia Spaziale Italiana, I-00133, Roma, Italy*
[2] *Istituto Nazionale di Fisica Nucleare, Sezione di Perugia, I-06123, Perugia, Italy*
[3] *Space Science Division, Naval Research Laboratory, Washington, DC 20375-5352, USA*

Science questions – The rapidly evolving socialization drivers of the globalization development, enabled by the internet networking era and the exponential grow of computing power and data storage, indicate that citizen society (i.e. the participation to the governance by citizens/taxpayers) and citizen science (scientific data exploration conducted by volunteer individuals) will have a substantial development in the next couple of decades. This is true also for citizen astronomy [13] based on open data and having non-negligible consequences for space missions and agencies supported by public funds. The hunt for alien worlds and the search for life in the Universe, is a very fascinating topic for citizen astronomy. Citizen astronomers are motivated by being of service to science, as well as by their interest in the subject. A basic question is therefore: how high-energy missions and instruments dedicated to the observation of the γ-ray sky can have a distinctive, and more compelling role in inspiring interest in the wider citizen and public outreach (E&PO) through the search for signs of extraterrestrial intelligent (ETI) life in newly discovered exoplanets and in extragalactic systems?

As of October 2017, 3691 planets in 2766 planetary systems, with 620 multiple-planet systems are counted [15]. The future path for the exoplanets science includes advanced searches for Earth-size and super-Earth-size habitable planets, their physical, geological and astrobiology characterization, the search for liquid water and understanding of their atmospheres and, at last, the search for signs of elementary life. Three recent discoveries have substantially impacted the media, enlarging the large public interest for missions motivated partially and primarily to exoplanet detection and characterization (e.g., CoRoT, Kepler, CHEOPS, PLATO, ARIEL, TESS, and also Spitzer, Gaia, JWST, WFIRST, LUVOIR). The Earth-size planet in Proxima Centauri (at 4.2 ly); the first known system of seven Earth-size planets (TRAPPIST-1) at 40 ly; the irregular and unusual optical flux dips, flickering and dimming in the star KIC 8462852 (Tabby's star). This F-type star system KIC 8462852 placed at 1280 ly, is interpreted as a swarm of dusty comet fragments, or a large number of orbiting small masses in tight formation, but more exotic theories are proposed, like patterns and signs of an exo-civilization associated with a construction of Dyson swarm [7, 17], that is a popular concept for a Type II extraterrestrial civilization in the Kardashev scale [9].

Despite the general scientific skepticism[1], KIC 8462852 has now been identified as an exceptional target for searches for extraterrestrial intelligence (SETI) signals and transmissions. Historically the SETI initiative have not considered γ-ray energies, therefore a second question is: how a next large γ-ray space telescope characterized by large field of view and improved sensitivity in the MeV band can be useful in the new era of revived scientific and SETI-related projects in the guise of multifrequency time-domain/survey astronomy?

Importance of gamma-ray observations – The intriguing fast radio bursts (FRBs) were first discovered in 2007. These are ultrafast radio transients with inferred extragalactic origin based on large dispersion meaures, with typical millisecond durations and $\sim$GHz flux densities of $\sim$1Jy. There is no concensus explanation for their progenitors [10] and they could in fact originate from multiple source populations. Although there could be thousands of detectable events per day, less than two dozen FRBs have been discovered. An FRB in our Galaxy is predicted at least every $\sim$300 years – at < 20 kpc distances, it would be spectacularly bright with a flux density of 10^{10} Jy,

[1] ''`Look for what's detectable, not for what's probable`'' (Freeman Dyson 2009).

detectable by low-cost radio receivers [12]. Some fraction of FRBs could have a short γ-ray flash following the radio pulse [6, 14], in the hypothesis of a merger of compact binaries (BH/NS). Short GRBs with temporally-extended emission in hard-X rays and medium-energy γ rays are expected to be observed in the 0.2 MeV−3 GeV band and this would be important to clarify the nature of FRBs and the related prediction of gravitational wave emission also for some class of FRBs, that could be already detected by advanced LIGO/VIRGO and in future by LISA (launch in 2034). As a remark, supergiant fast X-ray transients, believed to be produced by high mass X-ray stellar binary systems as short, sporadic and bright flares are likely not related to FRBs, but this do not in principle, exclude that millisecond-duration gamma-ray flashes (MGFs) from other galaxies might exist.

Much more exotic conjectures point out that FRBs could be produced by some activity of extragalactic advanced exo-civilizations (Kardashev II or III types). In some cases (like for the repeating FRB 12110) they are observed to repeat several times also years later, in agreement with the hypothesis for alien artificial beacons. When the Fermi Paradox on intelligent civilizations [8] was initially proposed, it was thought that planets themselves were very rare, contrary to the actual evidence that the hundreds of exoplanets found since 1992 are only the tip of the iceberg[2]. Some FRBs might originate from radio and coherent beams supplied by stellar energy that would power enormous light sails for spaceships capable of attaining relativistic speeds [11]. Energetic and engineering constraints both yield similar result on sail size (comparable to a super-Earth planet) and the optimal powering frequency similar to the detected FRB frequencies. Well observable leakage radiation may well be from the use of power millimeter-wave beaming to transfer energy and accelerate such spaceships, with effective isotropic radiated power of $\sim 10^{25}$ erg s^{-1} [3]. Advanced civilizations that have reached a technological singularity (abruptly runaway technological growth) could intentionally transmit a two-millisecond pulse encoding 10^{18} bits of information [2]. GRBs may be also used by civilizations as synchronizers for beamed and short duration SETI transmissions [4]. Considering that civilizations are bathed in optical light, the absorption/reddening of optical/UV light on the Galactic plane and the terrestrial/solar interference at radio bands, to send transmissions over the Galaxy is convenient to choose energy bands where the isotropic background and stellar output is low as like the wide MeV-GeV γ-ray band [1]. Under all the astrophysical/citizen-science/large-public outreach scenarios, a SETI approach based on γ-ray data (γ-SETI) could be of particular interest, especially if we consider MeV thermonuclear and matter-antimatter annihilation processes.

Signatures of an advanced exo-civilization in our Galaxy or other galaxies can, more easily, emerge if we observe the sky at MeV/sub-GeV γ-ray energies with respect to other photon frequencies, and include the following basic categories of technological progenitors. Artificial objects in central star transiting orbits; Dyson complexes; deliberate communication signals [1]; directed impulsive beaming for accelerating spacecrafts [3, 11]; leakage in the electromagnetic spectrum (spectral lines from nuclear fissile waste disposal in stars, tritium leakage, etc.); artifacts such as evidence for energy production/consumption/transportation or for huge space colonies with large-scale industrial engineering, furnaces for antimatter or fusion plants; manipulation of the central star and mining star material (for example the Shklovskii gamma-ray laser mining, or "graser"); protective blast shields against nearby merging NSs, GRBs or SN; self-destruction of civilizations by global thermonuclear wars and other observational signatures [16]; and the unexpected.

Expected results with e-ASTROGAM – Possible artificial and candidate γ-SETI signals from technologically advanced civilizations can be identified by searching for unusual spectral or temporal (dips, periodicy, unusual flickering) features, and with per-photon analysis, using MeV/sub-GeV data obtained by a high-sensitivity and large field of view surveying space telescope like e-ASTROGAM [5]. Beyond the search for possible spectrally/temporally unusual γ-ray

[2] ``Alien Worlds Galore'' (M. Cruz & R. Coontz 2013, introduction to a special issue of Science).
``If we are alone in the Universe, it sure seems like an awful waste of space.'' (Carl Sagan 1972 paraphrasing Thomas Carlyle as reported in "Accepting the Universe" by John Burroughs, 1920).

signals, the possibly repeating subset of millisecond γ-ray flashes (MGFs) or other type of mini-bursts are optimal targets for per-photon data studies. It is also of interest to investigate the association/coincidence of multiple γ-ray events with the FRBs [18]. The expected number of detectable γ rays from a FRB within a direction Ω_j at redshift z in a MGF search within a time interval Δt is given as $N_\gamma = \Delta t \int_{0.2\ \mathrm{MeV}}^{3\ \mathrm{GeV}} d\epsilon_{\mathrm{obs}} A_{\mathrm{eff}}(T_i, \Omega_j)[dF_\gamma(\epsilon_{\mathrm{obs}}; z, \xi)]/[d\epsilon_{\mathrm{obs}}]$, where ξ is the γ-ray to radio luminosity ratio in the rest-frame of a FRB. Gamma-ray photon pairs or multiplets within an energy and/or time range, for example with time search windows of $\Delta t = 1, 2, 5, 10$ msec are considered for every reference photon and other photons are searched, in blind mode, within a spatial distance compatible with per-photon angular resolution and within Δt from the reference photon event. These simple per-photon analyses have possible implementations in citizen-science (i.e., within the context of a "γ-SETI at home" program or even more interactive platforms). To outline conclusive candidates, Poisson statistics of steady γ-ray fluxes from bright point sources or diffuse γ-ray background have to be taken into account. Another example of a possible γ-SETI analysis is to search for spectral, also variable, annihilation signature in different regions of the γ-ray sky exploiting the excellent spectral energy resolution of e-ASTROGAM. Such a signal could be produced by artificial $p\overline{p}$ annihilation used for applications requiring portability like spaceships propulsion. If they exist, this might be detectable in case of solar neighborhood star directions.

An obvious disadvantage of artificial signal searches in γ rays is the large power output requirements for exo-engineering, but the history of science teach us that unexpected could be greater than expected. On the other hand it is time to include γ rays in SETI and citizen-astronomy frames, especially considering that the hard-X-ray and soft/medium energy (MeV) sky is the most promising portion of the electromagnetic spectrum, joined with existing radio and optical-wavebands for such searches. This also contributes to increase the potential of the e-ASTROGAM mission in terms of public outreach and synergy with studies of the potentially many, habitable exoplanets expected to be discovered in the forthcoming decades.

References

[1] Arnold, L. 2013, Internat. Journ. Astrobiology, 12, 212
[2] Ball, J. A. 1996, AIP Conf. Ser., 384, 719
[3] Benford, J. N., & Benford, D. J. 2016, ApJ, 825, 101
[4] Corbet, R. H. D. 1999, PASP, 111, 881
[5] De Angelis, A., Tatischeff, V., Tavani, M., et al. 2017, Experim. Astron., 44, 25
[6] DeLaunay, J. J., Fox, D. B., Murase, K., et al. 2016, ApJ Lett., 832, L1
[7] Dyson, F. J. 1960, Science, 131, 1667
[8] Jones, E. 1985, Los Alamos Tech. rep. LA-10311-MS
[9] Kardashev, N. S. 1964, Soviet Astron., 8, 217
[10] Katz, J. I. 2016, Modern Physics Lett. A, 31, 1630013
[11] Lingam, M., & Loeb, A. 2017, ApJ Lett., 837, L23
[12] Maoz, D., & Loeb, A. 2017, MNRAS, 467, 3920
[13] Marshall, P. J., Lintott, C. J., & Fletcher, L. N. 2015, ARA&A, 53, 247
[14] Murase, K., Mészáros, P., & Fox, D. B. 2017, ApJ Lett., 836, L6
[15] Schneider, J., Dedieu, C., Le Sidaner, P., Savalle, R., & Zolotukhin, I. 2011, A&A, 532, A79 (http://exoplanet.eu ; https://twitter.com/voexoplanet).
[16] Stevens, A., Forgan, D., & James, J. O. 2016, Internat. Journ. Astrobiology, 15, 333
[17] Wright, J. T., & Sigurdsson, S. 2016, ApJ Lett., 829, L3
[18] Yamasaki, S., Totani, T., & Kawanaka, N. 2016, MNRAS, 460, 2875

Author Index